AUGUST 1970 REPORT NO.

AN INVESTIGATION OF NONEQUILIBRIUM EFFECTS ON COMBUSTION IN SUPERSONIC STREAMS

by

R.M. JENSEN
C.A. BRYCE
B.A. REESE

NASA GRANT ~~NsG 592~~ NGR-15-005-013

Jet Propulsion Center
School of Mechanical Engineering
Purdue University

National Aeronautics and Space Administration
Lewis Research Center
21000 Brookpark Road
Cleveland, Ohio 44135

ABSTRACT

Theoretical and experimental studies have demonstrated the potential for aircraft capable of operating at hypersonic speeds within the atmosphere with an air breathing engine employing supersonic combustion. Duplication of true flight conditions in ground testing these propulsive systems requires a significant extension of existing facility capabilities and operating ranges. However, the nature of the flow at these extreme conditions does not completely simulate the actual flight conditions experienced by the Supersonic Combustion Ramjet (SCRAMJET) engine because the flowing gas stream is not in complete thermal and chemical equilibrium.

This research program is a theoretical and experimental investigation of the effect of nonequilibrium conditions upon the performance of combustors employing supersonic flows. Calculations and experiments are made regarding the effects on the ignition of hydrogen of the nonequilibrium species (free radicals, atoms, water vapor, etc.) obtained using vitiated air.

In the experimental effort, a gas generator burning nitrogen tetroxide and hydrazine, plus a nitrogen diluent is employed to produce the vitiated air which has approximately 19 percent by weight of water, replacing an equal volume of nitrogen in real air, 26 percent oxygen and 55 percent nitrogen. Test section conditions simulate a free flight Mach number of 6.5 and an altitude of 80,000 ft. The gas generator products expand through a converging-diverging nozzle to a supersonic velocity where heated hydrogen is injected and supersonic burning occurs. Hydrogen is introduced into the combustion process through an annulus at

a velocity corresponding to sonic conditions. Injection is parallel to the mainstream gases to minimize shock interactions, thereby simplifying the analysis of both the theoretical and experimental results.

Analysis of the inlet conditions and subsequent combustion process necessitates the use of finite-rate chemistry calculations to determine (1) the composition of the entering streams and (2) the composition variation with time during ignition. Ignition delays are then calculated using a one-dimensional, reacting gas program which assumes constant temperature during the delay period. Results of this program were verified against existing data for ignition delays in real air and hydrogen. Subsequent analysis for vitiated air at specific experimental conditions investigated showed that hydrogen would ignite approximately 1.5 in. downstream of the injection station. It also showed that if both streams (hydrogen and vitiated air) were in chemical equilibrium prior to mixing, the ignition would take place approximately 12 in. from the point of injection. Thus, the nonequilibrium free-radical content of the incoming streams tends to accelerate the ignition process to a significant degree.

In the experimental effort, the ignition delay length was determined visually from high speed (550 frames per second) motion pictures of the exhaust flow. The results showed the ignition delay distance to be a direct function of the hydrogen injection temperature. The observed distances varied from 8 to 19 in. and compared favorably with the analytical values when the assumption of limited rather than complete mixing of the two streams prior to ignition was employed.

Results of this investigation show that the nonequilibrium free-radical content from a vitiated air source will cause early supersonic

ignition of the hydrogen. An analysis of heated air expanded from a high temperature source to test section conditions also indicates that there is sufficient free-radical content in the incoming flow to cause early ignition. Therefore, neither vitiated air nor heated air will simulate the equilibrium supersonic ignition phenomenon in the regime where the reaction times are rate controlling. Water vapor was also found to reduce the ignition delay period.

TABLE OF CONTENTS

Page

LIST OF TABLES

LIST OF FIGURES

NOMENCLATURE

Symbol	
A	area
C^*	effective exhaust velocity
C_e	electrical capacitance (see Appendix B)
C_p	pressure coefficient (see Appendix G)
C_{th}	thermal capacitance (see Appendix B)
c_p	specific heat
E	activation energy
G	mass velocity (see Appendix G)
H	total enthalpy (see Appendix G)
h	absolute enthalpy, film heat transfer coefficient
h_s	sensible enthalpy (see Appendix G)
K	equilibrium constant
k	reaction rate constant, thermal conductivity
L	length of simulated section, length
M	effective third body concentration, Mach number
N	number of nodes (see Appendix B)
P_c	chamber pressure
P_t	total pressure
P_t'	impact pressure
p_s	static pressure
p_s'	cone-static pressure

Symbol	
Q	heat transfer flow rate
Q_{chm}	heat of reaction (see Appendix G)
q	dynamic pressure (see Appendix G)
R_u	universal gas constant
R_e	electrical resistance (see Appendix B)
R_{th}	total thermal resistance (see Appendix B)
R_{thn}	thermal convective resistance (see Appendix B)
R_{thn1}	thermal resistance encountered by traversing Δr_{n1} (see Appendix B)
R_{thn2}	thermal resistance encountered by traversing Δr_{n2} (see Appendix B)
r_i	inner radius of section (see Appendix B)
r_o	outer radius of section (see Appendix B)
r_{mn}	mean radius of nth division (see Appendix B)
r_n	radius of nth node (see Appendix B)
T	temperature, time scaling factor
T_{aw}	adiabatic wall temperature (see Appendix B)
T_c	chamber temperature
T_s	static temperature
T_t	total temperature
t_e	electrical time (see Appendix B)
t_{th}	thermal time (see Appendix B)
V	velocity, volume of element
$\dot{w}$	weight flow rate
X	third body mole fraction

Greek Symbol

γ	specific heat ratio
ΔH_R	heat of reaction
Δr_{n1}	radii difference between nth node and inner boundary (see Appendix B)
Δr_{n2}	radii difference between nth node and outer boundary (see Appendix B)
δ	cone-static probe half angle (see Appendix G)
η	species mole fraction
η_c	combustion efficiency
τ	time
τ_{ID}	ignition delay time
τ_R	reaction time
ϕ	equivalence ratio

Subscripts

cp	combustor products
e	combustor exit
EXP	experimental
f	fuel
ID	ignition delay, induction period
ox	oxidizer
R	reaction
SIL	simplified ignition lag
w	combustor wall conditions
1	combustor inlet
2	fuel exit
3	combustor exit

INTRODUCTION

Propulsion systems utilizing supersonic combustion have recently been recognized as having strong potential for vehicles operating in the hypersonic flight regime. The emergence of these new classes of engines capable of operating at very high speeds within the atmosphere introduces new problems in experimental aerodynamics. In particular, the duplication of true flight conditions in testing these hypersonic air breathing engines requires the significant extension of existing facilities, capabilities and operating ranges. As flight velocities are increased above Mach number 6, the stagnation temperatures and pressures required for meaningful ground test duplication becomes increasingly difficult to achieve, particularly where large test sections and long experimental run times are required. A typical supersonic combustion ramjet engine (SCRAMJET) cruising at a Mach number of 6 at an altitude of 80,000 feet would encounter stagnation temperatures and pressures in the realm of 2500°K and 1500 psia with air mass flows of 150 pounds per second. Dr. Antonio Ferri pointed out in his Lanchester Memorial Lecture [1]* on application of supersonic combustion that the most urgent problem to be solved before a supersonic combustion engine could be perfected was the development of ground facilities for testing these engines. Within the present

*Number in brackets indicate references in the Bibliography.

state-of-the-art of ground test facilities, it is just about impossible to test a complete engine under conditions duplicating all the parameters corresponding to high Mach number flight, particularly for a time duration sufficient to investigate the time-dependent facets of the combustion process. In the supersonic combustion problem as applied to the SCRAMJET, the chemical composition of the flowing medium, the mixing of the streams of fuel and air, the chemical reactions taking place, and the reaction rates involved are the important factors to be considered [2]. Therefore, the primary parameters requiring actual duplication in the test cell are the static temperature, static pressure, composition of the gases, residence time in the combustor, and the velocity relationship between the mixing streams. Duplication of the severe environments associated with low altitude high Mach number flight regimes using state-of-the-art ground test facilities, is possible at Mach numbers up to approximately 6 but it would be prohibitively expensive due to the size and operational cost of a clean air heater capable of delivering the necessary high temperature, pressure and quantity air mass flows. An alternate approach to this problem is to generate a fluid medium which possesses the primary influencial properties of true air, along with the inherent characteristics of high stagnation temperature and pressure. This chemically generated fluid medium is labelled "vitiated air" and is implied to mean a synthetic mixture of gases having the same percentage oxygen content and molecular weight as true air. The most significant difference between vitiated air and true air is the contaminating constituents such as water vapor and carbon dioxide emanating from the

chemical reaction of generation. These contaminating constituents are responsible for uncertainties in the results, as compared to true air, when employing vitiated air for high temperature combustion research. On the other hand, facilities employing vitiated air possesses the favorable characteristics of ability to operate at temperatures up to approximately 4500°F and pressures up to 2-3000 psi together with high flow rate capabilities.

Therefore, since vitiated air possesses all of the required primary properties of a high temperature fluid medium with the exception of known combustion characteristics, meaningful supersonic combustion development with state-of-the-art fuels could be conducted inexpensively if the effects of the contaminating constituents could be reliably predicted and correlated with results of air as experienced in free flight.

This research program is a theoretical and experimental investigation of the effects of nonequilibrium conditions--thermal and chemical--upon the performance of combustors employing supersonic flows. Specifically, the effects of free radicals, atoms and third-body species such as water vapor (a contaminating constituent in vitiated air), upon the combustion process are determined. Calculations and experiments are made regarding the effects on the combustion of heated hydrogen of the nonequilibrium species obtained using vitiated air.

Scope of Present Investigation

This research program is a continuation of the work initiated and performed by Dr. Charles A. Bryce which was submitted to Purdue University as a partial fulfillment of the requirements for the Degree of Doctor of Philosophy [3]. Dr. Bryce completed most of the analytical work on the ignition delay portion of this investigation and laid the foundation for the continuing experimental program. Therefore, much of Dr. Bryce's findings and conclusions are included in this thesis for the purpose of clarity, continuity and completeness.

In the supersonic burning of gaseous hydrogen there is a finite distance required for mixing and subsequent ignition and combustion of the two gas streams. If a combustor is operated at a high static temperature ($T > 1200°K$) the reaction times for autoignition and combustion are sufficiently fast that mixing becomes the rate controlling factor in determining the combustor length [1]. At static temperatures corresponding to low flight Mach numbers ($T < 1200°K$) reaction times for autoignition are slow and the reaction rate determines the combustor length. The present investigation is in the latter regime where reaction times are significantly longer than mixing times. Therefore, the primary emphasis is on defining the effects of vitiated air on the ignition characteristics with supersonic combustion. In a further attempt to identify the effects of vitiation on the supersonic combustion of gaseous hydrogen, an experimental investigation is described which could determine empirically these effects on the combustion efficiency.

In the experimental ignition delay and proposed combustion efficiency phases of the research investigation, a gas generator burning nitrogen tetroxide (N_2 O_4) and hydrazine (N_2 H_4) plus a gaseous nitrogen (N_2) diluent was employed to produce the vitiated air. This synthetic air has approximately 19 percent water, replacing a corresponding volume of nitrogen in real air, 26 percent oxygen and 55 percent nitrogen, by weight. The stagnation temperature (2200°K) and stagnation pressure (1000 psia) are characteristic experimental conditions in the gas generator, which, when expanded to a Mach number of 3 simulates a supersonic combustor's entrance conditions corresponding to a flight Mach number of M_∞ = 6.5 at an altitude of approximately 80,000 feet. The simulation was achieved by expanding the gas generator products (vitiated air) through a converging-diverging nozzle into a diverging (5° half angle) supersonic combustor where heated gaseous hydrogen is introduced with subsequent ignition and burning. The hydrogen was injected into the combustor through an annular type manifold surrounding the vitiated air stream, at a velocity corresponding to sonic conditions. Injection was parallel to the mainstream gases to minimize shock interactions, thereby simplifying the analysis of both the theoretical and experimental results. During the ignition delay experiments the supersonic combustor section was removed and the gas generator stagnation pressure and mass flows were reduced. These actions reduced the gas generator nozzle exit pressure to ambient pressure and permitted visible observation of the ignition phenomenon.

The purpose of the program was to investigate, both analytically and experimentally, the effects of vitiated air upon the performance of a combustor employing supersonic flows. Analysis of the inlet conditions and subsequent combustion process necessitates the use of finite-rate chemistry calculations to determine (1) the composition of the entering streams and (2) the composition variation with time during the ignition and combustion process. A comparison of the analysis and experiments with vitiated air against analytical results for real air is used to illustrate the degree of simulation that can be achieved.

Review of Pertinent Literature

The majority of the literature published concerning supersonic combustion has been classified for security purposes. The classified literature has been reviewed, but only the unclassified reports will be considered herein. Of the unclassified information available, the author was unable to find any reports which dealt specifically with the effect of vitiation on supersonic combustion. However, there are several articles concerning ignition delay in supersonic flows for hydrogen and real air. The unclassified articles considered most significant for comparison with the results of present programs are discussed in the following paragraphs.

Ferri [Ref. 1]

This is a review paper which summarizes primarily the work conducted by the General Applied Science Laboratories (GASL) on supersonic burning prior to 1964. In examining ignition delay, GASL

developed a computer program to solve the conservation equations for a reacting flow system. Species considered in this program were H, H_2, O, O_2, OH, H_2O and M, where M represents a third body. The assumption is made that the forward and backward rate constants are related by the equilibrium constant. Eight reactions, four bimolecular and four recombination (third body), were considered pertinent to hydrogen-air combustion. Starting conditions required for the analysis included the initial chemical composition of the mixture and the static temperature, pressure and velocity of the mixture. To simplify the analysis the static pressure was assumed constant throughout the combustion process, although the program was capable of handling a prescribed variation in static pressure.

Results of the analysis showed the bimolecular reactions dominate the ignition delay region and that these reactions take place at essentially constant temperature. In the ignition delay region free radicals increase to their peak concentrations. Ferri defines the ignition delay period as the time required to reach peak concentration for the hydrogen radical. During the latter portion of the induction period the free radicals begin to disappear. The heat release associated with the disappearance of the free radicals produces a rapid temperature rise to the final combustion temperature. The latter period is designated the reaction time.

From the analysis and a correlation of data from References 4 and 5, Ferri suggests the following simplified expression for calculating the ignition delay time.*

---

*The symbols are defined in the Nomenclature.

$$\tau_{ID} = \frac{8\times10^{-3}}{P} \exp[9600/T]$$

Based on the results of the numerical analysis, the following empirical expression was formed to define the reaction time.

$$\tau_R = \frac{\exp[-1.12T/1000]}{P^{1.7}}$$

One may observe from the above equation that the total reaction time is inversely proportional to temperature and pressure with temperature having the more significant effect. Thus, with high initial static temperatures ($T > 1200°K$), reaction times are almost negligible and mixing becomes the rate controlling mechanism in supersonic combustion. But in the low temperature regime ($T < 1100°K$) the overall reaction time is rate controlling and the mixing times can be neglected.

Nicholls, Adamson, and Morrison [Ref. 6]

Previous experiments by the first author showed a distinct separation between the flame and shock front for standing detonation waves with hydrogen-air mixtures. The distance between the flame front and shock front is said to represent the ignition lag length. In the referenced article the authors developed a simplified relation for the time delay based on solving the differential equations for the kinetics (assuming the hydrodynamic variables constant).

Nine reactions, five bimolecular and four third body, are considered pertinent to the delay zone and these only proceed in the

forward direction. Species considered were H, H_2, O, O_2, OH, H_2O, and M. The rate equations were written and terms were eliminated which were considered sufficiently small. This resulted in three linear equations written in terms of O, OH, and H and these equations could be solved explicitly after the introduction of a linear transformation. The solutions were expressions which described the free-radical concentrations as a function of time. Selecting as their criteria for ignition delay the inflection point in the atomic hydrogen versus time curve, the following expression was obtained for the induction period.

$$\tau_{ID} = \frac{RT}{2\,\eta_{O_2}\,PA_6} \exp\,[E_6/RT]\; \ell n \left[\frac{\eta_{O_2}^2\, k_6}{\eta_{H_2}\, k_2 + \eta_{H_2}\,\eta_{O_2}\, k_5}\right]$$

where $k_6 = PA_6/RT \exp[-E_6/RT]$ is the forward reaction rate equations or the rate controlling reaction ($O_2 + H \xrightarrow{k_6} OH + O$). The authors' conclusions regarding the ignition delay time for this system are:

1. τ decreases with increasing pressure and increasing temperature because of the exponential term.
2. τ is primarily dependent on reaction 6, a chain branching reaction usually consider controlling in the H_2 - O_2 system.
3. τ decreases slightly with initial oxygen content, the log term being small.
4. τ is weakly dependent on the initial H_2 concentration.

Brokaw [Ref. 7]

In this article, the differential equations governing the rate of change of free-radical concentration during the induction period were solved explicitly assuming constant temperature and negligible depletion of reactants. The reactions considered were as follows:

$$OH + H_2 \xrightarrow{k_1} H_2O + H$$

$$H + O_2 \xrightarrow{k_2} OH + O$$

$$O + H_2 \xrightarrow{k_3} OH + H$$

$$H + O_2 + M \xrightarrow{k_6} HO_2 + M$$

$$HO_2 + H_2 \xrightarrow{k_{11}} H_2\ O_2 + H$$

The first three are the standard bimolecular reactions considered with the H_2 - O_2 system while the latter two were felt to be significant at low temperatures. Employing only the forward reaction rates and eliminating the initiation rates, Brokaw solved, simultaneously, the equations for the growth of free radicals with time.

Three types of solutions were obtained and these tended to correspond qualitatively to the three explosion limits of the H_2 - O_2 system. The region of short ignition delays is of interest for application to supersonic combustion. Here Brokaw obtained an approximate analytical solution for the ignition delay in hydrogen-air flow systems. This solution assumes the induction period ends when the concentration of the OH radical reaches 10^{-6} moles/liter

[suggested in Reference 8]. The results of this method are shown to compare favorably with the more sophisticated numerical methods of Momtchiloff, et al. [4] and Belles and Lauver [9].

Brokaw indicated the importance of considering the HO_2 species for finding ignition delays at low temperatures. The three bimolecular reactions produce free radicals while the third-body reactions inhibit the build up of atomic hydrogen. This effect results in an increase in ignition delay period over that predicted by neglecting the latter two reactions. Of particular significance to applications with vitiated air and hydrogen combustion is the fact that water vapor is an effective third body. This is illustrated by the reaction rate expression given for k_6.

$$k_6 = 3.27\times10^{15} \left(X_{N_2} + 0.35\, X_{O_2} + 0.43\, X_{Ar} + 0.2\, X_{He} + 14.3\, X_{H_2O} + \cdots\right) T^{-1.92} \quad \frac{(\text{liters})^2}{(\text{mole})^2\ \text{sec}}$$

where X represents the mole fraction of the various third bodies. Since water vapor is an effective third body and tends to promote reaction 6, the overall effect should be to increase the ignition delay for hydrogen burning in vitiated air as compared to hydrogen burning in real air.

Momtchiloff, Taback, and Buswell [Ref. 4]

This article describes the development of a computer program for calculating ignition delays in hypersonic ramjets. The program combines the reaction rate equations with the one-dimensional gas

dynamics equations to form a series of simultaneous non-linear differential equations. Numerical methods were employed to obtain solutions for hydrogen-air flowing in an adiabatic, frictionless duct.

Starting conditions for the analysis were: (1) each stream is defined by its equilibrium composition at the local static temperature and pressure, and (2) instantaneous mixing is assumed to occur at the duct entrance. The assumption of instantaneous mixing is justified by their results which show that equivalence ratio has a very small effect on ignition delay in the range, $0.25 < \phi > 2.5$. A total of ten reactions are included in their program, six bimolecular and four third body. Species considered are O, O_2, H, H_2, OH, H_2O, N, N_2 and NO. This was the first attempt to include the effect of nitrogen reactions on the combustion process. However, their conclusion was that the nitrogen reactions are relatively unimportant at reactant temperature below 4000°R.

Several ignition criteria were examined by Momchiloff, et al., to show their effect on the theoretical delay time. The criteria considered were:

1. Time for OH radical to reach 10^{-6} moles/liter,
2. Time at the intersection of the slopes for the initial and maximum temperature rise,
3. Time for the temperature to reach 5% above the initial temperature, and
4. When the slope of the temperature versus time curve reaches 10^6 degrees R/second.

Results of this comparison showed the relative magnitudes of the delay times for different ignition criteria were within a factor of two over a wide range of initial temperatures. The first criterion for hydroxyl concentration was somewhat arbitrarily selected for defining the ignition period.

In order to substantiate their analytical technique, a comparison was made with experimental delay time data. This comparison is shown as Figure 1. The authors rationalize that the large difference shown for Das Gupta's [10] data is partly due to mixing time being included in the delay period and they also question the experimental accuracy of Nicholls' [6] data. In general, the comparison tends to substantiate the validity of the analytical procedure. As a final comment, the authors note that by a simple adjustment to the initial concentrations, one could predict the effect of simulated air on ignition delay.

Rhodes [Ref. 13]

This is the first author to suggest that nonequilibrium, free-radical concentration may have a significant effect on ignition delay with supersonic combustion. Examining the four bimolecular reactions which govern the rate of growth of free radicals, the author shows the ignition delay was primarily controlled by the reaction rate for:

$$O_2 + H \rightarrow OH + O$$

After several simplifications, an expression was derived for the initial rate of reaction in terms of the rate controlling reaction and

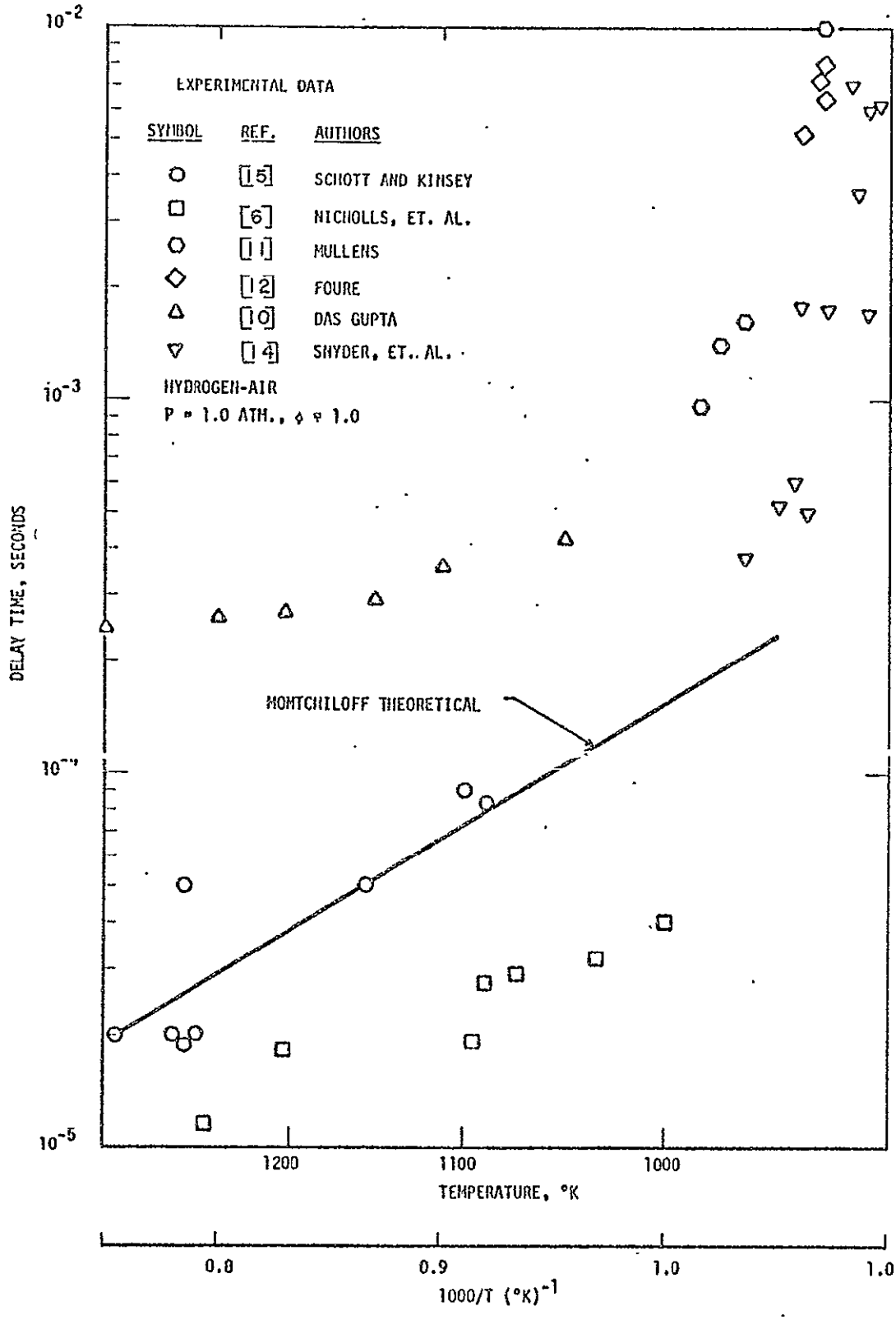

FIGURE 1 MOMTCHILOFF'S ANALYSIS COMPARED WITH EXPERIMENTAL RESULTS

the free-radical concentration. Rhodes then correlates the delay time (from the complete kinetics program of GASL) against the initial rate of reaction expression and found it conveniently plotted as a straight line on log-log coordinates. From this plot, the following expression was obtained for the ignition delay in terms of the initial free-radical concentration:

$$\tau_{ID} = \frac{1.27\times10^{-3}}{p^{4/3}} \left[\frac{T}{X_{O_2}{}_0 \, X_{FR_0}}\right]^{1/3} \exp[3020/T]$$

where

$$\left[X_{FR}\right]_0 = \left[X_H\right]_0 + \left[X_{OH}\right]_0 + 2\left[X_O\right]_0$$

From the above expression it may be noted that an order of magnitude increase in free-radical content for the incoming stream will reduce the delay time by a factor of two. There are two conditions in this equation which are somewhat inconsistent with other ignition lag correlations: one is the pressure dependence to the four-thirds power and the other is the rather significant effect of initial oxygen content. Since the author claims that this method will only predict times within a factor of two, these anomalies are not sufficient to invalidate the overall correlation.

The most significant conclusion that can be drawn from this article is that nonequilibrium, free-radical species can affect induction time in supersonic combustion. In ground test facilities heated air is expanded from a high-temperature to a supersonic test section where hydrogen or some other fuel is injected and combustion

occurs. During the expansion process some recombination freezing will occur and the excess free radicals in the incoming air will cause ignition to occur earlier than would occur in the engine in flight. The same effect will be seen in ground testing with vitiated or synthetic air as the primary fluid. However, a free-flight system may incur an increased ignition delay because the free-radical concentration produced by the inlet compression may be less than the corresponding equilibrium values.

Snyder, Robertson, Zanders, and Skinner [Ref. 14]

This report contains the results of an extensive experimental investigation of ignition delay for hydrogen-air mixtures. The work was conducted using shock tube techniques. Induction times were found by taking the difference between the time to peak pressure for the reflected shock and the time of sharp rise in ultraviolet emission at a specific axial location. Experimental conditions were varied over the following ranges: equivalence ratio ($0.5 \leq \phi \leq 1.0$), test section pressure ($1.5 \leq P \leq 130$ psia), and temperature ($800 < T < 1100°K$). The effect of several contaminants on the induction characteristic of hydrogen-air was also studied. Additives investigated experimentally included water vapor, nitric oxide, nitrogen dioxide and ammonia.

Experimental results for the undiluted mixtures were utilized as an input to a nonlinear regression program and the following equation is presented as a best fit to the data.

$$\tau_{ID} = \frac{7.92\times10^{5}}{(P)^{0.4}\phi} \exp[15.950/T]$$

Limits for application of this expression are fuel concentrations less than stoichiometric and initial static temperatures between 800 and 1100°K.

Some interesting results were obtained from the experiments investigating the effect of contaminants on the ignition reaction. Water vapor, nitric oxide, and nitrogen dioxide were found to reduce the ignition delay, while ammonia had essentially no effect. Water vapor was added in concentrations of 10, 15, and 20 mole percent in experiments at equivalence ratios of 0.5 and 1.0. At the lower equivalence ratio, the induction time was reduced by almost an order of magnitude. A plot of the experimental data illustrating the reduction in delay time with 15 mole percent water vapor is shown in Figure 2, which presents delay time as a function of temperature. A similar effect was shown at higher temperature ($\sim$ 1000°K) for the equivalence ratio of 1.0 experiments but a slight inhibiting effect was found in the low temperature region.

Results from the nitric oxide experiments (also shown in Figure 2) were much more dramatic. The addition of only 0.5 mole percent NO resulted in a reduction in induction time of approximately two orders of magnitude. Nitrogen dioxide exhibited essentially the same magnitude reduction. Several different concentrations were examined in the nitric oxide experiments ranging from 0.1 to 8.0 mole percent. Significant reductions (at least one order of magnitude) were found

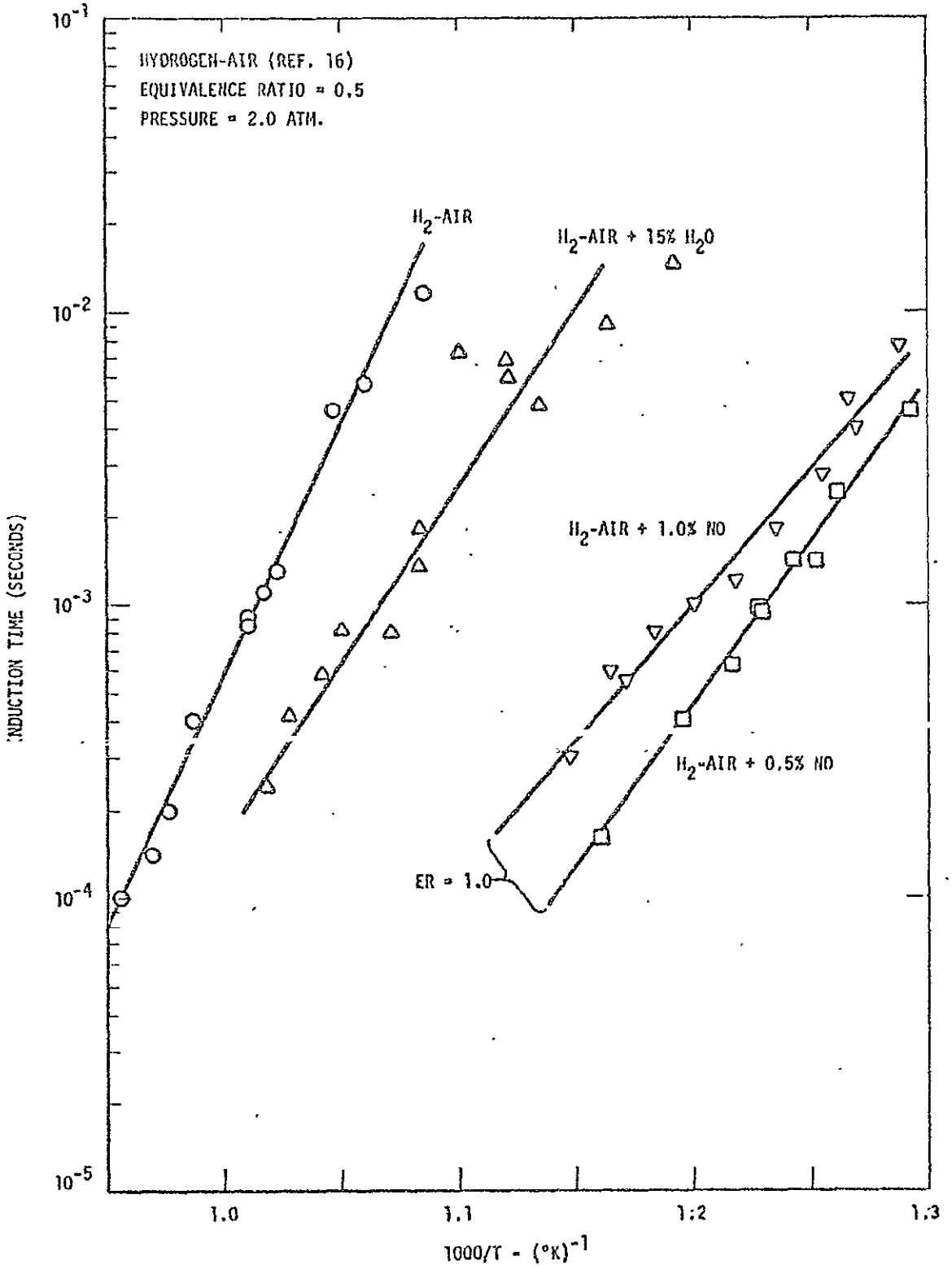

FIGURE 2 EFFECT OF CONTAMINANTS ON INDUCTION TIMES

in each case with the peak reduction occurring in the neighborhood of 0.5 mole percent. This indicates that nitric oxide catalyzes the hydrogen-air reaction. Ground test facilities using heated air or synthetic air can have an appreciable quantity of NO entering the supersonic test section. Therefore, induction times for ground testing may be considerably shorter than that experienced under the corresponding free-flight conditions.

ANALYTICAL PROGRAM

Most of the theoretical and experimental work concerning the combustion of hydrogen and air is based on the assumption that complete thermal and chemical equilibrium exists at the combustor inlet. In the shock tube work of Schott and Kinsey [15] and the standing detonation wave work of Nicholls [5], the combined streams are assumed in equilibrium immediately downstream of the shock front. With this type of experiment, the assumption of equilibrium starting conditions may be justified on the basis that the agreement between analysis and experiments is reasonably good.

For certain cases of shock-induced combustion, Rubins [16] has shown the possible existence of deviations from thermal equilibrium. In these cases, the different modes of energy storage are not in equilibrium, resulting in a translational temperature overshoot. By accounting for the overshoot in the reaction rate expression, they are still able to predict ignition delays for shock-induced combustion of hydrogen-air using the assumption of chemical equilibrium as a starting condition for finite-rate calculation. Therefore, most ignition delay data for hydrogen-air can be described theoretically by assuming (1) that the premixed gases are in chemical equilibrium just prior to ignition or (2) that each stream exists as its corresponding equilibrium state prior to mixing. The latter assumption applies to

combustion without shocks where the two gases are initially mixed at the combustor entrance.

An Ideal Supersonic Combustion (ISSC) program was employed by the author to determine the operating conditions of the gas generator and to size the gas generator, test section, and combustor exit. This program combines the one-dimensional gas dynamic equations with the equilibrium thermochemical relations to:

1. Determine the products of combustion in the gas generator,
2. Isentropically expand the products (shifting equilibrium) to the test section entrance,
3. Calculate the properties of hydrogen at the injection station, and
4. Calculate the results of mixing and burning the two streams at constant pressure.

A Finite Rate Reacting Gas (FRRG) program was used by the author to determine the nonequilibrium free-radical concentrations in the vitiated air as it enters the combustor. This program integrates the one-dimensional gas dynamic relations for a chemically reacting flow system throughout the expansion process. Reaction rates used with the FRRG program were identical to those used in the ignition lag program (discussed below) for situations where the same reactions were found to be applicable.

Induction times were determined by a Simplified Ignition Lag (SIL) program. This program solves the species reaction rate relations, assuming constant pressure and temperature, using a matrix technique. The validity of this program is established by a comparison of the

program results against existing experimental induction data for heated air. This comparison requires that the SIL program be run with initial species concentration data from the ISSC program because of the nature of the experimental results.

There is an abundance of reaction rate data for the hydrogen-oxygen system. A fairly up-to-date source of reaction rate information is provided in a study conducted by TRW [Ref. 17]. This study attempts to identify the significant reactions which affect the kinetic performance of typical liquid propellant systems. After identification of important reactions, a summary was made of existing rate data and the degree of uncertainty was established. In general, the bimolecular reaction rates seemed reasonable, however, the third-body reaction rates do not include an activation energy term. This omission would not significantly affect rocket performance predictions based on kinetics calculations; however, it could make some difference in the species concentration determinations when attempting to establish the free-radical content. After initially beginning the analysis utilizing the TRW reaction rates, it was decided to change to a more consistent set of rate expressions. The rates selected for the final analysis were supplied by E. A. Lezberg of NASA Lewis Research Center. The general agreement of these rates with those employed by other authors [Refs. 1, 4, and 17] is considered acceptable, since uncertainties of at least one order of magnitude are quite common in reaction rate data.

Description of Computer Programs

The computer programs used in the analytical effort are discussed in the following paragraphs. The discussion includes:

1. Basic assumptions,
2. Program description,
3. Input requirements,
4. Output results, and
5. Limitations.

Ideal Supersonic Combustion (ISSC) Program

Ideal performance calculations are useful, in many instances, for determining the maximum theoretical performance that can be derived for different propellant combinations. This program performs the basic thermochemical calculations necessary to design the gas generator assembly as well as the supersonic combustion test section. When making thermochemical calculations assuming shifting equilibrium conditions the following assumptions are made:

1. Chemical equilibrium is maintained both in the combustor and during the expansion process.
2. The combustion products behave as an ideal gas mixture.
3. The expansion processes are adiabatic and reversible (isentropic).
4. The reactants burn to completion at a specified pressure.
5. Supersonic combustion takes place adiabatically and at constant pressure.

The program combines the one-dimensional conservation equations for an ideal gas with the equilibrium thermochemical relations to compute the combustion and expansion processes. Specifically, the program first computes conditions in the primary combustor and then expands these gases (shifting equilibrium) to various area ratios which may be chosen as inputs to the program. The secondary stream is heated hydrogen with a temperature which corresponds to the input enthalpy of the reactants. Equilibrium dissociation is maintained as this stream is expanded to a pressure corresponding to that at which mixing takes place. It is assumed the streams are mixed instantaneously and burned at constant pressure. The latter step represents the supersonic combustion process. Provision is made for additional isentropic expansions and for calculation of the equilibrium stagnation pressure Mach number and temperature of the combined stream.

In the calculations for the production of vitiated air for these experiments, the required flow rates of nitrogen tetroxide, hydrazine, and nitrogen are a function of the desired chamber temperature. The flows are proportioned such that the vitiated air has the same weight percent oxygen as real air. Calculations of the flow rate requirements for setting the operational conditions of experimental hardware were made utilizing the equilibrium thermochemical program. Typical results are shown in Figure 3 which presents gas generator operating conditions as a function of chamber temperature. The final selection of a design operating condition is discussed in the section titled "Experimental Program."

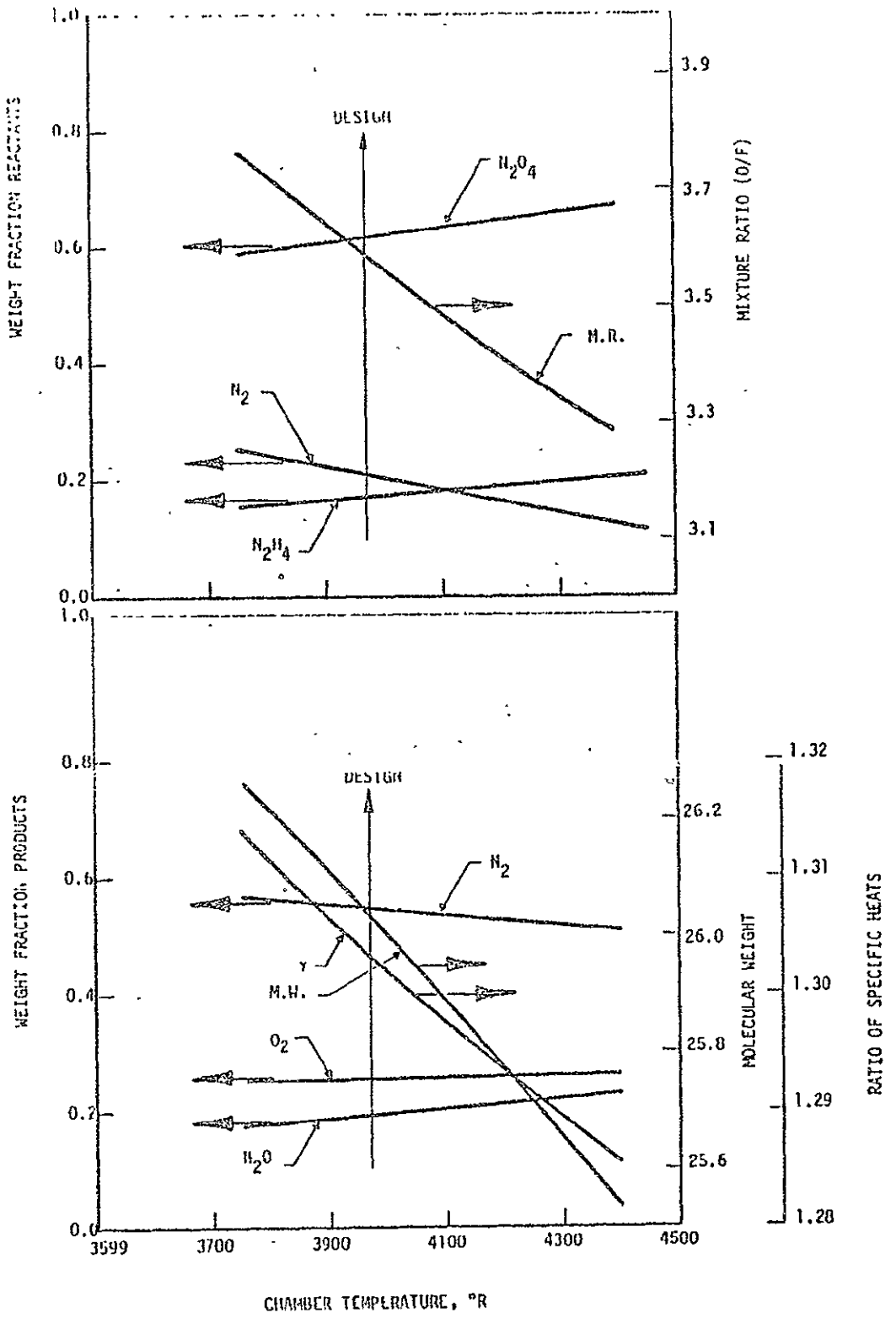

FIGURE 3 GAS GENERATOR OPERATING CONDITIONS

The ISSC program can also be operated with the characteristics of heated air serving as input to the program as the primary gas stream. It is then possible to compare the ideal supersonic combustion performance of vitiated air and heated air. The equilibrium species concentrations for the test section entrance as determined by this program are used as input to the ignition lag program. It is thus possible to determine ignition lag for equilibrium inlet conditions for comparison with the nonequilibrium conditions generated by the following computer program. Data input procedures and operating instructions are expanded in Reference 18.

Finite Rate Reacting Gas (FRRG) Program

This computer program was developed by TRW Systems for NASA (MSC) under Contract NAS-4358. Inputs to the program included reaction rate information, nozzle geometry, propellant data (i.e., moles of fuel and oxidizer plus their heats of formation). The program solves the equations for inviscid, one-dimensional flow of a reacting gas mixture. The following assumptions are made when deriving the conservation equations:

1. The expansion process is adiabatic.
2. All species behave as ideal gases.
3. Viscous effects are neglected.
4. All internal modes of energy storage are in equilibrium.

The reaction rate parameters employed in the FRRG program are listed in Table 1. Only the constants for the forward rate expression are used as input to the program. The reverse reaction rates are

TABLE 1

REACTION RATES FOR FRRG PROGRAM

J	Reaction	A(J) (gr. cm.)	B(J) (kcal/mole)	N(J)
1	$H_2O + M \rightleftharpoons OH + H + M$	1.9×10^{18}	119.9	-1.278
2	$H_2 + M \rightleftharpoons H + H + M$	3.2×10^{16}	102.9	-1.5
3	$N_2 + M \rightleftharpoons N + N + M$	1.0×10^{18}	--	-1.0
4	$NO + M \rightleftharpoons N + O + M$	6.0×10^{16}	--	-0.5
5	$OH + M \rightleftharpoons O + H + M$	2.0×10^{18}	--	-1.0
6	$O_2 + M \rightleftharpoons O + O + M$	3.59×10^{17}	118.0	-2.5
7	$H_2O + H \rightleftharpoons H_2 + OH$	1.43×10^{14}	20.94	--
8	$H_2O + O \rightleftharpoons OH + OH$	2.9×10^{14}	18.7	--
9	$H_2 + O \rightleftharpoons OH + H$	4.0×10^{13}	10.2	--
10	$H_2 + O_2 \rightleftharpoons OH + OH$	2.5×10^{12}	38.9	--
11	$N_2 + O \rightleftharpoons NO + N$	1.5×10^{13}	--	--
12	$N_2 + O_2 \rightleftharpoons NO + NO$	1.0×10^{13}	79.5	-2.5
13	$NO + H \rightleftharpoons OH + N$	5.3×10^{11}	5.62	0.5
14	$NO + O \rightleftharpoons O_2 + N$	1.8×10^{8}	6.0	1.5
15	$O_2 + H \rightleftharpoons OH + O$	1.0×10^{14}	16.0	--

where

$$k_f(J) = A(J)\ T^{N(J)}\ \exp\left[-B(J)/RT\right]$$

and

$$k_b(J) = k_f(J)/k_c(J)$$

computed internally from the forward rate and equilibrium constant (based on molar concentrations) by the following relation:

$$k_b(j) = k_f(j)/k_c(j)$$

There is some question as to the applications of this relation to three-body reactions, but it is known to be a good assumption for bimolecular reactions near equilibrium.

Numerical integration of the governing equations is accomplished using an implicit integration scheme. The advantage of this method is that it permits stable integration for step sizes of the same order of magnitude as the physical dimensions (nozzle throat size) for any flow condition (either near equilibrium or frozen). A similar program was developed earlier by Zupink, et al. [19] of United Aircraft. However, this program employs explicit integration methods which are unstable unless the step size is or order of the characteristic relaxation distance. For near equilibrium flows the relaxation distance becomes very small and explicit integration methods require excessive computer time. In addition a first guess as to the initial step size to be utilized in the combustion chamber is required as input to the United Aircraft program. Because of these limitations it was decided to conduct all further analysis of nonequilibrium flows using the TRW program.

The FRRG program calculates the nonequilibrium species concentrations at specified area ratios in the nozzle. Since the one-dimensional flow equations are used in this program, the concentrations are assumed uniform at each axial location. A check was made as to

the validity of the one-dimensional flow assumptions for the nozzle configuration employed in the experimental program. Results from a two-dimensional, axisymmetric flow program (also developed by TRW Systems), which employs the method of characteristics for chemically reacting gases, were used for this comparison. The species concentrations at the nozzle exit were essentially identical for the two programs. Since the one-dimensional program uses about one-third less computer time than the two-dimensional program, the additional sophistication of the latter program was not deemed necessary.

Results from the FRRG program are shown in Figure 4 which presents species concentrations as a function of temperature. As can be seen from the figure there is a significant difference in free-radical concentrations at the nozzle exit when finite rate chemistry is considered. For equilibrium flows the free-radical concentrations at the nozzle exit are quite small. However, the FRRG program predicts these concentrations are from two to ten orders of magnitude greater than their corresponding equilibrium values. These differences can be explained as follows. Free-radical recombination requires a third body to absorb the heat released by the reaction. The probability for three body collisions is quite small, so that termolecular reaction times become greater than the gas residence times. This effect is termed "recombination freezing," a subject which has received considerable attention in the past several years [Ref. 20]. In general, the concentration changes within regions of rapid acceleration of the gas stream are governed by the bimolecular reaction rates which are several orders of magnitude faster than the termolecular rates.

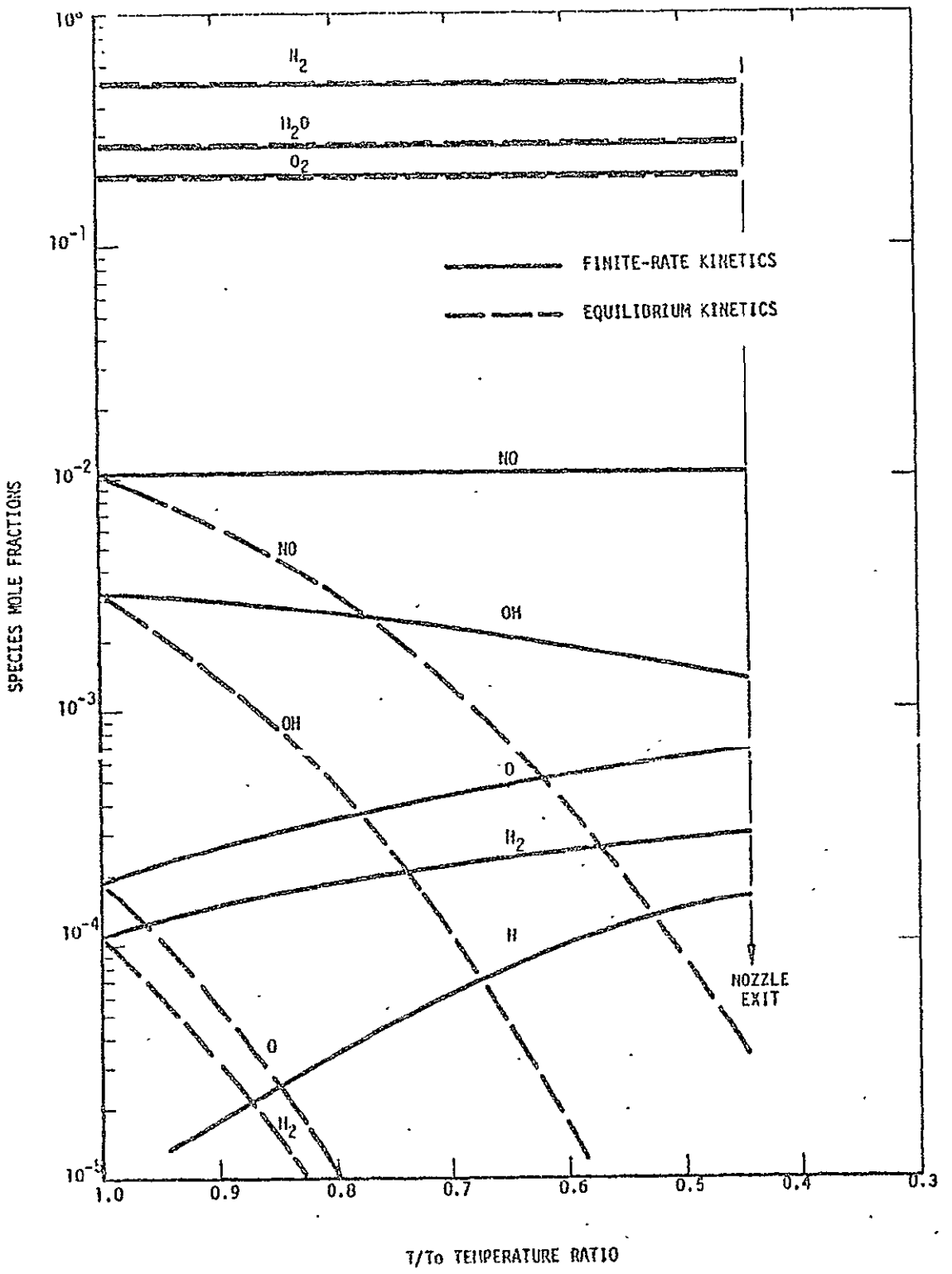

FIGURE 4 EQUILIBRIUM AND FINITE-RATE COMPOSITIONS FOR G.G. PRODUCTS

Simplified Ignition Lag (SIL) Program

The complete combustion process is assumed to occur in two steps as illustrated in Figure 5, which describes schematically the ignition model. During the induction period free radicals are exponentially produced by: (1) the initial chain initiating steps and (2) the chain-branching mechanisms of the bimolecular reactions. Throughout this period the temperature remains essentially constant because certain reactions are slightly exothermic and others endothermic. Towards the end of the induction period the free radicals begin to recombine exothermically and the temperature starts to rise exponentially. The period of rapid temperature increase is termed the reaction time. In the temperature regime of interest in this investigation, the reaction times are much shorter than the induction period. Therefore, the analytical effort is directed toward evaluating the effect of vitiation on the induction period.

The ignition model employed assumes the temperature is constant throughout the induction period. This simplification along with the assumption of constant pressure makes it possible to neglect the hydrodynamic equations and to solve the differential equations describing the reaction kinetics. The approach is to write the equations governing the rate of growth of free radicals and to solve these for species concentrations as a function of time using standard matrix techniques. The computer program is a simplification of a more general program developed by GASL. A source deck for the SIL program was supplied by E. A. Lezberg of NASA Lewis Research Center. The Lewis modifications to the program included the constant temperature

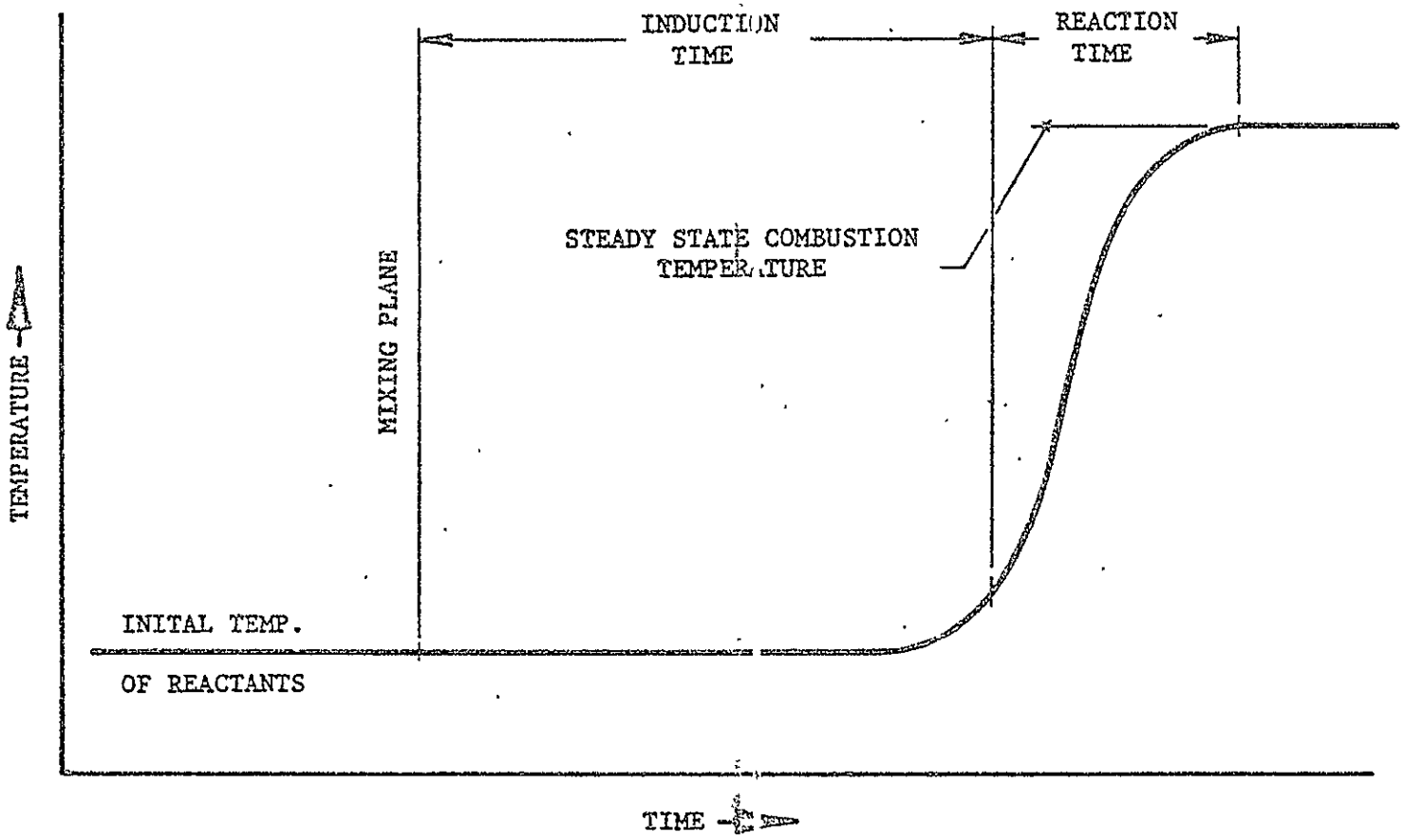

FIGURE 5 SCHEMATIC OF THE IGNITION MODEL

simplification and the inclusion of several additional hydrogen and oxygen reactions which may be important to the ignition kinetics at temperatures below 1000°K. A list of reaction rate expressions and rate constants employed in the program is presented in Table 2.

A total of nine species are considered by the program. These are H, O, H_2O, H_2, O_2, OH, N_2, HO_2, and H_2O_2. The latter two species enter into a chain-breaking step which tends to lengthen the induction period. Inclusion of these species in the induction analysis should result in a more favorable comparison of experimental and theoretical ignition delays at low temperatures.

Fifteen reactions are included in the SIL program. One of the advantages of this program is that a large number of reactions can be considered without significantly increasing the computing time. One limitation of this program is that it fails to include any NO or NO_2 reactions. The analysis of Momtchiloff indicated these reactions were comparatively unimportant below 4000°R. However, the experimental results of Skinner indicated that both NO and NO_2 have a catalytic effect on the induction process. This effect tends to reduce delay time by an order of magnitude. Since the mechanism which accelerates the reaction is not understood at this time, it is not possible to include any NO or NO_2 reactions in a manner that would be meaningful.

Results from the SIL program are the species concentrations as a function of time. Ignition lag is determined from the semilog plot of the hydroxyl radical concentration against time. The induction period is characterized by the region of essentially constant exponential growth of free-radical concentrations. The end of the induction

TABLE 2

REACTION RATES FOR SIL PROGRAM

J	Reaction	A(J) (gr. cm.)	B(J) (kcal/mole)	N(J)
1	$H + O_2 \rightleftharpoons OH + O$	1.0×10^{14}	16.0	--
-1		4.16×10^{12}		0.41
2	$O + H_2 \rightleftharpoons H + OH$	4.0×10^{13}	10.2	--
-2		1.85×10^{13}	8.39	--
3	$H_2 + OH \rightleftharpoons H + H_2O$	2.3×10^{13}	5.2	--
-3		1.43×10^{14}	20.94	--
4	$O + H_2O \rightleftharpoons OH + OH$	2.9×10^{14}	18.7	--
-4		2.03×10^{13}	1.13	0.26
5	$H_2 + M \rightleftharpoons 2H + M$	3.16×10^{16}	102.9	-1.5
-5		9.18×10^{15}	-0.97	-1.5
6	$H_2O + M \rightleftharpoons OH + H + M$	1.86×10^{18}	119.9	-1.278
-6		7.5×10^{16}	--	-1.0
7	$O_2 + M \rightleftharpoons 2O + M$	3.59×10^{17}	118.0	-2.5
-7		8.9×10^{15}	-1.57	-2.074
8	$H + O_2 + M \rightleftharpoons HO_2 + M$	4.3×10^{15}	-1.28	--
-8		8.9×10^{15}	46.12	-0.28
9	$H_2 + HO_2 \rightleftharpoons H_2O_2 + H$	2.0×10^{13}	23.72	--
-9		1.0×10^{14}	9.82	--
10	$H_2 + O_2 \rightleftharpoons OH + OH$	2.5×10^{12}	38.95	--
-10		4.77×10^{10}	19.87	--
11	$H_2O_2 + M \rightleftharpoons 2OH + M$	1.17×10^{17}	45.57	--
-11		8.4×10^{14}	-5.31	--
12	$H + HO_2 \rightleftharpoons OH + OH$	7.0×10^{13}	--	--
-12		4.37×10^{12}	39.2	--
13	$HO_2 + HO_2 \rightleftharpoons H_2O_2 + O_2$	1.8×10^{12}	--	--
-13		8.1×10^{12}	42.19	--
14	$H + H_2O_2 \rightleftharpoons H_2O + OH$	3.18×10^{14}	9.0	--
-14		5.6×10^{13}	78.0	--
15	$OH + H_2O_2 \rightleftharpoons H_2O + HO_2$	1.0×10^{13}	0.897	--
-15		2.8×10^{13}	32.76	--

where $k(J) = A(J)\ T^{N(J)}\ \exp[-B(J)/RT]$

period is considered to be the time when the hydroxyl concentration deviates from constant exponent growth. This definition for the end of induction is recommended by Hersch [21]. Other methods for defining the end of the induction period were considered in this study. The following comparison illustrates the variation in ignition delay periods for different methods of defining the end of induction.

Definition of End of Induction	Reference	Delay Time
1. End of exponential growth of (OH)	21	39 μ sec
2. OH concentration of 10^{-9} gram-moles/cm^3	15	30 μ sec
3. Hydrogen concentration = $1/2 \cdot (H_2)_0$	13	47 μ sec
4. End of exponential growth of (H)	6	40 μ sec

This comparison for heated air and hydrogen at 1200°K and one atmosphere pressure is shown in Figure 6, which presents the OH and H radical concentrations plus the hydrogen weight fraction as a function of time. Starting conditions assume each stream is in chemical equilibrium prior to mixing and an equivalence ratio of one for the combined streams. The comparative times indicate the method of defining the end of induction has some effect on the calculated delay time. However, Hersch [21] is able to show that method 2 is only a reasonable approximation of the delay period for temperatures greater than 1500°K. At the same time, method 3 is simply an approximation suggested by Rhodes [13]. Methods 1 and 4 yield essentially identical delay time so that both methods appear applicable. Hersch was able to compare method 1 with a detailed analytical model which included the temperature variations during the postinduction period. Conclusions

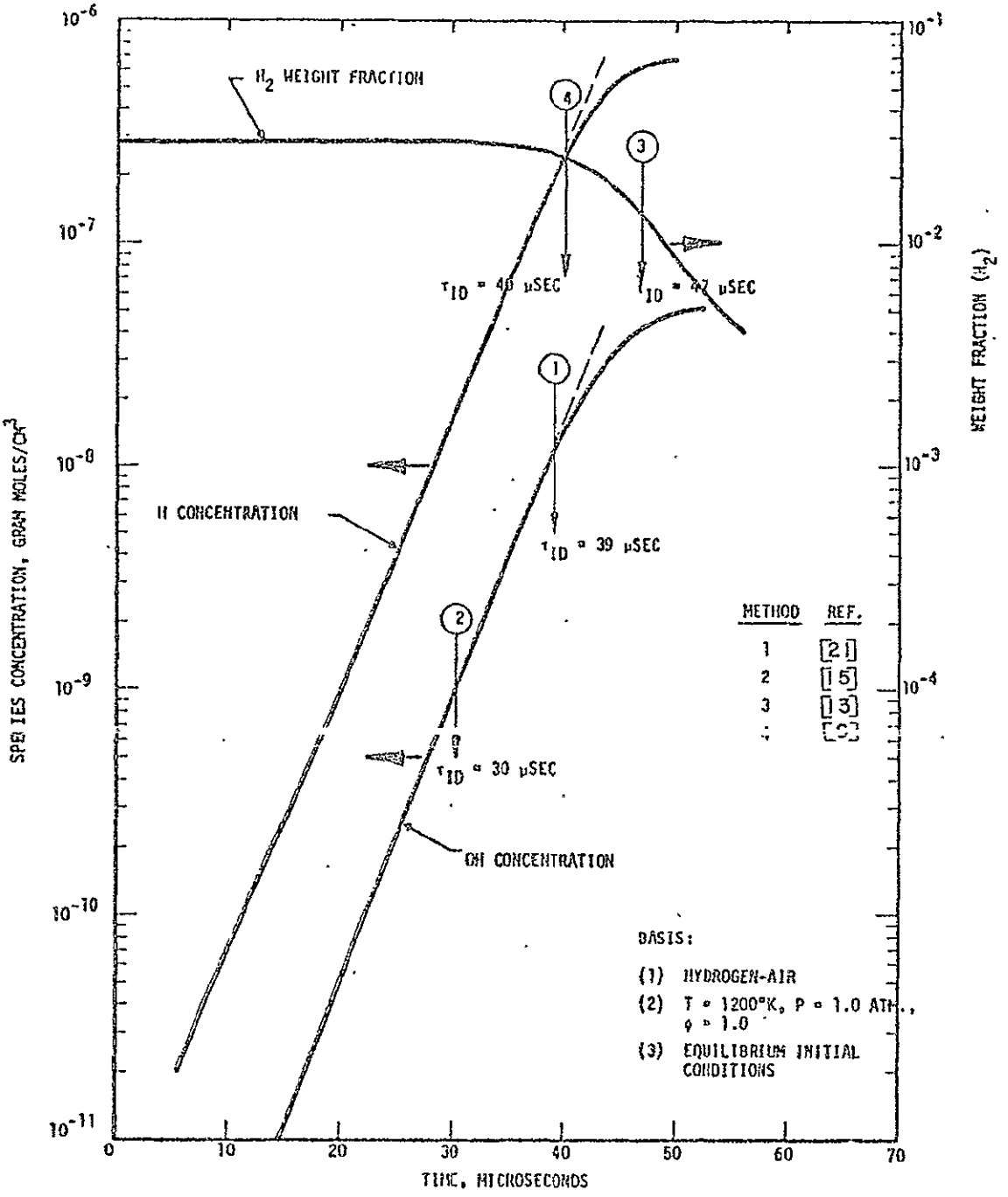

FIGURE 6 DEFINITIONS OF THE INDUCTION PERIOD

from this comparison were that method 1 was a reasonably good approximation to the induction limit over a wide range of initial temperatures ($1200 \leq T_i \leq 2500°K$). Therefore, this method was finally selected as most appropriate for application to the SIL program results.

When examining the results from the Lewis version of the SIL program, one modification was incorporated into the program. This modification is a revision of the method of defining the effective concentration of third-body species that enter into the three-body reaction rates. Brokaw [7] suggests that the third-body expression in reaction 8 in Table 2 is a strong function of water vapor content of the reacting species. He showed the relative third-body efficiencies are given by the following expression:

$$M = X_{H_2} + 0.35\, X_{O_2} + 0.43\, X_{N_2} + 0.2\, X_{A_r} + 14.3\, X_{H_2O}$$

where X is the mole fraction of each third body. In the Lewis version of the SIL program, the relative efficiency of water vapor was reduced from 14.3 to 6.0. When the Lewis version of the SIL program was utilized to calculate the effect of 10 percent water vapor content in the air on ignition delays at 1000°K an anomalous result was obtained: the ignition delay for hydrogen and air plus 10 percent water was six times longer than the corresponding dry air case. The magnitude of this difference is shown in Figure 7 which again presents OH concentration as a function of time. Also shown in this figure is the effect of further reducing the third-body contribution of water vapor. The third-body expression used in this comparison is as follows:

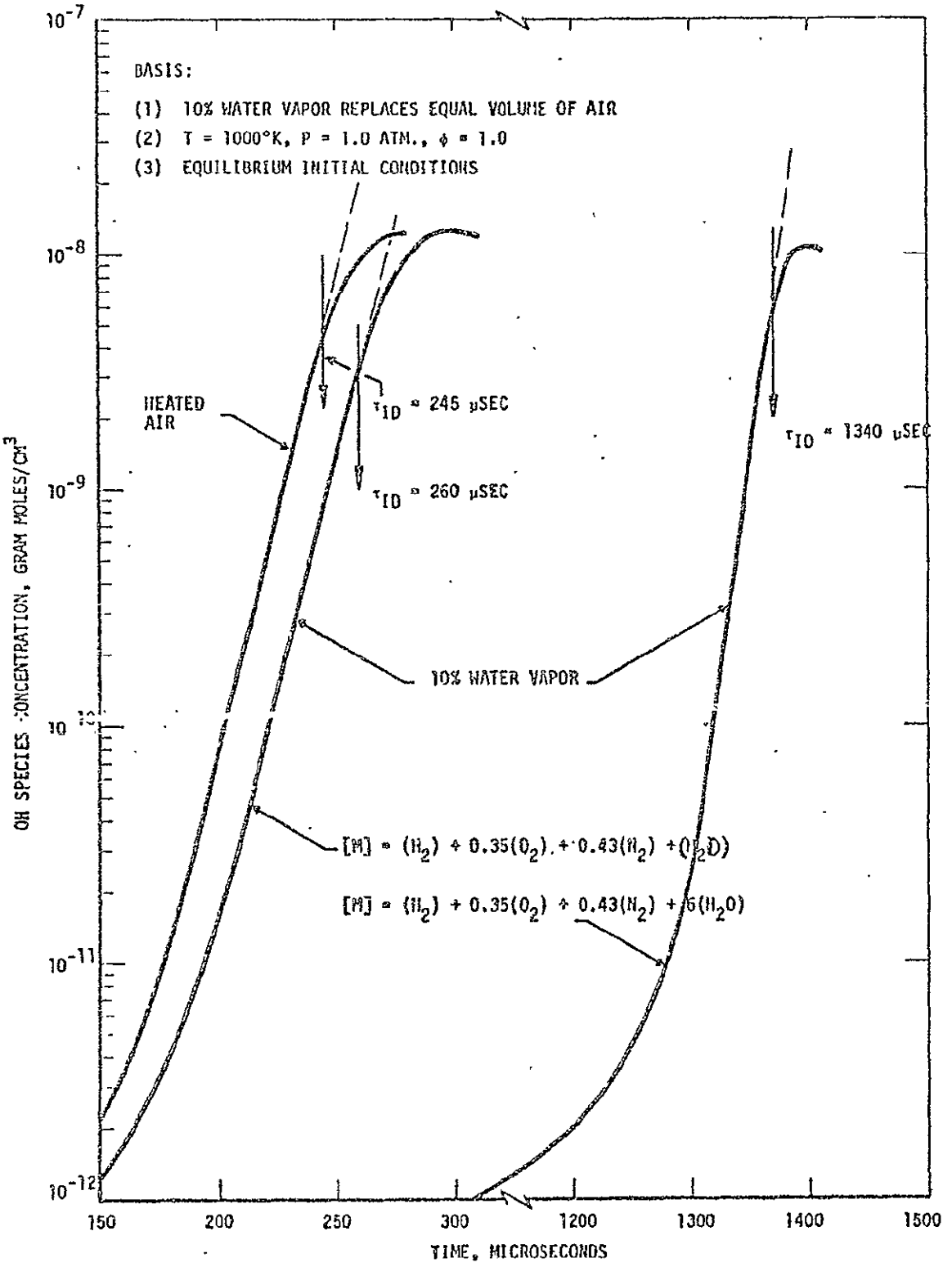

FIGURE 7 THIRD BODY EFFECTS ON DELAY TIMES

$$M = X_{H_2} + 0.35\ X_{O_2} + 0.43\ X_{N_2} + X_{A_r} + X_{H_2O}$$

When this expression for the third-body terms was employed in the SIL program the difference in delay times of hydrogen-air and hydrogen-air plus 10 percent water vapor is reduced to 15 micro-seconds.

The results in Figure 7 show that the third-body term may have a significant effect on delay times. This effect is quite pronounced under the following circumstances:

1. When relatively large concentrations of water vapor are present in the initial reactants;
2. When the initial temperature of reactants is low ($T < 1100°K$).

Further examination of the effect of the third-body term revealed that it had absolutely no effect when applied to dry air over a temperature range of 950 to 1200°K. One reason why this term has no effect for dry air is that the third-body term acts to reduce the build up of free radicals during the early part of the induction period. Water vapor does not appear in significant concentrations until the latter part of the induction period where the bimolecular reactions predominate the induction process. Thus the overall influence of the contribution of the effective water vapor concentration in the third-body expression is insignificant when applied to an initial mixture of hydrogen and uncontaminated air.

When this same type of comparison was made at 1200°K, the following results were obtained:

	Initial Composition	Third Body	Delay Time
1.	Hydrogen/Heated Air	M_1 or M_2	39 μ sec
2.	Hydrogen/Air + 10% H_2O	M_1	36 μ sec
3.	Hydrogen/Air + 10% H_2O	M_2	34 μ sec

where

$$M_1 = X_{H_2} + 0.35\ X_{O_2} + 0.43\ X_{N_2} + 6\ X_{H_2O}$$

$$M_2 = X_{H_2} + 0.35\ X_{O_2} + 0.43\ X_{N_2} + X_{H_2O}$$

These results indicate the effective water vapor concentration in the third-body term yields an almost negligible difference in delay times at temperatures of 1200°K or higher.

Experimental data of Snyder, et al. [14] showed that water vapor in the initial air resulted in a slight reduction in delay times over the corresponding case for hydrogen and uncontaminated air. When the SIL program was modified to employ M_2 as the third-body term, the agreement with Snyder's experimental results, while not entirely satisfactory, is considerably better than that shown by the Lewis version of the program. Obviously better agreement between theoretical and experimental induction times could be obtained by further reducing the effective concentration of water vapor in the third-body term. However, there is no theoretical and very little experimental justification for making the effective concentration less than unity. Consequently the third-body term defined by M_2 was employed for all subsequent SIL programs.

Typical results from the SIL program are shown in Figures 8 through 13 which present OH radical concentration as a function of

time. The results presented in these figures are discussed in the next section which is an extensive verification of the simplified induction model employed in the computer analysis.

Verification of the Simplified Ignition Lag Program

Before applying the SIL program to the analysis of ignition lag with vitiated air, it is first necessary to establish the validity of the program results. Since most of the theoretical and analytical work on ignition lag is concerned with real air and hydrogen, the verification is made for these gases. Initially, a base case was selected for making this comparison. Temperature for the base case is 1200°K, pressure is one atmosphere, and equivalence ratio is one. As a starting condition, both streams are assumed to be in chemical equilibrium at the assigned temperature and pressure prior to mixing. The combined stream is no longer in chemical equilibrium.

Results from the SIL program for the base case species are shown in Figure 8, which presents the OH radical concentration as a function of time. The induction period is defined by the end of the constant exponential growth for the OH radical. An induction time of 39 microseconds is obtained for the base case conditions. Several approximate relations for determining ignition delays are discussed in the review of literature. A summary of the equations presented by the different authors is given in Table 3 along with the range of temperatures over which they apply. These approximate relations are used to calculate the ignition lag for the base case conditions and the delay times are also shown in Figure 8. (Note that the empirical expression of Skinner does not apply above 1100°K.) The relation of Ferri predicts

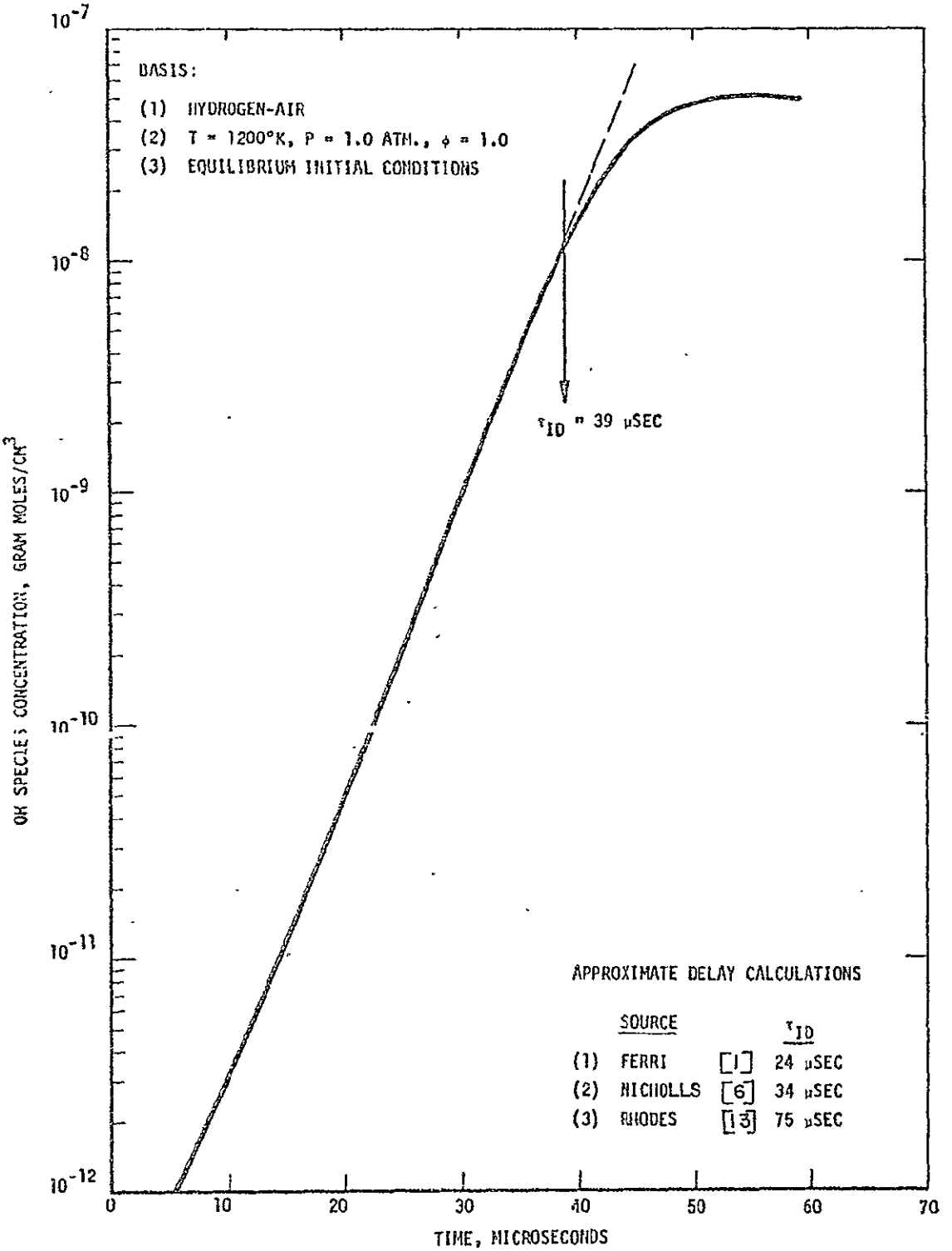

FIGURE 8 IGNITION DELAY FOR BASE CASE SPECIES

TABLE 3

APPROXIMATE LAG THEORIES

(1) Ferri:

$$\tau_{ID} = \frac{8\times10^{-3}}{P} \exp[9600/T]$$

(2) Nicholls: $(1100° \leq T \leq 2000°K)$

$$\tau_{ID} = \frac{4.1\times10^{-7}\ T}{\eta_{O_2}\ P} \exp[8.05/T]\ \ell n \left[\frac{\eta_{O_2}^2\ k_6}{\eta_{H_2}\ k_2 + \eta_{O_2}\ \eta_{H_2}\ k_5}\right]$$

(3) Skinner: $(800° \leq T \leq 1000°K)$

$$\tau_{ID} = \frac{7.92\times10^{-3}}{P^{\eta_{O_2}}\ \phi} \exp[15.950/T]$$

(4) Rhodes: $(800° \leq T \leq 1800°K)$

$$\tau_{ID} = \frac{1.27\times10^{-3}}{P^{4/3}} \left[\frac{T}{[X_{O_2}]_0\ [X_{FR}]_0}\right]^{1/3} \exp[3020/T]$$

$$[X_{FR}]_0 = [X_H]_0 + [X_{OH}]_0 + 2\ [X_O]_0$$

much shorter delay times than the SIL program, while Rhodes predicts a considerably longer induction period. There is a relatively close agreement between Nicholls' result and that of the SIL program.

The effect of peripheral reactions and different reaction rate data are illustrated in Figure 9, which presents OH concentration as a function of time. Here the same starting conditions are applied to each case, but only the first nine reactions shown in Table 1 are considered. The latter six reactions in this table were expected to show minor effect on the induction time for the base case conditions. The difference between nine and fifteen reactions (using identical rate data for corresponding reactions) only amounts to eight micro-seconds variation in delay time. However, this represents a 20 percent variation in induction period so that the latter six reactions are more important than originally anticipated. When the reaction rates of Ferri were used in the nine reaction system, a considerable decrease in delay time is evidenced (47 μ sec → 28 μ sec). In general, the forward reaction rates employed by Ferri are faster than those shown in Table 2, so that a reduction in delay time is not surprising. However, the magnitude of the difference shown here is hardly significant in terms of induction lengths for supersonic combustion. Even with gas velocities of 10,000 feet per second, the difference in induction distances is still less than 3 inches.

The effect of temperature on induction times is shown in Figure 10, in which hydroyxl radical concentrations as a function of time are shown at three separate temperature levels. Starting conditions for each case assume the heated air and hydrogen streams

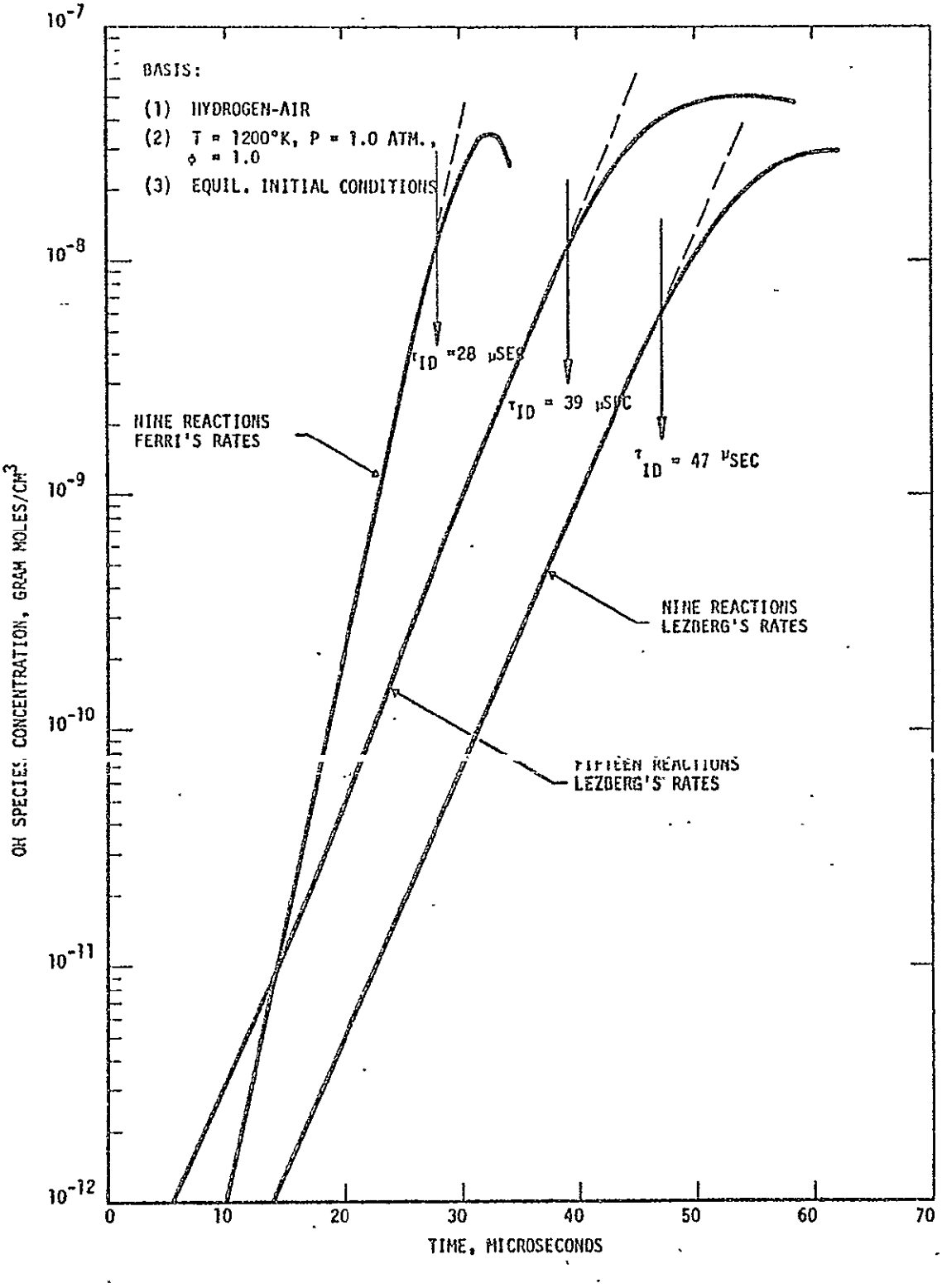

FIGURE 9 EFFECT OF REACTIONS AND RATE DATA ON DELAY TIMES

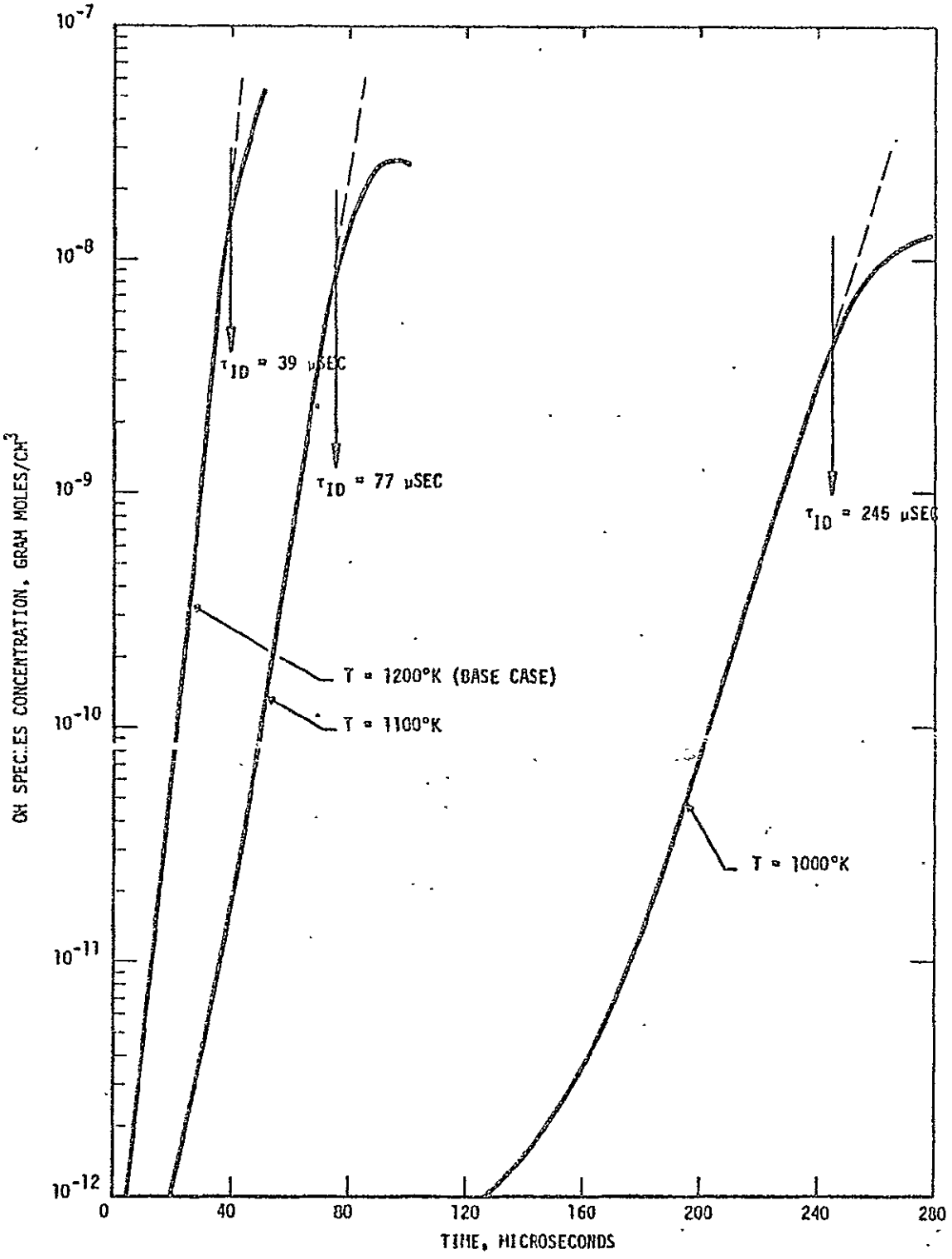

FIGURE 10 EFFECT OF TEMPERATURE ON INDUCTION TIMES

are in chemical equilibrium prior to mixing at constant temperature and pressure. The results show that a hundred degrees reduction in temperature over the base case, just about doubles the induction time. However, a further reduction of the same magnitude, results in a factor of six difference in induction time over the base case. The effect of initial temperature is best illustrated by plotting the induction times against the reciprocal of temperature on semi-log coordinates. This type of information is presented and discussed later in this section.

Figure 11 illustrates the effect of equivalence ratio on induction times for the base case species concentration. Three values for equivalence ratio are presented in this figure. The results show that equivalence ratio has a very small effect on induction times in the range ($0.2 \leq \phi \leq 1.0$). Momtchiloff obtained similar results in a theoretical and experimental comparison of the effect of equivalence ratio on delay times. The analytical model of the induction process assumes instantaneous mixing for the two streams. This assumption is justified on the basis that local mixture ratio variations during the actual mixing process have essentially no effect on induction time.

The effect of pressure on ignition delay is illustrated in Figure 12, which again presents OH concentrations as a function of time. Higher pressure in the combustor tends to decrease ignition delays; the delay time being inversely proportional to the pressure. In this constant temperature comparison, two combustor pressures are examined with the starting condition for each case being the equilibrium species concentrations prior to mixing. At two atmospheres

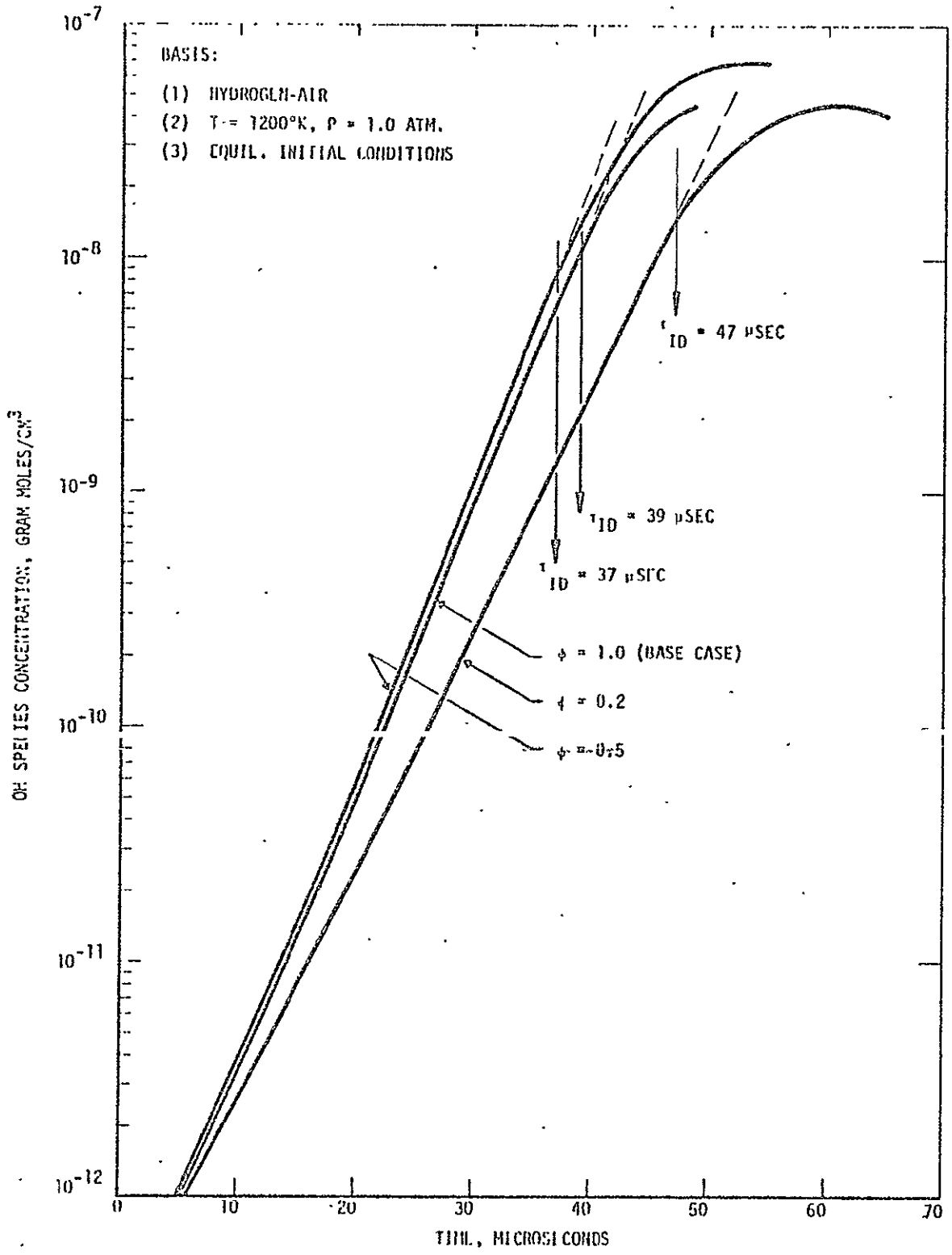

FIGURE 11 EFFECT OF EQUIVALENCE RATIO ON DELAY TIMES

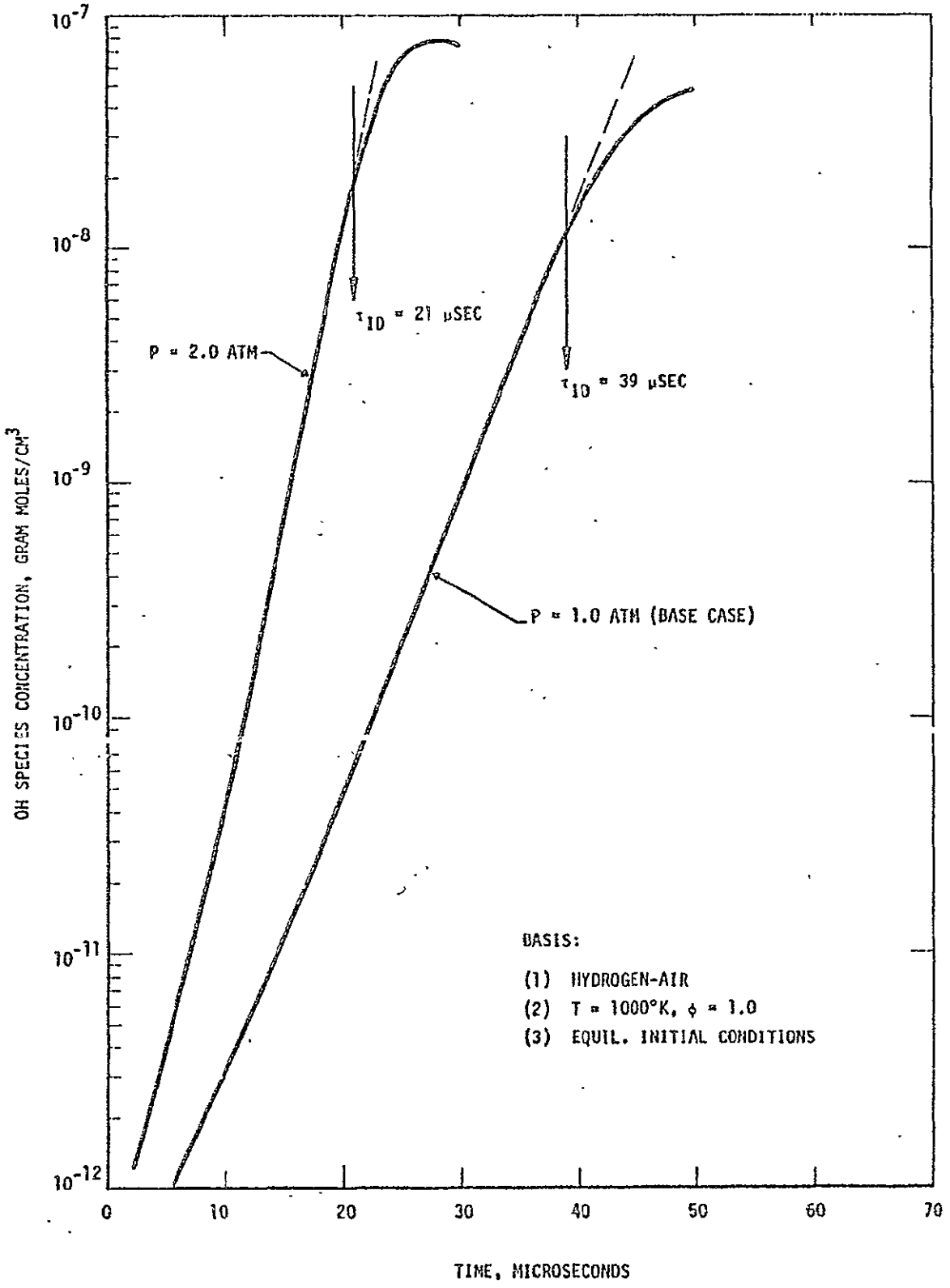

FIGURE 12 EFFECT OF PRESSURE ON INDUCTION TIMES

pressure the delay time is 21 microseconds compared with 39 microseconds at one atmosphere pressure. Relating the delay time to the inverse of pressure yields an exponent of 0.9 on pressure. The theoretical work of Momtchiloff reports this exponent is 1.09 at the same temperature conditions. Experimental data from Schott and Kinsey indicate this exponent is 1.0, while Das Gupta reports an average value of 0.9. The agreement of the SIL program results with the experimental findings is relatively good for this case and possibly even better than for the more detailed theoretical model of Momtchiloff. Any variations between the two theoretical approaches can probably be traced to the different reactions and reaction rate data used in the SIL program.

Production of vitiated air usually implies the presence of water vapor as a contaminant in the gas stream. The effect of water vapor on induction time is illustrated in Figure 13, which presents OH concentrations with time for the base case species and for 10 percent water vapor additive. In the case investigated, 10 percent water vapor replaces an equal volume of air. Temperature, pressure and equivalence ratio are fixed in this comparison. Water vapor is known to reduce the induction time by a small amount. The experimental results of Snyder also showed water vapor slightly reduced the ignition time. The effect may be related to the additional free radicals present at the start of the induction period due to reaction 3 in Table 2.

Several authors have derived either analytical or empirical relations for predicting the ignition delay times for the hydrogen-air

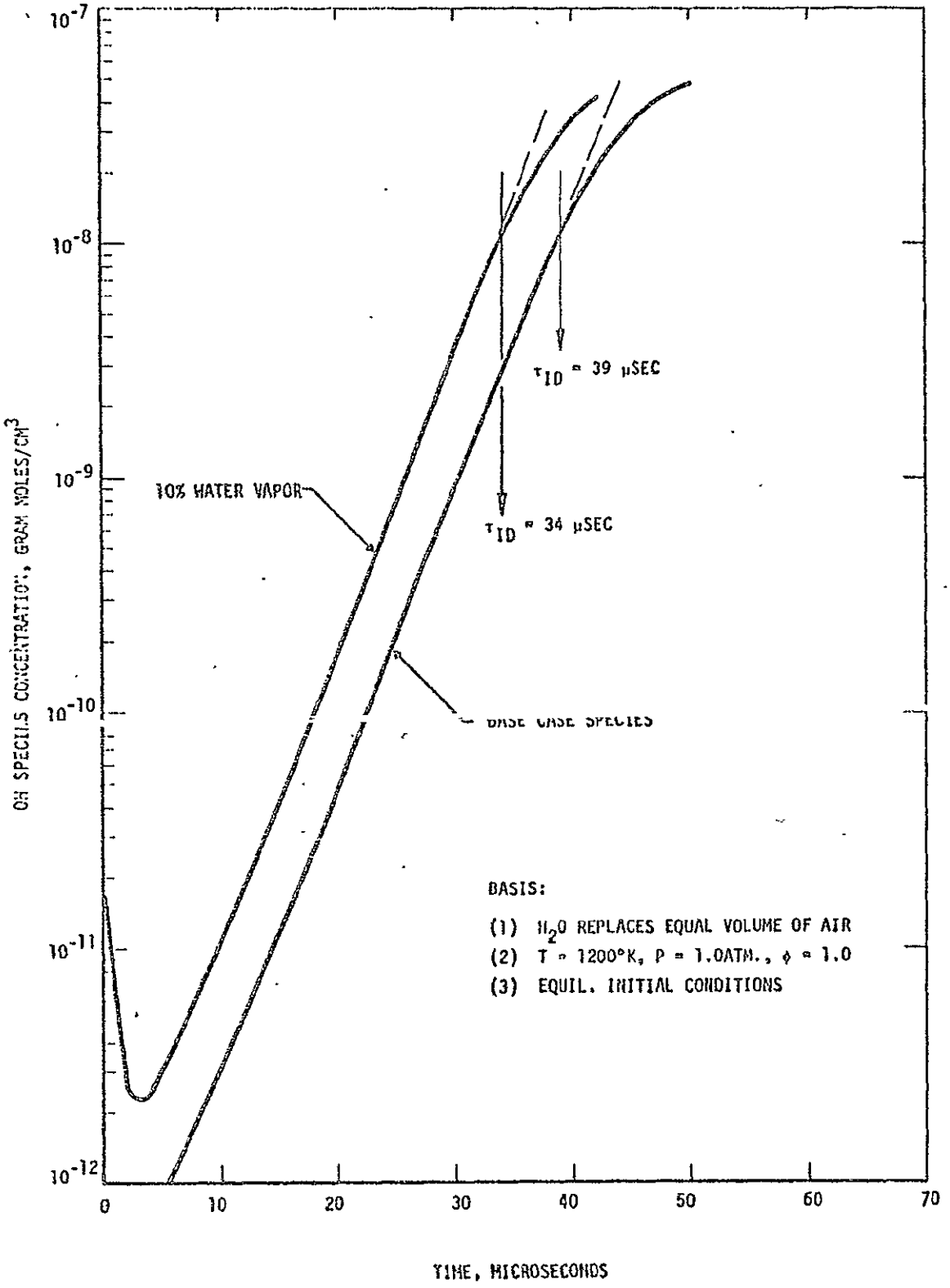

FIGURE 13 EFFECT OF WATER VAPOR ON INDUCTION TIMES

system. A comparison of their results with those obtained from the SIL program are shown in Figure 14, which presents the delay time as a function of the reciprocal of temperature with the following parameters held constant:

1. The pressure is one atmosphere,
2. The equivalence ratio is one, and
3. Both streams are in chemical equilibrium prior to mixing.

The correlations shown here are terminated at their respective temperature range of application. Note that most of the correlation presented are plotted as a straight line in this figure. Even the sophisticated analytical model employed by Momtchiloff [4] yields a straight line in these coordinates. However, the SIL program results deviate considerably from straight line behavior, especially at low temperatures. The reason is that the SIL program includes the effect of the HO_2 species on the ignition times. This species has often been observed in hydrogen-oxygen flames as an intermediate product that disappears rapidly as the reaction progresses. Brokaw [7] is the only other author to include this species and the point shown in Figure 14 includes his postulated mechanism by which the HO_2 species influences the delay time.

In the high temperature range ($T \rightarrow 1000°K$) the SIL program results agree reasonably well with the approximate lag calculations of Nicholls [6] and Ferri [1]. It agrees even better with the more detailed theoretical analysis of Momtchiloff [4]. At 950°K the simplified model agrees with the empirical relations of Snyder [14] and Rhodes [13]. Momtchiloff's analysis does not include the effect

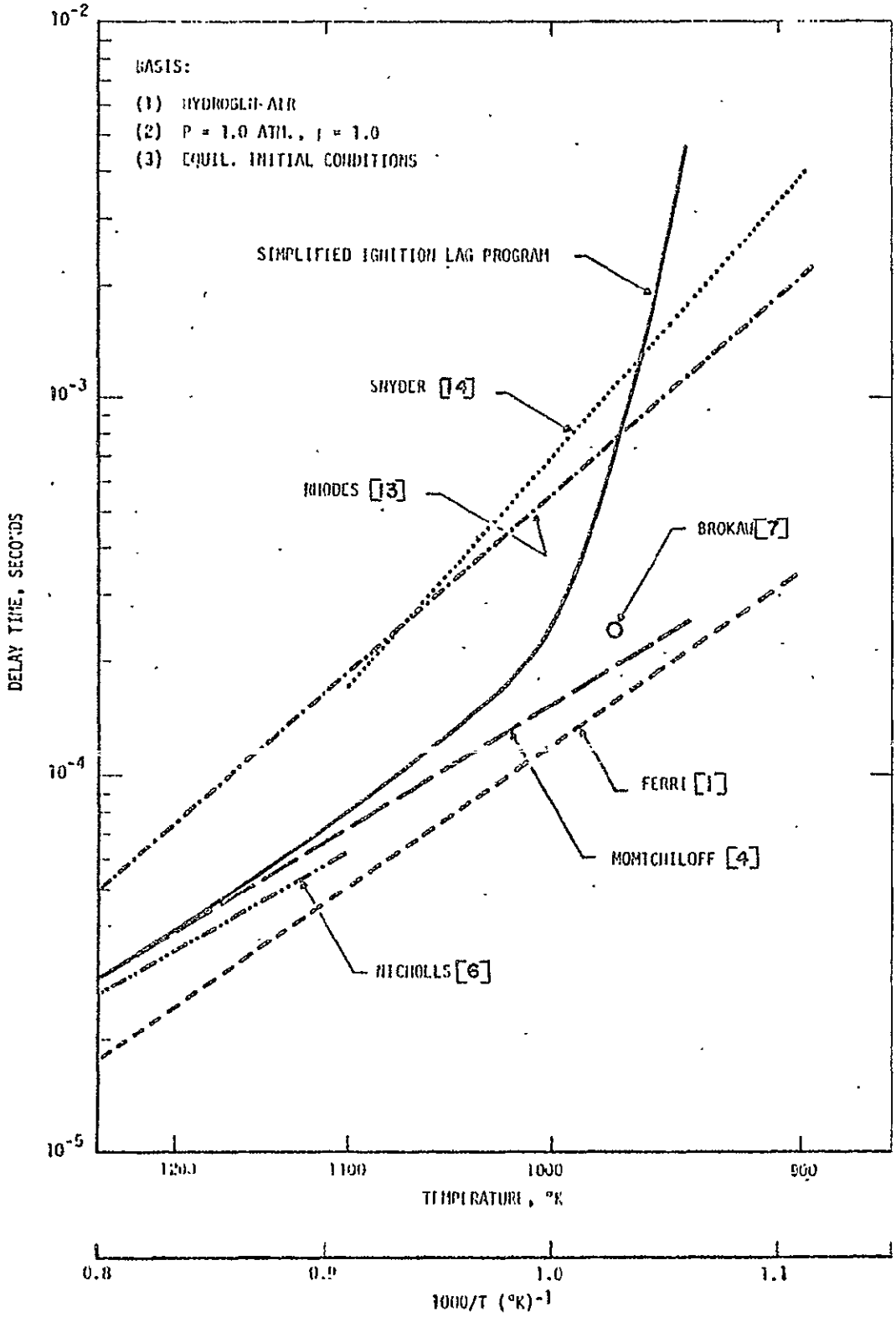

FIGURE 14 IGNITION DELAY TIMES FOR DIFFERENT CORRELATIONS

of HO_2 on induction times. This may explain the large differences between Momtchiloff's results and those of the SIL program in the low temperature range.

A comparison of the SIL program results with experimental data for ignition delay at low temperatures is made in Figure 15. Above 1000°K the SIL program predicts delays close to those of Momtchiloff [4], who was able to justify his theoretical model with experimental results as shown previously in Figure 1. The low temperature experimental results of Snyder [14] show very poor agreement with Momtchiloff's analysis. However, the SIL program results follow the basic trend of Snyder's shock tube data even though the agreement is not entirely satisfactory. The fact is that the SIL program consistently predicts longer delays than were found experimentally for the test conditions indicated in Figure 15. (Snyder's empirical relation used on the previous figure represents a correlation of all his data by a nonlinear regression program.) However, the general agreement of the SIL program with experimental data tends to support the argument that ignition delays increase significantly at low temperatures due to the self-inhibition of the reactions by HO_2 formation.

In summary, examination of the ignition model employed in the SIL program has shown that most of the relevant parameters influencing induction times are predicted with a reasonable degree of accuracy. The assumption of starting conditions where both streams are in chemical equilibrium is an essential part of this analysis because

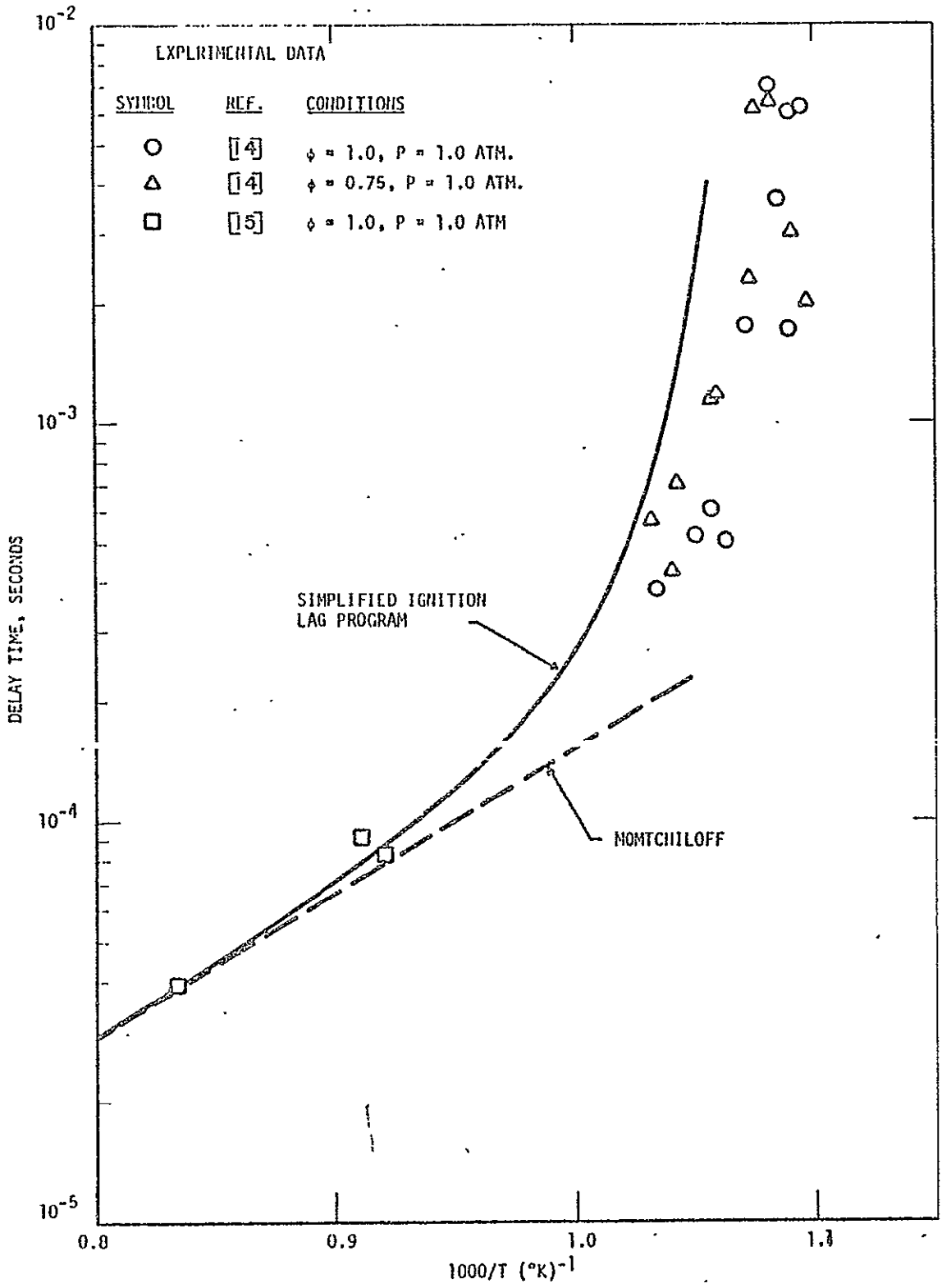

FIGURE 15 COMPARISON OF ANALYTICAL AND EXPERIMENTAL RESULTS

1. The experimental data used for comparison with the program results were obtained under conditions where equilibrium species concentrations at the combustor inlet is a reasonable approximation.
2. Most of the theoretical approaches for calculating ignition delays employ the assumption of chemical equilibrium as a starting condition.

In the next section, the effect of nonequilibrium starting conditions is examined using the SIL program, and an analysis is made to show the effect of vitiated air on ignition delays in supersonic combustion.

Analysis for Vitiated Air

The vitiated air composition is made up of the products of combustion in the gas generator. A combination of nitrogen tetroxide, hydrazine and nitrogen serve as reactants for the gas generator. In the ignition lag experiments described in the Experimental Program Section, the design mixture ratio of reactants is such that the theoretical flame temperature is 2200°K at a chamber pressure of 600 psia. The products of combustion are expanded to atmospheric pressure (14.7 psia) where hydrogen is injected parallel to the mainstream gases. Injection velocity for the hydrogen corresponds to sonic condition and mixing and combustion takes place at constant pressure. A complete analytical description of this system has not been made in the present program. A model has been made which incorporated the following simplifying assumptions into the analysis

in order to obtain a qualitative answer to the effect of vitiation on ignition lags:

1. All viscous effects are neglected.
2. Instantaneous mixing of the mainstream gases and hydrogen occur at the point of injection.
3. Constant temperature and pressure are assumed to exit throughout the induction period.

Of these three assumptions only the second is believed to be of significance.

The nonequilibrium composition of the vitiated air at the entrance to the supersonic test section is calculated utilizing the Finite Rate Reacting Gas (FRRG) program. Computed composition changes during the expansion were shown previously in Figure 4. The hydrogen stream at the test section entrance is assumed to have a free-radical composition corresponding to stagnation conditions in the hydrogen manifold. The recombination of atomic hydrogen is a relatively slow three-body reaction and the assumption of frozen flow is quite reasonable for the temperatures and pressures employed in the experimental program. The vitiated air and hydrogen streams are mixed at constant pressure and the resulting species concentrations are input as initial conditions into the Simplified Ignition Lag (SIL) program.

The SIL program results for vitiated air and hydrogen are shown in Figure 16, which presents the OH radical concentration as a function of time. These results indicate the induction period for vitiated air and hydrogen may be as short as 20 microseconds. Under the experimental conditions of this program, ignition should occur less

than 1.5 inches downstream of the test section entrance. However, mixing times are neglected in this analysis, so that the actual distance to the ignition front may be located somewhat further downstream than predicted by the SIL program.

Figure 16 also includes the delay time calculated assuming chemical equilibrium for both the vitiated air and hydrogen stream prior to mixing. Notice the test section temperature is 1030°K for that case compared to 1000°K for the previous calculation assuming finite rate chemistry. Both the finite rate and equilibrium calculations are started at the same timperature and pressure in the gas generator. The heat release associated with additional recombination of free radicals when assuming chemical equilibrium results in higher temperatures throughout the expansion process. An induction time of 158 microseconds was determined for vitiated air and hydrogen utilizing the assumption of equilibrium initial conditions. This delay corresponds to a distance of approximately 11.5 inches downstream of the test section entrance for the ignition front.

A comparison was also made to show the effect of employing heated air to perform the same type experiments. Conditions at the inlet to the supersonic test section (i.e., temperature, pressure and equivalence ratio) are identical to those employed in the vitiated air analysis.

The SIL program results for heated air and hydrogen are shown in Figure 17, which again presents OH radical concentration as a function of time. An induction time of 30 microseconds was obtained for non-equilibrium inlet conditions to the supersonic test section. This

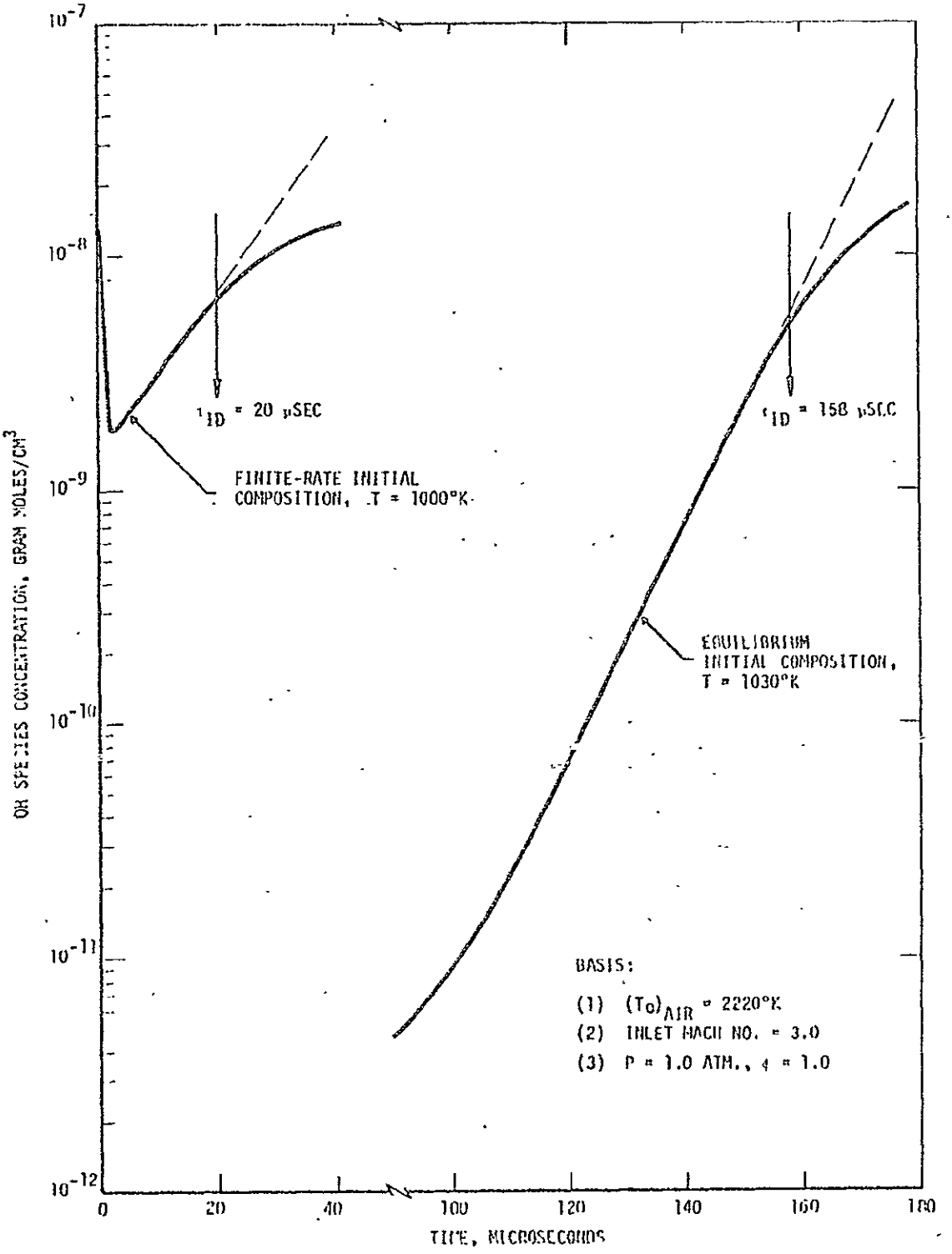

FIGURE 16 IGNITION DELAY FOR VITIATED AIR/HYDROGEN

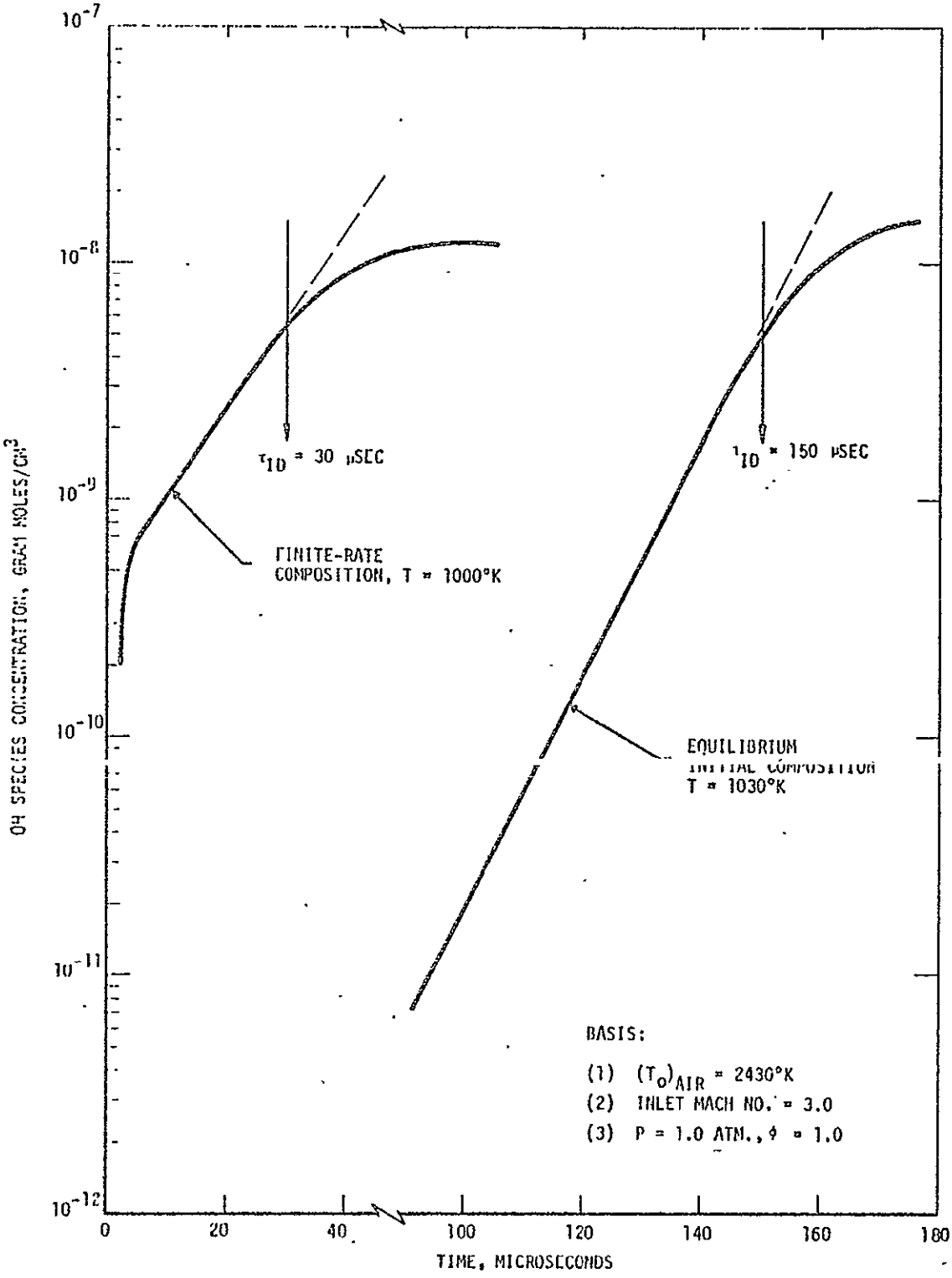

FIGURE 17 IGNITION DELAY FOR HEATED AIR/HYDROGEN

delay time corresponds to a flame front location of 2.2 inches downstream of the test section inlet. When equilibrium initial conditions were assumed for the heated air and hydrogen the delay time increased to 150 microseconds. This induction time corresponds to a lag length of 10.8 inches.

A comparison of the vitiated air and heated air analytical results indicates that vitiated air does, to some extent, simulate heated air from the standpoint that the ignition lag lengths are almost equal. For nonequilibrium inlet conditions, the free-radical content of the vitiated air and hydrogen is present in sufficient quantity to cause the ignition to be almost spontaneous. Heated air contains no hydroxyl radical at the test section inlet, but the nonequilibrium concentrations of atmoic hydrogen and oxygen are sufficient to cause rapid build-up of hydroxyl radical through the bimolecular reactions. Again the ignition is almost spontaneous. Another factor which has not been included in this analysis is the effect of NO and/or NO_2 content on the ignition delay. These species have been shown to have a catalytic effect on the ignition process. Nonequilibrium inlet conditions for both the vitiated air and heated air have enough NO present to catalyze the induction process. This further tends to substantiate the argument that the use of heated air or vitiated air for ground testing of supersonic combustion with hydrogen will yield extremely short ignition delays under the conditions investigated. This may mean that mixing will be rate-controlling such that the distance between the test section entrance and the flame front may represent for the most part the mixing length.

Supersonic combustion under free-flight conditions may correspond more closely to equilibrium initial conditions. In that event neither heated air nor vitiated air can be used to simulate supersonic combustion performance under free-flight conditions in the regime where reaction times are rate-controlling.

EXPERIMENTAL PROGRAM

The experimental program discussed in this report was concerned primarily with the effects of vitiated air on ignition delay. A proposed follow-on effort, as described in Appendix G, would have investigated the effects of vitiated air on the overall combustion efficiency. The method of procedure, design and fabrication of the hardware and associated instrumentation of the follow-on program is reported herein. Exhaustion of the project's allotted time and funding precluded the completion of this specific experimental task.

Since the ignition delay and combustion efficiency programs complemented one another, all hardware was designed and fabricated simultaneously in an effort to conserve time and money. Therefore, some of the hardware described herein was not actually utilized for the purpose of obtaining ignition delay data, but would have been employed in the overall combustion efficiency experimental effort.

Sizing of the experimental apparatus was based on the criteria that the supersonic test section should be large enough to minimize scale effects but small enough to reduce run costs. It was also desirable that the design conditions simulate a flight regime in which the SCRAMJET vehicle might be expected to operate. This regime was chosen so that ignition delay times would be relatively long so that they could be measured.

Design conditions selected for the gas generator were: chamber pressure = 1000 psia, chamber temperature = 2200°K and flow rate = 15 lb/sec. The design operating conditions for the gas generator and supersonic combustor are shown schematically in Figure 18. These conditions approximately simulate a flight Mach number of 6.5 at an altitude of 80,000 ft., a regime that should be of interest for SCRAMJET application. The equipment size and propellant flow rates were well within the limits of the existing research facilities at the Zucrow Engineering Research Center, Purdue University.

In the ignition delay experiments, the gas generator pressure and hydrogen pressure were selected so that they expanded to atmospheric pressure. The combined streams were permitted to mix and burn in an unconfined manner as a free jet. The absence of a confining wall made it possible to visually observe the flame front and determine the ignition delay distance. A solid wall near the reaction zone often catalyzes the combustion process by either surface reactions or through a temperature increase due to viscous dissipation. In addition, the flow pattern (recirculation) becomes more complex. By examining ignition in a free jet, the ignition delay effects should be theoretically predicable providing the reaction mechanism is selected properly.

Design pressure for the supersonic combustor section is 25 psia. Since the ignition delay study was conducted with the test section at 14.7 psia, the gas generator was operated at 600 psia for the ignition delay experiments, while the basic hardware remained unchanged, except

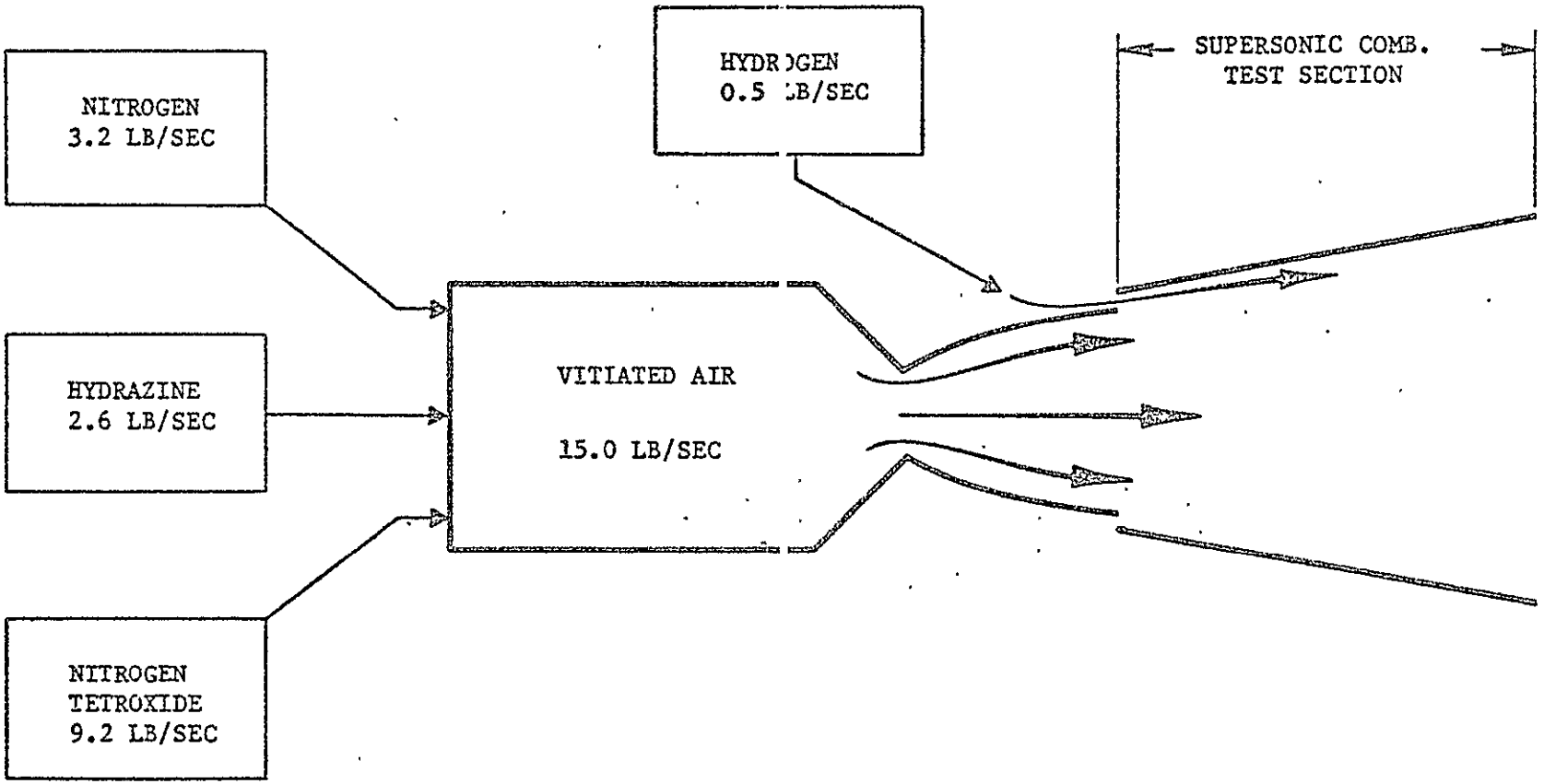

FIGURE 18 SCHEMATIC OF EXPERIMENTAL SET-UP

for the removal of the supersonic combustor and constant area mixing sections.

Description of Experimental Apparatus

In this section, the main elements of the experimental apparatus are discussed briefly under separate headings.

Gas Generator

The components of the gas generator include an injector, two chambers, a turbulence ring and a converging-diverging contoured (parallel flow) nozzle. An assembly drawing of the gas generator components with the supersonic combustion test section is presented as Figure 19.

In the initial phase of this program the gas generator and the supersonic combustion test section were fabricated of type 347 stainless steel. The hot surfaces of this uncooled apparatus were coated with a high temperature ceramic material (zirconium oxide) to form a thermal barrier between the stainless steel wall and the hot ($T = 2200°K$) chamber gases. This material has relatively good heat resisting qualities and is compatible with both nitrogen tetroxide and hydrazine. Unfortunately, after a short series of experimental runs, it became evident that due to spalling and cracking of the zirconium oxide coating, the life duration of the gas generator nozzle throat was limited. This precluded operation of the hardware for run times in excess of 1 sec. of steady state operation. At this time research was initiated into the possibility of employing an all copper system. The remaining portion of the life span of the stainless steel

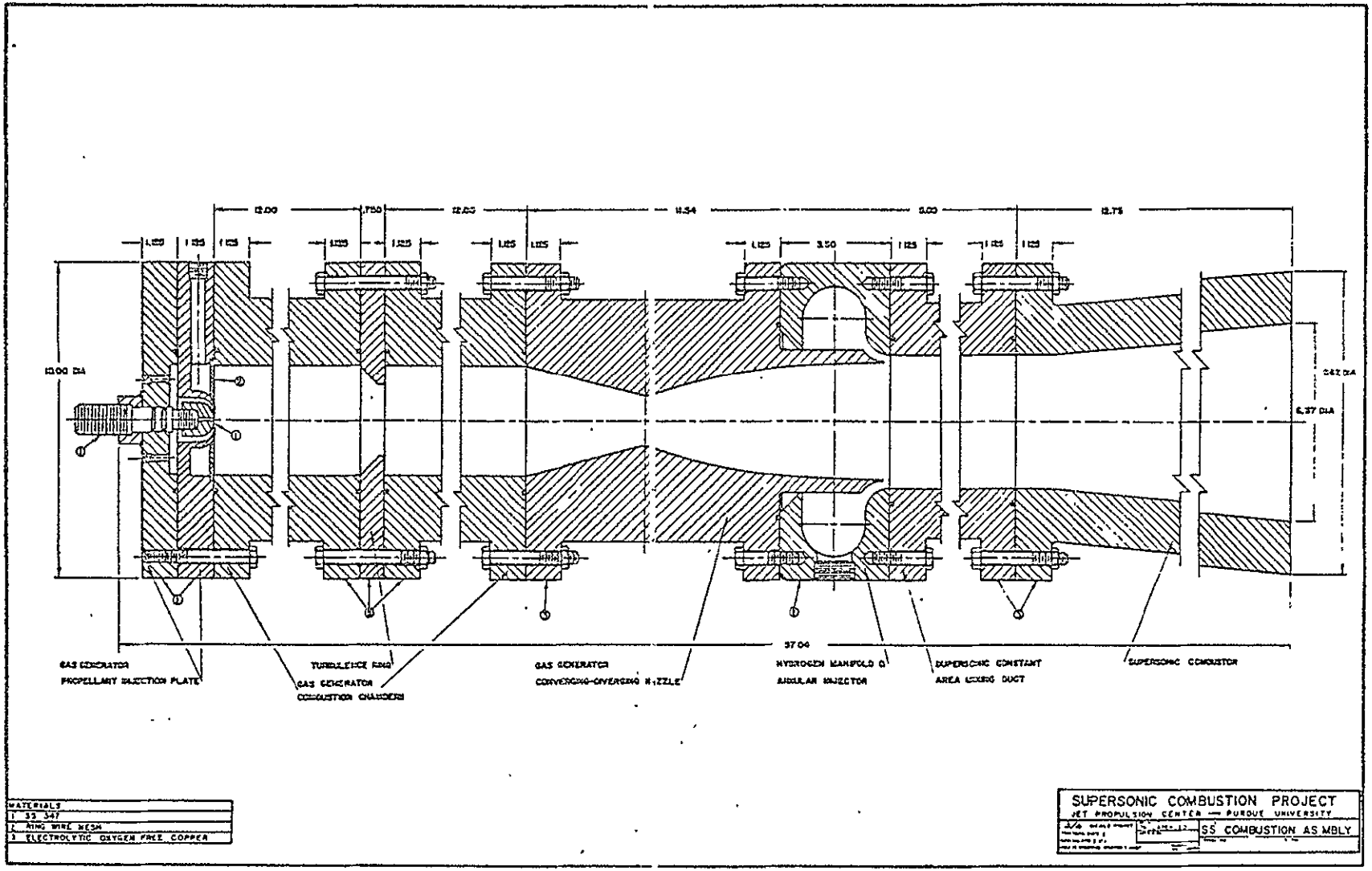

FIGURE 19 SUPERSONIC COMBUSTION SYSTEM ASSEMBLY DRAWING

system was devoted to determining optimum propellant flow rates for design operational conditions and confirming system design integrity for supersonic combustion. The experimental data generated during this portion of the investigation are not reported because this series of runs had to be repeated in the follow-on phase employing the newly fabricated experimental apparatus. Nevertheless, during this unreported series of test, system integrity was confirmed and meaningful propellant flow rate data were developed prior to the expected nozzle failure. Details concerning this series of runs are reported in Reference 3.

The possibility of employing an all copper system was discussed in a meeting between members of NASA Lewis and the Zucrow Engineering Research Center. The primary reason for not using an all copper system initially was due to the known erosive nature of nitrogen tetroxide and its by-products when in contact with copper. It was pointed out that this erosive phenomenon is most prevalent when the reacting agents are in their condensed phase and if these agents could be neutralized before this phase is reached, their effect would be minimal. The relative high thermal conductivity of copper makes it extremely attractive for uncooled high temperature apparatuses. A preliminary heat transfer analysis (see Appendix B) indicated that an uncooled copper gas generator system subjected to the experimental chamber conditions mentioned previously could theoretically operate for run times up to 14 sec. before failure. A maximum of 4 sec. of steady state operation, which entails approximately 6 sec. of total gas generator run time, is necessary for any of the prescribed

investigations. A saturated solution of sodium bicarbonate was suggested as an economical and effective neutralizer of the erosive reactants.

The decision to employ an all copper system was finalized after careful review of all the pertinent facts. The new hardware's design was basically the same as that of the stainless steel apparatus except that the material is now oxygen free, electrolytic tough pitch copper with a minimum wall thickness of 2.1 in. An assembly drawing of the new system is shown in Figure 19. Since copper is difficult to weld, the flanges and its associated section were machined out of a single solid 10 in. round of copper stock. During the machining process of the flange, only enough material was removed from the outside diameter of the copper round to allow clearance for the connecting bolts and their associated washers. This permitted maximum residual material for "heat sink" purposes. The combustion chambers and nozzle sections are flanged on both ends with "O" ring grooves on the sealing surfaces. Material for the "O" rings is type 316 stainless steel with a 0.003 in. thick tungsten coating. During the investigation the seals held up satisfactorily with minimum leakage. When signs of leakage was detected, that particular section was disassembled and the "O" ring seal replaced. Prior to the initial assembly, each sealing surface was relieved approximately 0.010 of an inch for better sealing characteristics.

The two combustion chamber sections are separated by a turbulence ring as shown in Figure 19. The purpose of the turbulence ring is to

promote mixing in the hot gases in order to insure a relatively uniform exhaust stream.

The gas generator injector has three separate elements: the oxidizer inlet housing, fuel injection pintle and a porous metal surface in the area exposed to the combustion gases. The diluent nitrogen is introduced into the combustion chambers through this porous metal surface and thus serves to cool the entire injector face. The fuel injection pintle serves to introduce the hydrazine into the combustion chamber and together with the nitrogen inlet housing forms an annulus for injecting the nitrogen tetroxide oxidizer. A close-up photograph of the injector face and fuel pintle is presented in Figure 20. The pintle contains 10 hydrazine injection ports of 0.0625 in. diameter for high flow rate runs ($\dot{w}$ = 15 lb/sec) and 10 injection ports of 0.0156 in. diameter for low flow rate runs ($\dot{w}$ = 9 lb/sec).

The width of the annular passage for the oxidizer can be varied by turning the pintle assembly. This feature permits some adjustments of the injector pressure drop to help avoid low frequency combustion instability problems.

The gas generator nozzle was designed for uniform, parallel flow across the exit plane. Design of the exit contour was accomplished by utilizing a computer program which solves the two-dimensional, axisymmetric flow relations by the method of characteristics. This program requires as input

1. The gas properties,
2. The upstream converging and downstream diverging blend radii,

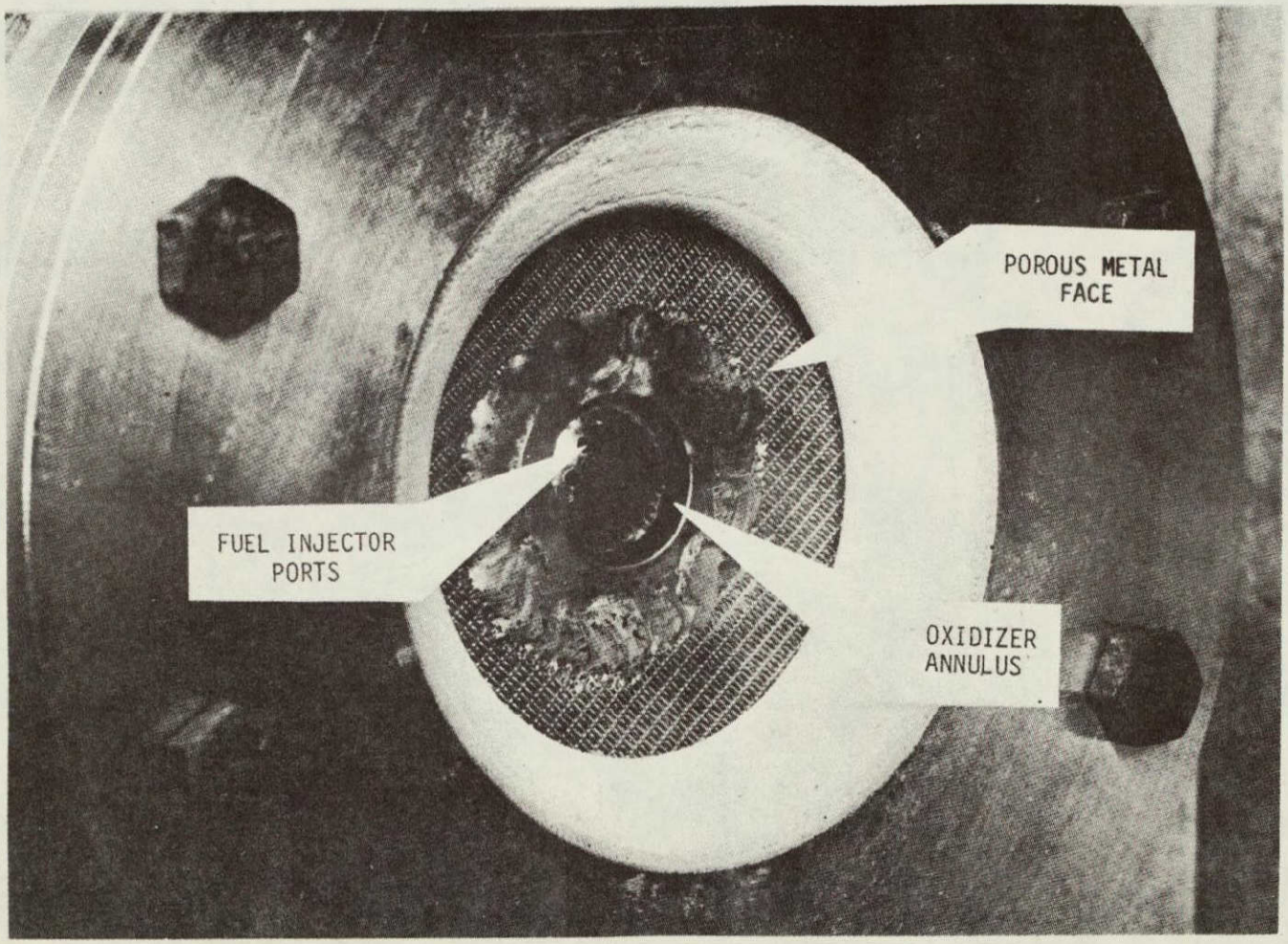

FIGURE 20 GAS GENERATOR INJECTOR ASSEMBLY

3. The throat radius, and

4. The design Mach number.

A start line is calculated in the nozzle throat region using Sauer's method. A solution to the flow in the kernal is continued to the point where the Mach number on the axis corresponds to the design value. Then the exit characteristic is generated assuming the flow angle is zero. The exit characteristic is terminated when the mass flow equals that computed for the start line. A complete wall contour is calculated by solving the characteristic relations in the previously undefined region. A plot showing the complete characteristic network for the parallel flow nozzle is presented in Figure 21. This is a cross-sectional view of the nozzle exit section divided at the centerline. The computer program assumes constant values for the ratio of specific heats and for the molecular weight of the mixture. This assumption, while esthetically displeasing, yields a good approximation to the contour coordinates calculated for real gas conditions. The parallel flow nozzle has a throat diameter of 1.596 in. and an overall area ratio of 5.38. A photograph of the assembled gas generator apparatus is shown in Figure 22.

Hydrogen Heater

The hydrogen heater was designed and fabricated by Thermal Transfer Corporation of Monroeville, Pennsylvania. This unit consists of a large stainless steel coil which is heated by convection and radiation from the combustion products of three propane burners. A photograph of the installation of the hydrogen heater is presented in Figure 23. The heater is located outside the test cell perimeter as

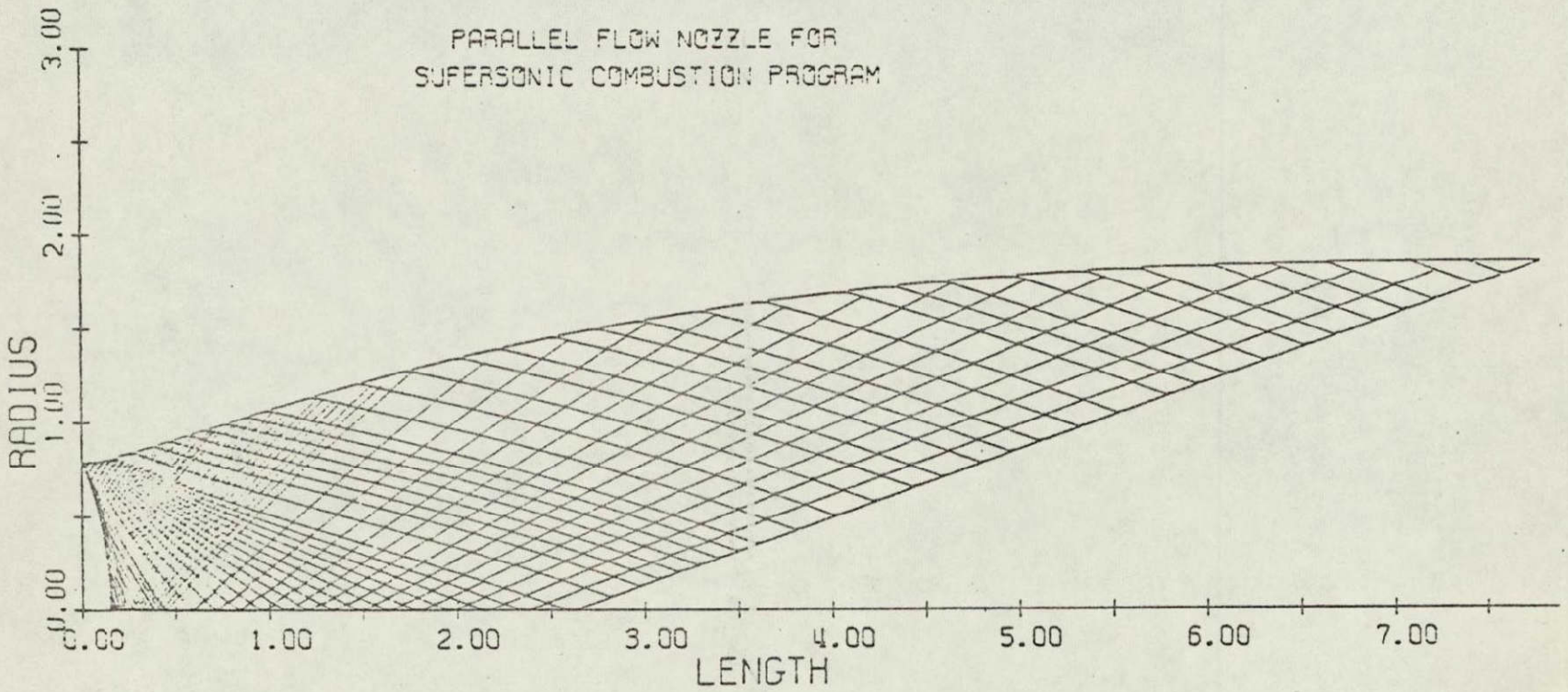

FIGURE 21 CHARACTERISTIC NETWORK FOR PARALLEL FLOW NOZZLE

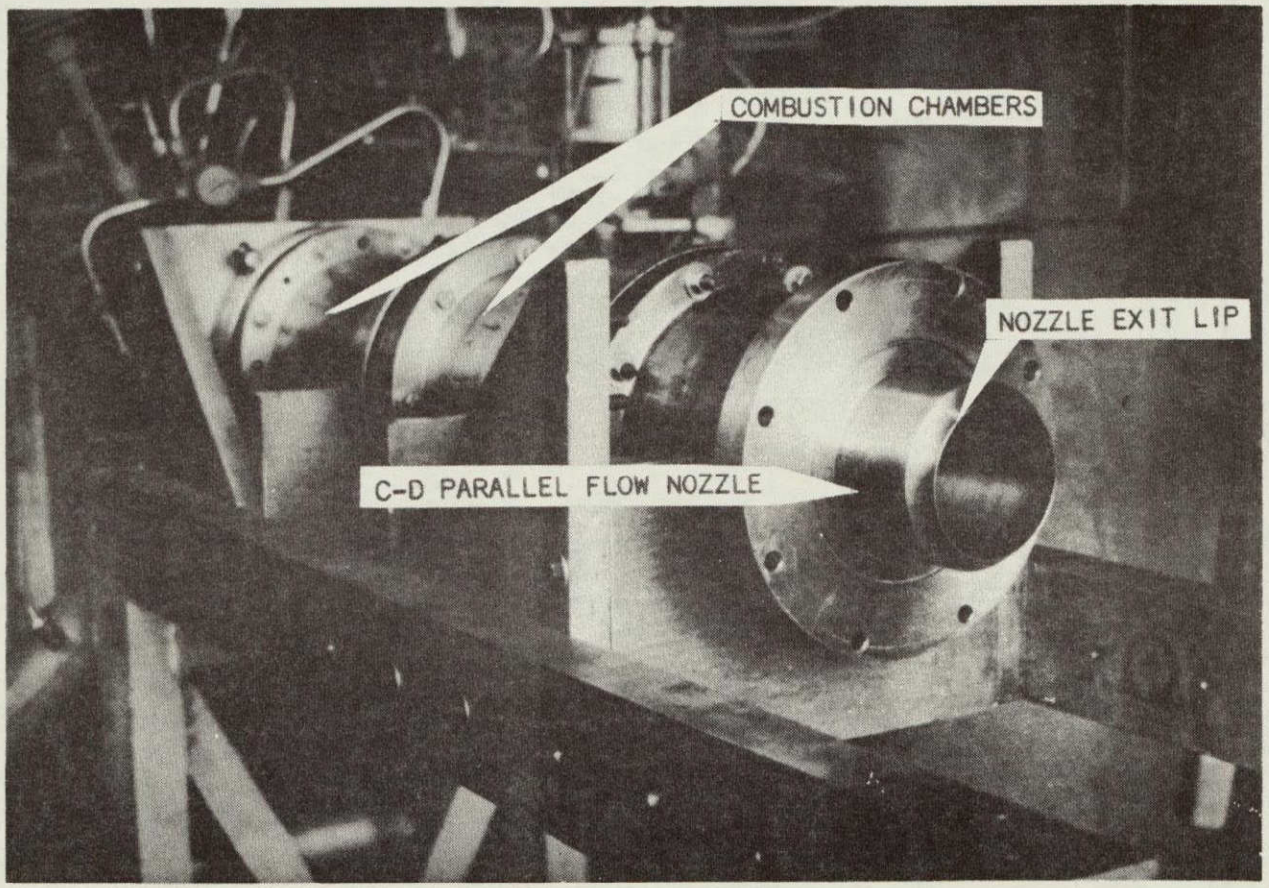

FIGURE 22 GAS GENERATOR ASSEMBLY

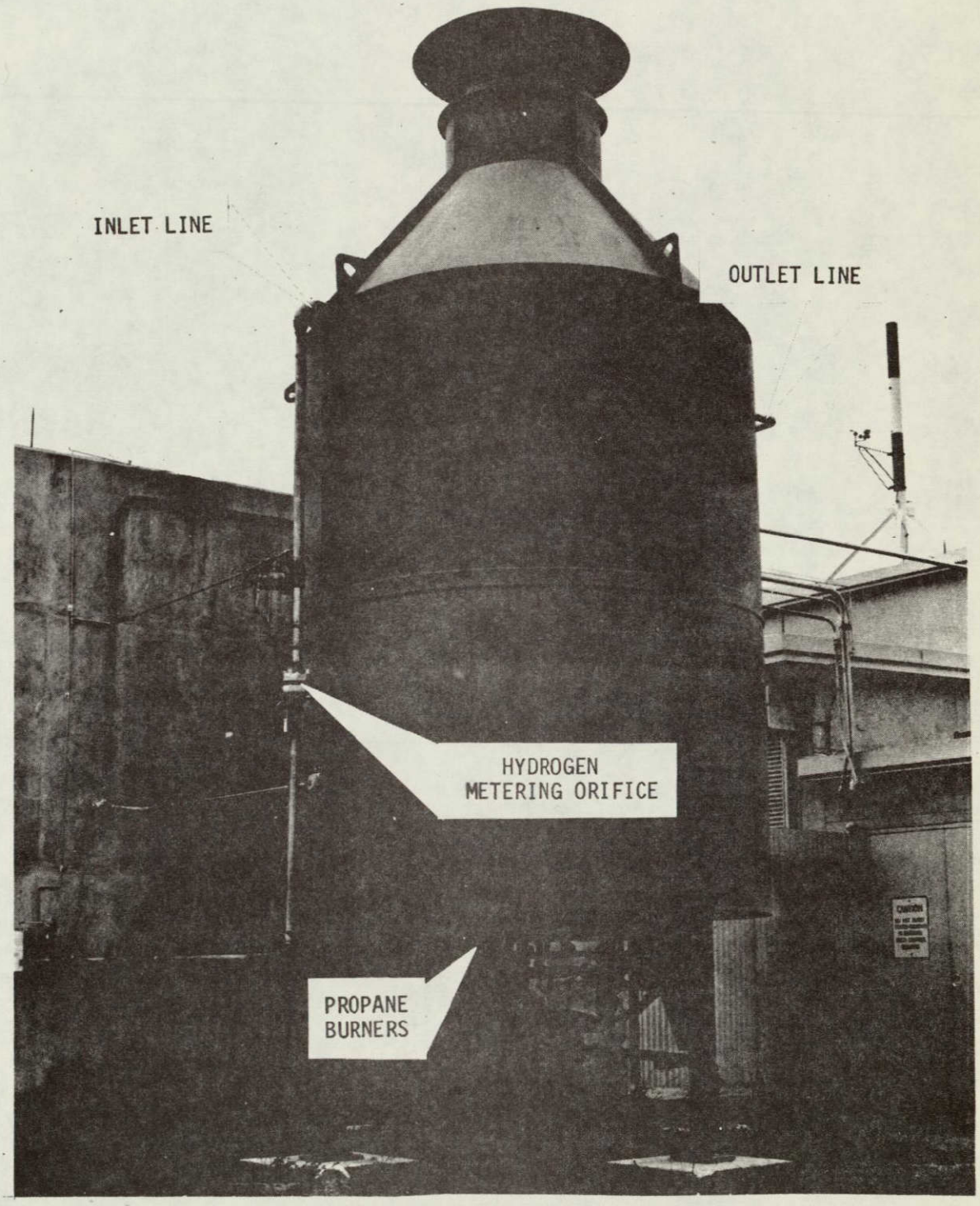

FIGURE 23 HYDROGEN HEATER INSTALLATION

a safety precaution. Design specifications on the hydrogen heater are presented in the following tabulation:

Hydrogen Heater Specifications

Total Heat Input	BTU/HR	20.0×10^6
Design Operating Pressure	PSIG	325
Excess Combustion Air	%	50
Waste Gas Volume	S.C.F.M.	3,190
W.G. Temp.-entry	°F	2,700
W.G. Temp.-exit	°F	1,400
Thermal Efficiency	%	30
Hydrogen Flow	lb/sec	0.5
Hydrogen Temp.-entry	°F	70
Hydrogen Temp.-exit	°F	1,040

The combustion system for the heater consists of a main shut-off valve, which can be operated either manually or automatically, and a multiple National Airoil burner arrangement equipped with spark ignited pilots. A flame safety system shuts off fuel to the burners in the event of excessive temperatures measured on the tube wall or in the exhaust stack gases. The heater is relatively simple to operate and performed well.

Supersonic Test Section

Three separate components make up the supersonic test section. These are the hydrogen manifold, the constant area mixing section and the divergent supersonic combustor. The latter two components were not employed in the ignition delay experiments but would have been

utilized if the effect of vitiated air on the overall combustion efficiency investigation had been completed.

The hydrogen manifold was machined from a single billet of type 347 stainless steel. After careful alignment, the manifold was bolted to the exit section of the parallel flow nozzle. The mating of the hydrogen manifold and nozzle exit section is such that an annulus is formed between them. The hydrogen gas is expanded to sonic conditions as it passes through this annulus. The pressure in the hydrogen system manifold is maintained at a sufficient level to keep the flow through the annulus choked. A photograph showing the hydrogen manifold mounted on the gas generator is presented as Figure 24. The exit lip of the parallel flow nozzle and the internal exit diameter of the hydrogen manifold form the above-mentioned annular injector. The lip is 0.050 in. thick and was purposely made as small as possible to minimize flow recirculation problems in this area, but large enough to maintain some structural strength.

The constant area mixing section has an inside diameter of 4.25 in. and is 5.0 in. long. The supersonic combustor section has a conical shaped wall which diverges at a 5 degree half angle. This divergent area combustor design was selected to permit essentially constant pressure combustion and to minimize the undesired condition of thermal choking caused by excessive heat addition. Overall length of the combustor is 12.75 in. with a 6.37 in. exit diameter. Both the constant area mixing section and the divergent supersonic combustor are fabricated out of oxygen free electrolytic tough pitch

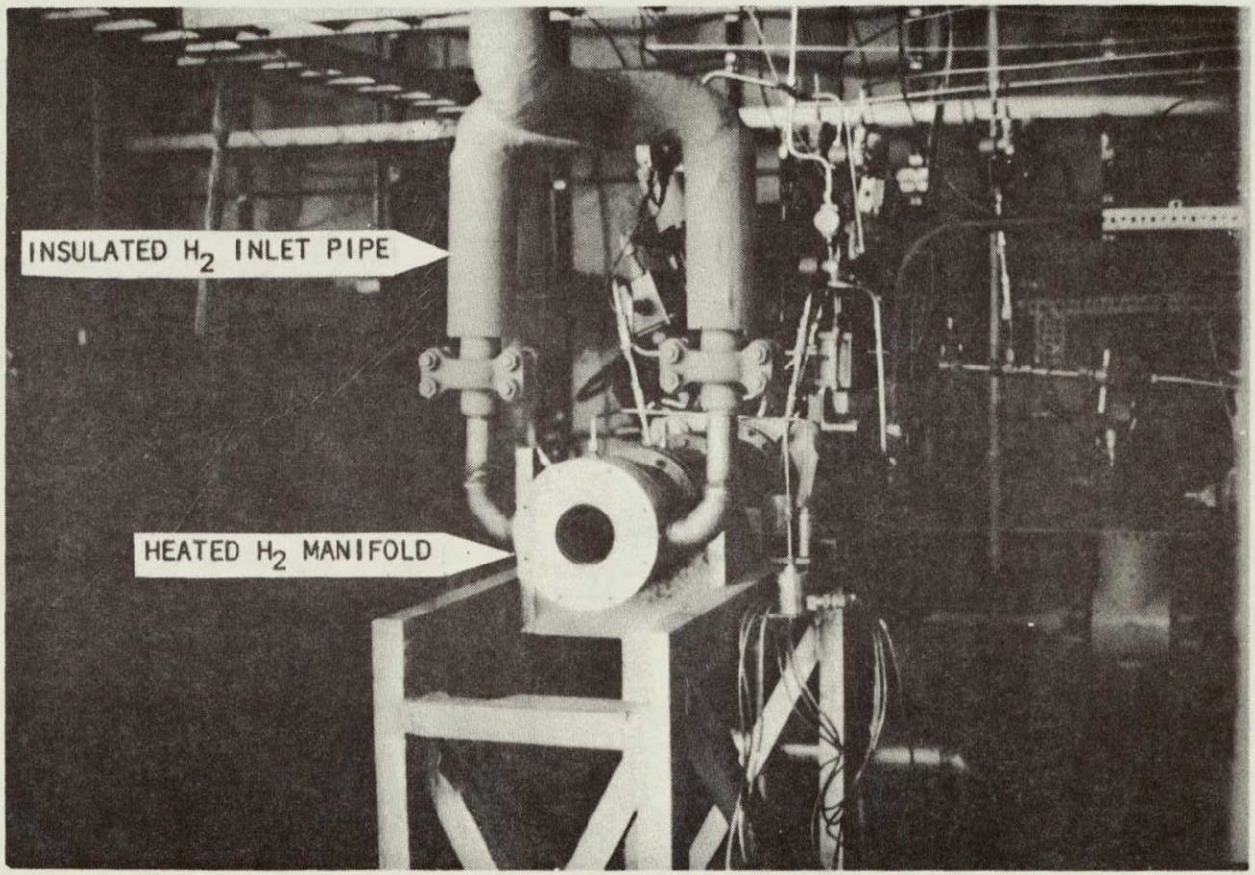

FIGURE 24 HYDROGEN MANIFOLD - GAS GENERATOR ASSEMBLY

copper. An aft view of the entire supersonic test section assembly is shown in Figure 25.

Description of Instrumentation

The basic instrumentation employed in the experimental program is summarized in Table 4. This tabulation includes the pressure transducers, flow meters and thermocouples utilized in the ignition delay investigation. A photocon transducer was employed in a few of the earlier gas generator performance evaluations to determine whether the system exhibited any high frequency pressure oscillations. During these experiments the photocon output data indicated that there were no instability problems within the system.

In the proposed overall combustion efficiency investigation, in order to more completely describe combustor performance from experimental results, a thorough knowledge of the spatial distribution of pressure (total and static), temperature and specie concentration of the combustor exit plane is required. From these properties the overall combustion efficiency can be defined by comparison with the parameters that would result from an ideal process. This technique involves measuring as many properties as possible and determining the others through iteration of the integral equations of flow (see Appendix G).

Flow in the supersonic combustor is assumed to be axisymmetric. Therefore, measurement of flow properties at several radial locations would have provided data throughout the measurement plane. A water-cooled cruciform instrumentation rake, with each arm of the rake assembly designed to measure either gas composition, temperature,

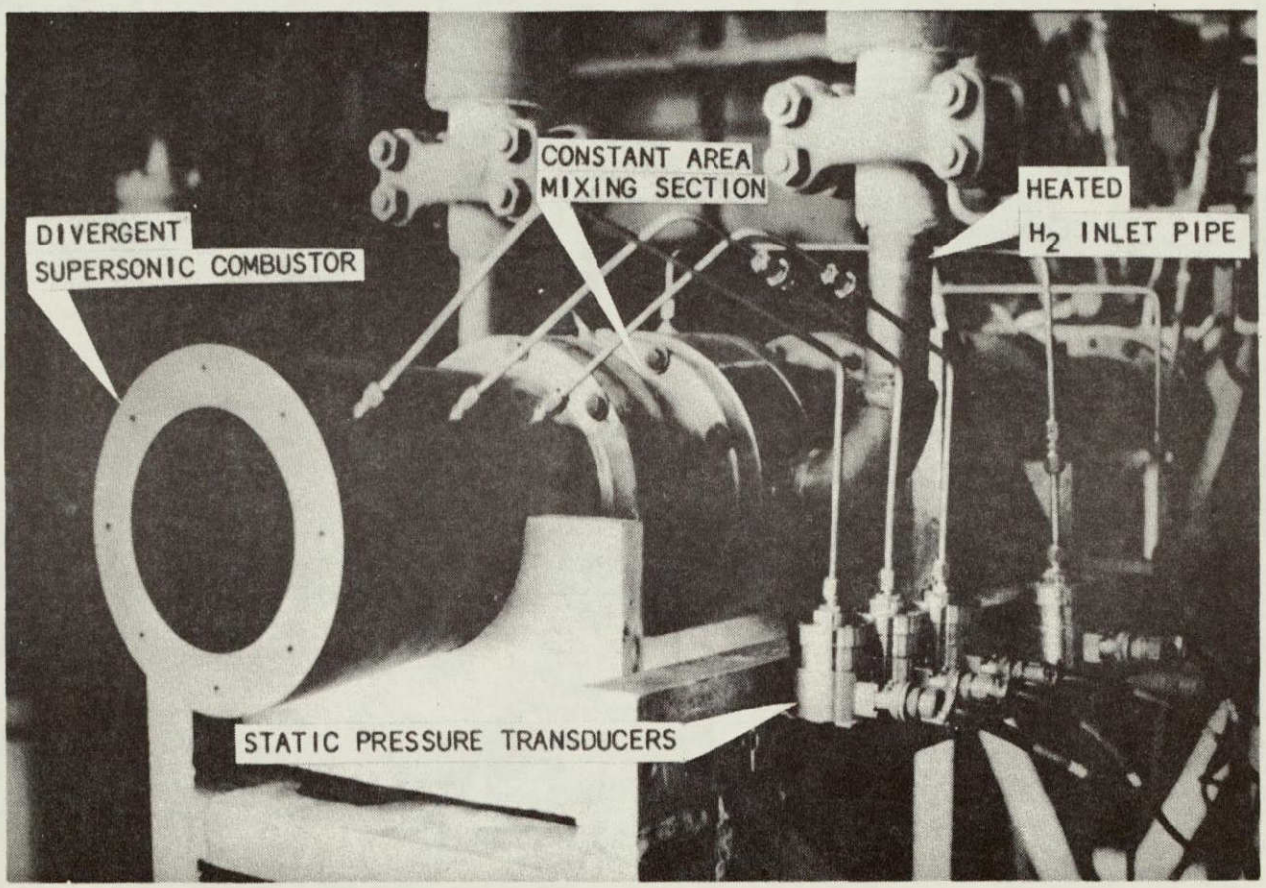

FIGURE 25 SUPERSONIC TEST SECTION ASSEMBLY

TABLE 4

INSTRUMENTATION SUMMARY

Parameter to be Measured	Instrumentation Manufacturer & Model No.	Operating Range	Recording Instrument
1. G.G. Chamber Pressure	Tabor, 206-DB	0-1500 psig	Strip Chart, Oscillograph & Digital Tape
2. N_2 Line Pressure	Tabor, 206-DB	0-2000 psig	Strip Chart & Digital Tape
3. N_2 Orifice Differential Pressure	Tabor, 2102	±120 psid	Strip Chart, Oscillograph & Digital Tape
4. Fuel Tank Pressure	Tabor, 2301	0-2000 psig	Strip Chart, Digital Tape
5. Oxidizer Tank Pressure	Tabor, 250	0-5000 psig	Strip Chart, Digital Tape
6. H_2 Manifold Pressure	Tabor, 254	0-50 psig	Oscillograph & Digital Tape
7. H_2 Line Pressure	Tabor, 206	0-350 psig	Strip Chart & Digital Tape
8. H_2 Orifice Differential Pressure	Tabor, 210?	±200 psid	Strip Chart, Oscillograph & Digital Tape
9. Fuel Flow Rate	Pottermeter, 3/4 inch-5550	0-30 gpm	Strip Chart, Oscillograph & Digital Tape

TABLE 4 (continued)

	Parameter to be Measured	Instrumentation Manufacturer & Model No.	Operating Range	Recording Instrument
10.	Oxidizer Flow Rate	Pottermeter, 2 1/2 inch-5971	0-400 gpm	Strip Chart, Oscillograph & Digital Tape
11.	H_2 Manifold Temperature	Iron-Constantan Thermocouples	0-833 °K	Strip Chart, Oscillograph & Digital Tape
12.	G.G. Chamber Temperature	40% Iridium-60% Rhodium vs Iridium Thermocouples	0-2100 °K	Strip Chart & Digital Tape
13.	N_2 Line Temperature	Iron-Constantan Thermocouples	0-833 °K	Strip Chart, Oscillograph & Digital Tape
14.	G.G. Chamber Wall Temperature	Chromel-Alumel Thermocouples	0-762 °K	Strip Chart, Digital Tape

impact pressure, or static pressure at equal distances from the centerline, was to be employed. These measurements would have provided the required properties in a plane across the entire flow field. Figure 26 shows a schematic of the water-cooled instrumentation rake assembly. A photograph of the rake installed on the supersonic combustor's exit is presented in Figure 27.

The integral components which comprise the cruciform instrumentation rake assembly are shown in Figures 28 through 34. These components will be briefly discussed in the following paragraphs.

The impact pressure and gas sampling probe, as shown in Figure 28, is a modified version of a probe assembly successfully utilized at the Applied Physics Laboratory of the John Hopkins University. Five impact pressure probes and five gas sampling probes are made from concentric pairs of type 316 stainless steel tubes, in which water in the annulus is discharged approximately 0.09 in. downstream of the probe tip, as indicated in Figure 29. The indicated pressure from the impact pressure probes would have been measured by Teledyne Model No. 206 gauge pressure transducers with a range of 0 to 1500 psig. A detached normal shock wave forms in front of the impact probe and the exit stagnation pressure P_{t_e} must be calculated from the indicated impact pressure P'_t. If the assumption is made that the gas composition does not shift through the shock, or in the short distance from the shock to the probe, the frozen normal shock relation can be used:

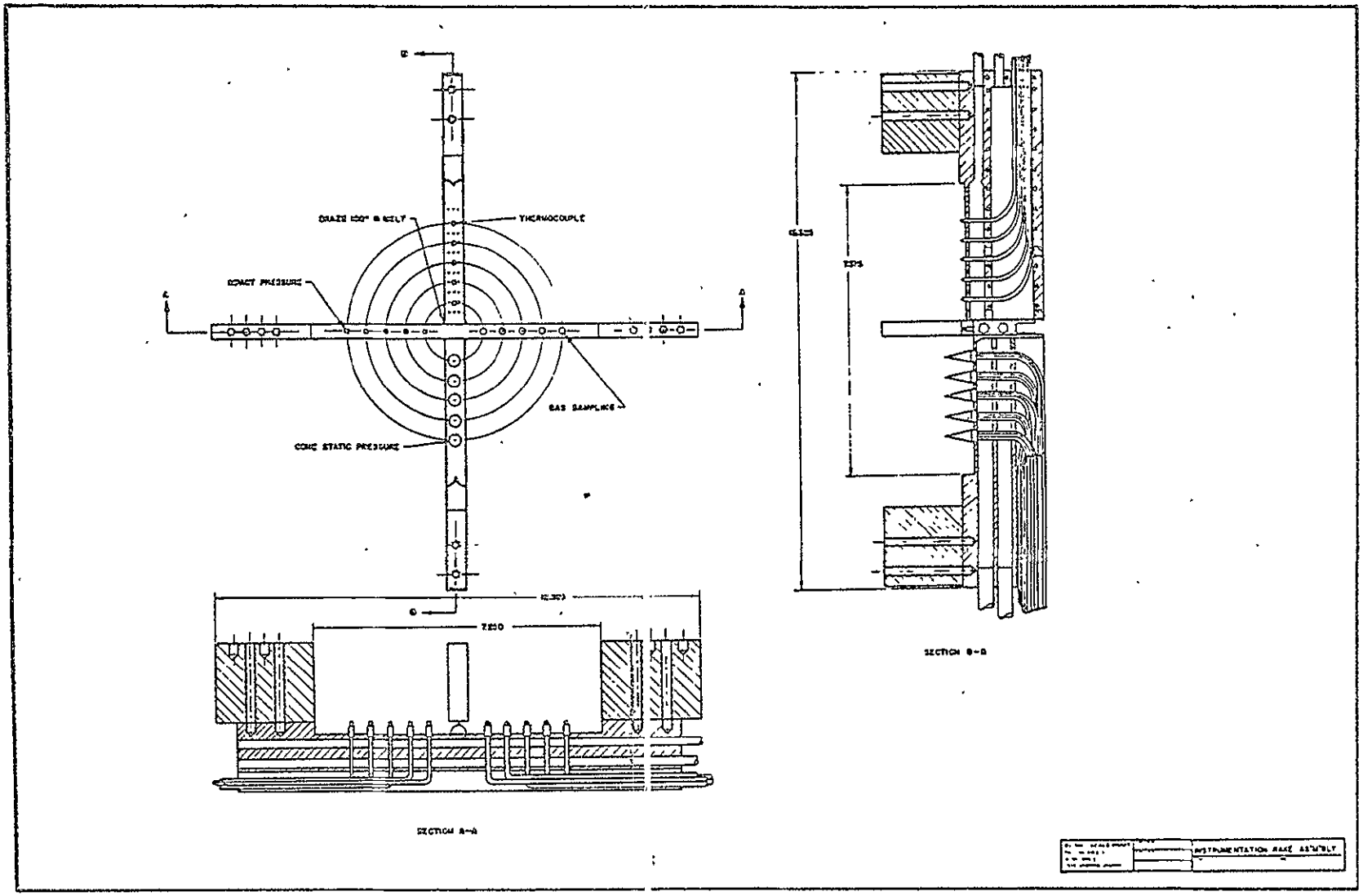

FIGURE 26 SCHEMATIC OF COOLED INSTRUMENTATION RAKE ASSEMBLY

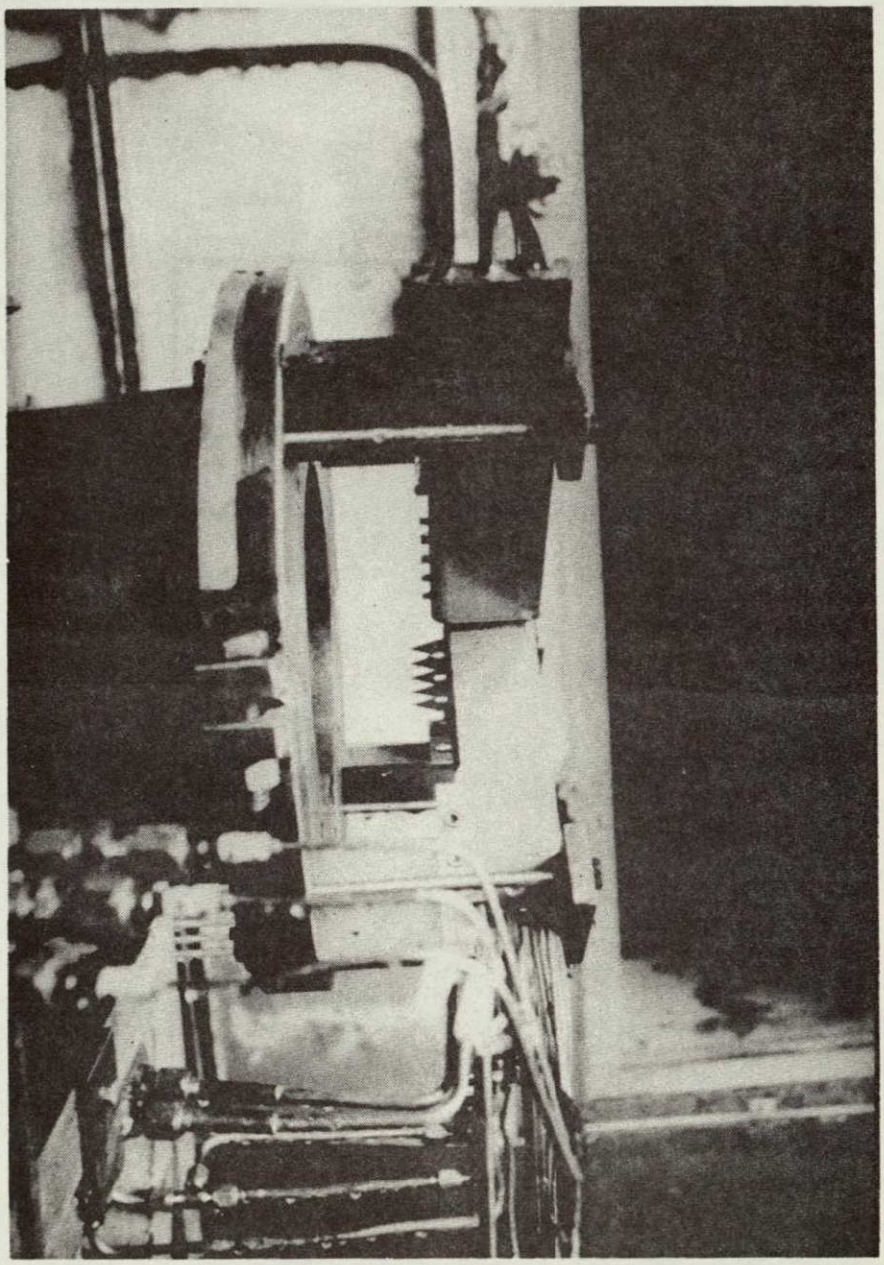

FIGURE 27 INSTALLATION OF INSTRUMENTATION RAKE

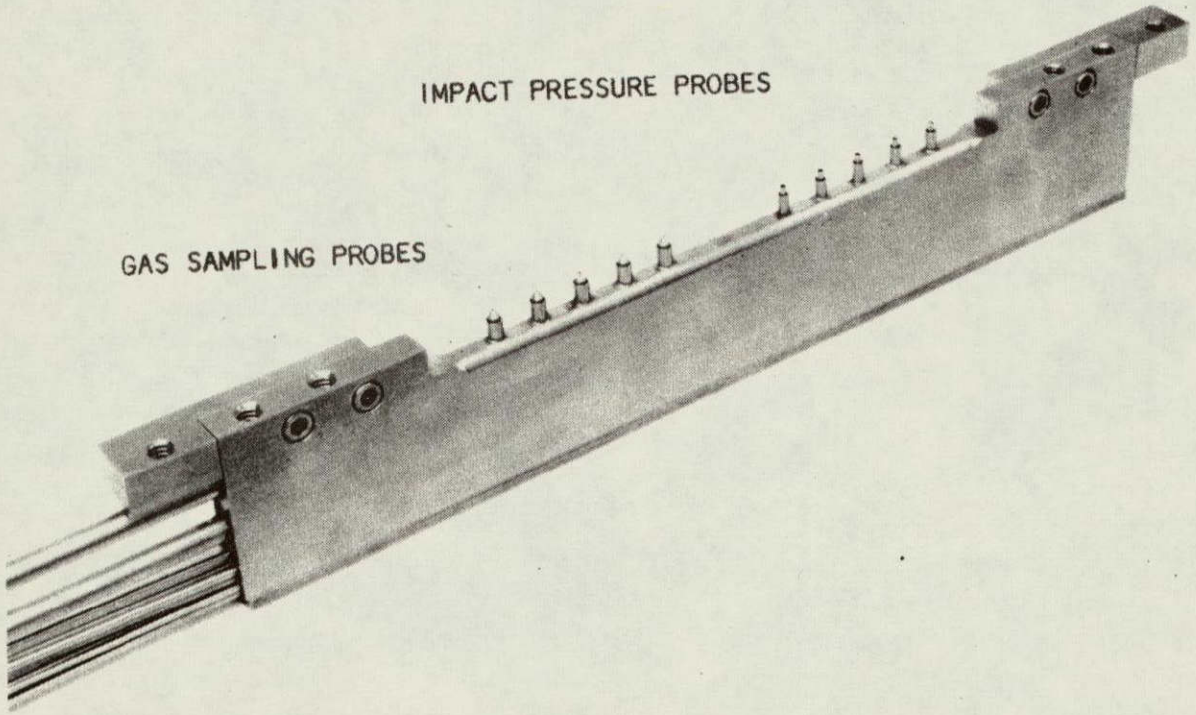

FIGURE 28 IMPACT PRESSURE AND GAS SAMPLING PROBE ASSEMBLY

FIGURE 29 SCHEMATIC OF IMPACT PRESSURE AND GAS SAMPLING PROBE ASSEMBLY

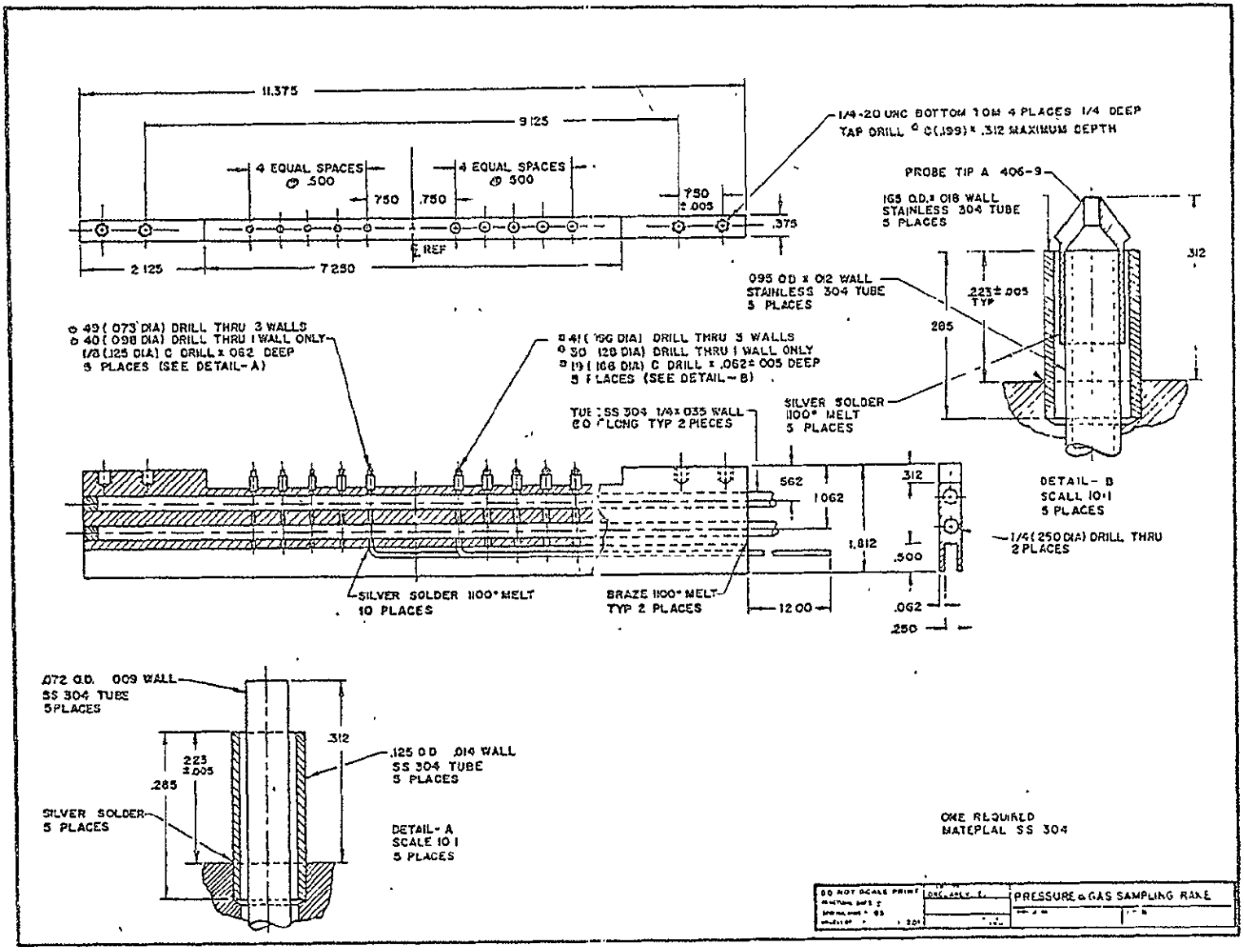
11.375
9.125
4 EQUAL SPACES @ .500
4 EQUAL SPACES @ .500
.750
.750
.750 ±.005
.375
2.125
7.250
1/4-20 UNC BOTTOM TOM 4 PLACES 1/4 DEEP
TAP DRILL Q C(.199) x .312 MAXIMUM DEPTH
PROBE TIP A 406-9
.165 O.D. x .018 WALL STAINLESS 304 TUBE 5 PLACES
.312
.095 O.D. x .012 WALL STAINLESS 304 TUBE 5 PLACES
.223 ±.005 TYP
.285
SILVER SOLDER 1100° MELT 5 PLACES
DETAIL- B SCALE 10:1 5 PLACES
Q 49 (.073 DIA) DRILL THRU 3 WALLS
Q 40 (.098 DIA) DRILL THRU 1 WALL ONLY
1/8 (.125 DIA) C DRILL x .062 DEEP
5 PLACES (SEE DETAIL-A)
Q 41 (.096 DIA) DRILL THRU 3 WALLS
Q 30 (.128 DIA) DRILL THRU 1 WALL ONLY
Q 19 (.166 DIA) C DRILL x .062± .005 DEEP
5 PLACES (SEE DETAIL-B)
TUBE SS 304 1/4 x .035 WALL
60 LONG TYP 2 PIECES
.562
.1062
.312
1.812
.500
1/4 (.250 DIA) DRILL THRU 2 PLACES
SILVER SOLDER 1100° MELT 10 PLACES
BRAZE 1100° MELT TYP 2 PLACES
1.200
.062
.250
.072 O.D. .009 WALL SS 304 TUBE 5PLACES
.312
.223 ±.005
.285
.125 O.D. .014 WALL SS 304 TUBE 5 PLACES
SILVER SOLDER 5 PLACES
DETAIL- A SCALE 10:1 5 PLACES
ONE REQUIRD
MATERIAL SS 304
DO NOT SCALE PRINT
PRESSURE & GAS SAMPLING RAKE

FIGURE 29

$$P_{t_e} = P'_t \frac{\left\{\left[\frac{2\gamma}{(\gamma+1)}\right] M_e^2 - \left[\frac{(\gamma-1)}{(\gamma+1)}\right]\right\}^{(1/\gamma-1)}}{\left\{\frac{[(\gamma+1)/2]\, M_e^2}{1 + [(\gamma-1)/2]\, M_e^2}\right\}^{(\gamma/\gamma-1)}}$$

The calculation requires iteration, due to the exit Mach number M_e being a function of the static pressure, p_{s_e}, and the ratio of specific heats γ_e. This discussion is presented in Appendix G.

The external shock experienced by the gas sampling probe tip is swallowed by evacuating the manifold connected to the five probe lines. The gas sample is quenched by rapid expansion through the probe with an internal area ratio of 12:1. The low probe internal pressure increases the molecular mean free path to slow down reaction rates. Quenching is further aided by the water cooling system. The gas samples was to be collected in stainless steel 10 ml storage bottles and later analyzed using a Bendix Time-of-Flight Mass Spectrometer. The gas sample analysis would have permitted the determination of the mass fraction x_j of each representative specie in the combustion product mixture, subject to errors resulting from finite rate quenching, probe wall catalysis, and other factors resulting in changes in chemical composition from actual exit conditions. These errors are not felt to be critical since an approximate value of the specific heat ratio of the combustion product mixture is sufficient to permit calculation of the combustion efficiency. Specific heat at constant pressure c_p is determined from

JANAF Thermochemical Data for the constituent species at the exit static temperature by the equation

$$c_{p_e} = \sum_j x_j \, c_{p_j}$$

The specific heat ratio at the exit plane γ_e is calculated from

$$\gamma_e = \frac{c_{p_e}}{c_{p_e} - R_u}$$

Again, the calculation is iterative and is presented in detail in Appendix G.

The static pressure probes of the cruciform instrumentation rake assembly consists of five 15° semi-vertex angle conical probes as shown in Figure 30. Four static pressure taps on each probe are aligned parallel and perpendicular to the probe arm. Figures 30 and 31 are respectively a photograph and assembly drawing of the probes. The tantalum-10 tungsten probe tips are cooled by water impingement on the inside of each tip, with subsequent discharge overboard through the coolant overflow ports. The indicated pressure was to be measured by Teledyne Model No. 206 gauge pressure transducers with a range of 0 to 300 psig. The shock wave system around the cone static probes is expected to present a complex pattern. In the plane parallel to the rake arm, it is anticipated that the interaction of the conical shock waves attached to the probes, together with the normal shock standing in front of the rake arm would generate an unpredictable shock pattern. Analysis indicated that for a 15° semi-vertex angle cone, shock

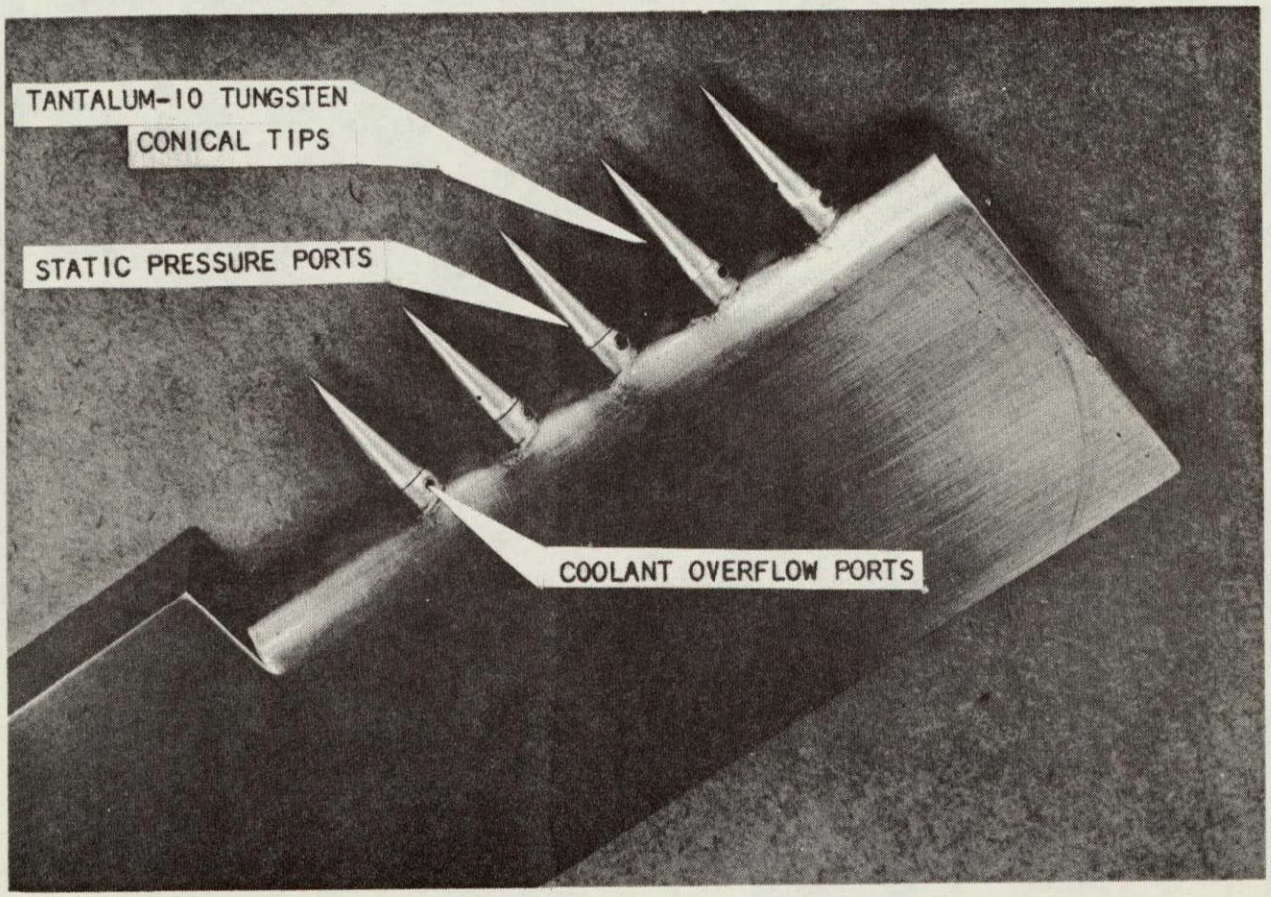

FIGURE 30 CONE STATIC PRESSURE PROBE ASSEMBLY

FIGURE 31 SCHEMATIC OF CONE STATIC PRESSURE PROBE ASSEMBLY

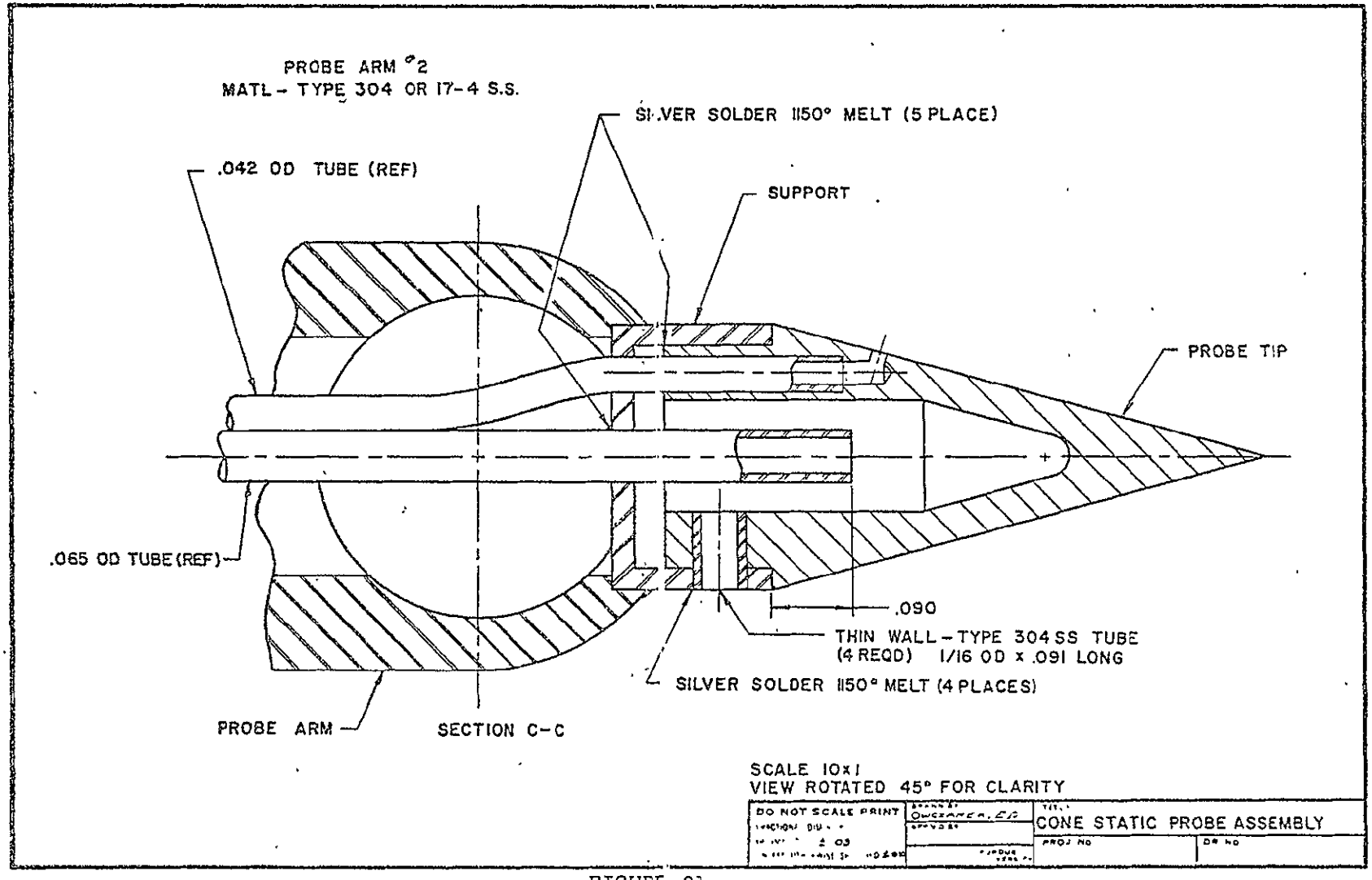
PROBE ARM #2
MATL - TYPE 304 OR 17-4 S.S.
SILVER SOLDER 1150° MELT (5 PLACE)
.042 OD TUBE (REF)
SUPPORT
PROBE TIP
.065 OD TUBE (REF)
.090
THIN WALL - TYPE 304 SS TUBE
(4 REQD) 1/16 OD x .091 LONG
SILVER SOLDER 1150° MELT (4 PLACES)
PROBE ARM
SECTION C-C
SCALE 10x1
VIEW ROTATED 45° FOR CLARITY
DO NOT SCALE PRINT
CONE STATIC PROBE ASSEMBLY
PROJ NO
DR NO

FIGURE 31

attachment will be maintained down to a Mach number of 1.12. (The supersonic combustor was designed for an exit Mach number of 2.0.) The taps aligned perpendicular to the arm should, however, see basically a conical shock pattern. Individual measurements from each of the four taps in each probe during calibration should help to resolve this problem and perhaps indicate that only these two tap positions should be used during operation. The relation between the cone static pressure p_s' and the exit static pressure p_{s_e} is discussed in Appendix G.

Radial temperature measurement presented a particularly difficult problem under the anticipated experiment conditions. Two methods were to be employed. The first provides static, temperature measurements using an optical system developed by Hofmann [22] at the Zucrow Engineering Research Center, Purdue University in 1968. The apparatus for making these measurements was developed in the initial phase of this program. Several preliminary experiments were run to evaluate the basic concept and to prove that the system would perform in the test environment. In these experiments, the optical system was operated in conjunction with the gas generator and employed to measure the static temperature of the vitiated air exhausting from the parallel flow nozzle.

The optical system consisted of a modified sodium line reversal pyrometer mounted on a base which moved vertically to permit the pyrometer to scan the hot gases across the plane of the combustor exit. Calibrated light from a tungsten strip lamp was focused on the center of the exhaust stream. This light beam is mechanically chopped

at a rate of 120 times per minute by a four bladed element driven by a synchronous motor. The resultant light is focused by a second condensing lens on the entrance slit of a monochromator where the intensity of the Sodium D-line is measured by a photomultiplier tube. Two intensity levels were observed, one with the flame plus strip lamp and the other with the flame alone. Since the tungsten strip lamp had been calibrated so that its temperature, as a function of voltage supplied (at the wavelength of the Sodium D-line) is known, the difference in intensity levels permitted a calculation of the "line of sight" average temperature of the flame. The line of sight intensity measurements were converted mathematically to a radial intensity-to-temperature profile using the Abel integral transform technique. The above-mentioned experiments met with limited success because the static temperature ($T_s \approx 1000°K$) at the nozzle exit was too low to produce a usable signal with the instrumentation available. Under these conditions the dissociation of sodium hydroxide is very small, but there still should have been a measurable adsorption and emission in this range. During the majority of the experiments, the emission detected was obscured by the noise level of the recording instruments. The signal-to-noise radio was continually improved as the experiments progressed and sufficient data were recorded to give a temperature measurement within 180°K of the calculated equilibrium temperature. It was felt that with the higher static temperatures generated in the combustion of vitiated air and gaseous hydrogen and additional refinements on the instrumentation, that the pyrometer could operate in the test environment and produce meaningful results.

Additional details concerning the mathematical and operational procedures used to determine the temperature profile can be found in Reference 22, along with a comprehensive description of the optical system.

The second method of temperature measurement employs a film cooled thermocouple probe to measure impact temperature. This probe consists of a film cooled arm with positions for five 40 percent iridium / 60 percent rhodium versus iridium thermocouples in inconel sheaths insulated with magnesium oxide. The thermocouple material was selected to provide normal operating temperature measurements up to 2367°K with the possibility of short duration operation up to the melting point of 2644°K in an oxidizing atmosphere.

Film cooling is provided by passing water through 34 cooling ports 0.026 in. in diameter in the leading edge of the probe arm. This is illustrated in the photographs and assembly drawing of the probe as presented in Figures 32, 33, and 34. The thermocouple hot junctions are positioned in an aspirated copper tubing for the purposes of structural protection and to provide radiation shielding. This method of temperature measurement in a flowing stream has been successfully employed at NASA Lewis in their supersonic combustion program.

Blackburn and Caldwell [23] published reference tables for conversion of the 40 percent iridium / 60 percent rhodium versus iridium emf output in millivolts to temperature from 273°K to 2373°K. Uncertainties in the range of 1644°K to 2367°K are believed to vary from 156°K to 158°K. The calibration uncertainties, however, are expected to be minor compared to other anticipated measurement errors.

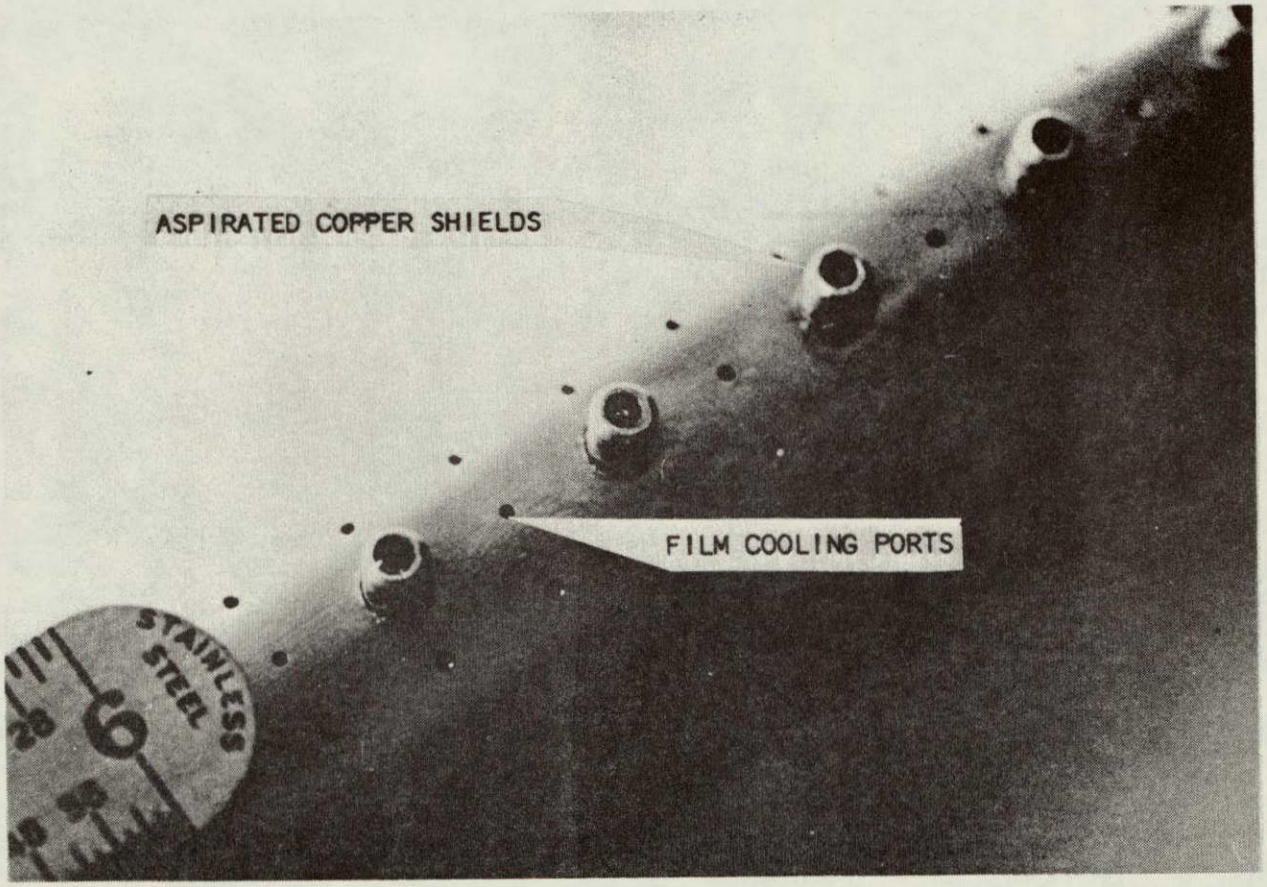

FIGURE 32 HIGH TEMPERATURE THERMOCOUPLE PROBE

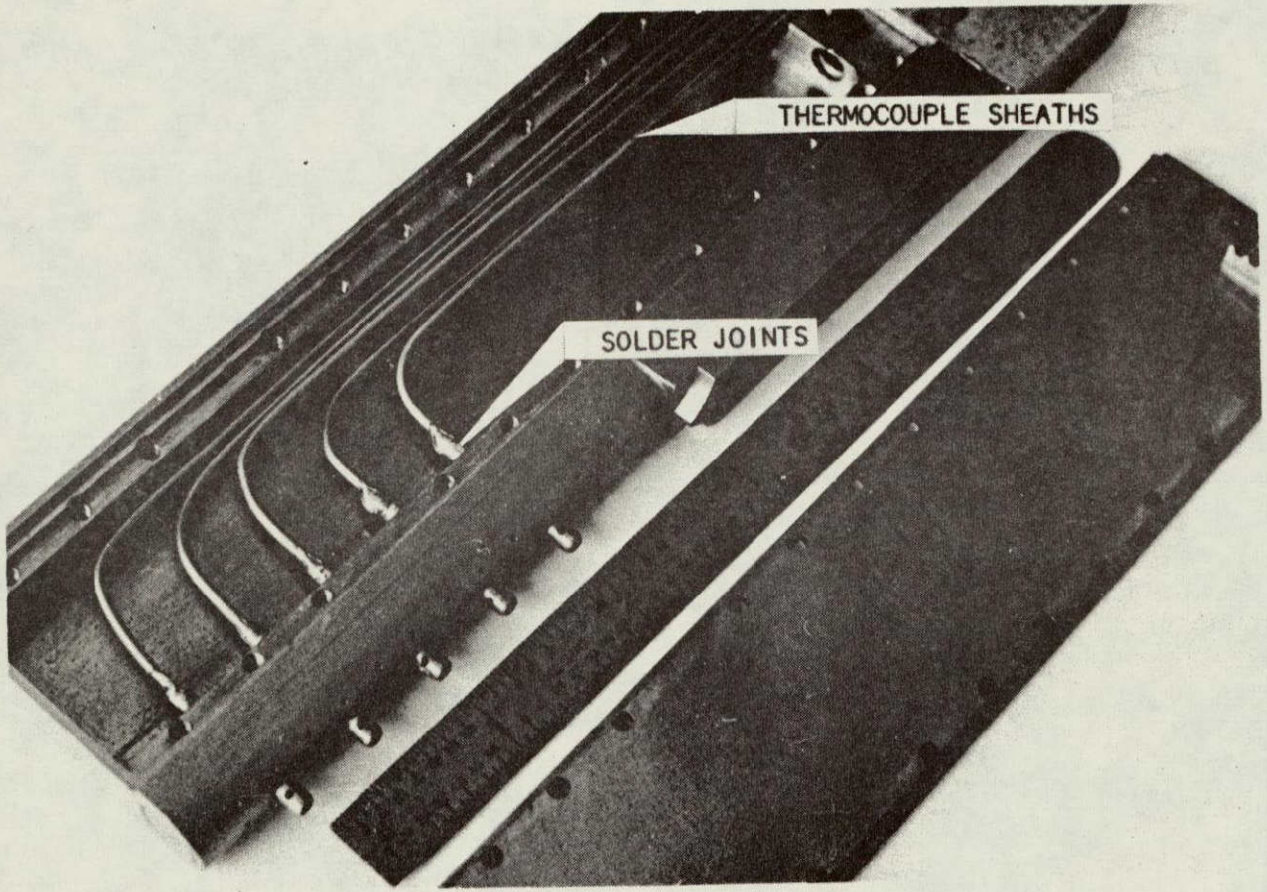

FIGURE 33 INTERIOR OF HIGH TEMPERATURE THERMOCOUPLE PROBE

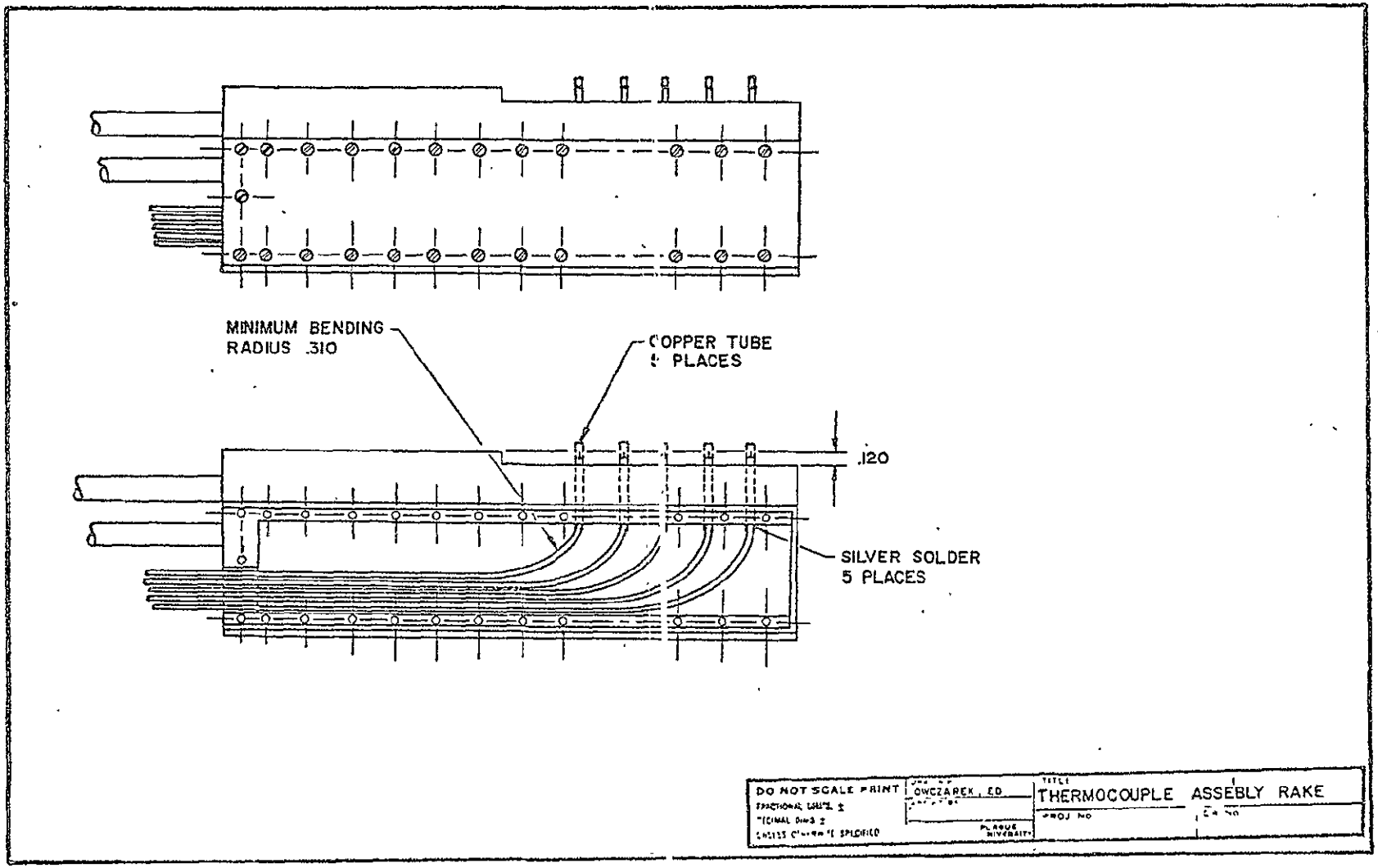

FIGURE 34 SCHEMATIC OF THERMOCOUPLE ASSEMBLY

The recovery factor for this type of probe would normally be expected to be about 98 percent, introducing a 4°K - 6°K error in the 2222°K - 2800°K range. However, significant errors which may result in recovery factors greater than unity may result from radiation in the high-water-content combustion products and from possible dissociated hydrogen recombination on the thermocouple junctions. Additional errors are introduced by the necessity of cooling the thermocouple sheaths. The magnitude of these errors are not predictable or measurable.

It would have been necessary to calculate the exit static temperature, T_{s_e}, from the impact temperature, T_{t_e}, which is equal to the total temperature (T_t) across an assumed adiabatic normal shock formed in front of the probes. The appropriate equation which can be employed is

$$T_{s_e} = \frac{T_{t_e}}{\left[1 + (\gamma_e - 1)/2\ M_e^2\right]}$$

Since the specific heat ratio, γ_e, and exit Mach number, M_e, are also unknown, this calculation will be iterative. This discussion is presented in Appendix G.

It was anticipated that the sodium-line/reversal technique for static-temperature measurement would provide a reasonable check on the thermocouple method.

Experimental Results

The experimental program was conducted essentially in two phases. In the first phase, the gas generator was developed to a level where it could be operated with a high degree of reliability. It was also necessary to demonstrate that the gas generator would operate repeatedly at high combustion efficiencies ($\eta_c \geq 93\%$) in order that the gas composition and state properties could be reasonably estimated by theoretical techniques. To attempt to achieve high combustion efficiency, the gas generator had a large characteristic length ($L^* \sim 120$ in.) and a turbulence ring to promote mixing and complete combustion of the exhaust products. Subsequent to the achievement of satisfactory operation of the gas generator, the supersonic combustion ignition delay experiments were undertaken. This constituted the second phase of the experimental program. Results from each phase of this program are discussed separately in the following sections. A limited number of supersonic combustion experiments which were intended as a prelude to the overall combustion efficiency investigation are also briefly discussed. A summary of the performance results from the overall experimental effort, except for the investigation accomplished with the initial system fabricated from stainless steel, is presented in Table 5. The tabulation presents stabilized propellant tank pressures, flow rates, chamber pressure and temperature when measured, hydrogen conditions, ignition delay data, a characteristic velocity (C^*) determined from measured values, and a C^* efficiency. The theoretical characteristic velocity employed to determine the C^* efficiency was calculated from an equilibrium thermochemistry computer

TABLE 5

GAS GENERATOR AND SUPERSONIC COMBUSTION EXPERIMENTS

Propellants: $N_2H_4/N_2O_4/N_2$ & $N_2H_4/N_2O_4/N_2 + H_2$

Run No:	1	2	3	4	5
Date:	3/27/69	3/27/69	4/1/69	4/1/69	4/1/69
Oxidizer System					
Tank Pressure (psig)	800	775	730	700	650
Flow Rate (lb/sec)	9.65	6.95	6.76	6.15	5.08
Fuel System					
Tank Pressure (psig)	780	1420	1290	1290	1290
Flow Rate (lb/sec)	1.09	1.74	1.58	1.58	1.59
Diluent N_2 System					
Line Pressure (psig)	890	840	900	940	950
Flow Rate (lb/sec)	2.86	2.08	1.75	1.92	1.98
Hydrogen System					
Line Pressure (psig)	-	-	-	-	-
Flow Rate (lb/sec)	-	-	-	-	-
G.G. Chamber Conditions					
Chamber Pressure (psia)	427	577	555	565	555
Measured Chamber Temp (°K)	§	§	§	§	§
Total Flow Rate (lb/sec)	13.6	10.77	9.09	9.65	8.65
Steady State Run Time (sec)	1.1	1.1	1.1	1.1	1.1
C^* (Measured) (ft/sec)	2013	3434	4000	3770	4099
C^* (Theoretical) (ft/sec)	3199	4072	4530	4070	4160
C^* Efficiency	0.63	0.84	0.88	0.93	0.99
Measured Ignition Delay (in)	-	-	-	-	-
Theoretical Ignition Delay (in)	-	-	-	-	-
H_2 Measured Manifold Temp (°K)	-	-	-	-	-
Equivalence Ratio	-	-	-	-	-
Purpose of Run	|——— Balance System ———|				
Remarks	|—— Loose N_2 Line ——|				

§Not Measured

TABLE 5 (continued)

Propellants: $N_2H_4/N_2O_4/N_2$ & $N_2H_4/N_2O_4/N_2 + H_2$

Run No:	6	7	8	9	10
Date:	4/1/69	4/4/69	4/5/69	4/5/69	5/13/69
Oxidizer System					
Tank Pressure (psig)	700	700	675	700	1000
Flow Rate (lb/sec)	5.70	5.80	5.62	5.76	-
Fuel System					
Tank Pressure (psig)	1290	1290	1290	1280	1290
Flow Rate (lb/sec)	1.59	1.58	1.58	1.58	-
Diluent N_2 System					
Line Pressure (psig)	980	990	950	950	960
Flow Rate (lb/sec)	1.94	2.11	1.88	1.95	-
Hydrogen System					
Line Pressure (psig)	-	171	150	150	-
Flow Rate (lb/sec)	-	0.29	0.24	0.23	-
G.G. Chamber Conditions					
Chamber Pressure (psia)	555	563	555	559	-
Measured Chamber Temp (°K)	§	§	§	§	-
Total Flow Rate (lb/sec)	9.23	9.48	9.08	9.29	-
Steady State Run Time (sec)	3.3	3.4	3.4	3.2	1.1
C^* (Measured) (ft/sec)	3832	3820	3950	3880	-
C^* (Theoretical) (ft/sec)	4118	4120	4145	4145	-
C^* Efficiency	0.93	0.93	0.96	0.95	-
Measured Ignition Delay (in)	-	§	§	§	-
Theoretical Ignition Delay (in)	-	-	-	-	-
H_2 Measured Manifold Temp (°K)	-	§	533	582	-
Equivalence Ratio	-	1.05	0.9	0.86	-
Purpose of Run	Balance System	Balance System with H_2			Rebalance System with Larger ΔP Across Oxidizer Injector
Remarks					Line Failure

§Not Measured

TABLE 5 (continued)

Propellants: $N_2H_4/N_2O_4/N_2$ & $N_2H_4/N_2O_4/N_2 + H_2$

Run No:	11	12	13	14	15
Date:	5/29/69	5/29/69	5/29/69	6/4/69	6/4/69
Oxidizer System					
Tank Pressure (psig)	1000	950	1000	1100	1050
Flow Rate (lb/sec)	8.62	4.85	5.08	5.93	5.08
Fuel System					
Tank Pressure (psig)	1310	1310	1310	1280	1310
Flow Rate (lb/sec)	1.59	1.62	1.62	1.58	1.62
Diluent N_2 System					
Line Pressure (psig)	960	960	930	1010	940
Flow Rate (lb/sec)	1.94	1.96	1.91	2.1	1.92
Hydrogen System					
Line Pressure (psig)	-	-	-	171	171
Flow Rate (lb/sec)	-	-	-	0.28	0.28
G.G. Chamber Conditions					
Chamber Pressure (psia)	570	549	550	570	565
Measured Chamber Temp (°K)	§	§	§	§	§
Total Flow Rate (lb/sec)	12.15	8.42	8.61	9.61	8.62
Steady State Run Time (sec)	1.1	1.1	3.2	3.4	3.4
C^* (Measured) (ft/sec)	3006	4179	4091	3800	4200
C^* (Theoretical) (ft/sec)	3832	4220	4214	4043	4219
C^* Efficiency	0.78	0.99	0.97	0.94	1.0
Measured Ignition Delay (in)	-	-	-	§	§
Theoretical Ignition Delay (in)	-	-	-	-	-
H_2 Measured Manifold Temp (°K)	-	-	-	506	521
Equivalence Ratio	-	-	-	0.96	1.1
Purpose of Run	|— Rebalance System —|				Ambient Air Entrainment Effect
Remarks	Not Desired Mixture Ratio			NO H_2 Ignition	NO H_2 Ignition H_2 Temp Too Low

§Not Measured

TABLE 5 (continued)

Propellants: $N_2H_4/N_2O_4/N_2$ & $N_2H_4/N_2O_4/N_2 + H_2$

	16 6/4/69	17 7/23/69	18 7/23/69	19 7/23/69	20 7/23/69
Oxidizer System					
Tank Pressure (psig)	1050	1075	910	810	810
Flow Rate (lb/sec)	6.78	7.78	6.3	5.24	5.30
Fuel System					
Tank Pressure (psig)	1300	1284	1280	1244	1260
Flow Rate (lb/sec)	1.60	1.54	1.54	1.54	1.54
Diluent N_2 System					
Line Pressure (psig)	1010	970	960	960	960
Flow Rate (lb/sec)	2.1	2.0	1.95	1.95	1.95
Hydrogen System					
Line Pressure (psig)	172	-	-	-	-
Flow Rate (lb/sec)	0.28	-	-	-	-
G.G. Chamber Conditions					
Chamber Pressure (psia)	585	540	540	533	533
Measured Chamber Temp (°K)	§	§	§	§	§
Total Flow Rate (lb/sec)	10.48	11.82	9.79	8.73	8.79
Steady State Run Time (sec)	3.4	1.1	1.1	1.1	3.4
C^* (Measured) (ft/sec)	3576	3057	3534	3912	3886
C^* (Theoretical) (ft/sec)	3972	3862	4019	4127	4132
C^* Efficiency	0.90	0.79	0.88	0.95	0.94
Measured Ignition Delay (in)	§	-	-	-	-
Theoretical Ignition Delay (in)	-	-	-	-	-
H_2 Measured Manifold Temp (°K)	357	-	-	-	-
Equivalence Ratio	0.89	-	-	-	-
Purpose of Run	Ambient Air Entrainment Effect	Rebalance System			
Remarks	NO H_2 Ignition H_2 Temp Too Low and Fuel Pintle Burned	New Fuel Pintle Installed			

§Not Measured

TABLE 5 (continued)

Propellants: $N_2H_4/N_2O_4/N_2$ & $N_2H_4/N_2O_4/N_2 + H_2$

Run No:	21	22	23	24	25
Date:	7/25/69	7/25/69	7/25/69	7/25/69	8/3/69
Oxidizer System					
Tank Pressure (psig)	840	840	810	830	850
Flow Rate (lb/sec)	5.08	5.08	4.93	5.08	5.39
Fuel System					
Tank Pressure (psig)	1260	1280	1260	1260	1260
Flow Rate (lb/sec)	1.58	1.62	1.6	1.58	1.50
Diluent N_2 System					
Line Pressure (psig)	975	950	960	960	920
Flow Rate (lb/sec)	2.0	1.94	1.96	1.95	1.80
Hydrogen System					
Line Pressure (psig)	172	172	175	177	98
Flow Rate (lb/sec)	0.27	0.27	0.27	0.28	0.15
G.G. Chamber Conditions					
Chamber Pressure (psia)	553	545	543	540	533
Measured Chamber Temp (°K)	§	§	§	§	§
Total Flow Rate (lb/sec)	8.66	8.64	8.49	8.61	8.69
Steady State Run Time (sec)	3.3	3.3	3.3	3.3	3.3
C^* (Measured) (ft/sec)	4018	4042	4093	4019	3891
C^* (Theoretical) (ft/sec)	4157	4204	4204	4173	4129
C^* Efficiency	0.97	0.96	0.97	0.96	0.94
Measured Ignition Delay (in)	14	14	14	10	10
Theoretical Ignition Delay (in)	-	-	-	-	-
H_2 Measured Manifold Temp (°K)	680	683	654	731	757
Equivalence Ratio	1.06	1.03	1.06	1.01	0.59
Purpose of Run	⟵ Ambient Air Entrainment Effect ⟶				
Remarks	3 inch Plexi-glas Collar	3 inch Plexi-glas Collar	6 inch Plexi-glas Collar		

§Not Measured

TABLE 5 (continued)

Propellants: $N_2H_4/N_2O_4/N_2$ & $N_2H_4/N_2O_4/N_2 + H_2$

Run No:	26	27	28	29	30
Date:	8/3/69	8/4/69	8/4/69	8/4/69	8/8/69
Oxidizer System					
Tank Pressure (psig)	850	1550	1500	1450	1450
Flow Rate (lb/sec)	5.92	9.39	9.86	8.93	9.29
Fuel System					
Tank Pressure (psig)	1270	1440	1350	1300	1230
Flow Rate (lb/sec)	1.50	3.08	2.77	2.69	2.54
Diluent N_2 System					
Line Pressure (psig)	960	1500	1550	1580	1630
Flow Rate (lb/sec)	1.90	2.72	3.04	2.98	3.20
Hydrogen System					
Line Pressure (psig)	69	-	-	-	-
Flow Rate (lb/sec)	0.11	-	-	-	-
G.G. Chamber Conditions					
Chamber Pressure (psia)	537	990	975	915	909
Measured Chamber Temp (°K)	§	§	§	§	§
Total Flow Rate (lb/sec)	5.53	15.19	15.67	14.6	15.03
Steady State Run Time (sec)	3.3	1.1	1.1	1.1	1.1
C^* (Measured) (ft/sec)	3645	-	-	3976	3838
C^* (Theoretical) (ft/sec)	4038	-	-	4228	4080
C^* Efficiency	0.90	-	-	0.94	0.94
Measured Ignition Delay (in)	10	-	-	-	-
Theoretical Ignition Delay (in)	-	-	-	-	-
H_2 Measured Manifold Temp (°K)	745	-	-	-	-
Equivalence Ratio	0.39	-	-	-	-
Purpose of Run	Ambient Air Entrainment Effect	Balance System for High Chamber Pressure and High Flow Rate		Balance System for Supersonic Combustor Experiments	
Remarks					

§Not Measured

TABLE 5 (continued)

Propellants: $N_2H_4/N_2O_4/N_2$ & $N_2H_4/N_2O_4/N_2 + H_2$

Run No:	31	32	33	34	35
Date:	8/8/69	8/8/69	9/15/69	12/5/69	12/19/69
Oxidizer System					
Tank Pressure (psig)	1450	1450	1400	1400	1400
Flow Rate (lb/sec)	9.29	9.47	9.09	§	§
Fuel System					
Tank Pressure (psig)	1230	1220	1260	1260	1260
Flow Rate (lb/sec)	2.54	2.54	2.55	§	§
Diluent N_2 System					
Line Pressure (psig)	1640	1620	1590	§	§
Flow Rate (lb/sec)	3.22	3.18	3.22		
Hydrogen System					
Line Pressure (psig)	300	300	310	-	-
Flow Rate (lb/sec)	0.43	0.43	0.43	-	-
G.G. Chamber Conditions					
Chamber Pressure (psia)	918	900	938	-	-
Measured Chamber Temp (°K)	§	§	§	§	§
Total Flow Rate (lb/sec)	15.05	15.19	14.86	-	-
Steady State Run Time (sec)	3.3	3.3	3.3	-	-
C^* (Measured) (ft/sec)	3870	3759	4005		
C^* (Theoretical) (ft/sec)	4086	4086	4102		
C^* Efficiency	0.95	0.92	0.98		
Measured Ignition Delay (in)	-	-	-		
Theoretical Ignition Delay (in)	-	-	-		
H_2 Measured Manifold Temp (°K)	788	804	745		
Equivalence Ratio	0.98	0.97	1.0		
Purpose of Run	Supersonic Combustion Experiment with Combustor		Extend H_2 Burn Time to 2.0 sec Steady State	Overall Supersonic Combustion Efficiency Experiments	
Remarks				Aborted Both Runs	

§Not Measured

TABLE 5 (continued)

Propellants: $N_2H_4/N_2O_4/N_2$ & $N_2H_4/N_2O_4/N_2 + H_2$

Run No:	36	37	38	39	40
Date:	1/10/70	1/12/70	1/13/70	1/14/70	1/15/70
Oxidizer System					
Tank Pressure (psig)	1400	850	850	850	850
Flow Rate (lb/sec)	8.9	-	-	5.62	5.54
Fuel System					
Tank Pressure (psig)	1260	1260	1260	1260	1260
Flow Rate (lb/sec)	2.63	-	-	1.58	1.55
Diluent N_2 System					
Line Pressure (psig)	1620	980	980	970	970
Flow Rate (lb/sec)	3.3	-	-	1.98	2.0
Hydrogen System					
Line Pressure (psig)	-	-	-	175	186
Flow Rate (lb/sec)	-	-	-	0.28	0.29
G.G. Chamber Conditions					
Chamber Pressure (psia)	927	-	-	555	558
Measured Chamber Temp (°K)	§	-	-	1680	1569
Total Flow Rate (lb/sec)	14.83	-	-	9.18	9.10
Total Run Time (sec)	3.3	-	-	3.3	3.3
C^* (Measured) (ft/sec)	3965	-	-	3835	3893
C^* (Theoretical) (ft/sec)	4136	-	-	4108	4086
C^* Efficiency	0.96	-	-	0.93	0.95
Measured Ignition Delay (in)	-	-	-	8	15
Theoretical Ignition Delay (in)	-	-	-	7.6	8.0
H_2 Measured Manifold Temp (°K)	-	-	-	750	645
Equivalence Ratio	-	-	-	1.03	1.09
Purpose of Run	Gas Sample G.G. Products	Balance System for Ignition Delay Experiments		Ignition Delay Experiments	
Remarks		Aborted Both Runs, Fuel Valve Failure			

§Not Measured

TABLE 5 (continued)

Propellants: $N_2H_4/N_2O_4/N_2$ & $N_2H_4/N_2O_4/N_2 + H_2$

Run No:	41	42	43	44	45
Date:	1/15/70	1/15/70	1/16/70	1/16/70	1/16/70
Oxidizer System					
Tank Pressure (psig)	850	850	830	830	830
Flow Rate (lb/sec)	5.7	5.7	5.5	5.7	5.5
Fuel System					
Tank Pressure (psig)	1260	1260	1260	1260	1260
Flow Rate (lb/sec)	1.54	1.54	1.53	1.5	1.5
Diluent N_2 System					
Line Pressure (psig)	944	996	940	940	970
Flow Rate (lb/sec)	1.92	2.04	1.94	1.92	2.0
Hydrogen System					
Line Pressure (psig)	184	137	186	93	70
Flow Rate (lb/sec)	0.29	0.21	0.29	0.13	0.08
G.G. Chamber Conditions					
Chamber Pressure (psia)	555	558	540	540	543
Measured Chamber Temp (°K)	1551	1534	1588	1476	1476
Total Flow Rate (lb/sec)	9.18	9.29	8.90	9.12	9.04
Total Run Time (sec)	3.3	3.3	3.3	3.3	3.3
C^* (Measured) (ft/sec)	3834	3809	3835	3757	3886
C^* (Theoretical) (ft/sec)	4106	4067	4095	4060	4052
C^* Efficiency	0.93	0.94	0.94	0.93	0.96
Measured Ignition Delay (in)	10	16	19	11	14
Theoretical Ignition Delay (in)	7.9	7.97	8.7	7.53	7.19
H_2 Measured Manifold Temp (°K)	710	691	590	681	705
Equivalence Ratio	1.07	0.75	1.12	0.48	0.31
Purpose of Run	Ignition Delay Experiments				
Remarks					

[§]Not Measured

program. A typical data reduction analysis is presented and discussed in Appendix F.

Gas Generator Experiments

The objective of the first six runs was to balance the propellant flow rates and confirm the integrity of the system as a reliable apparatus. Line and injector resistances generated in the early series of experiments utilizing the stainless steel system [Ref. 3] were used to set the propellant tank pressure for the desired propellant flow rates. 1.25 moles of liquid nitrogen tetroxide, 1.0 moles of liquid anhydrous hydrazine and 1.4 moles of gaseous diatomic nitrogen comprised the propellant combination utilized to generate 9 lb/sec and 15 lb/sec of vitiated air at 600 psia and 1000 psia respectively in the gas generator.

As can be seen in Table 5, after the first three runs the system operated quite stably. The apparatus fabricated from copper gave no indications of overheating as the gas generator run times were increased. The nozzle's throat was measured before and after each run and no erosion or growth was found. Color photographs were taken of each gas generator run. The gas generator burns with a transparent (to visible wavelengths) exhaust.

Supersonic Combustion Experiments

The supersonic combustion experiments were primarily directed towards determining the effect of vitiated air on the ignition delay times when burning hydrogen. Mixing and subsequent combustion of the heated hydrogen took place in the gases flowing as a free jet without

any confining walls. Both streams were operated with a static pressure of 14.7 psia at the injection station in an attempt to minimize shock interactions in the exhaust gases due to the surrounding stmospheric conditions. By permitting the gases to mix and burn in an unconfined exhaust stream, the flame front could be visually observed and photographically recorded. A solid wall in the vicinity of the flame front can often have a catalytic effect on the ignition process. The absence of a confining duct should permit the experimentally determined flame front to be a function of the chemical kinetics of the reacting system of gases. There is a possibility of induction of ambient air into the mixing region of the hydrogen and vitiated air which could reduce the effective temperature of the mixture (longer delay times). This effect was investigated in a short series of experiments and is discussed later in this section.

The vitiated air enters the supersonic test section at Mach 2.9 with an average static temperature of 1000°K and a static pressure of 14.7 psia. The contoured nozzle of the gas generator was designed to produce these conditions with a chamber pressure of 600 psia. The hydrogen stream can be heated to a maximum temperature of 867°K in a stored energy heater which burns propane to heat a large stainless steel coil. Injection conditions for the hydrogen are Mach 1.0 with a static temperature of 500°K to 800°K (depending on objectives of the run) and a static pressure of 14.7 psia. The relative velocity ratio for the two streams at injection conditions is 1.08 (hydrogen/vitiated-air). These experiments had relatively large differences in static temperatures for the hydrogen (500°K - 800°K) and vitiated air

system (1000°K) at test section conditions. The relative temperature difference for these two streams makes it difficult to establish an "effective" mean temperature of the gases prior to ignition. An analytical attempt to establish such a temperature was made in order to correlate analytical and experimental data. The results of this attempt are discussed in the section entitled "Discussion of Analytical and Experimental Results." Injection of both streams at essentially the same temperature would eliminate this problem. If the hydrogen system was designed for a static temperature at injection equivalent to the vitiated air temperature, the heater would have to be designed to operate at 1200°K. The 867°K limit on the total temperature for the hydrogen was selected as a compromise to allow the use of relatively inexpensive materials in the construction of the hydrogen heater and downstream hardware.

Operation of the full supersonic combustion experiments was considerably more complex than operation of only the gas generator. Safety is a primary concern when handling hydrogen. Precautions were taken to assure that the gas generator products did not enter the hydrogen manifold at any time. A nitrogen purge system was employed to keep the hydrogen lines, heater, and manifold full of inert gas when the main hydrogen valve was shut off. This was accomplished by operating the main fuel valve for the hydrogen and the nitrogen purge valve off of the same pilot valve. Then, when the main hydrogen valve is in the off-position, the nitrogen purge valve is open and when the hydrogen valve opens, the nitrogen purge valve closes. A separate

valve located further upstream in the nitrogen purge line provides shut-off capability when the purge is not required.

Proper valve timing is essential for the supersonic combustion experiments. The main control valve for the hydrogen system is a Jamesbury ball valve which is pneumatically actuated. This valve opens relatively slowly, and is the last valve to open in the start-up sequence. The "signal" for the hydrogen valve to open is from a pressure switch which indicates that the gas generator has reached the desired operating pressure level. Opening time for the main hydrogen valve is approximately 1 sec. The time required to fill the heater, lines and manifold is also approximately 1 sec., so that 2 sec. of steady state gas generator operation are necessary before the hydrogen reaches the supersonic test section. Thus, for 2 sec. of steady state operation of supersonic hydrogen combustion, the gas generator must be operated for at least 4 sec. This has been done successfully with the all copper apparatus which has a theoretical capability of operation for 14 sec. prior to failure.

The objective of runs 7, 8, and 9 was to reconfirm system integrity and the ability to demonstrate the phenomenon of hydrogen ignition in a supersonic ($M = 2.9$) vitiated air stream. This phenomenon was photographically recorded on black and white motion pictures taken at 550 frames per second with a Fastex camera. Upon reviewing the motion pictures, the film velocity (frames per second) was sufficient to slow down the ignition process so that an approximate ignition delay length could be measured. This measurement is based on the position where the flame front (first emitted light) first appears.

A photographic history of the ignition phenomenon is shown in Figure 35. These six consecutive frames show the instant just prior and subsequent to ignition. Frame 1 (upper left) depicts the transparent nature of the gas generator products (vitiated air). Flow is from left to right. In the next frame (lower left) hydrogen ignition is assumed to have occurred because of the presence of the visible luminous flame front. At this state in the investigation no deliberate effort was made to accurately measure the actual ignition delay length, although it was possible to estimate this distance by comparison with known component dimensions in the photograph. A rough comparison of the annular hydrogen injector dimensions (10 in. in diameter) with the distance from it to the hydrogen flame front, measures an ignition delay length of approximately 10 in. In the three runs made during this short exploratory series (runs 7 through 9) with hydrogen injection, this same approximate distance was realized. As shown in frames 3, 4, 5, and 6, the hydrogen flame front propagates towards the point of injection and stabilizes approximately 2 in. downstream. This phenomenon occurred in all of the ignition delay investigations, but at slightly longer distances.

An attempt in run 10 to improve the C^* efficiency of the gas generator by increasing the pressure drop across the oxidizer injector (150 psi) to match that across the fuel injector (640 psi) resulted in a fuel line failure which severed one of the oxidizer inlet lines thereby causing a flash fire. Fortunately, the sequenced run time duration was at its minimum setting (1 sec. steady state) and negligible damage, except for a few singed transducer wires, was realized. Prior

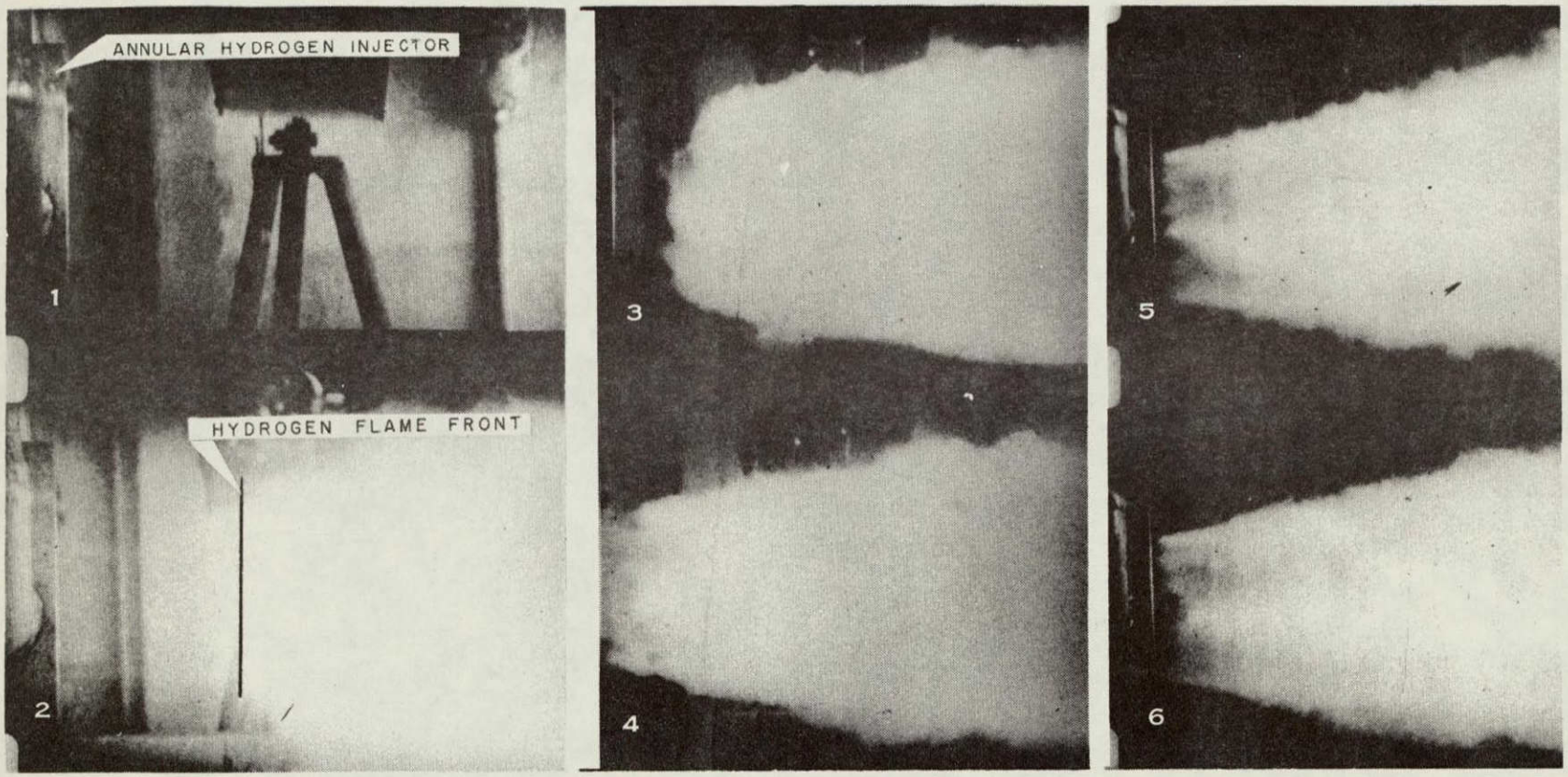

FIGURE 35 HISTORY OF IGNITION PHENOMENON OF VITIATED AIR AND HYDROGEN

to this stage in the investigation, the propellant feed system was plagued with occasional line failures either in the line itself or in the associated check valves. After a careful re-examination of the propellant feed system's design, the cause was identified and corrected. A discussion of these incidents is presented in the following paragraph.

In the design of the sequencing system which automatically schedules the experimental run, the prefire purge is allowed to terminate prior to activation of the fire initiation switch. This operation is necessary in order that the pneumatic propellant valve activation, which is also supplied by the purge line pressure, would have a positive response. The valve operation schedule has the oxidizer valve opening 0.05 sec. prior to the fuel valve. Since the purge is off at this instant, the oxidizer flows into the chamber and upstream in the fuel line toward the check valve. Consequently, the fuel first contacts the oxidizer in this line and ignition takes place. This point of contact is a function of the oxidizer tank pressure. Prior to run 10 in which the failure occurred, there was evidence of this type of over pressure. A slight bulge was discovered in the line connecting the fuel pintle injector and the check valve. It was believed at that time that this over pressure may have occurred during the very first gas generator runs which were slightly off mixture ratio. Nevertheless, the line was replaced prior to run 10 and closer observations were taken on subsequent firings.

The "fix" consisted of installing an auxiliary nitrogen fuel purge line which parallels the main fuel purge valve. This auxiliary

line which operates off of a manually operated switch on the control console permits the fuel line purge flow to continue after the main fuel purge valve has closed. A check valve was also installed in this auxiliary nitrogen purge line so that once the fuel flow pressure increased above that of the nitrogen purge, the nitrogen flow would be terminated until the fuel pressure diminished. Even though the fuel line continues to be purged during valve operation, the purge pressure is regulated at a low level so that valve operation is not compromised.

Runs 11 through 13 were used to verify the aforementioned cure and to rebalance the propellant flow system. The result of increasing the differential pressure across the oxidizer injector did not substantially improve the C^* efficiency but it did afford better control over the oxidizer flow rate, which is inherent with large injector pressure differentials.

During the course of the research for possible methods for the detection of the ignition delay length in a free jet, it became obvious that the physical characteristics of the hydrogen injection and combustion apparatus might generate false ignition data. It was suspected that the ambient air may have had a quenching effect on the synthetic-air/hydrogen mixture. The problem stems from the entrainment effect that the hydrogen injection stream's velocity has on the quiescent ambient air. The hydrogen stream flowing at sonic velocity entrains the cool ambient air and mixes it with the hydrogen. This mixture may be, in turn, mixed with the synthetic air. The overall result could be reduction in the rate of free radical production due to the lower temperature environment and a shortening of the ignition

delay length. Another possibility is that the oxygen supplied by the ambient air even though at a low temperature, may be an additional reacting source for OH radicals which would tend to lengthen the ignition delay. It was felt that since the hydrogen/ambient-air mixture is below the theoretical ignition temperature, that of the two aforementioned effects, the quenching effect would be dominant. The fact that the ambient air does have an effect on a test apparatus of this nature has been indicated experimentally in Reference 24.

The three experimental test runs (14, 15 and 16) made during this series were directed towards the determination of the ambient air entrainment effect. These particular runs were made with plexiglas collars of various fixed lengths (3 and 6 in.) fastened to the hydrogen injection manifold to isolate the hydrogen/vitiated-air mixture from the ambient air until ignition occurs. In all three runs problems were encountered. The results indicated the absence of sustained hydrogen ignition because of abnormally low hydrogen gas injection temperatures.

This conclusion was confirmed analytically and is discussed in the section of the thesis entitled "Discussion of Analytical and Experimental Results." The reason for the low hydrogen gas injection temperatures was attributed to the lack of "Process Gas Temperature Drop versus Time" data for the hydrogen gas heater. The temperature of the prepurge nitrogen process gas which flows through the hydrogen heater is monitored at the exit of the heater and at the hydrogen injector manifold--a distance of about 55 ft. of exposed tubing. Depending on the ambient conditions, the temperature drop between these

two points was as much as 167°K. The method employed on previous heated hydrogen runs was to flow nitrogen through the heater until the desired process gas temperature was obtained at the hydrogen injector manifold and then immediately firing the gas generator and flowing the hydrogen before the tubing had a chance to appreciably cool. This same technique could not be applied during this specific experiment because the hot nitrogen process gas would melt the plexiglas. This was demonstrated on the second heated hydrogen run of this series when the 6 in. plexiglas collar melted and distorted prior to the gas generator ignition. The method subsequently employed was to bring the process gas temperature up to the desired level, place the plexiglas collar on the hydrogen manifold, bring the fuel and oxidizer pressures up and then fire. Unfortunately, during the interim the tubing cooled excessively thus lowering the hydrogen inlet temperature below an ignition temperature. To alleviate this problem all exposed tubing was insulated and weather-proofed. In addition, a series of experiments were performed on the hydrogen gas heater in order to get reliable information on process gas temperature drop versus time. These experiments indicated that once the insulation was heated, the temperature drop, for a period of approximately 1 min. was as low as 32°K. In subsequent system experiments which employed the hydrogen heater (to be reported later in this section) measured hydrogen gas exit temperatures as high as 803°K were obtained. All experiments which required heated hydrogen were initiated when the nitrogen gas, which is the process gas, had a measured heater exit temperature of at

least 840°K. The maximum process gas temperature of the hydrogen gas heater is 867°K.

Once these heater checks were completed, a repeat of the ambient air entrainment effect investigation was accomplished. This experimental effort consisted of four runs (21, 22, 23 and 24). Two of the four runs were made with the 3 in. collar, one with the 6 in. collar and the remaining run without any collar for comparison. All four experimental runs were held to similar operating conditions within the limitations of the system, as noted in Table 5. It is felt that the operating conditions maintained in all four runs were within the constraints which would make a comparison of ignition delay with and without the plexiglas collar meaningful. High speed Fastex 16 mm motion pictures taken at a rate of 550 frames per second, using 4X - reversal black and white film, was the instrumentation used to determine the effect of the ambient air entrainment on the ignition delay. Although the Fastex camera is capable of taking pictures at a rate of 15,000 frames per second, the system is limited to 550 frames per second because of the available light or luminosity of the hydrogen/vitiated-air mixture upon reaction.

The ignition delay lengths were determined by comparing the position where the flame front first appears on the film with a graduated scale also photographed. The flame front was quite pronounced as demonstrated in previous experimental runs in which high speed photographs were taken of the ignition process. This pronounced flame front lent itself to easy measurement. The result is that relatively speaking, the effect of ambient air entrainment, even though evident

(14 in. versus 10 in.), is minimal. Another observation in this series of experiments is that it was possible to observe the stabilization of the supersonic hydrogen/vitiated-air combustion's flame front relative (∿ 2 in.) to the hydrogen injection point well within the plexiglas collar. This observation confirmed the fact that mixing of the hydrogen and vitiated air streams is rapid enough to react well within the constant area mixing duct of the complete engine. Once combustion stabilized, the plexiglas collar melted and was blown away.

In the next sequence, two preliminary runs (25 and 26) were made to determine the effect on the ignition delay of varying the equivalence ratio. One run was made at an equivalence ratio of 0.586 and the other at 0.39. Again an ignition length of approximately 10 in. was measured with operating conditions similar to those tabulated previously. The observation of the independence of the ignition delay on equivalence ratio is supported by theory, as discussed in the analytical section of this thesis.

The next experimental series consisted of nine runs (27 through 35) in which the first four were used to balance the propellant system, for 15 lb/sec of vitiated air at a chamber pressure of 1000 psia. The last five runs (31 through 35) were made employing the whole copper engine (gas generator plus constant area mixing section and the diverging area supersonic combustor). Prior to this series the complete gas generator was disassembled, inspected and reassembled. The mating flanges between combustion chambers, injector face and nozzle were refinished to insure better sealing qualities at the elevated chamber pressures. After 30 firings the only change in the

gas generator, except for discolorations, was that the nozzle throat diameter had decreased from 1.596 in. to 1.583 in. or approximately 0.814 percent. This throat area reduction has been taken into account in the determination of the C^* efficiency; it is negligible.

Runs 31 and 32 were the first runs made with the supersonic combustor and constant area mixing duct assembled to the gas generator. Hydrogen and vitiated air combustion was detected by static pressure measurement along the divergent supersonic combustor section and by color photography. As indicated by the pressure measurements and 35 mm color slides, sustained stable hydrogen and vitiated air supersonic combustion was achieved in both runs. A photograph showing this phenomenon is presented as Figure 36.

The results of these two runs indicated that the engine design is capable of performance which would have given meaningful results in the overall combustion efficiency investigation. Both runs were slightly oxidizer rich, with the design flow rate of 9.17 lb/sec. The off mixture ratio accounted for the relatively low chamber pressure. Experience indicates that this engine design is quite sensitive to the design mixture ratio. If the mixture ratio is varied from the design by approximately 14 percent, the C^* efficiency decreases significantly. In the calculation of the C^* efficiency the most important parameter is the gas generator chamber pressure. As indicated in Table 4, the chamber pressure during an experimental run is recorded simultaneously on a strip chart, an oscillograph and a digital tape. The output of these instruments when compared, indicated reliable measurements of the chamber pressure within ± 30 psi of the tabulated values. This

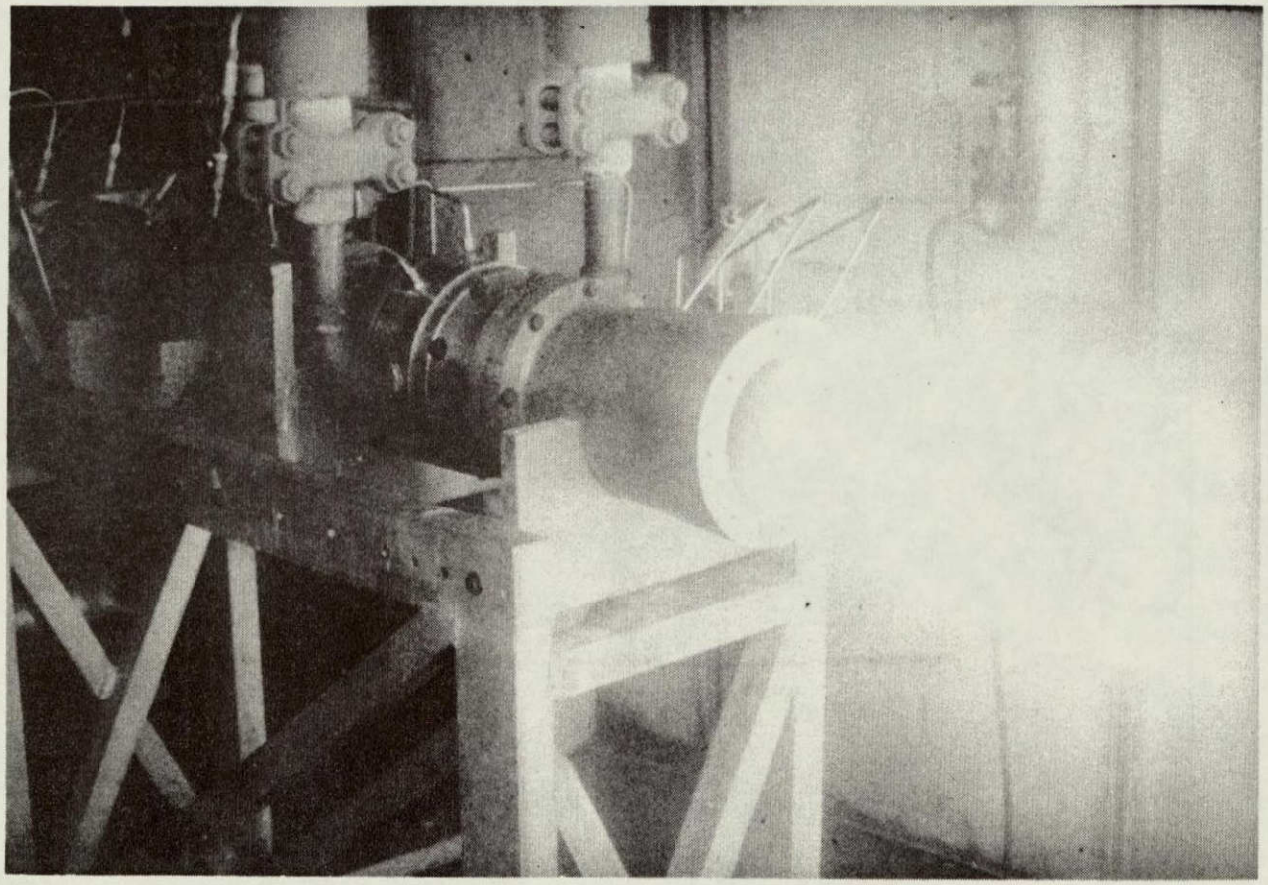

FIGURE 36 SUPERSONIC COMBUSTOR FIRING

accuracy is considered acceptable for the range of pressures measured ($P_c \sim 930$ psia).

Even though 1.4 sec. of hydrogen burn time was obtained, only 0.5 sec. was at steady state. Therefore, in order to get more accurate results from the instrumentation, the hydrogen steady state burn time should be extended to at least 2 sec. In run 33 the hydrogen burn time was increased to 3.5 sec. with approximately 2.0 sec. of steady state operation. In this run the propellant flow conditions were close to design with the results being an increase in chamber pressure and C^* combustion efficiency. The increase in hydrogen burn time was made without increasing the gas generator burn time by increasing the timing relay setting on the hydrogen injector supply valve. An external energy source (oxy-acetylene torch) was positioned downstream of the system as an ignition device in case there should be residual hydrogen gas flow during gas generator shut-down. Since safety is a requirement, when the engine's propellant flow sequencing schedule was first developed prior to running with the hydrogen system, approximately 3 sec. of gas generator operation was included after the initiation of the closing of the hydrogen fuel valve. This insured that in case of a hydrogen fuel valve interruption, there would be vitiated air present for reaction. Experience has proven the reliability of the hydrogen valve, and the valve was scheduled to remain open for an additional 2.0 sec., giving the desired increased hydrogen burn time.

The pressure measurements taken on the constant area mixing section and divergent supersonic combustor indicated stable hydrogen combustion for approximately 2.0 sec. A slightly greenish color flame

appeared for the first time in the color slides which were taken of the longer hydrogen burn time run. Upon a post inspection of the engine, a small peripheral area just downstream of the hydrogen annular injection station showed signs of some sort of reaction which might account for this slightly greenish flame. The surface appeared dark and felt slightly rough to the touch. All other parts of the combustor were smooth and showed no signs of the previous described conditions. This greenish color flame was not observed during the prehydrogen ignition gas generator operation phase of the run.

The results of run 33 indicated that the system was operating as close to design as could be expected. Preparations were initiated for the preliminary overall supersonic combustion efficiency experiments. The required instrumentation, as described previously, was installed and checked out for operational reliability. During the interim (3 weeks) between runs 33 and 34 the project was beset by sub-zero ambient conditions which inherently generated formidable problems. Hydrazine which freezes at 275°K (34°F) was the cause of primary concern. With the aid of auxiliary test cell heaters to prevent hydrazine fuel and instrumentation coolant line freeze ups, runs 34 and 35 were attempted. Both ended in aborts due to hydrazine fuel valve activation failures. Since the project's allotted time and funding were rapidly approaching the point of exhaustion, the decision was made to concentrate the remaining portion of the project on the investigation of the effects of vitiated air on ignition delay. No additional experimental runs to obtain data on the overall supersonic combustion efficiency were made.

In order to completely describe the vitiated air effects on ignition delay, as many properties of the gas generator and its products of combustion (vitiated air) as possible must be measured. Since the high temperature iridium 60 percent rhodium/iridium thermocouples and gas sampling probes which were to be used in the overall combustion efficiency phase of the project were already fabricated, minimum time and effort were spent preparing these items for use in the measurement of the gas generator chamber temperature and the sampling of the vitiated air stream.

The primary objective of run 36 was to capture a vitiated air gas sample for analysis. The hydrogen system was not employed during this specific task. Successful operation of the gas sampling system resulted in the capturing of a representative sample of the vitiated air stream. A comprehensive description of this system is expanded in Appendix E. The captured sample was analyzed by the Chemistry Department, Purdue University on a Bendix Time-of-Flight Mass Spectiometer. Interpretation of the resultant spectra was done at the Air Force Aerospace Research Laboratory, Wright-Patterson Air Force Base under the guidance of Dr. Thomas O. Tiernan.

The fundamental objective of gas sampling is to obtain a sample which is representative of the composition of the fluid at the sampling point. One of the most prominent sources of errors in this type of measurement is that the sample can change during its passage through the sampling system due to condensation of vapor phases. In this particular system, water vapor theoretically accounts for 19 percent of the total weight in the vitiated air stream. If this

vapor should condense, it would most likely do so in the sample collection bottle. The effect of this would be to form aqueous solutions of various components such as nitric acid, etc., thereby destroying the original sample composition. Since accurate water estimates are not required for the analysis, water vapor is effectively removed by passing the captured sample through a Type 3A, Linde Molecular Sieve adsorbent. 1/16 in. pellets were the size employed. Type 3A Molecular Sieve adsorbs all molecules with an effective diameter of less than 3 angstroms, including water, ammonia and methanol [25]. Unfortunately, diatomic oxygen has an effective diameter of 2.8 angstroms and is slightly adsorbed also, but not as actively as the water vapor. This slight disadvantage in the use of this particular type of adsorbent should not seriously effect the results of the gas composition analysis.

The purpose of obtaining a vitiated air gas analysis was to attempt to determine the amount of nitric oxide (NO) and nitrogen dioxide (NO_2) in the vitiated air, and to compare the actual gas composition with that which was theoretically calculated by the Finite Rate Reacting Gas (FRRG) program. This specific computer program is discussed in the analytical section of this thesis. Theory and experiments indicate that nitric oxide and nitrogen dioxide have a catalyzing effect on the ignition process [12]. If this is so, then knowing the mass fraction or existence of these two constituents in the vitiated air stream should help justify experimental results. Also, the presence of nitrogen dioxide in the gas is a measure of the incompleteness of the gas generator combustion process. Nitrogen

dioxide is not one of the products of the complete reaction of nitrogen tetroxide and hydrazine.

The analysis of the vitiated air gas sample indicated that no nitrogen dioxide was present in the air stream. This means that the combustion process in the gas generator must have gone to completion and that the inefficiency as manifested in the less than 100 percent C^* efficiency was due to heat transfer and boundary layer effects. A heat transfer analysis across the chamber walls was done and is discussed later in this section.

In analyzing the gas sample spectra, the relative abundance of species by weight was shown to be O_2 = 17 percent, NO = 5.7 percent and N_2 = 76.0 percent. The remaining 1.3 percent of the sample was not determined. The analysis was accomplished by performing a mass spectrometer sensitivity check for known amounts of diatomic nitrogen, diatomic oxygen, water vapor, nitric oxide and nitrogen dioxide. These results were then applied to the gas sample's mass spectra output and the relative abundance calculated. The water vapor peak (m/e = 18) as compared to the background level was too small to be considered even though water vapor theoretically comprises 19 percent of the vitiated air composition. This insignificant presence of water vapor in the captured gas sample confirms the effective use of the Molecular Sieve adsorbent. It must be emphasized that the relative abundance of species previously reported are the relative amounts captured subsequent to passage through the Molecular Sieve adsorbent. Therefore, in order to ascertain the relative abundance of species in the vitiated air stream, the water vapor and any oxygen adsorbed by

the Molecular Sieve must be determined. The adsorbent bottle was weighed before and after the run in anticipation of being able to calculate the amount of water captured. However, after analyzing the gas sample, it became evident that some unknown amount of the oxygen must have been adsorbed also, thereby making any attempt to account for the water vapor adsorbed, fruitless. Nevertheless, meaningful information was obtained in the fact that there was a substantial amount of nitric oxide present in the sample. At first it was believed that the majority of the nitric oxide measured was due to the possible decomposition of nitrogen dioxide in the sample bottle by the reaction

$$NO_2 \rightarrow NO + O \ , \ \Delta H_R = 62 \text{ Kcal}$$

This reaction was found to be nonexistent at the level of temperature and pressure in the gas sample bottle. Approximately 62 Kilocalories of energy is required for the above endothermic reaction to proceed. To reconfirm the absence of nitrogen dioxide in the vitiated air stream, the fragmentation patterns for nitrogen dioxide and nitric oxide at 70 ev as found in Reference 26, were reviewed. The fragmentation pattern spectra for nitrogen dioxide showed that if nitrogen dioxide was present initially in the gas sample that there would be a representative nitrogen dioxide peak (m/e = 46). Since no significant nitrogen dioxide peak was found, it was concluded that nitrogen dioxide was never present in the gas sample.

If the assumption is made that the excess diatomic nitrogen which serves as the diluent in the overall gas generator combustion process does not significantly contribute to the reaction, then the known relative input amount of diatomic nitrogen should serve as a basis for comparison of the relative specie abundance measured, with that calculated by the FRRG program. Therefore, the relative abundance by weight of diatomic nitrogen measured 76 percent should be equivalent to the known relative amount input 55 percent. Utilizing this basis of comparison, the relative abundance by weight of the oxygen is changed from 17.0 percent to 12.3 percent and the nitric oxide from 5.7 percent to 4.0 percent. The remaining 28.7 percent is assumed to consist of the water vapor and diatomic oxygen adsorbed by the Molecular Sieve. Table 6 shows the relative abundance of species measured compared to that calculated by the FRRG program. The relatively good agreement between the data measured and that calculated by the FRRG program justifies using the results from the FRRG program for the analytical portion of the investigation.

Runs 37 and 38 whose purpose was to rebalance the system for lower chamber pressure (600 psia) and flow rate (9 lb/sec) in preparation for additional ignition delay runs were aborted due to hydrazine fuel valve failures. The fuel valve was dismantled and inspected. A loose cam set screw which allowed the cam shaft to rotate without rotating the cam was responsible for the malfunctions. This particular cam when rotated along with fuel valve actuation, activates a sequencing microswitch which allows the gas generator firing sequence to progress. Without this positive microswitch

TABLE 6

COMPARISON OF RELATIVE SPECIE ABUNDANCE BY WEIGHT

MEASURED VERSUS (FRRG) CALCULATED

Species	Measured	Calculated
O_2	12.3%*	23.80%
N_2	55.0%	55.00%
NO	4.0%	0.36%
H_2O	*	19.00%
	71.3%	98.16%

*Part of specie O_2 and practically all of specie H_2O which accounts for 26.86% is assumed captured by the Molecular Sieve adsorbent.

activation, the sequencing mechanism senses that the fuel valve did not operate and automatically terminates the run. The problem was corrected and the investigation proceeded.

The remaining runs of the investigation were directed towards the collection of ignition delay data as a function of hydrogen temperature and equivalence ratio. Gas generator chamber wall heat transfer rates and chamber temperatures were also obtained. The average heat transferred through the chamber walls during the experimental runs is shown to account for at least a 2 percent decrease in C^* efficiency.

The heat transfer rate through the gas generator chamber walls was measured simultaneously with the chamber temperature and ignition delay lengths on all of the remaining runs (39 through 45). This was accomplished by mounting in the chamber wall two chromel alumel thermocouples at a depth of 0.813 and 1.563 in. respectively. The distance from the deeper thermocouple (1.563 in.) to the hot side of the chamber wall is 0.54 in. After each run the slope of the temperature increase for each thermocouple was compared for a quasi-steady temperature difference. The averaged difference was 86°K. Knowing the thermal conductivity of oxygen free electrolytic copper and the distance between the thermocouples, it was a relatively simple matter of applying Fourier's one-dimensional law of heat conduction for a hollow cylinder to get an approximate heat transfer flux rate of 1.54 BTU/in^2-sec. This efflux of heat was analytically accounted for in the measured C^* combustion efficiency of the gas generator.

To measure the gas generator chamber temperature two iridium 60 percent rhodium/iridium thermocouples mounted inside the chamber

cavity at depths of 0.37 and 1.125 in. respectively from the hot wall, were employed. The components of the thermocouple consist of a 0.062 in. inconel sheath with a magnesium oxide layer which insulates the two 0.010 in. diameter iridium 60 percent rhodium/iridium wires. A bead joining the two exposed thermocouple wires at a distance of 0.25 in. from the sheath material, formed the hot junction of the instrument. The thermocouples held up satisfactorily during the course of this investigation. Measurements were taken on all seven runs and were relatively consistent as indicated in Table 5. Temperature differences between the two thermocouples during the runs when averaged were approximately 76°K. The values of chamber temperature as listed in Table 5 are the uncorrected readings from the thermocouple positioned closest to the hot gas core (1.125 in.). A radiation and conduction thermocouple heat transfer error analysis was carried out according to the method outlined in Reference 27.

Results of the analysis indicated an average heat transfer error of approximately 5°K and 80°K for radiation and conduction respectively. The primary objective for measuring the chamber temperature was to verify the accuracy of the temperatures computed by the Finite Reaction Rate Gas (FRRG) program. Temperatures ($\sim$ 1700°K) measured and corrected for thermocouple losses did not compare favorably with corrected theoretical temperatures ($\sim$ 2100°K) calculated by the FRRG program. Reasons for the discrepency were not resolved since time was at a premium and the resulting effects of this discrepency on the investigation were felt to be minimal. However, due to the many unknowns associated with high temperature thermocouple

measurements, the temperatures computed by the FRRG program were considered to be the more accurate of the two. Therefore, the corrected theoretical temperatures were subsequently employed to generate an input temperature which is used in the Simplified Ignition Lag (SIL) program to calculate the theoretical ignition delay distance. The theoretical ignition length is compared with that experimentally measured for correlation. This correlation is discussed in the section "Discussion of Analytical and Experimental Results."

The actual ignition delay length data were photographically recorded on Kodak 4X-Reversal black and white film using a Fastex 16 mm camera at a film velocity rate of 550 frames per second. A photograph of the apparatus for observing and measuring the ignition phenomenon is presented as Figure 37. The apparatus is basically the same as when used as a simulated supersonic combustor except that the constant area mixing section and divergent combustor are removed and a graduated measuring scale is mounted on the side of the test stand for determining the ignition delay length. Since the vitiated-air/hydrogen mixture burns with a diffuse consistency, the dark background horizontal slot in the measuring scale emphasized the ignition distance and subsequent reaction phenomena. Each white stripe is an inch apart. The left side of the horizontal slot is in the exit plane of the hydrogen annular injector and thereby forms the datum point from which the exact ignition delay length is measured. The distance measured from this datum to the point of first light apparition is defined to be the ignition delay length. Figures 38, 39 and 40 are typical photographic data results of the experimental runs. Each figure

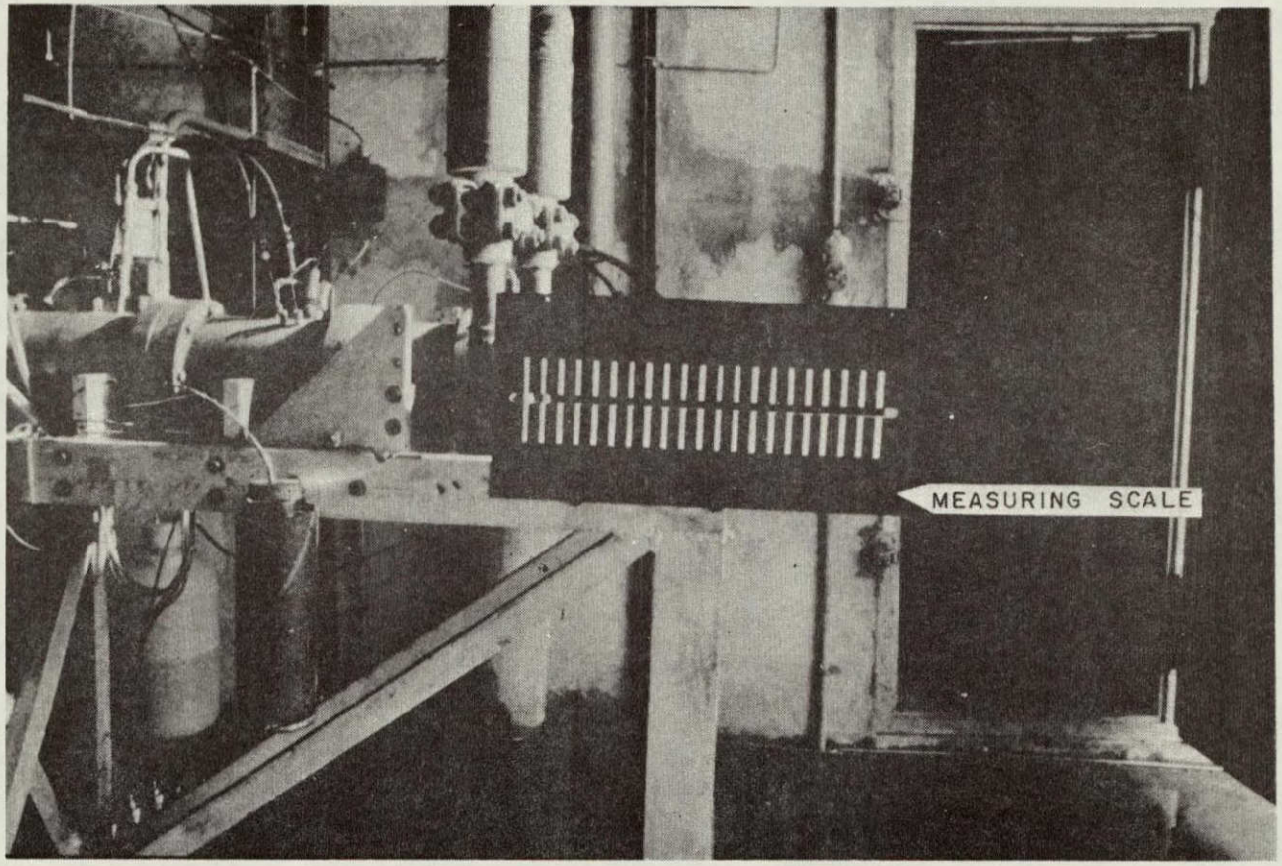

FIGURE 37 IGNITION DELAY MEASURING APPARATUS

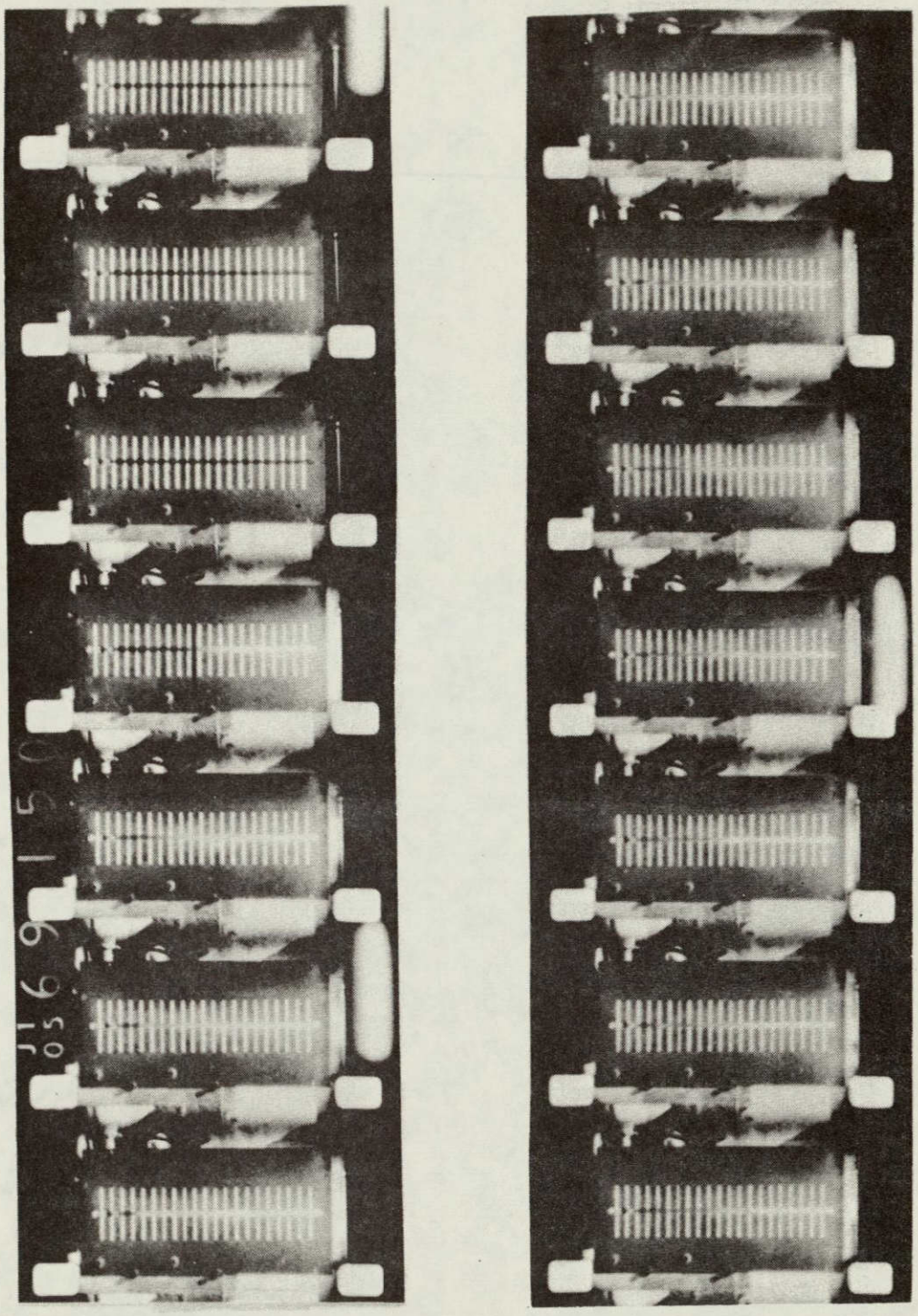

$L_{ID(EXP)}$ = 10 INCHES

T_{H_2} = 710°K

ϕ = 1,07

FIGURE 38 IGNITION DELAY - RUN 41

depicts 14 consecutive frames showing the instant before and after the onset of ignition. As can be seen in the photograph, the vitiated-air/hydrogen flame front lends itself to easy observation and measurement. In Figure 38, the fourth frame down shows the point of ignition. Counting the stripes from left to right indicates a distance of 10 in. The inked-in line highlights the line of demarcation between the dark background of the horizontal slot in the measuring scale and the vitiated-air/hydrogen combustion flame front. The white elongated marks on the extreme outer edge of the film strip are the film velocity timing marks which are generated at a frequency of 100 per sec. From this measurement the film velocity is calculated and verified. The film velocity as shown is approximately 550 frames per second. Careful review of the succeeding frames subsequent to the point of ignition, reveals that the flame front propagates towards the plane of hydrogen injection to about 3 in. and then oscillates between 3 and 7 in. This effect is believed to be a recirculation phenomenon and a function of the nozzle/injector-lip geometry.

In run 43 (Figure 39), the temperature of the heated hydrogen (T_{H_2} = 590°K) was just slightly above the autoignition temperature. It was demonstrated in runs 14 and 15 that hydrogen injected at a temperature of 506°K and 521°K would not ignite in this apparatus. Nevertheless, in run 39, ignition was realized but with a relatively long ignition delay length. Concentrating on the third and fourth frames down and in the immediate area to the extreme right side of the measuring scale, the onset of ignition is indicated by the illumination of this section. However, the flame front does not

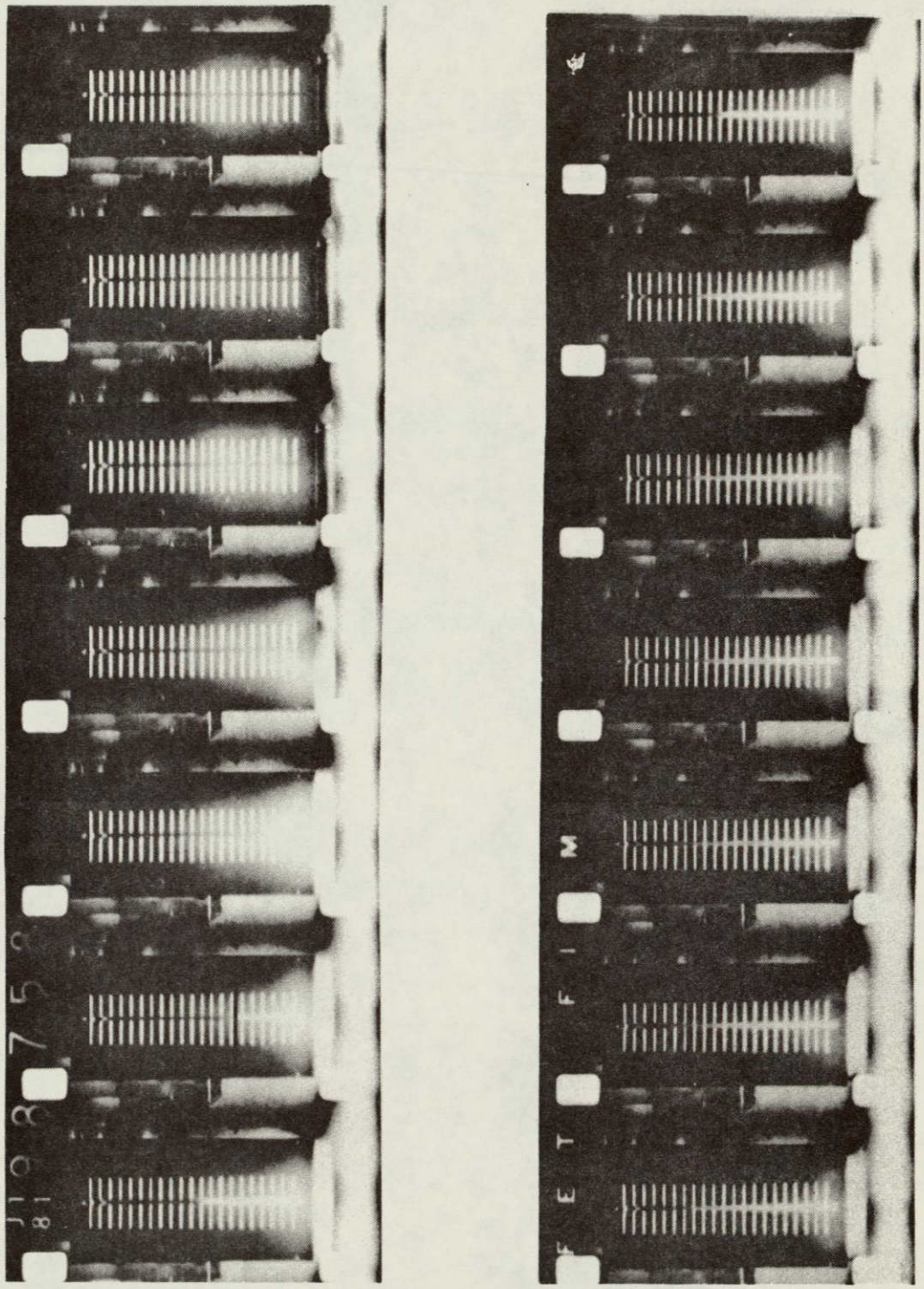

$L_{ID(EXP)}$ = 19 INCHES

T_{H_2} = 590°K

ϕ = 1.12

FIGURE 39 IGNITION DELAY - RUN 43

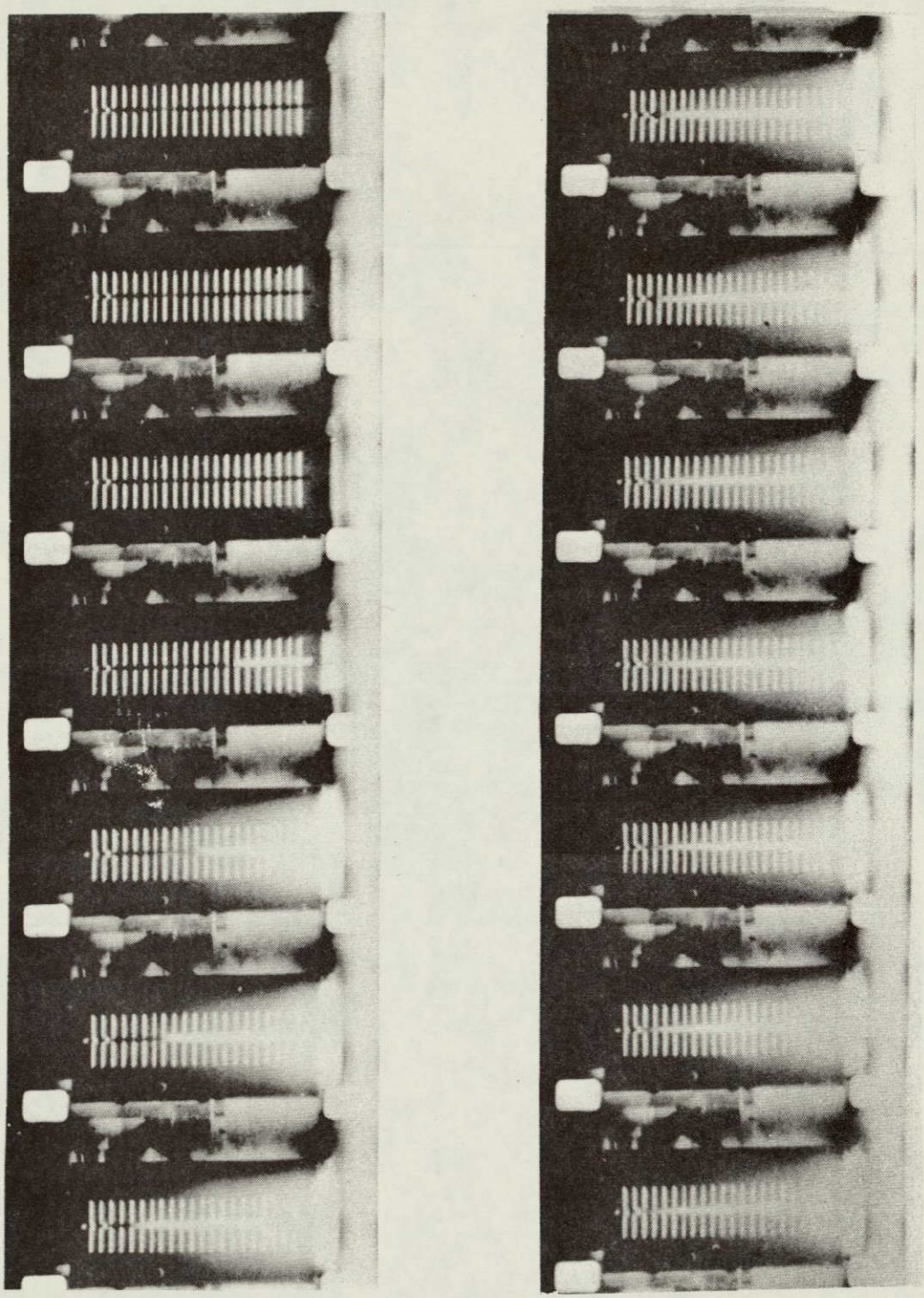

$L_{ID(EXP)}$ = 14 INCHES

T_{H_2} = 705°K

ϕ = 0.31

FIGURE 40 IGNITION DELAY - RUN 45

sharply appear until frame number 6. This indicates that the point of ignition is somewhere near the extremity of the measuring scale. By considering the flame front propagation speed (approximately 2 in. per frame) and assuming it constant, the point of ignition is calculated to be approximately 19 in. In this particular run the flame front stabilized at a distance of 8 in., which indicates hydrogen temperature as well as geometry may have a profound influence on the point of stabilization. No attempt was made to resolve this uncertainty.

Photographic data results of the other four runs are similar in nature to these presented. However, due to the lack of detail photographic sharpness in reproduction, they were purposely omitted. A compilation of the ignition delay data as a function of hydrogen manifold temperature and equivalence ratio is presented graphically as Figures 41 and 42. A comparison of these results with the analytical findings is discussed in the following section.

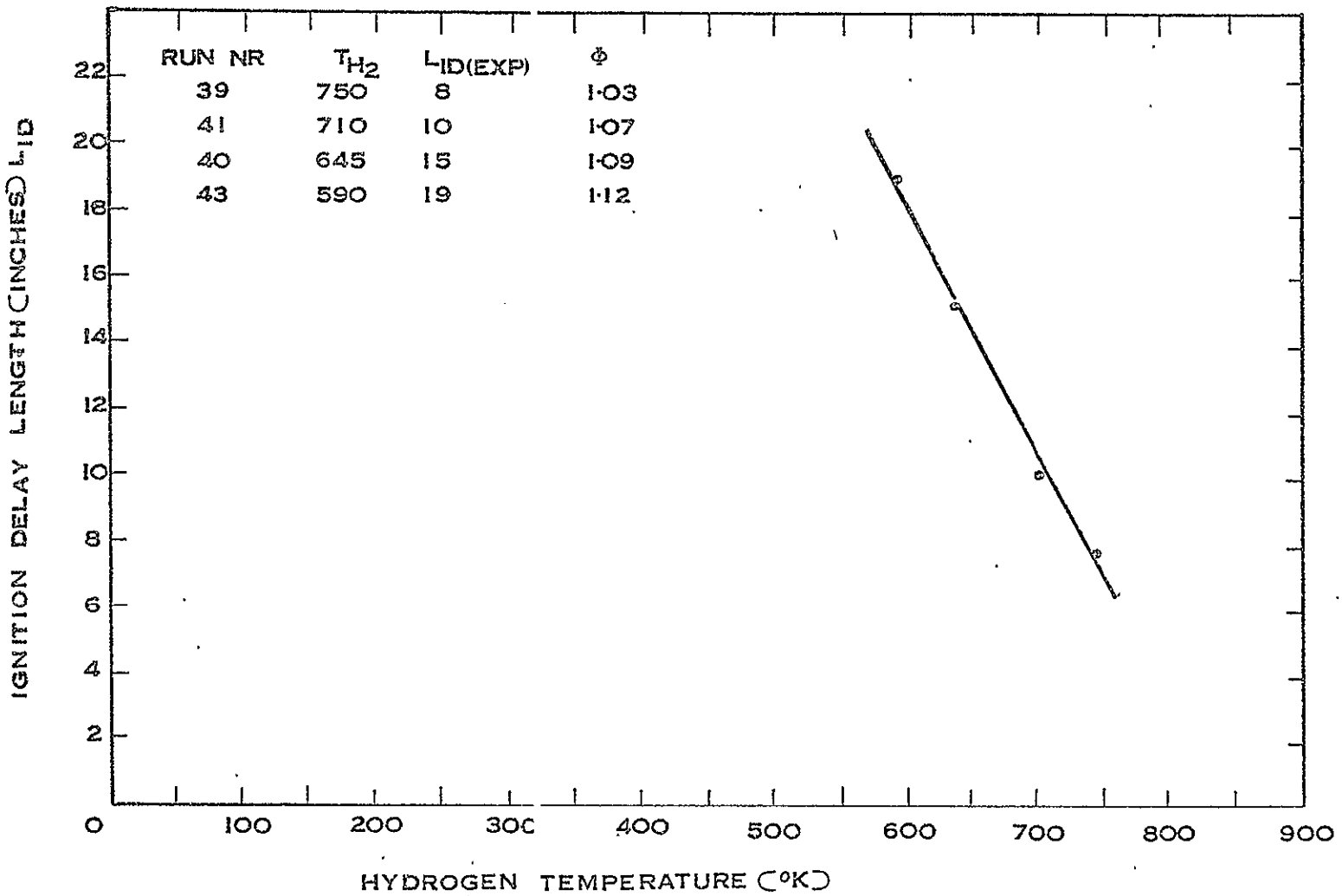

FIGURE 41 GRAPH IGNITION DELAY VERSUS H_2 TEMPERATURE

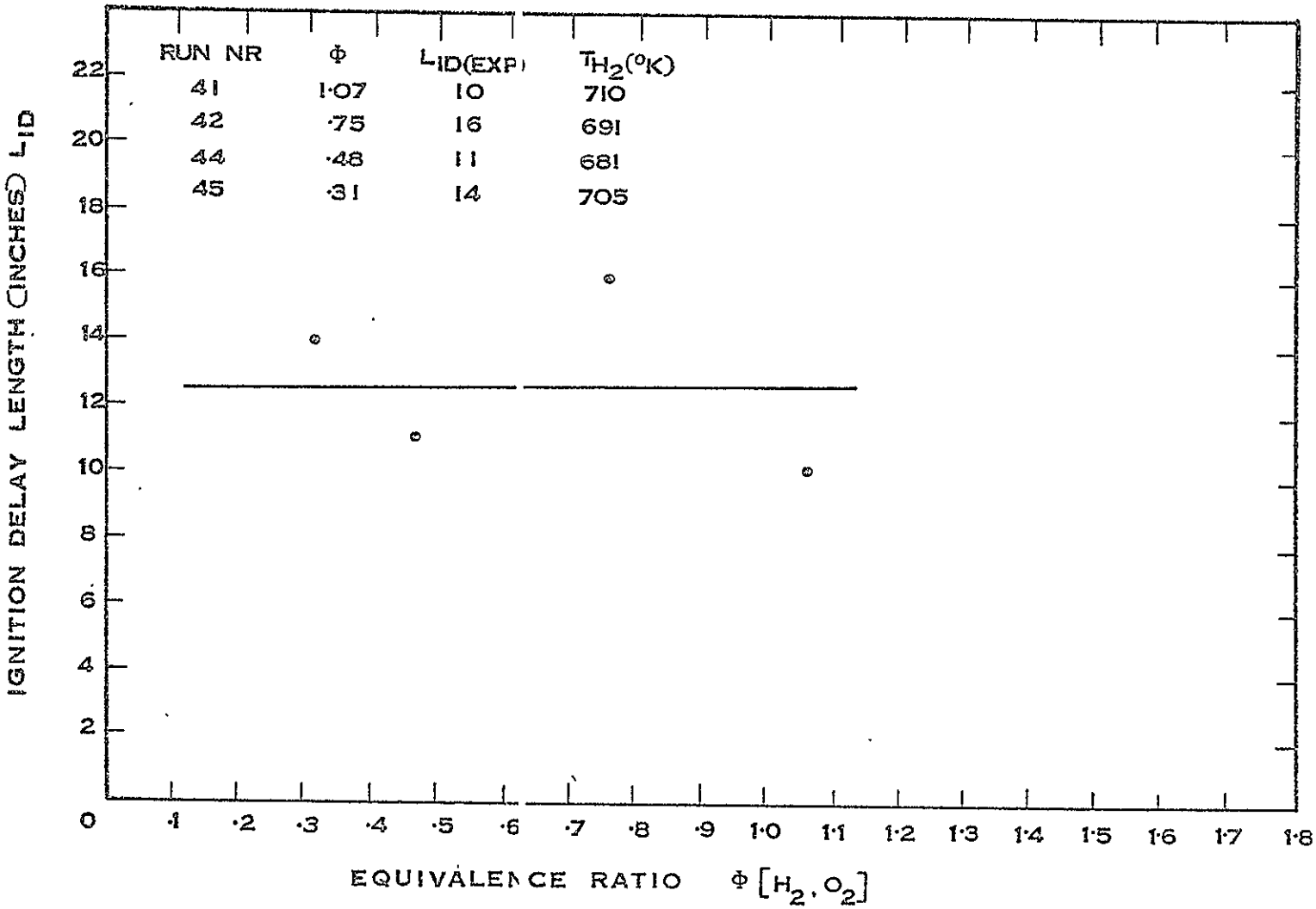

FIGURE 42 GRAPH IGNITION DELAY VERSUS EQUIVALENCE RATIO

DISCUSSION OF ANALYTICAL AND EXPERIMENTAL RESULTS

The ignition delay for a reacting gas mixture is determined primarily by the number of free radicals initially present. At no time during the ignition and subsequent combustion process does the mass fraction of free radicals become a large portion of the total gas mixture. Under conditions of relatively long ignition delays (low static temperatures), the ignition process can be accelerated significantly by small amounts of free radicals. An extensive analysis was undertaken to determine the effect of vitiation on the ignition delay characteristics of hydrogen. The analysis showed that the nonequilibrium free-radical content of the vitiated air system as it enters the supersonic combustion chamber would result in relatively short ignition delay times. The effect is not entirely a function of the vitiated air composition but was shown to be related to the nonequilibrium expansion process by which the gas is accelerated to test section conditions (recombination freezing). In that sense real air exhibits the similar effect on the ignition delay characteristics with hydrogen when the air is expanded to the supersonic test section Mach number from a high temperature source.

The nonequilibrium analysis for a test case typical of the experimental conditions resulted in a calculated ignition delay length of 1.5 in. for the vitiated air. This calculation assumes the hydrogen and vitiated air to be instantaneously mixed at a constant mixture

temperature of 1000°K and an equivalence ratio of unity. It also assumes nonequilibrium gas compositions for both streams prior to mixing. When equilibrium compositions were employed in these calculations, the ignition delay length was computed to be 11.5 in. This is approximately a factor of eight increase in distance over the nonequilibrium case. Therefore, should the experimentally observed ignition delay distance be significantly less than 11.5 in. for mixture temperatures of 1000°K or less, the effects of the nonequilibrium inlet conditions will have been demonstrated.

In the experimental program, the hydrogen gas was heated to manifold temperatures which varied from 500°K to 750°K prior to injection and mixing with the vitiated air. Vitiated air conditions at the test section inlet were a static temperature of approximately 1000°K and a 2.9 Mach number. The two streams were introduced parallel to each other at a constant static pressure of one atmosphere and permitted to mix as an unconfined flow system. The ignition delay distance was determined visually from high speed (550 frames per second) 16 mm Fastex motion pictures of the exhaust flow. These pictures showed that hydrogen ignition (which was primarily a function of hydrogen injection temperature) occurred at distances varying from 8 to 19 in. downstream from the plane of injection. The fact that ignition occurred in some cases at distances less than 11.5 in., does indicate the presence of nonequilibrium free radicals which have reduced the ignition delay phenomenon.

An additional theoretical analysis was undertaken to attempt to achieve better correlation between experimental and analytical program

results. In the experimental program, the hydrogen and vitiated air enters the test section area at different static temperatures. This fact complicates the analysis of the delay time since a mean mixing temperature for the reacting gases must be defined before computing the ignition delay distance. The operational procedure for this specific analysis was executed as follows:

1. In an experimental ignition delay run note the hydrogen manifold temperature and flow rate, gas generator chamber pressure, propellant flow rates, and observed ignition delay distance.

2. Input the required gas generator properties and parameters into the Finite Rate Reacting Gas (FRRG) computer program and calculate velocity, specie concentration, static temperature and pressure at the gas generator nozzle exit plane, which also serves as the entrance to the supersonic test section area.

3. Input into the Simplified Ignition Lag (SIL) computer program the specie concentrations computed above, together with the additional hydrogen injected, the mixture mean temperature, pressure and equivalence ratio.

4. Determine from the computer plotted output graph (OH radical concentration versus time) the point where the slope of constant OH radical growth starts to deviate from straight line behavior (end of ignition period).

5. Multiply the time indicated at this point of deviation by the velocity computed by the FRRG to determine the comparable ignition delay length.

In the initial attempt to compare the experimental and analytical results as outlined above, the mean temperature of the mixed stream (hydrogen and vitiated air) was determined by employing the gross over-simplification that the mean temperature can be obtained from the weighted heat content of the combined streams. Since the flow rate of the vitiated air stream was measured to be 9.0 lb/sec in contrast to the flow rate of 0.08 lb/sec to 0.29 lb/sec of the hydrogen stream, the mean temperature of the mixture, assuming instantaneous mixing, was for all practical purposes equal to that of the vitiated air stream ($\sim$ 980°K). The results of this preliminary effort are presented as Figures 43 through 49. A comparison of these analytical results with the experimentally measured ignition lengths is not satisfactory. Experimentally there is a factor of three difference in the measured ignition delay distances for the different hydrogen inlet conditions. The discrepancy between the analytical and experimental results is believed to be entirely an effect of the over-simplified assumption of instantaneous mixing of the two dissimilar streams.

A combined mixing and reaction kinetics analysis is beyond the scope of the present program. However, a simple rule of thumb used in free jet mixing studies states that mixing is usually complete in a distance of approximately 10 jet diameters from the injection plane. This distance would be about 45 in. in the existing system. The maximum ignition delay distance observed was 19 in.; therefore, it can be safely concluded that the onset of ignition occurs before the hydrogen gas has a chance to diffuse completely into the vitiated air core. Hence, the reaction zone of the mixture forms a conical sheath

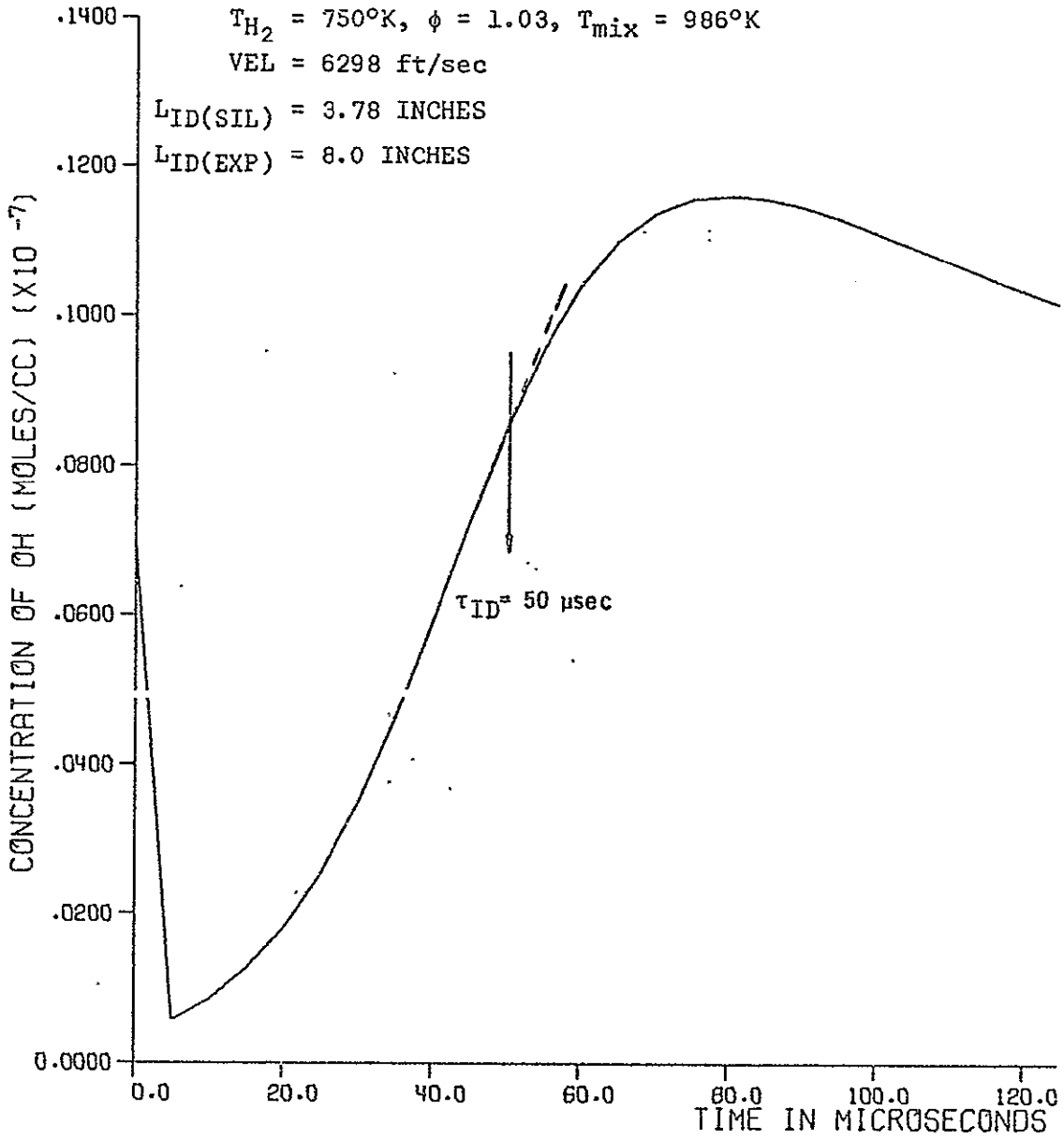

FIGURE 43 IGNITION DELAY 100% MIXING - RUN 39

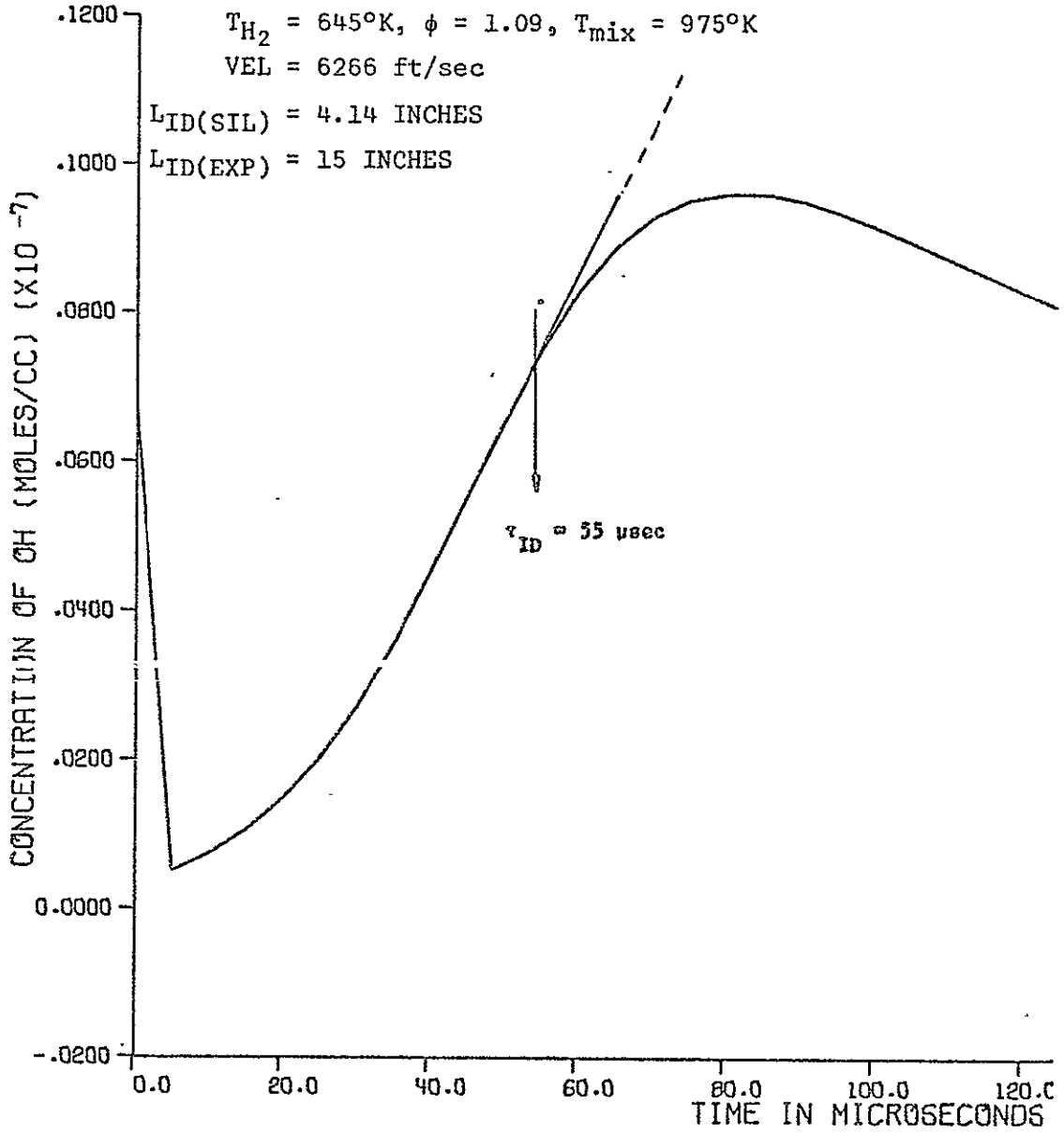

FIGURE 44 IGNITION DELAY 100% MIXING - RUN 40

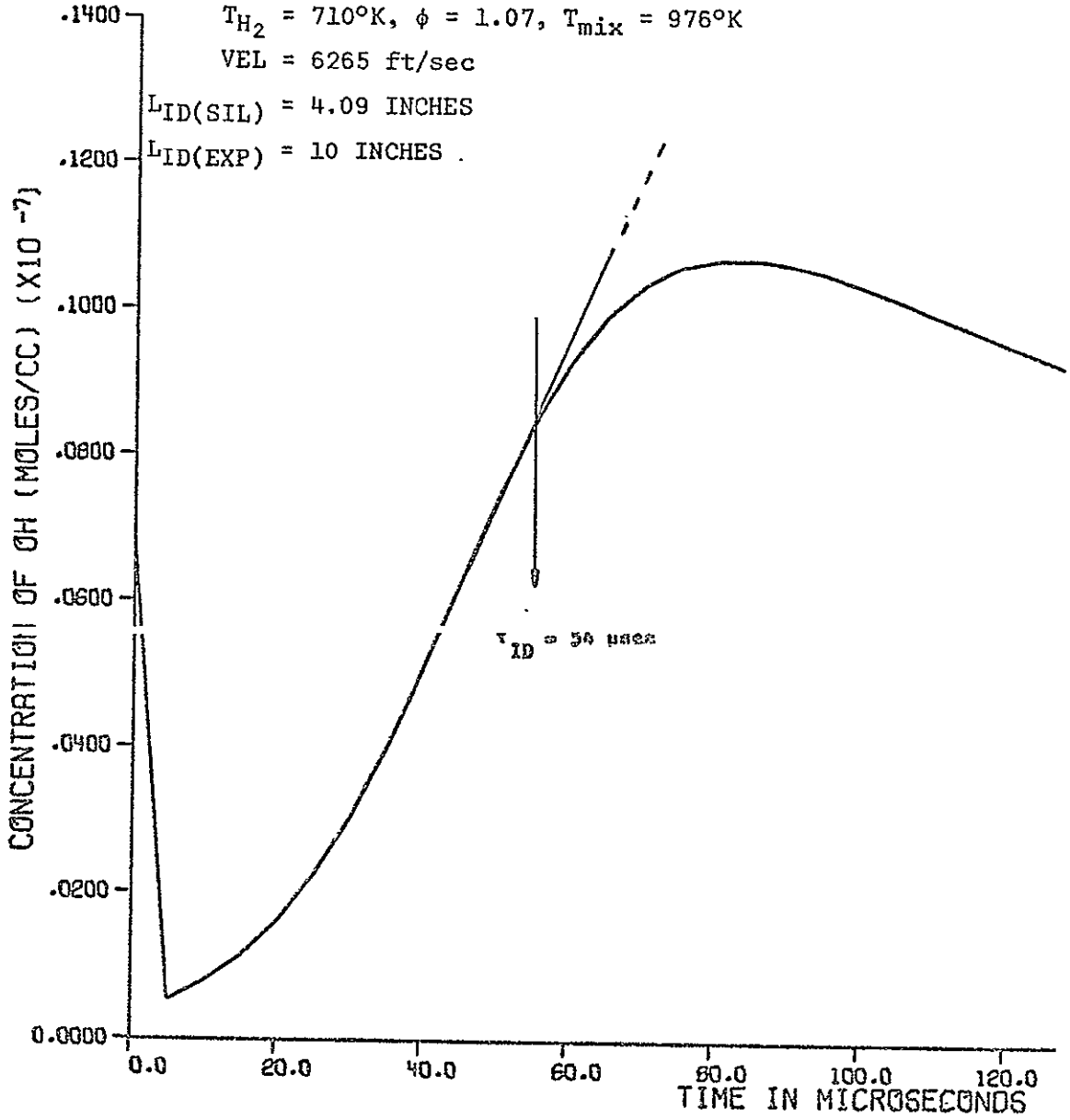

FIGURE 45 IGNITION DELAY 100% MIXING - RUN 41

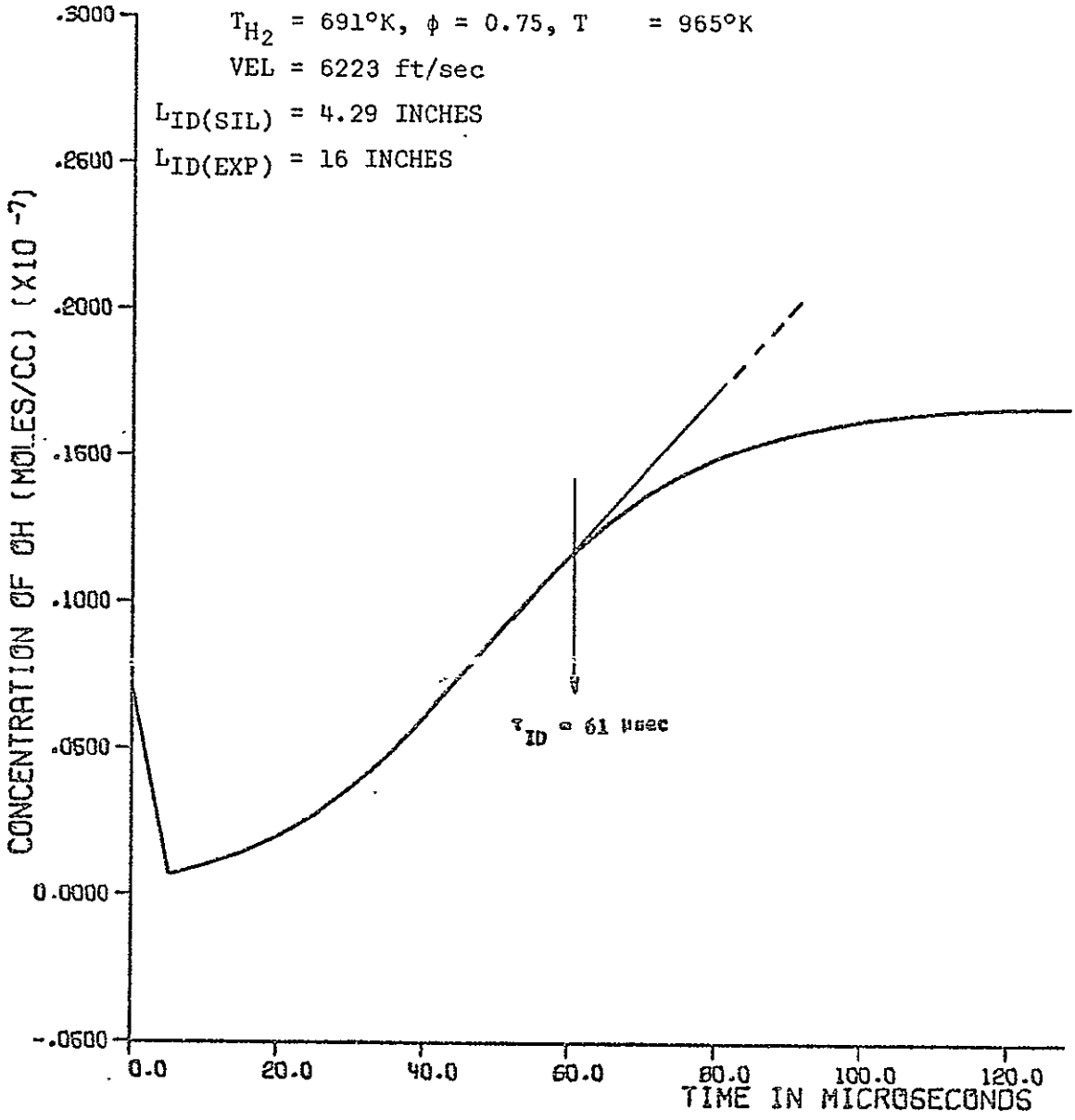

FIGURE 46 IGNITION DELAY 100% MIXING - RUN 42

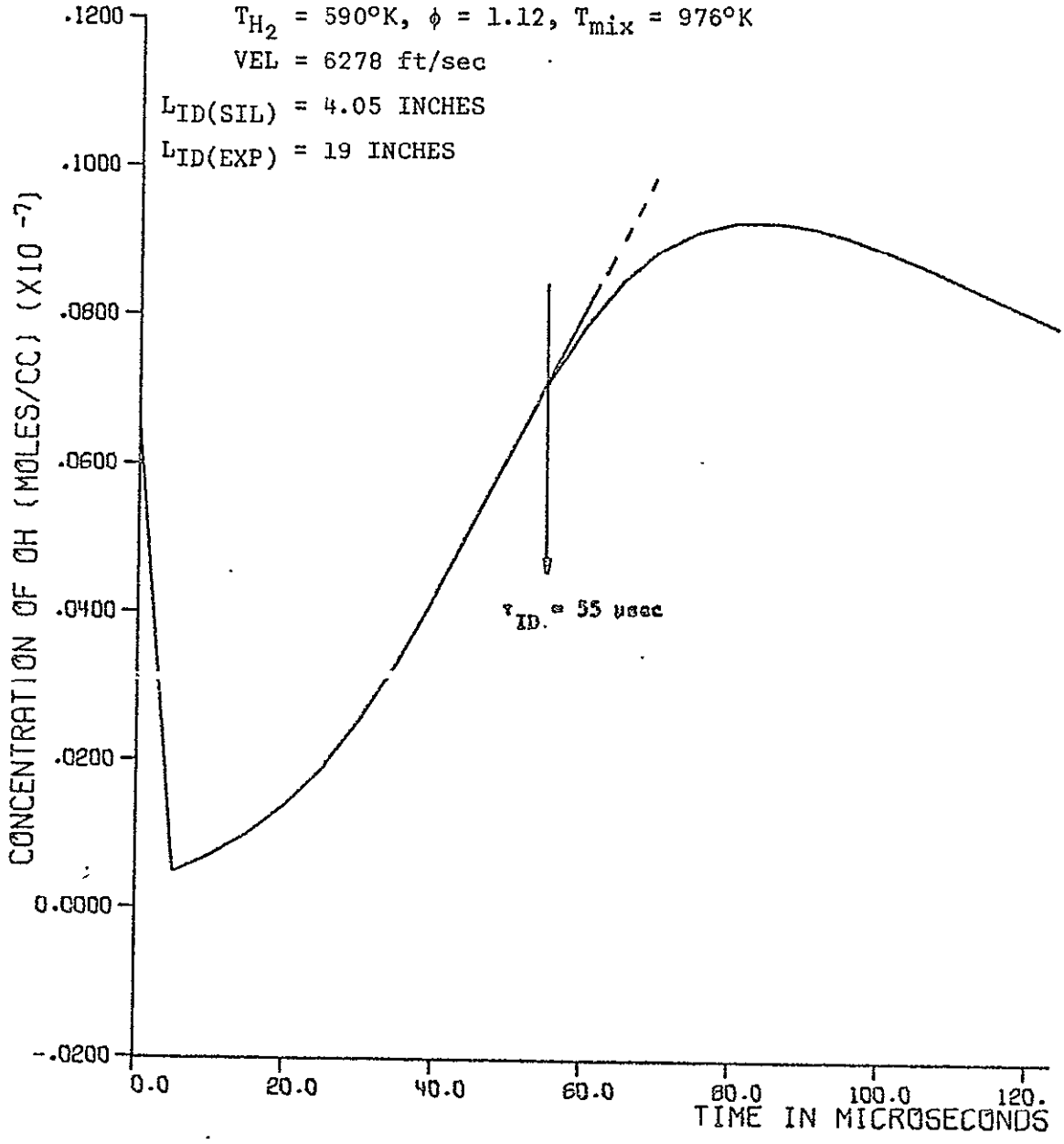

FIGURE 47 IGNITION DELAY 100% MIXING - RUN 43

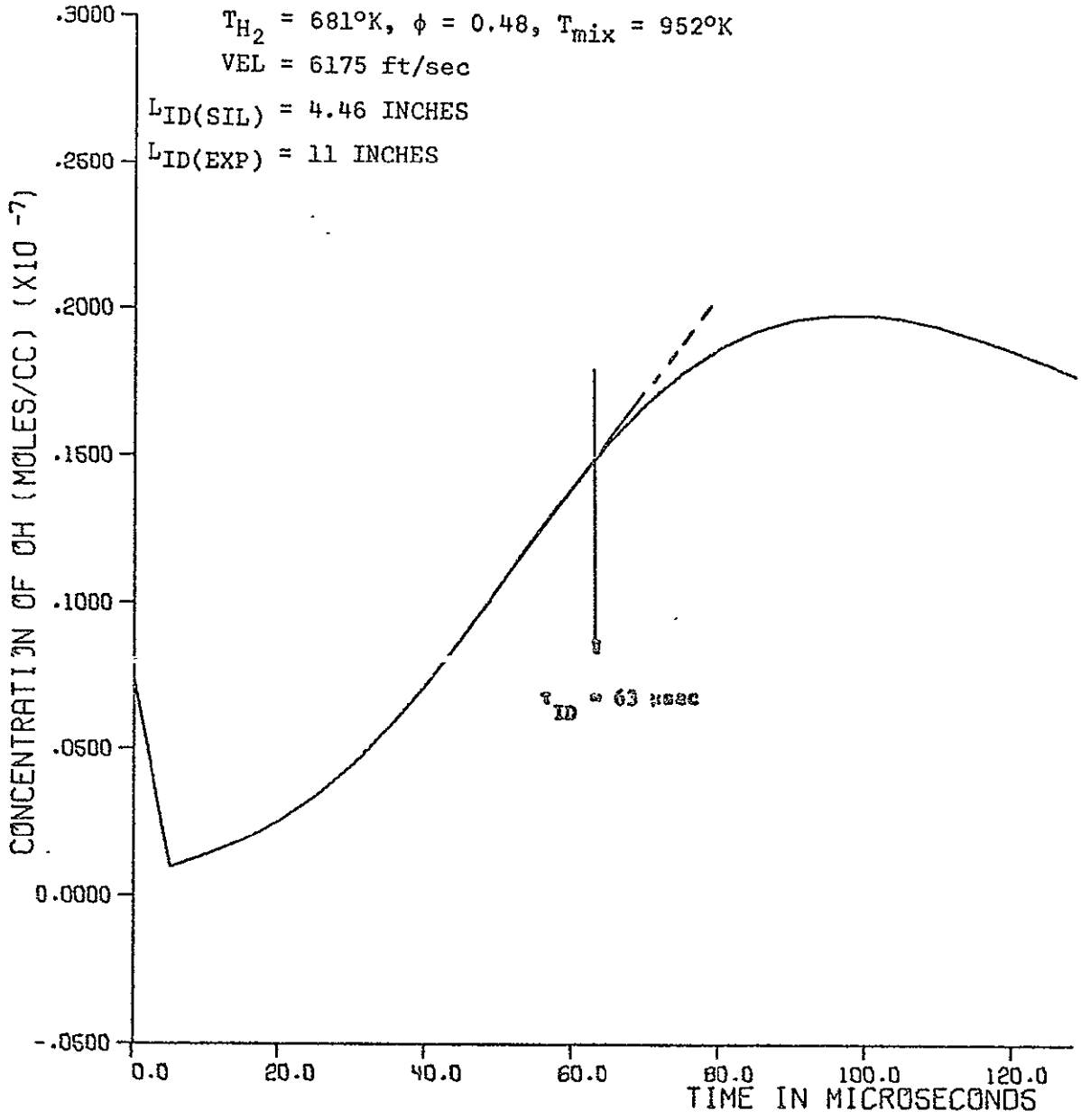

FIGURE 48 IGNITION DELAY 100% MIXING - RUN 44

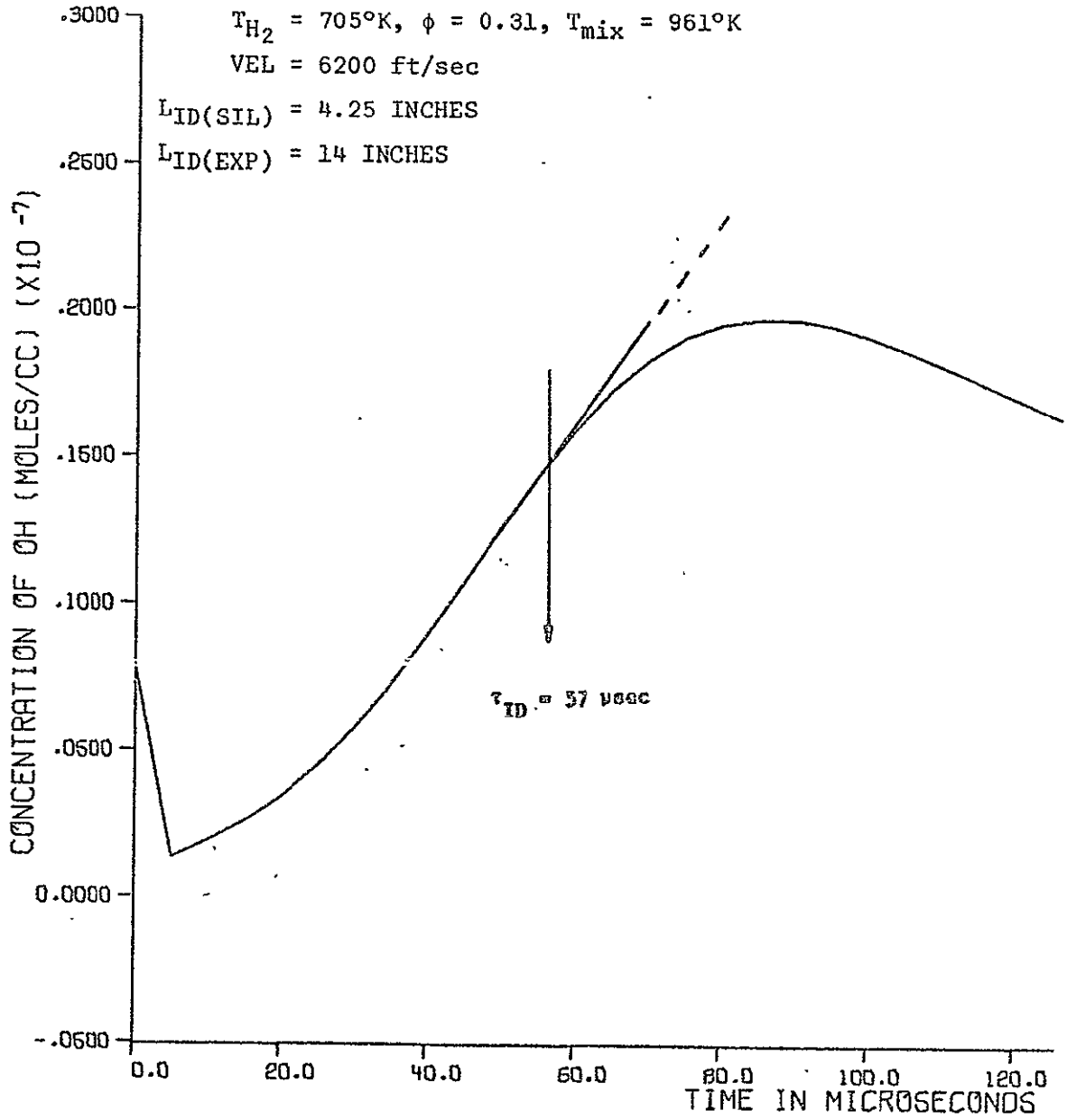

FIGURE 49 IGNITION DELAY 100% MIXING - RUN 45

about the vitiated air stream. The thickness of this zone was calculated to be approximately 0.4 in. Calculations were performed using the "Finite Rate Supersonic Combustion Mixing Analysis" computer program written by Siegelman and Fortune of the General Applied Science Laboratories [28]. The extensive use of this program for a more inclusive type of investigation is reported later in this section.

A short analytical investigation of the effects of vitiated-air/hydrogen mixture temperature on ignition delay as calculated by the Simplified Ignition Lag (SIL) computer program was accomplished in an attempt to improve the correlation of the experimental and analytical data. It was shown that the hydrogen does not completely penetrate the vitiated air core before ignition, therefore, it is only logical to conclude that the mean mixture temperature should be a direct function of penetration depth. The initial phase of this specific investigation used the simplified assumption that due to the limited penetration of the hydrogen into the air core, that ignition occurred at a mean mixture temperature equal to the injection temperature of the hydrogen. The static temperature of the hydrogen subsequent to passage through the sonic annular injector is the value used in all of the analytical ignition delay efforts. Hydrogen temperatures as listed in the tables and graphs are manifold or total temperatures. Results of this investigation are shown in the computer printed graphs indicated as Figures 50, 51 and 52. In all three cases considered, the OH radical concentration never increased. On the basis of this data it can be concluded that ignition never occurred. This fact analytically verifies the experimental results concerning the ambient

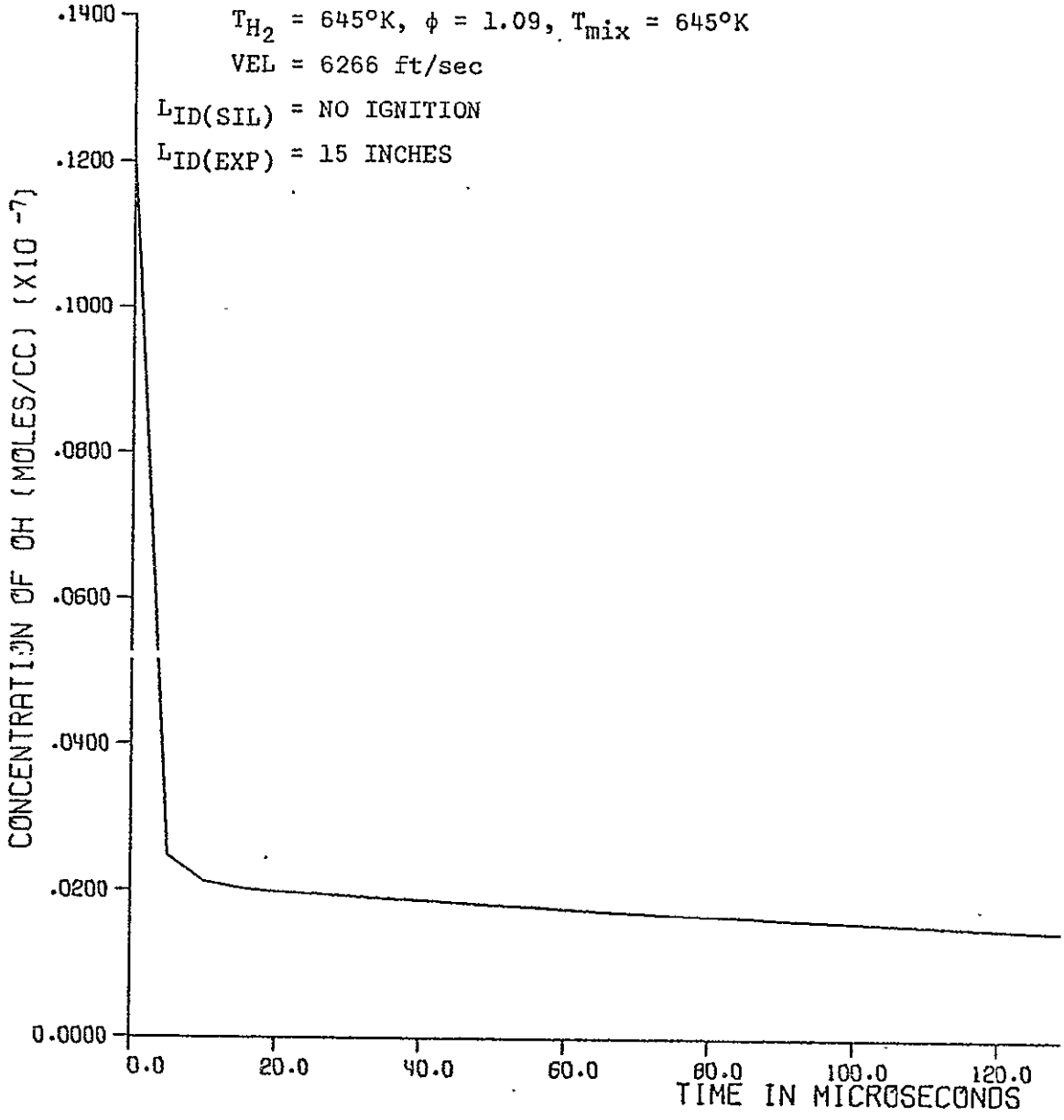

FIGURE 50 IGNITION DELAY MINIMAL MIXING - RUN 40

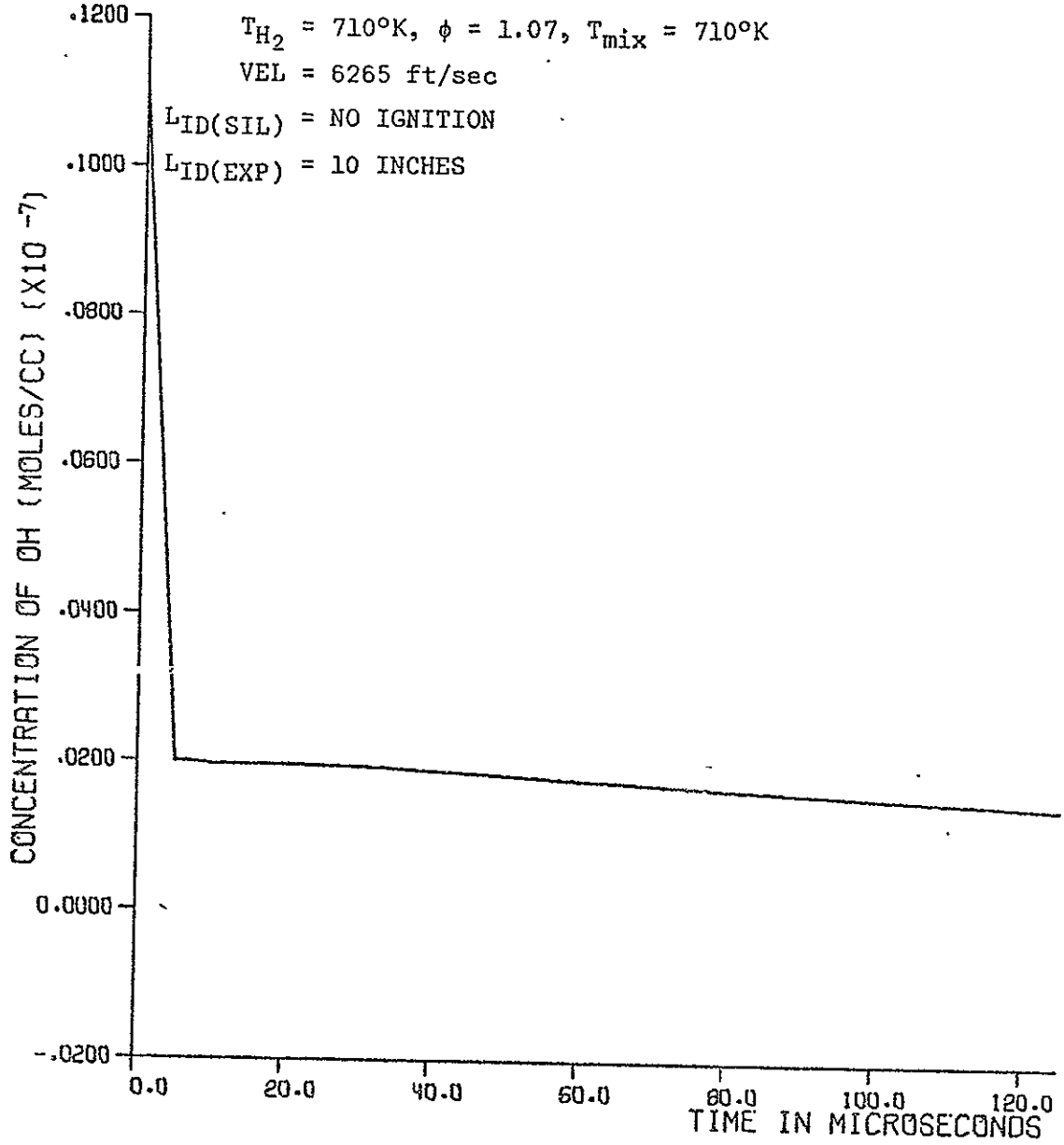

FIGURE 51 IGNITION DELAY MINIMAL MIXING - RUN 41

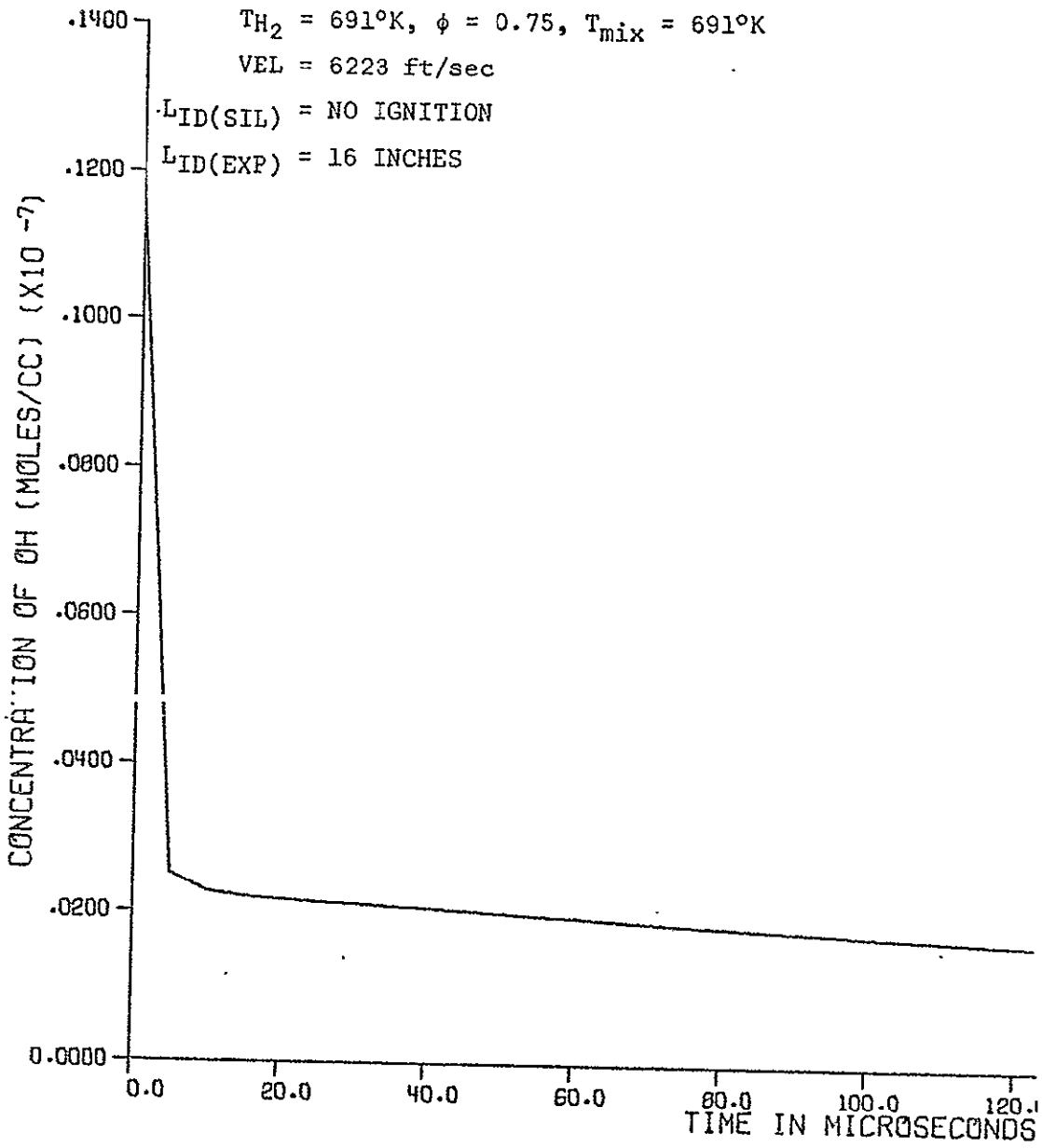

FIGURE 52 IGNITION DELAY MINIMAL MIXING - RUN 42

air entrainment effect on the ignition delay distance. It had been suspected that the oxygen in the ambient air entrained by the hydrogen stream provided a free-radical source for ignition. Due to the experimental fact that ignition was not realized, the requirement for a thermal ignition source greater than that supplied by the heated hydrogen alone is substantiated. In other words, the results of this analytical investigation supports the theory that the mixture resulting from ambient air entrainment does not possess the required energy for autoignition. The conclusion that the ignition delay length is primarily a function of the energy content of the vitiated-air/hydrogen mixture is therefore reconfirmed.

The experimental observation that ignition and sustained combustion did occur in runs 40, 41, and 42, invalidates the assumption of mixture temperatures equal to hydrogen injection temperatures. In order to more closely approximate the depth of hydrogen penetration into the hot vitiated air core and, in turn, to be able to generate a realistic mean mixture temperature for analytical needs, the GASL's "Finite Rate Supersonic Combustion Mixing Analysis" computer program was employed. This program describes the turbulent mixing of axisymmetric hydrogen-air jets inside a duct. It utilizes a finite-difference technique to trace the mixing process with either frozen or finite rate chemistry. Outputs from the program consists of the following parameters as a function of geometric grid point position in the reacting or nonreacting mixture: Mach number, velocity, static and total pressure, static and total temperature, specific heat, density, molecular weight, static and total enthalpy, ratio of specific

heats, acoustic velocity, specie concentration and the equivalence ratio of hydrogen to oxygen. Even though the program was written for ducted flow, the initial portion of the output is applicable to the mixing and ignition processes. This is only true when the processes are confined to a region located a considerable distance upstream from the point where the reaction zone would theoretically contact the duct wall. Figures 53, 54 and 55 are schematic drawings of the specie concentration profiles computed by the mixing program for a typical experimental ignition delay run. The abcissa is the species mass fraction. The ordinate (ψ) is the grid points which specifies discrete positions in the duct cross section. These points are related to the radial distances in the duct through a von Mises transformation.

As a starting point in the mixing analysis, it is necessary in the finite-difference mode of computation to input the initial number of grid points (ψ) and the distance between any two grid points ($\Delta\psi$). Hence, thirteen grid points (ψ) are initially used, ten for the hydrogen stream and three for the vitiated air stream. The distance between each grid point ($\Delta\psi$) is 0.0276 in. Additional grid points are generated as required by the program to account for the ever widening mixing zone.

The approximation of a mean mixture temperature was obtained by using the calculated penetration depth at which the equivalence ratio output of unity occurred. This value was located at grid point number 4 at an axial distance of 0.10 ft. from the plane of hydrogen injection. The specie concentration profile for this particular

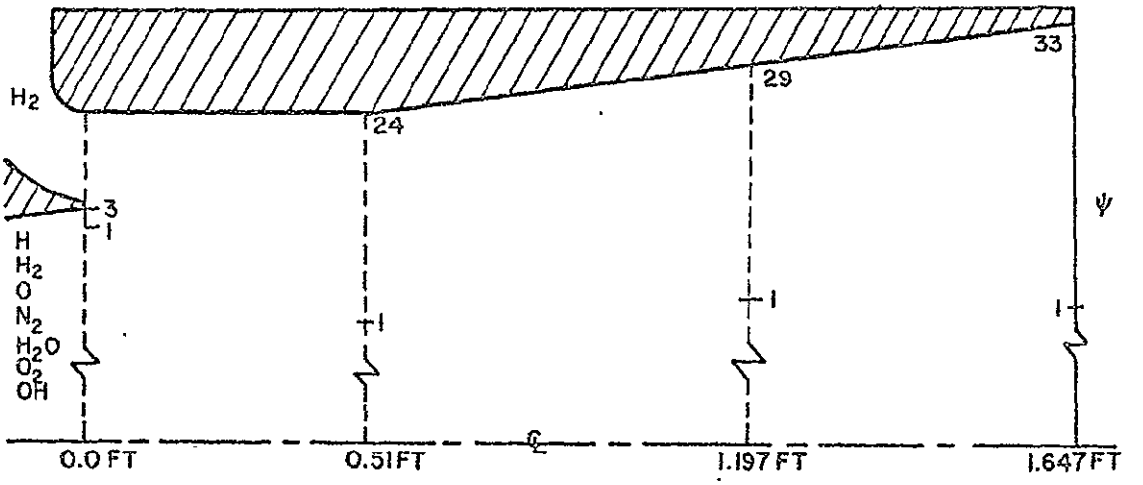

SUPERSONIC COMBUSTION INLET AND TEST SECTION

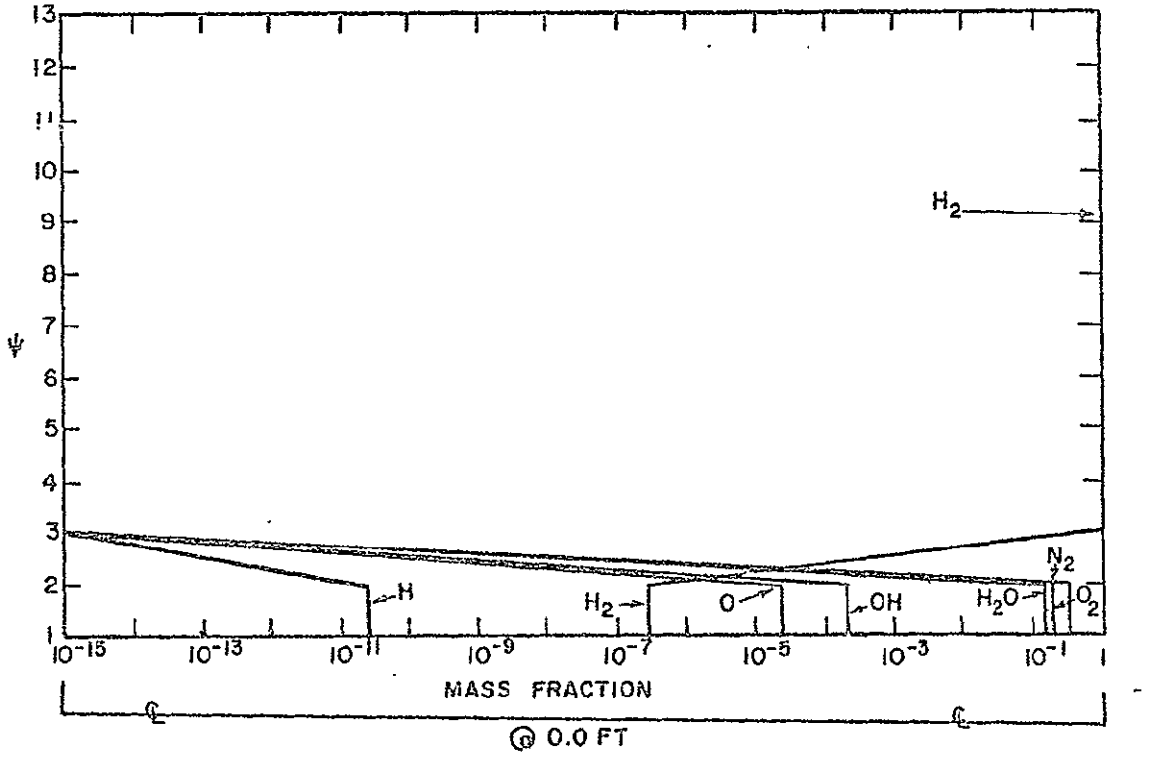

FIGURE 53 SCHEMATIC SUPERSONIC DUCT AND SPECIE CONCENTRATION PROFILE 0.0 FT - RUN 39

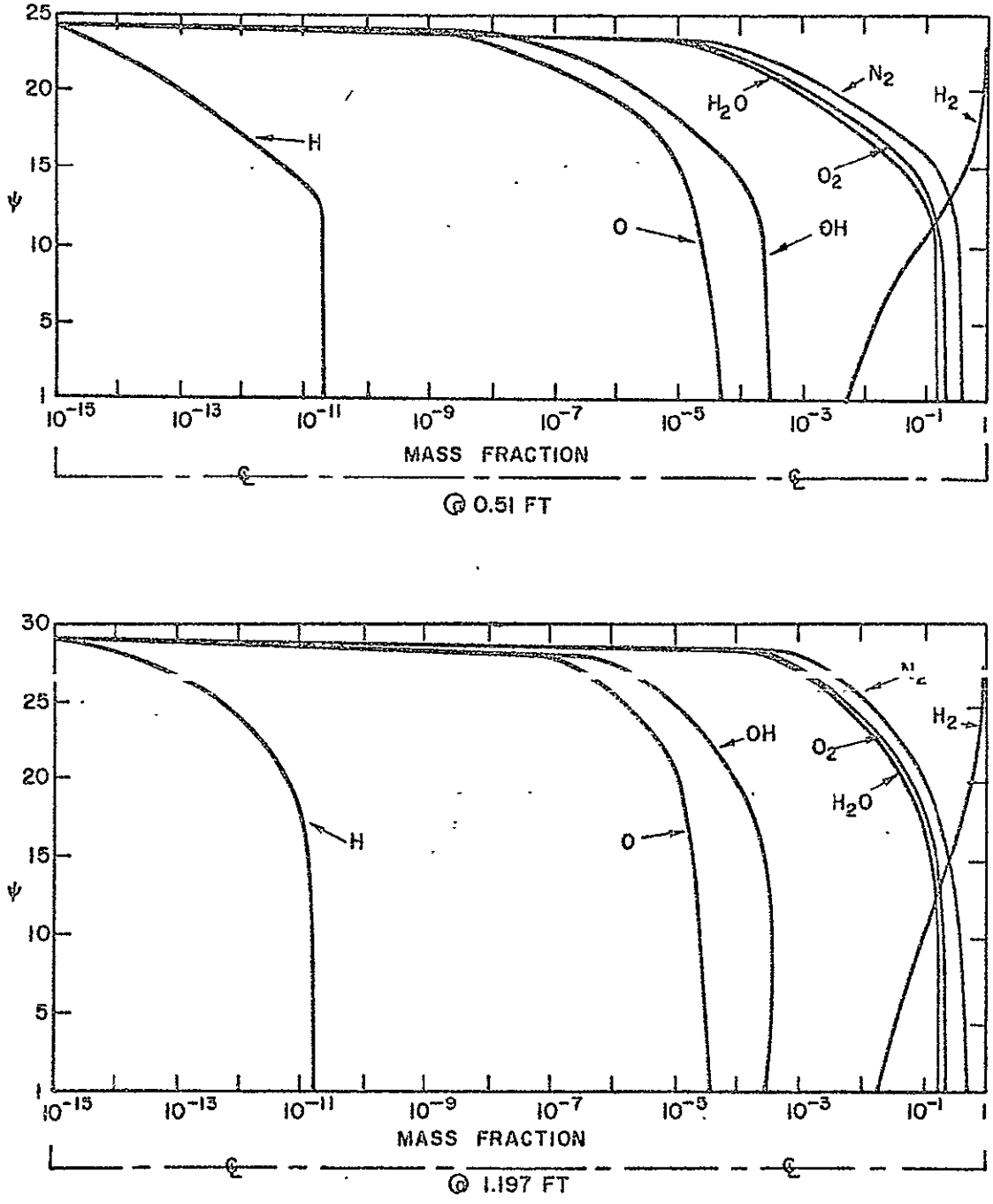

FIGURE 54 SPECIE CONCENTRATION PROFILES 0.51 FT AND 1.197 FT - RUN 39

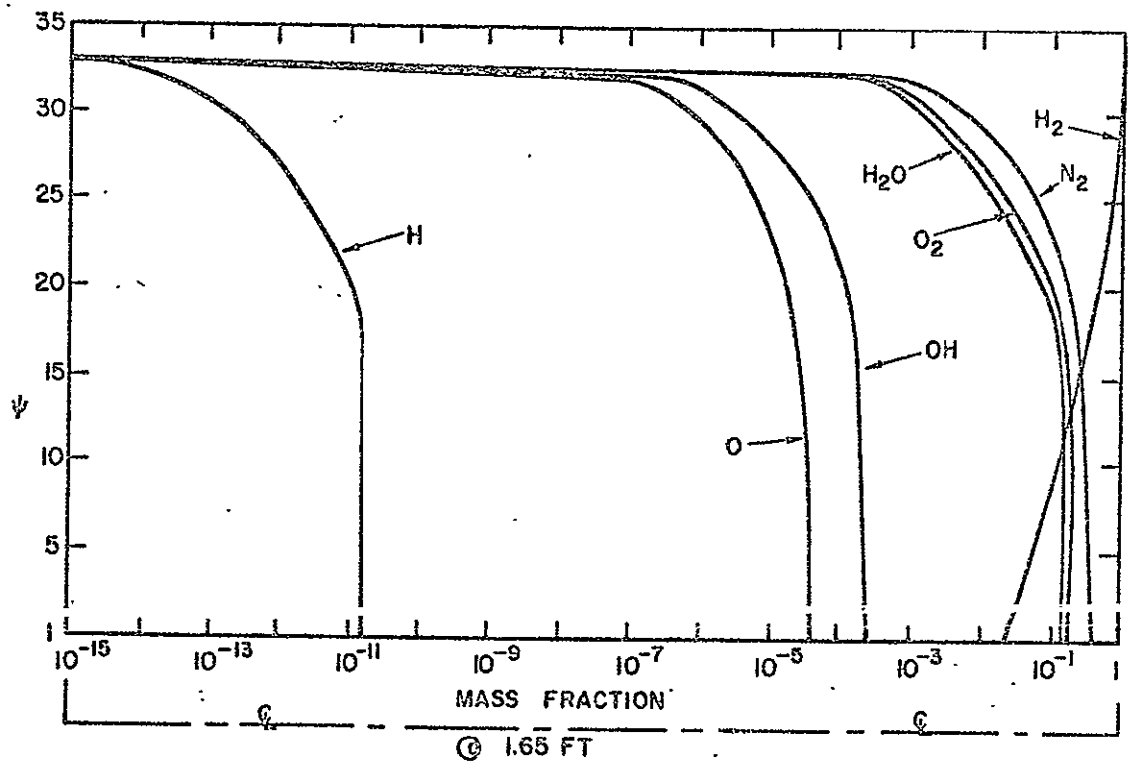

FIGURE 55 SPECIE CONCENTRATION PROFILE 1.65 FT

station is not shown in the associated figures. Nevertheless, grid point number 4 at this station is positioned at a depth of 0.414 in. into the periphery of the vitiated air core. It was therefore concluded that in the distance from the hydrogen injection plane out to this station (0.10 ft.) the hydrogen gas diffuses into the vitiated air core to a depth of 0.414 in. The volume percentage of the vitiated air core penetrated by the hydrogen gas in this distance amounts to approximately 40 percent. Therefore, the mean temperature of the mixture was arrived at by using only 40 percent of the total vitiated air flow in a vitiated-air/hydrogen weighted mean temperature calculation. This effort reduced the mean mixture temperature to a more realistic value and resulted in a better correlation between analytical and experimental data. The static temperature of the vitiated air core at the hydrogen injection plane was calculated to be 850°K. This value was arrived at by subtracting the temperature drop ($\Delta T \approx 133°K$) due to heat transfer effects in the combustion chamber and along the nozzle walls, from the theoretical static temperature (983°K) calculated by the FRRG program. In the heat transfer analysis it was found that the chamber temperature decreased by 67°K for a quasi-static heat transfer rate through the walls of 1.54 BTU/in^2-sec. It was therefore assumed that the additional temperature decrease through the nozzle section should be at least equal to that lost in the combustion chamber. With a modified vitiated air static temperature of 850°K versus the original theoretical static temperature of 983°K, it is felt that the species concentrations as calculated by the FRRG program at the original

IV

temperature (983°K) would not vary excessively due to this temperature difference. Hence, the species concentration as calculated originally at 983°K was input into the SIL program along with the mean temperature generated by using the modified temperature (850°K). The results of this analysis as shown in Figures 56 through 62 are manifested in the longer ignition delay times. It can also be observed that the analytical and experimental ignition delay lengths agree much better than in the previous comparison where it was assumed that the hydrogen and vitiated air streams mixed instantaneously and completely prior to ignition. This comparison would seem to indicate that the effect of different static temperatures for the hydrogen and vitiated air streams in addition to mixing rates, have a profound effect on any analytical ignition delay model.

Figures 63 and 64 are graphical plots comparing the experimental and analytical data as a function of hydrogen manifold temperature and equivalence ratio. As can be observed in Figure 63, the differences in delay length diverges as the hydrogen temperatures decrease. This effect may be caused by the effect of temperature on the mixing or diffusion rate in the two streams. It is shown in Reference 29 that the mass diffusivity in gaseous mixtures does increase with temperature. Another noteworthy observation is the trend of decreasing ignition length with increasing hydrogen temperature as manifested in both the analytical and experimental data results. This fact tends to reconfirm the validity of the analytical model in that ignition delay length decreases with increasing temperatures. In Figure 64, the experimental data deviate from the analytical theory of relative

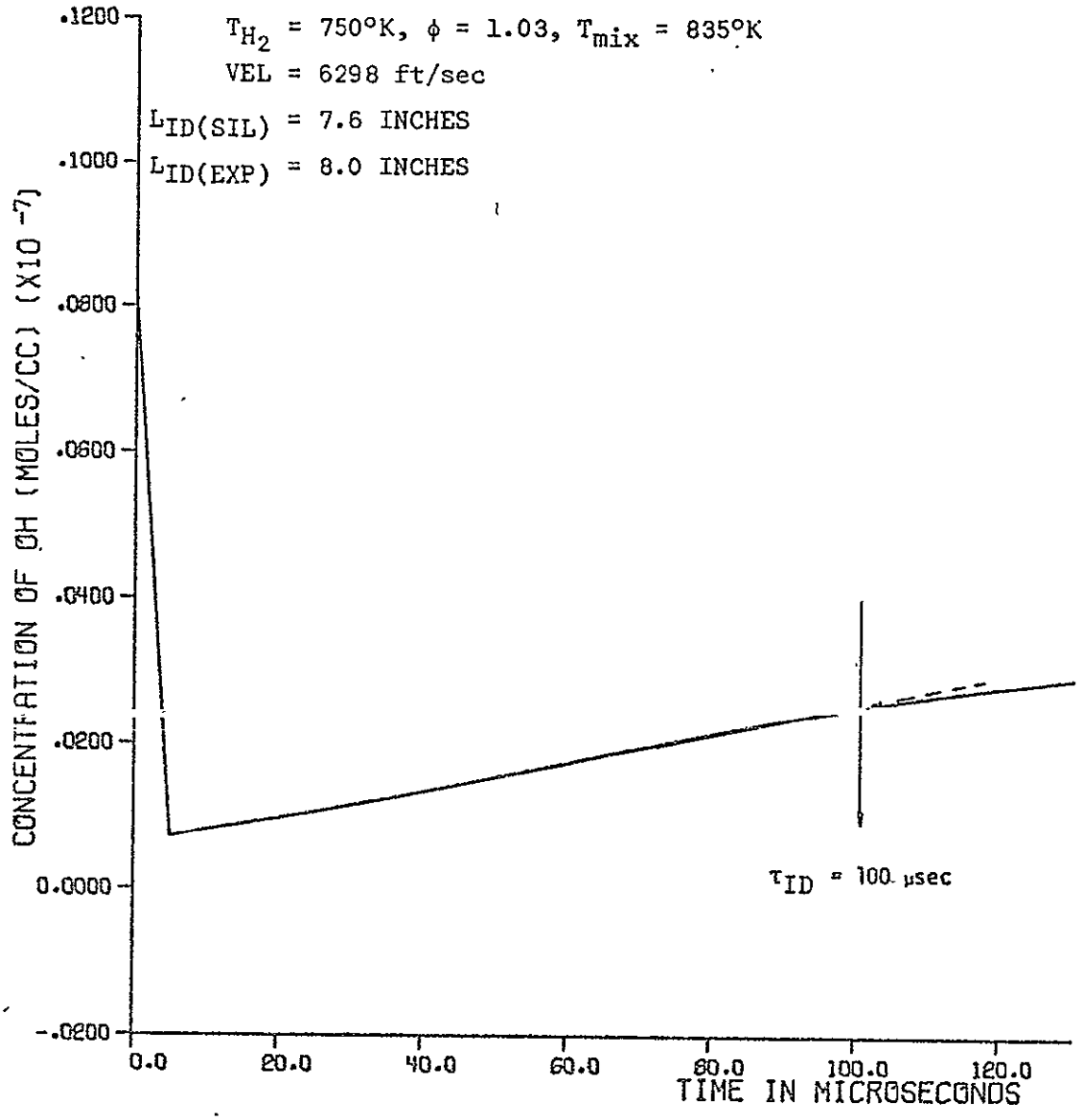

FIGURE 56 IGNITION DELAY 40% MIXING - RUN 39

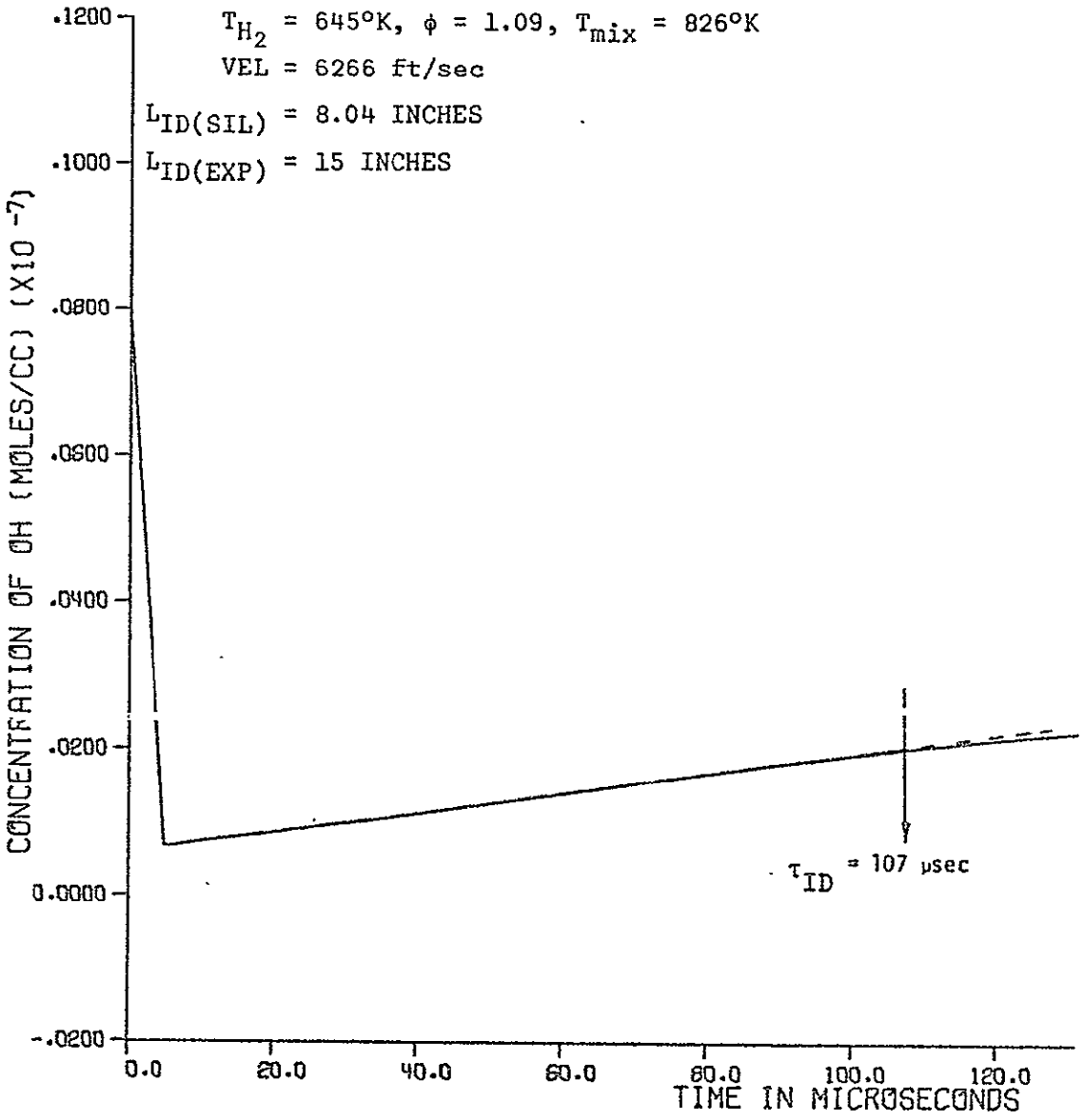

FIGURE 57 IGNITION DELAY 40% MIXING - RUN 40

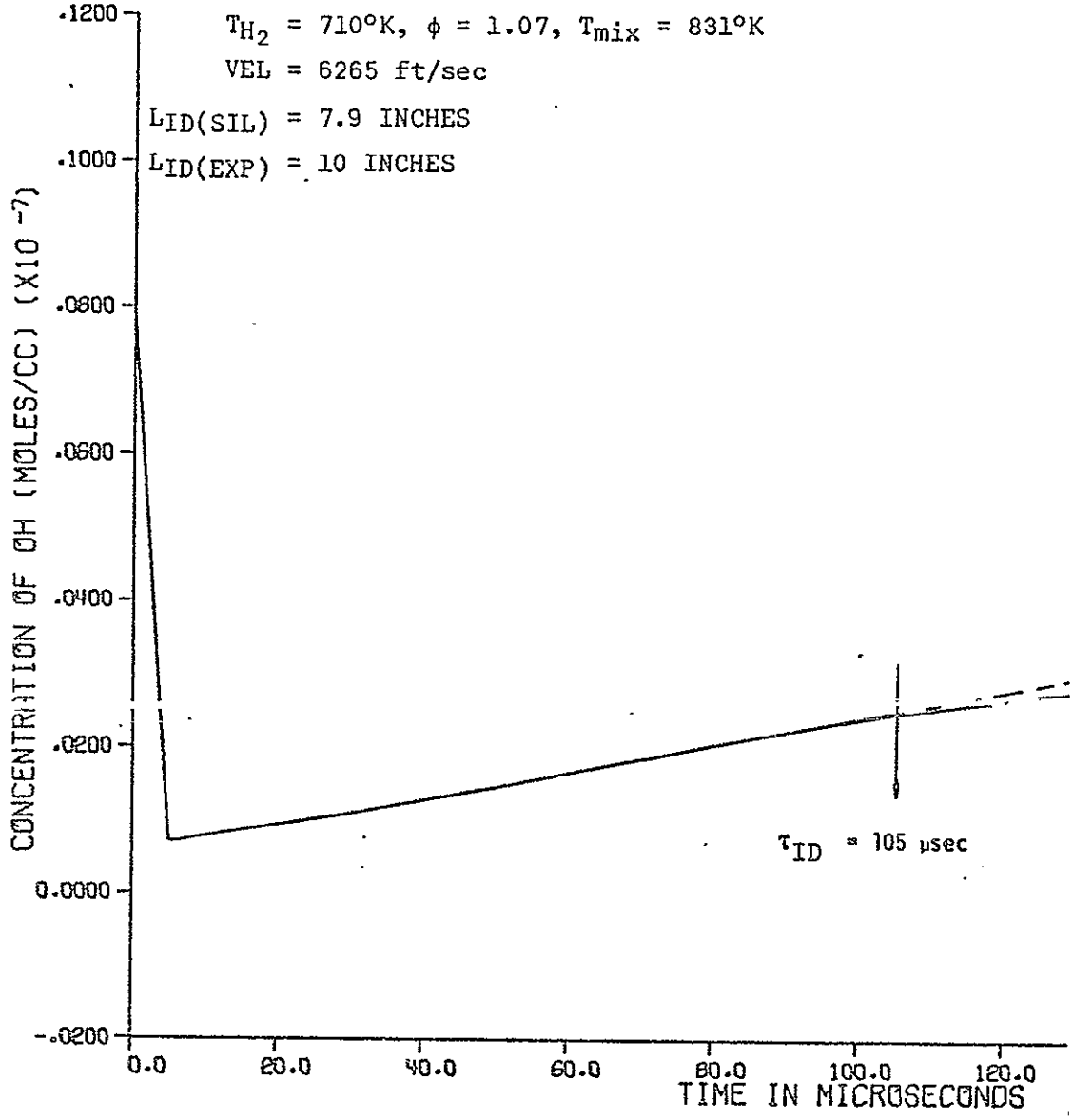

FIGURE 58 IGNITION DELAY 40% MIXING - RUN 41

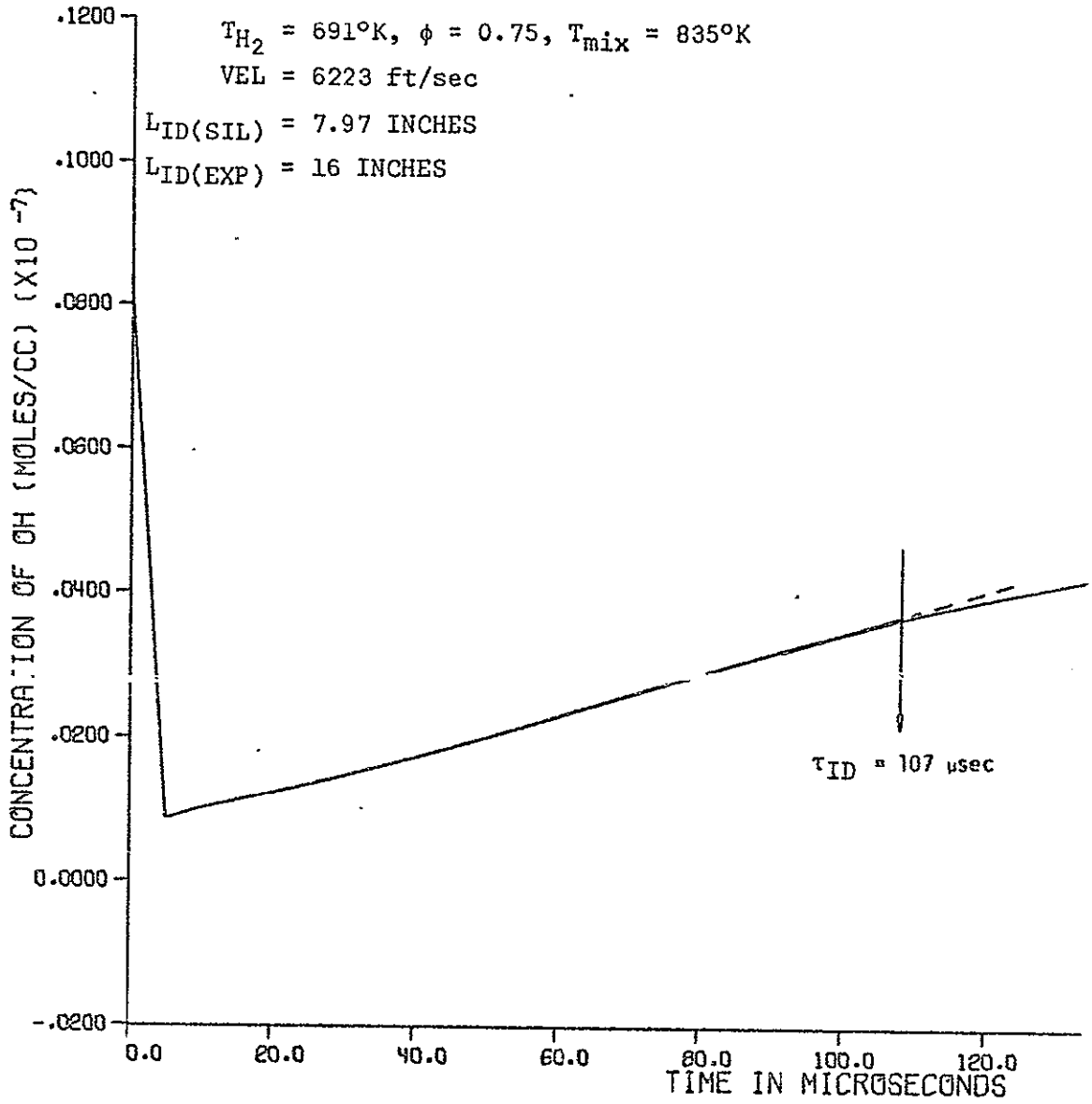

FIGURE 59 IGNITION DELAY 40% MIXING - RUN 42

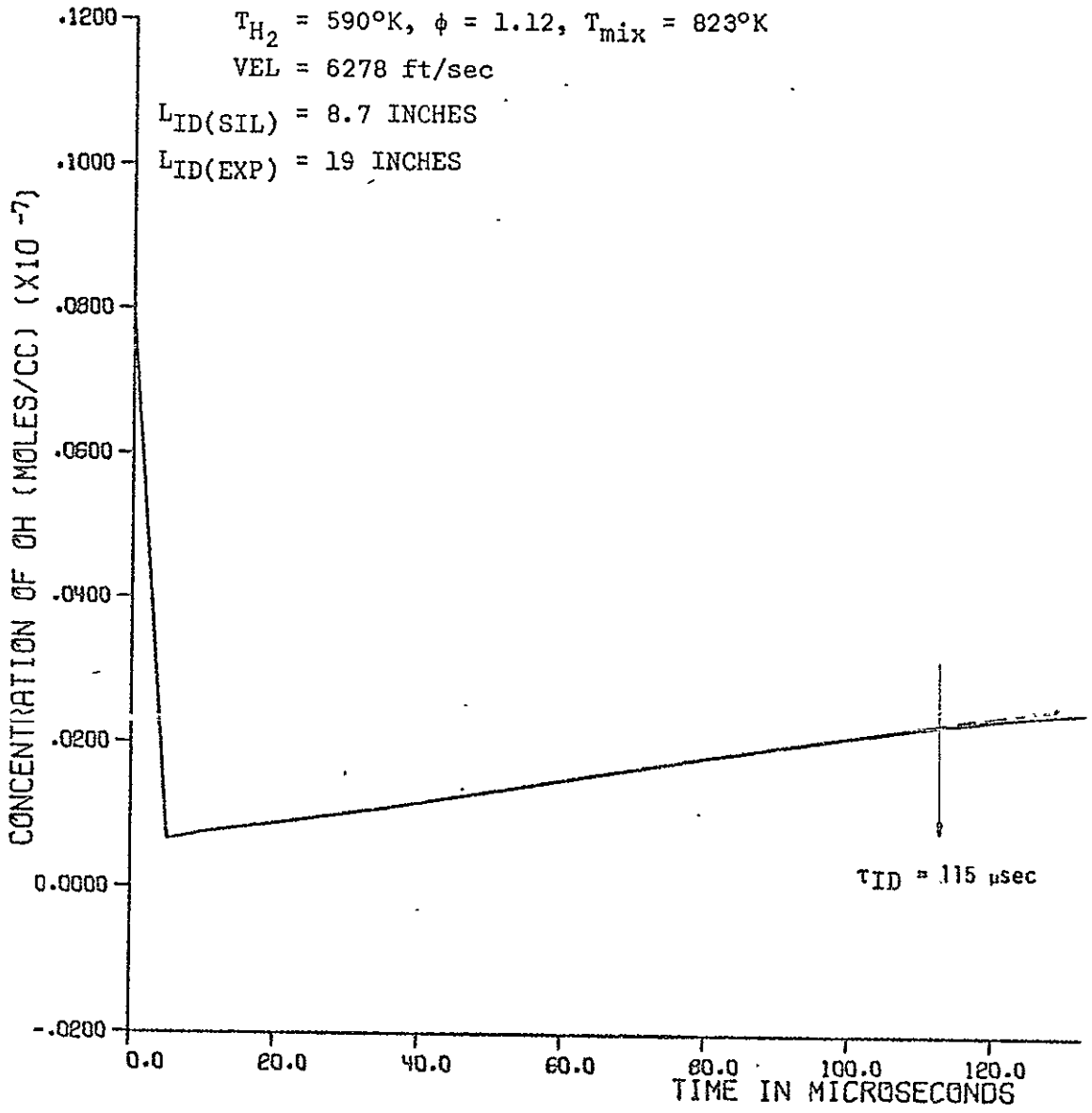

FIGURE 60 IGNITION DELAY 40% MIXING - RUN 43

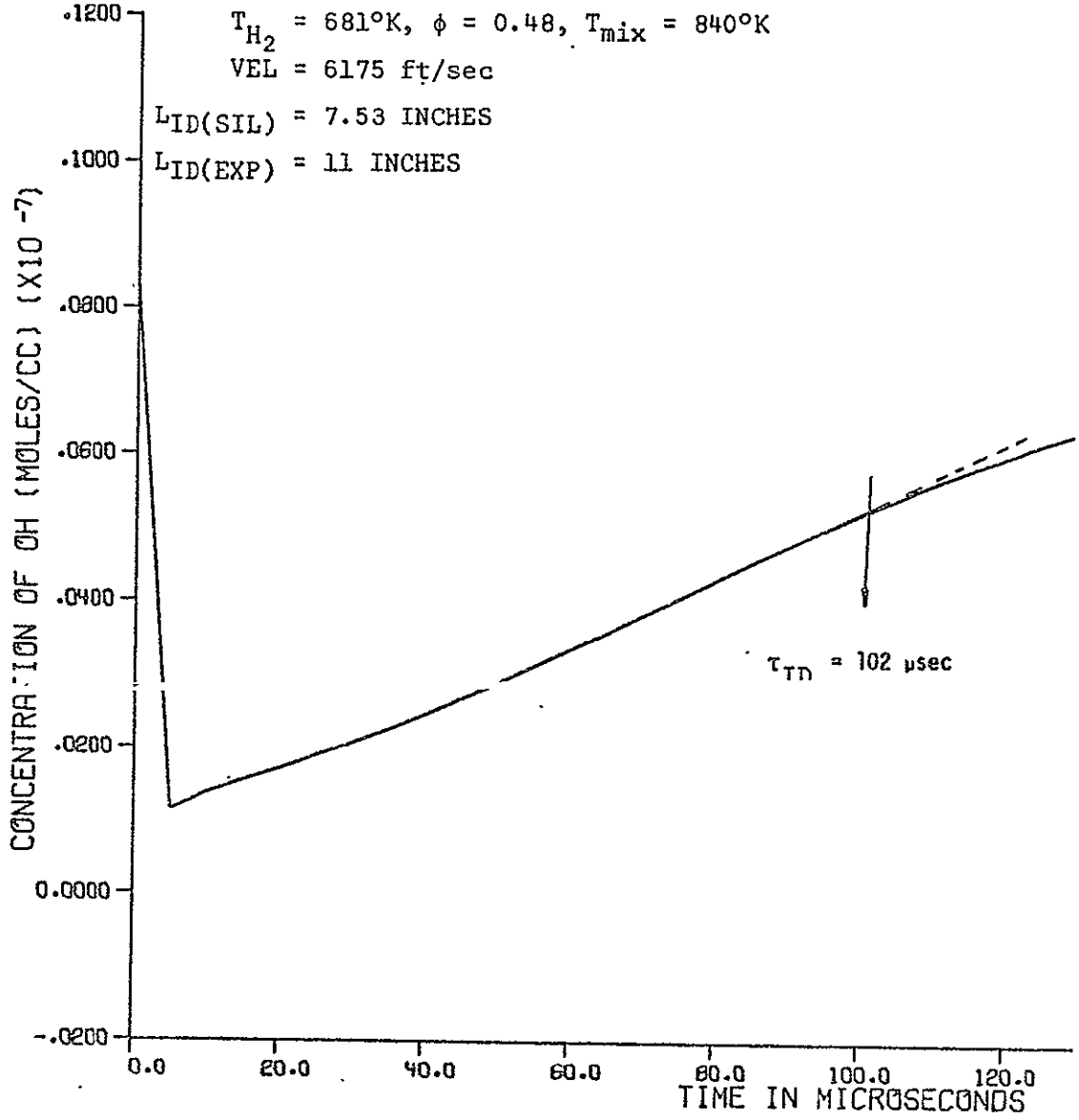

FIGURE 61 IGNITION DELAY 40% MIXING - RUN 44

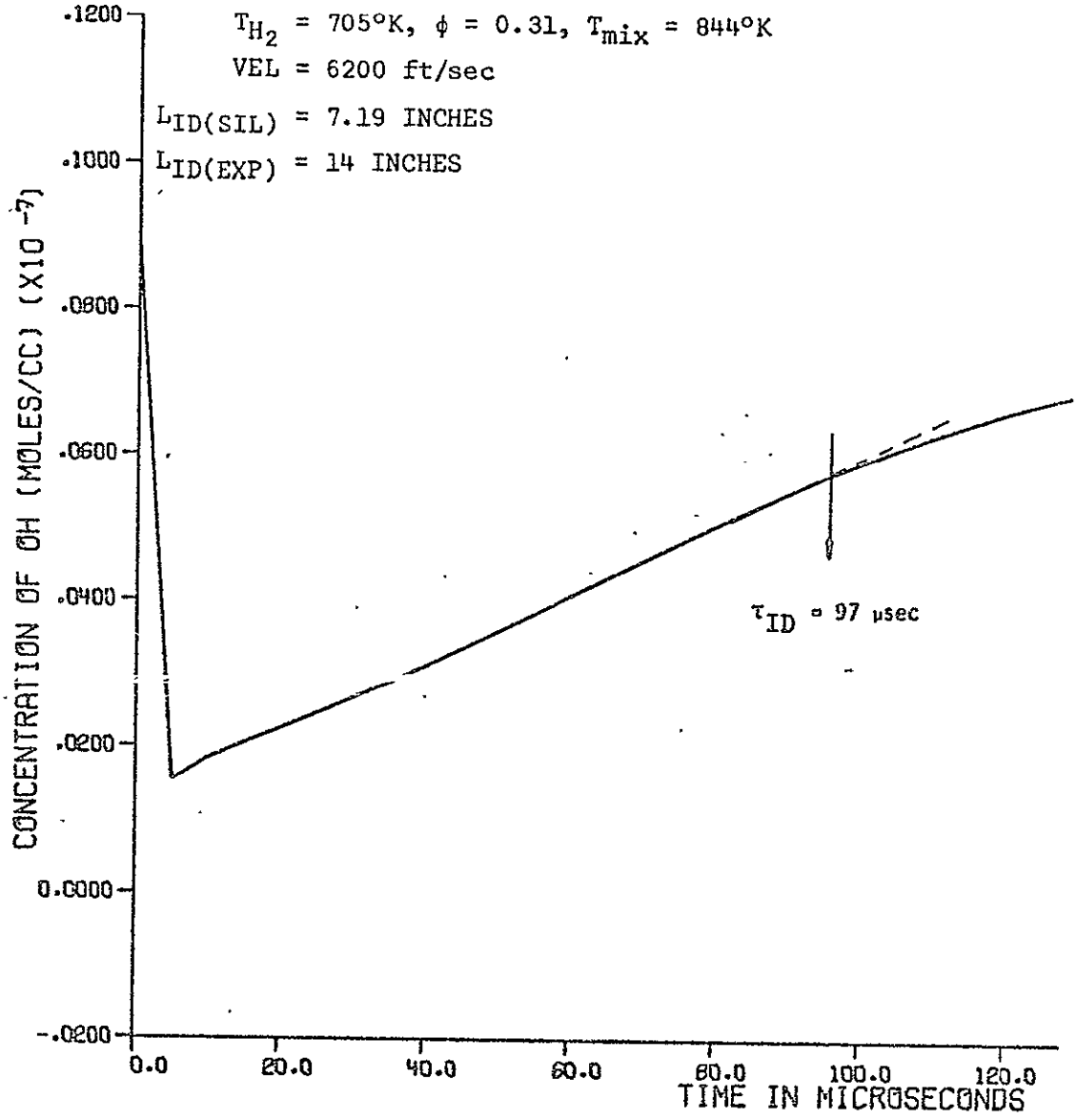

FIGURE 62 IGNITION DELAY 40% MIXING - RUN 45

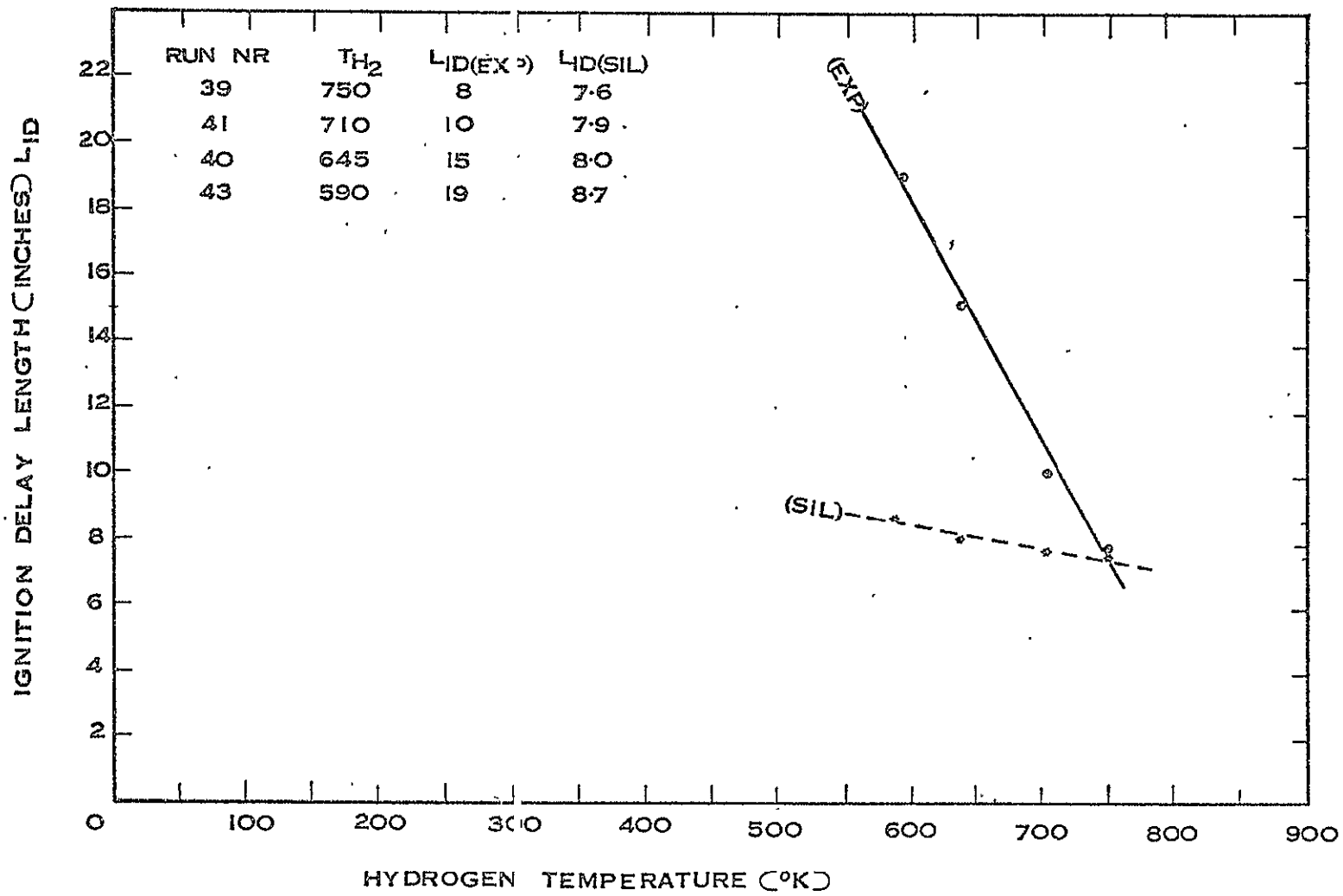

FIGURE 63 GRAPHICAL COMPARISON OF ANALYTICAL AND EXPERIMENTAL IGNITION DELAY RESULTS AS FUNCTION OF H_2 TEMPERATURE

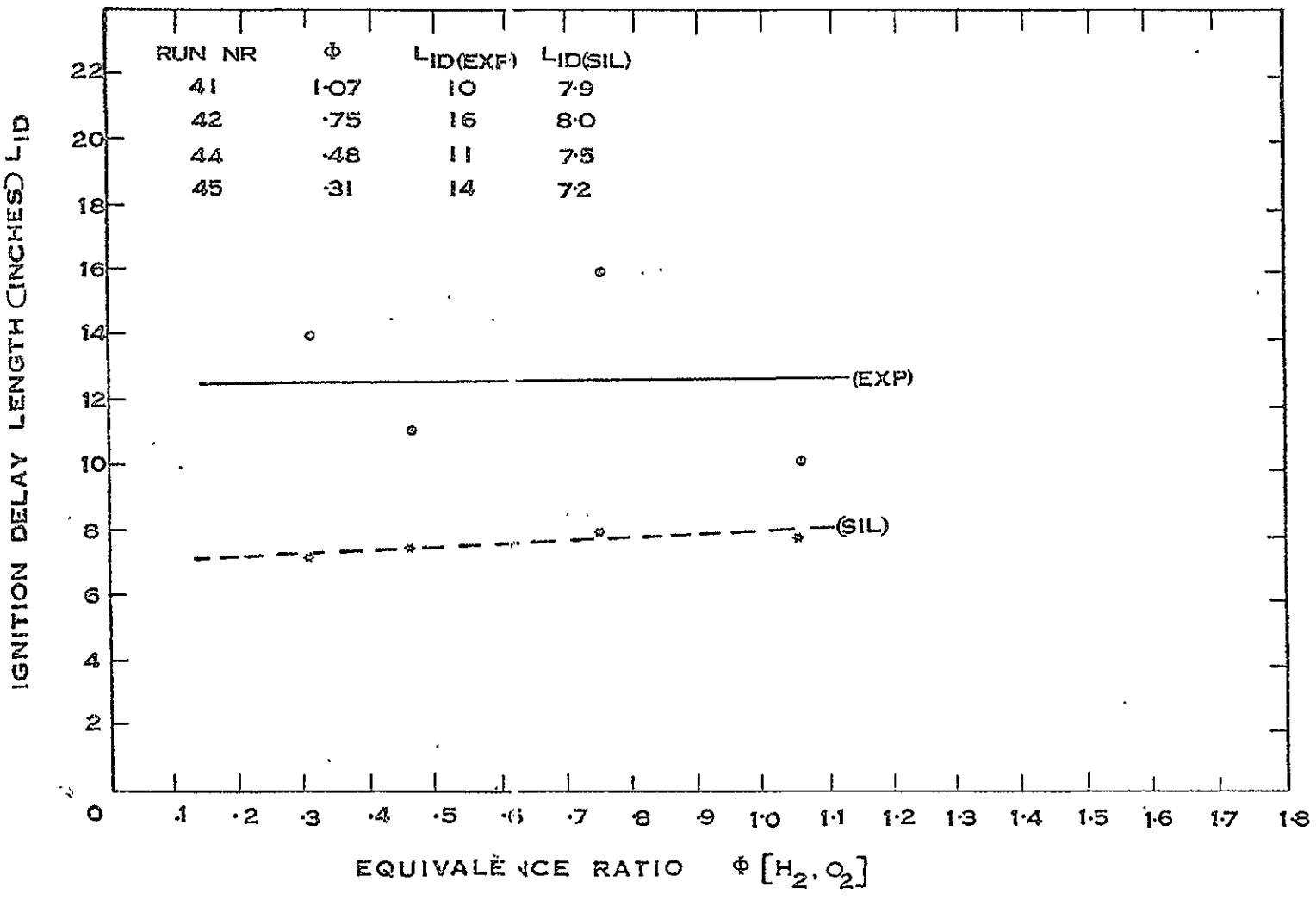

FIGURE 64 GRAPHICAL COMPARISON OF ANALYTICAL AND EXPERIMENTAL IGNITION DELAY RESULTS AS FUNCTION OF EQUIVALENCE RATIO

independence of ignition delay distances on equivalence ratio. The observed fact that the experimental data points do straddle a straight line when drawn equidistant from each point, provides some encouragement. An explanation as to why there is such scatter cannot be given at this time. Analytically, the data points do indicate a relatively constant ignition delay distance irregardless of equivalence ratio variance.

CONCLUSIONS

Detailed analytical and experimental measurements have been made in a mixing and reacting vitiated-air/hydrogen supersonic stream for the purpose of determining the effects of vitiation products (free radicals, third bodies, etc.) on the ignition delay phenomenon. On the basis of the experimental data and their subsequent application to the verification of the analytical model, it is concluded that:

1. The presence of water vapor in a combustor entrance flow can either increase or decrease the ignition delay time. This depends upon the initial temperature, pressure and concentration level which can either result in a significant generation of free radicals and increase the ignition length or cause an increase in heat sink effects and/or source for third body reactions thereby reducing ignition delay times. The present experimental system favors the latter effect because of the relatively low temperature test section environment.

2. No analytical ignition delay model, regardless of the temperature regime, can be completely independent of the mixing phenomenon. In general, the rate of a diffusion process is expected to be a quadratic function of depth and temperature. Therefore, in practical situations of interest, combustion and mixing are coupled and should be considered simultaneously.

3. Nonequilibrium free-radical content of the incoming stream accelerates the reaction process. This causes ignition to occur much sooner than would be expected if the incoming stream were near equilibrium as far as free-radical concentrations are concerned. While the vitiated air employed in this program was produced synthetically in a liquid rocket engine, similar effects would occur with any type of vitiated air system. In fact, air which is heated and subsequently expanded to the inlet condition of a supersonic combustor would result in earlier ignition than would occur in the situation where atmospheric air would be diffused to the supersonic combustor inlet conditions.

4. The results predicted by the ignition delay model are favorably substantiated by experimental data when the assumption of complete mixing is abandoned. This indicates that the use of vitiated air to simulate the ignition phenomenon for a SCRAMJET system will lead to erroneous data if the air entering the SCRAMJET combustor is near equilibrium conditions. It must be emphasized that these conclusions only apply in the low temperature supersonic regime. Therefore, direct ground simulation of supersonic ignition in the regime where reaction times are rate controlling is difficult and, without a knowledge of the equilibrium conditions leaving the diffuser, may be impossible to achieve experimentally.

5. In the temperature regime investigated ($\sim$ 850°K) the experimentally measured content (4 percent) of nitric oxide (NO) in the vitiated air was observed to have little effect on the ignition delay length. The catalytic accelerating effect as indicated in the literature was found to be nonexistent. Therefore, it is concluded

that while it is theoretically possible for NO to profoundly decrease the ignition delay time at temperatures greater than 1000°K, at the lower temperatures, its presence seems to be ineffectual in the existing experimental effort.

RECOMMENDATIONS

On the basis of the present investigation into the effect of nonequilibrium conditions on the combustion of hydrogen in supersonic streams, many precursory results were generated. To better define these findings and to reconfirm the conclusions specified, the following recommendations are offered:

1. To virtually eliminate the minor influence of the entrained ambient air and to closely as possible simulate the instantaneous and complete mixing of the two dissimilar streams, the experimental apparatus should be modified for centerline hydrogen injection. This would, in turn, place the CIL computer program and the experimental boundary conditions on a similar basis as far as the assumption of the ignition delay process being rate rather than mixing controlling in the low temperature regime.

2. Due to the fact that the point of deviation from straight line OH radical concentration growth was arbitrarily chosen from many equally valid ignition delay length criteria as the best method for analytically measuring this phenomenon, the reacting vitiated-air/hydrogen mixture should be axially probed for OH radical growth. This can be logically accomplished with a translating absorption-emission spectrometer. Then, the results can be simultaneously compared with the experimentally observed ignition delay length.

3. Since it has been shown that mixing cannot be completely ignored in any type of binary stream combustion process, a detail mixing investigation should be initiated to effectively determine how influential this effect is in a relative low temperature regime. Also, the presence of nonequilibrium species and excessive water content in the flowing medium (vitiated air) may have an applicable effect on the mixing process.

4. The ultimate objective for any vitiated air investigation is to obtain enough data to be able to predict the outcome of an experimental run made with clean air when compared to the same run made with synthetic air. Therefore, an effort should be made to rerun all of the ignition delay experiments employing a clean air source. This would generate experimentally the data necessary for comparison with the results of the analytical portion of the investigation concerning real air.

5. The investigation of the ignition process as an approach to determine the effect of vitiation on the combustion of hydrogen in a supersonic flowing stream is sufficient but only so far as an initial step in the overall understanding of the complete combustion process when practically applied to the ground testing of SCRAMJET propulsive systems. The primary goal envisioned is the understanding of the effect of vitiation on the complete supersonic combustion process. In this sense, work should be continued on the determination of these effects on the overall combustion efficiency (η_c). It is felt that the method as presented in Appendix G is apropos.

BIBLIOGRAPHY

1. Ferri, A., "Review of Problems in Application of Supersonic Combustion," The Seventh Lanchester Memorial Lecture, Royal Aeronautical Society, London, England, May 14, 1964.

2. Scaggs, N. and R. Dunn, "Development of a Facility for Supersonic Combustion Simulation," AIAA Paper No. 66-743.

3. Bryce, C.A., "An Investigation of Nonequilibrium Effects on Combustion in Supersonic Streams," Ph.D. Thesis, Purdue University, January 1969.

4. Momtchiloff, I.N., E.D. Taback, and R.F. Buswell, "Kinetics in Hydrogen-Air Flow Systems. I. Calculation of Ignition Delays for Hypersonic Ramjets," Ninth Symposium (International) on Combustion, Academic Press, 1963.

5. Nicholls, J.A., "Stabilization of Gaseous Detonation Waves with Emphasis on the Ignition Delay Zone," Ph.D. Thesis, University of Michigan, 1960.

6. Nicholls, J.A., T.C. Adamson, Jr., and R.B. Morrison, "Ignition Time Delay of Hydrogen-Oxygen-Diluent Mixtures at High Temperatures," AIAA Journal, Vol. 1, No. 10, October 1963.

7. Brokaw, R.S., "Analytical Solutions to the Ignition Kinetics of the Hydrogen-Oxygen Reaction," NASA-2542, December 1964.

8. Pergament, H.S., "A Theoretical Analysis of Nonequilibrium Hydrogen-Air Reaction in Flow Systems," General Applied Science Laboratory Technical Report No. 325A, November 1962.

9. Belles, F.E. and M.R. Lauver, "Origin of OH Chemiluminescence During the Induction Period of the H_2-O_2 Reaction Behind Shock Waves," Journal Chem. Phys., Vol. 40, No. 2, January 1964.

10. Das Gupta, N.C., McGill University, Department of Mechanical Engineering, Report No. SCS36, 1961.

11. Mullins, B.P., NATO AGARD AG5/P2, 1952.

12. Foure, C., Recherche Aeron., 33, 1954.

13. Rhodes, R.P., "The Effect of Nonequilibrium Free-Radical Concentration on Ignition Delay in the Hydrogen-Air-System," AEDC-TDR-64-241, November 1964.

14. Snyder, A.D., J. Robertson, D.L. Zanders, and G.B. Skinner, "Shock Tube Studies of Fuel-Air Ignition Characteristics," Technical Report AFAPL-TR-65-93, August 1965.

15. Schott, G.L. and J.L. Kinsey, "Induction Times in the Hydrogen-Oxygen Reaction," Journal Chem. Phys., Vol. 29, No. 5, November 1958.

16. Rubins, P.M. and R.P. Rhodes, "Shock-Induced Combustion with Oblique Shocks: Comparison of Experiment and Kinetic Calculations," AIAA Journal, Vol. 1, No. 12, December 1963.

17. Cherry, S.S., TRW Systems Report No. 08832-6001-T0000, May 1967.

18. Poulsen, P. and J.G. Skifstad, "A Thermochemistry Program for Air-Augmented Rocket Computations," 26 August 1968, Report No. RK-TR-68-14, Army Propulsion Laboratory and Center.

19. Zupnik, T.F., E.N. Nilson, and V.J. Sarli, "Investigation of Nonequilibrium Flow Effects in High Expansion Ratio Nozzles," Computer Program Manual, Report No. UACRL-C910096-11 (NASA CR-54042), September 1964.

20. Bray, K.N.C., "Atomic Recombination in a Hypersonic Wind Tunnel Nozzle," J. Fluid Mech., 6, 1959.

21. Hersch, M., "Hydrogen-Oxygen Chemical Reaction Kinetics in Rocket Engine Combustion," NASA TND-4250, December 1967.

22. Hofmann, J.R., "An Experimental Method for Measuring Temperature Profiles," M.S. Thesis, Purdue University, June 1968.

23. Blackburn, G.F. and F.R. Caldwell, "Reference Tables for 40 Percent Iridium-60 percent Rhodium Versus Iridium Thermocouples," Journal of Research of the National Bureau of Standards, Vol. 66-C, No. 1, January-March 1962, pp. 1-12.

24. Bar-Gadda, I. et al, "Supersonic Combustion" Republic Aviation Corporation Report, RD-TR-64-641, 5 December 1964.

25. Breck, D.W., "Crystalline Molecular Sieves," Journal of Chemical Education, Vol. 48, December 1964, p. 678.

26. Cornu, A. and R. Massot, "Compilation of Mass Spectral Data."

27. Scadron, M.D. and I. Warshawsky, "Experimental Determination of Time Constants and Nusselt Numbers for Bare-Wire Thermocouples in High Velocity Air Streams and Analytic Approximations of Conduction and Radiation Errors," NACA Technical Note 2599, January 1952.

28. Siegelman, D. and O. Fortune, "Computer Program for the Mixing and Combustion of Hydrogen in Air Streams," GASL TR 618, July 1966.

29. Bird, R., W. Stewart, and E. Lightfoot, "Transport Phenomena," paragraph 16.3, John Wiley and Sons, Inc., 1965.

30. Simon, W.E. and L.A. Walter, "Approximations for Supersonic Flow Over Cones," AIAA Journal, Vol. 1, No. 7, 1963.

31. Sutton, G.P., "Rocket Propulsion Elements," John Wiley and Sons, Inc., 1965.

APPENDIX A

FACILITY DESCRIPTION

The experimental research program discussed herein was conducted in the Combustion Research Laboratory at the Zucrow Engineering Research Center of Purdue University. This facility was constructed with flexibility to conduct combustion experiments as a prime design feature, however, one of the other criteria was to be able to investigate problems related to the combustion of storable liquid rocket systems. The storable propellant capability made this facility readily adaptable to the requirements of the present program.

The Combustion Research Laboratory also has an extensive control room for remote operation of combustion experiments. The control room contains instruments for data recording (i.e., strip charts, oscillograph, and a 60 channel magnetic tape unit) and a flow system control panel with an automatic sequencer for the main propellant valves. A photograph of the main control panel is presented in Figure A-1. Any pneumatically operated valve in the facility can be operated off the main control panel. The sequencing unit is set-up to automatically open each valve at the proper time and to check for operating malfunctions. Since the control room services two test cells and four separate experiments, the instrumentation had to be scheduled.

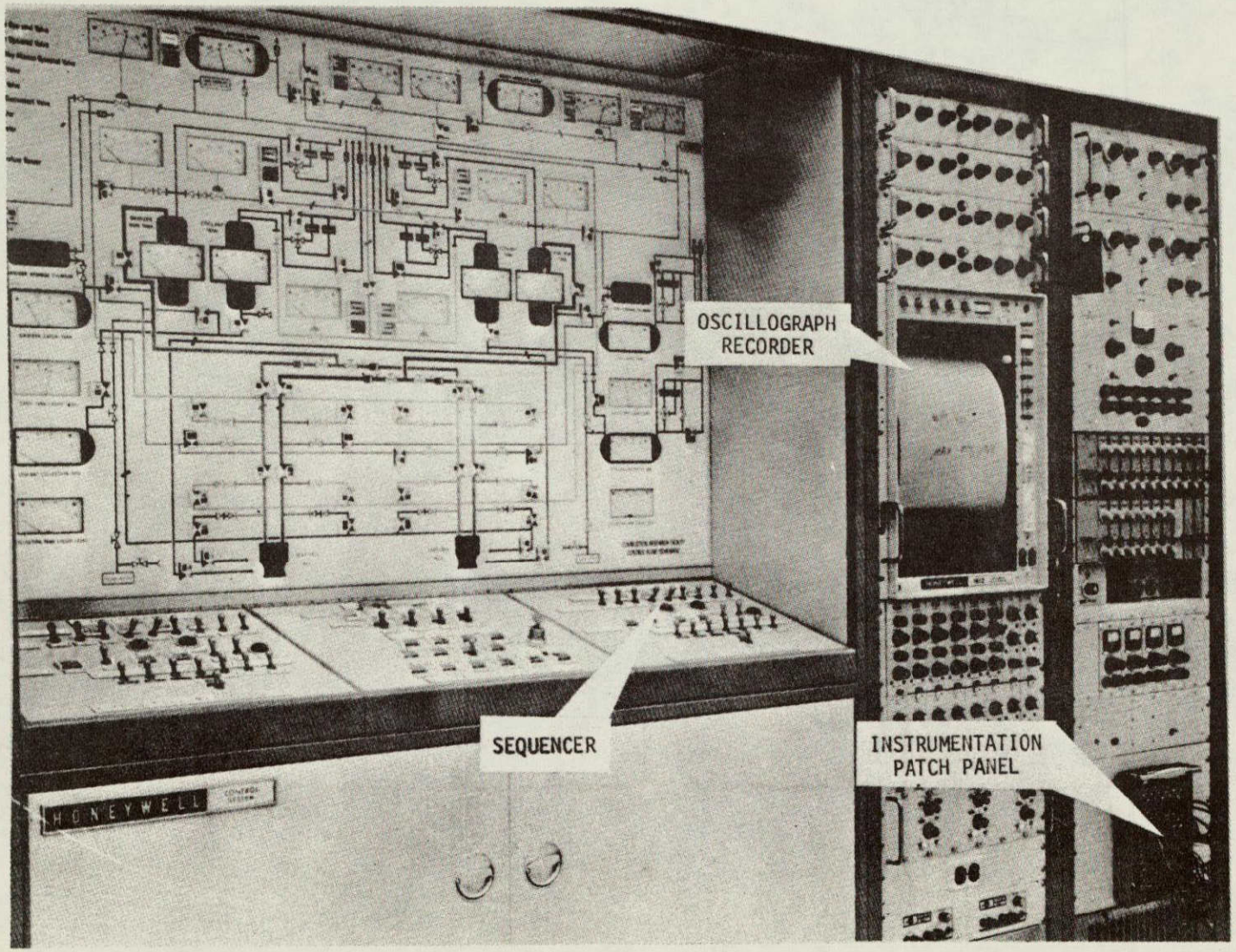

FIGURE A-1 MAIN CONTROL PANEL

Each researcher was provided with a prewired instrumentation patch panel to provide rapid changeover between different experiments.

The hydrogen heater was an addition made to the Combustion Research Facility specifically for this program. A separate control panel was also added for operating the hydrogen heater. A photograph showing the hydrogen control panel is presented as Figure A-2. The hydrogen heater is operated separately from the main flow control system. The heater is initially brought up to operating temperature prior to starting preparations for firing the gas generator. Flow of propane to the burners is controlled manually at the control panel. Two temperature controllers are provided for operating the hydrogen heater. One monitors tube wall temperature and the other the exhaust gas stack temperature. If either of these controls reaches a preset limit, the hydrogen heater is automatically shut down.

The propellant system in use at the Combustion Research Laboratory at the time of these experiments were nitrogen tetroxide and a 50/50 blend of hydrazine and unsymmetrical dimethylhydrazine. Since nitrogen tetroxide was employed in the present program, the existing oxidizer system was directly connected to the gas generator. A separate propellant supply system was added to handle the anhydrous hydrazine fuel to avoid interference with other programs. High pressure nitrogen was available at the test cell. Piping, valves and a regulator were added to provide the nitrogen diluent supply system. The hydrogen system was a new addition to this facility so that a complete system had to be installed for these experiments. A flow schematic of the propellant supply system for the supersonic

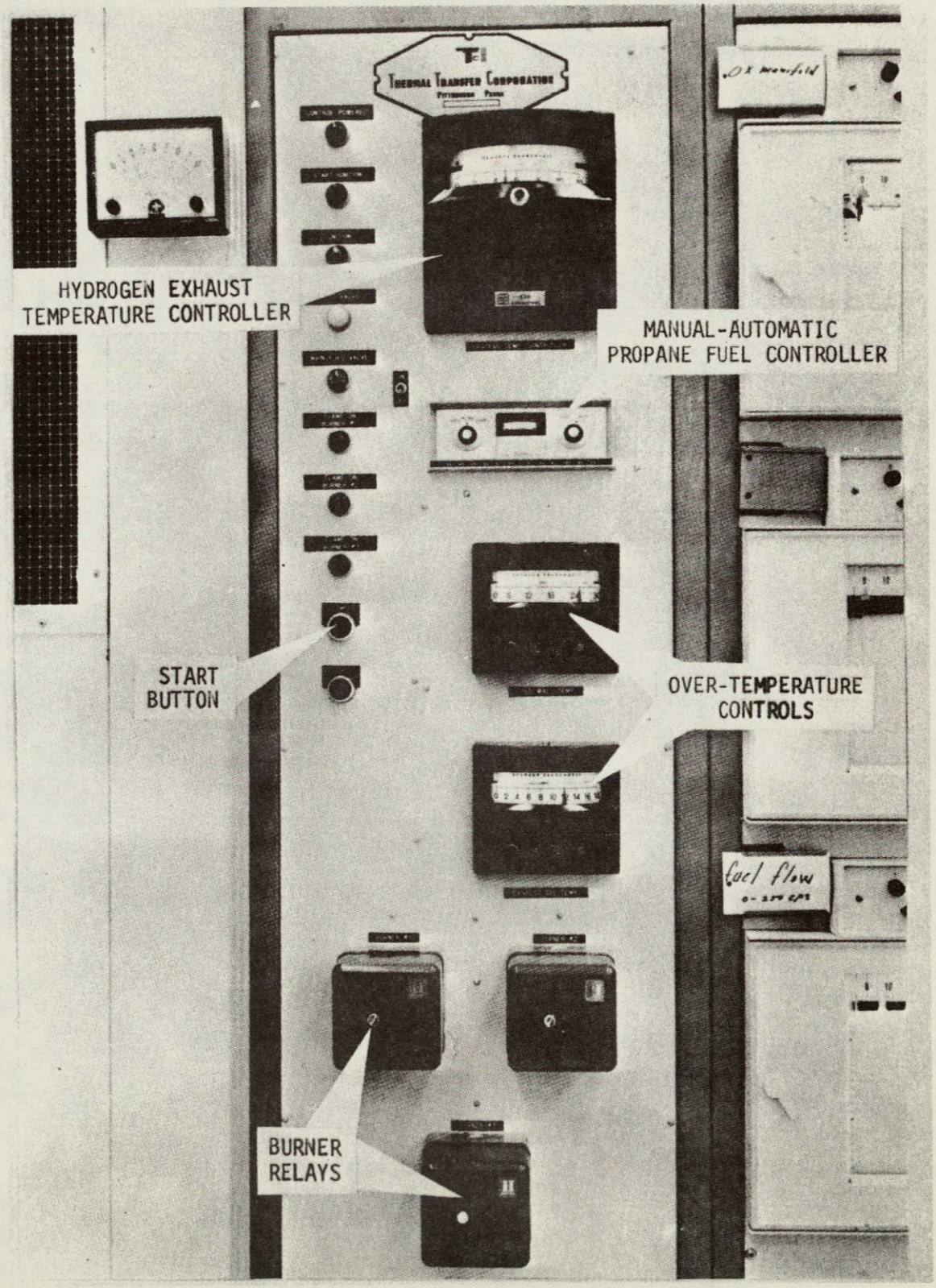

FIGURE A-2 HYDROGEN CONTROL PANEL

combustion experiments is presented as Figure A-3. The dotted lines on this figure represent the facility fuel supply system which was not employed in this program .

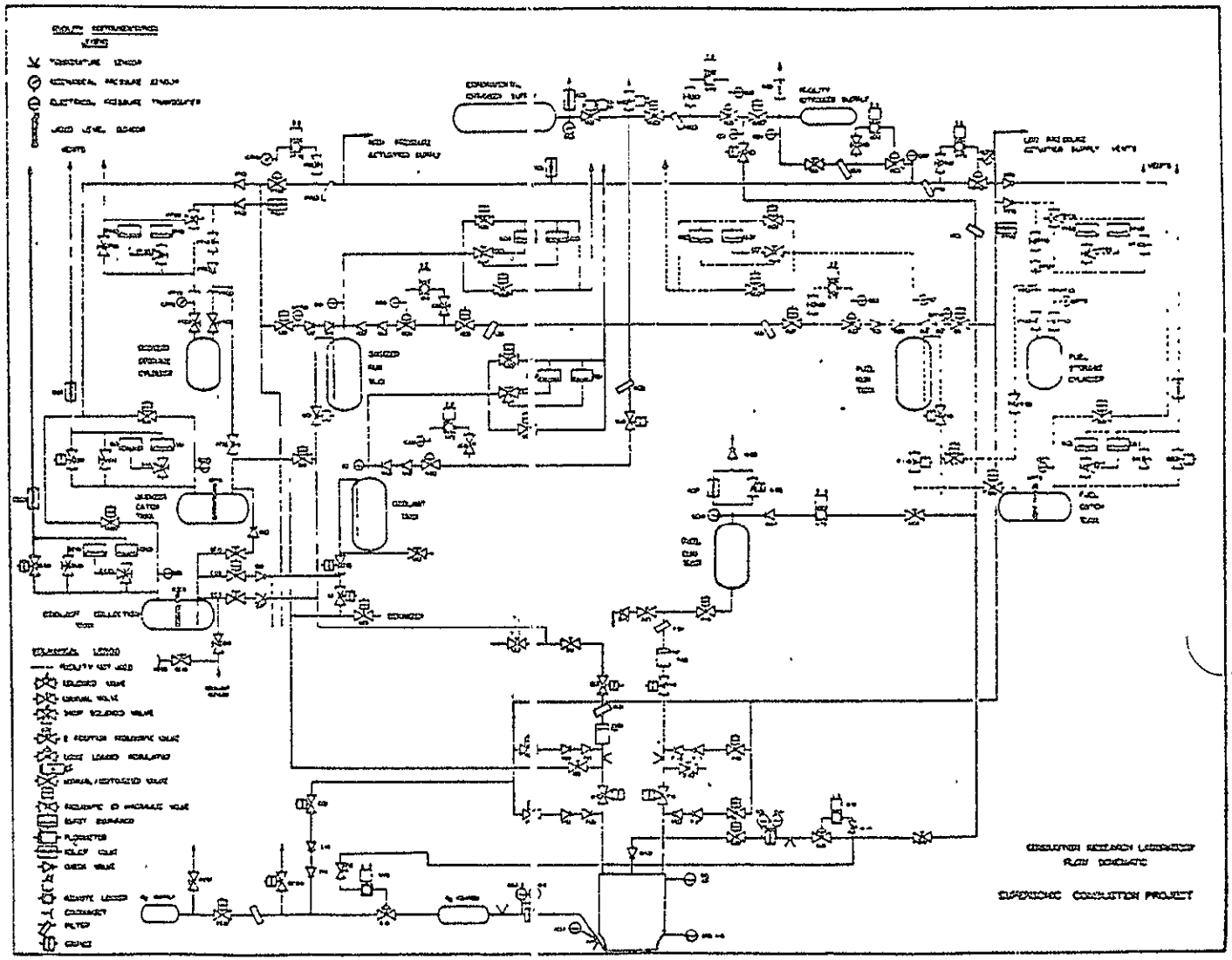

FIGURE A-3 PROPELLANT SUPPLY SYSTEM SCHEMATIC

APPENDIX B

HEAT TRANSFER ANALYSIS FOR COPPER ENGINE DESIGN

The objective of the following analytical effort was to determine the theoretical run duration failure limit of a gas generator fabricated from oxygen free electrolyte tough pitch copper. By using a resistor capacitor analog unit and a temperature input simulator, it is possible to obtain the temperature versus time curves for any radial section of the nozzle. Since the throat of the converging-diverging nozzle section is the location of the most severe heat transfer rates, the analysis was specifically directed towards determining the temperature versus time curves for the throat of the nozzle area.

The basic design values utilized in the analysis were P_c = 1000 psia, T_o = 4500°R and h = 1.04×10^{-3} BTU/in^2-sec-°R. The film heat transfer coefficient (h) was calculated using Bartz's equation [31]. Values of parameters used in this equation were generated by the Finite Rate Reacting Gas program.

Employing the analogy between thermal and electrical resistance/capacitance circuits in transient flows, temperature versus time curves were generated. The simulation was performed on the throat by assuming a step temperature input and using the most severe design conditions of heat transfer as previously specified. The output

response was traced by an Offner Dynograph. Numerical results were subsequently obtained by applying time and temperature scales factors to the graphical output trace.

The basic calculations were made by dividing the nozzle throat radial into equal volume elements. A schematic of this operation is presented in Figure B-1. Each volume element corresponds to equal thermal and electrical capacitance. The computation of their appropriate thermal resistances and capacitance was accomplished accordingly by the following relationships:

(1) $$\frac{1}{N}\left(r_0^2 - r_1^2\right) = \left(r_{n+1}^2 - r_n^2\right)$$

(2) $$C_{th} = \rho V\, c_p = \rho \frac{1}{N}\left(r_1^2 - r_0^2\right) c_p$$

(3) $$r_{mn} = \left(\frac{r_n^2 + r_{n+1}^2}{2}\right)^{1/2}$$

(4) $$\Delta r_{n1} = r_{mn} - r_n$$

(5) $$\Delta r_{n2} = r_{n+1} - r_{mn}$$

(6) $$R_{th} = \frac{\Delta X}{kA}$$

(7) $$R_{th_1} = \frac{\Delta r_{n1}}{k\pi\left(r_{mn} + r_{n+1}\right) L}$$

(8) $$R_{th_2} = \frac{\Delta r_{n2}}{k\pi\left(r_{mn} + r_{n+1}\right) L}$$

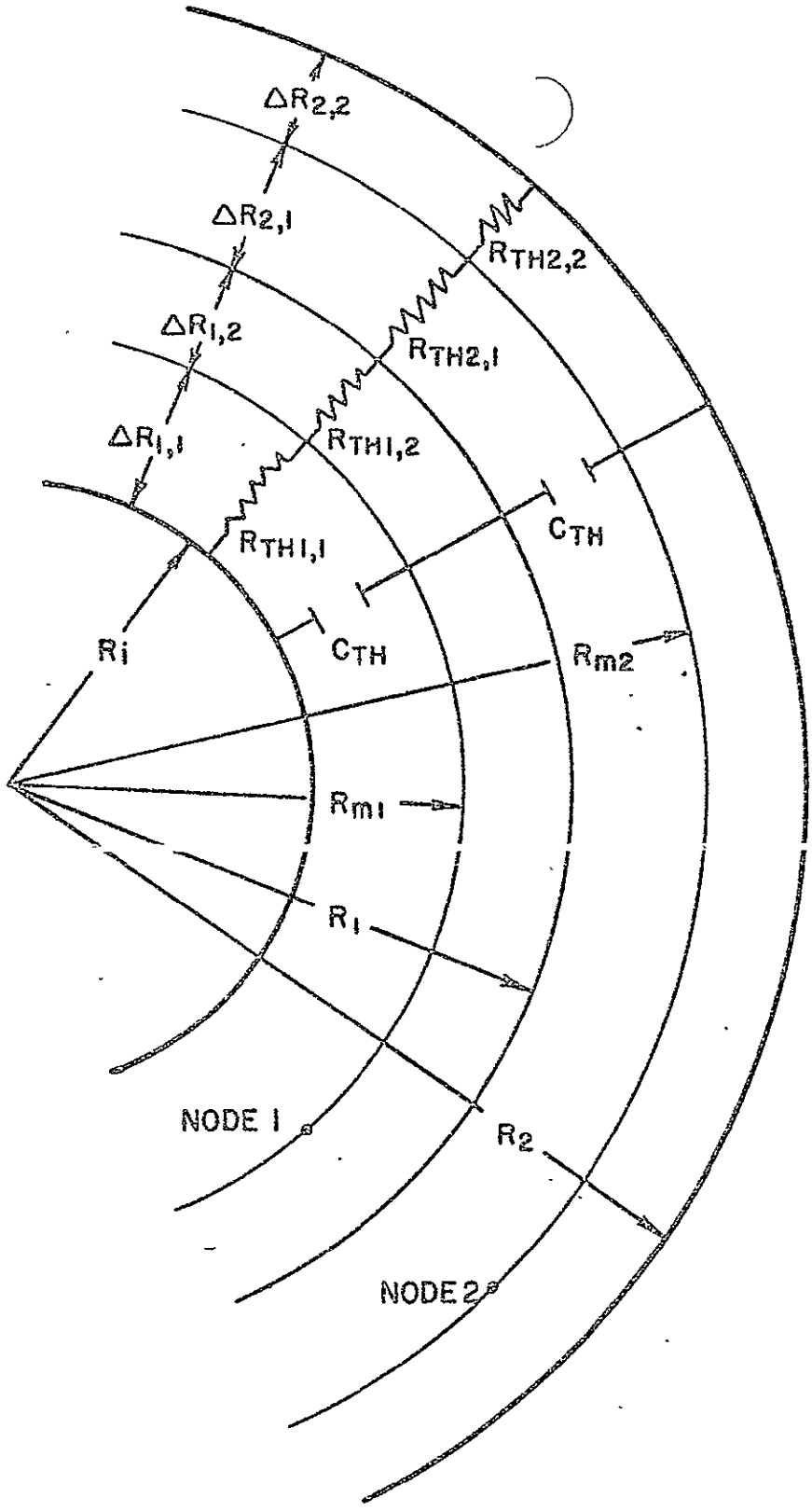

FIGURE B-1 SCHEMATIC OF ANALOGY BETWEEN THERMAL AND ELECTRICAL CIRCUITS

These computed values are converted to electrical values by arbritrarily setting the smallest thermal resistance equal to a variable value (to be discussed later) and normalizing the other resistances with this value. The thermal capacitance is then equated to a chosen electrical capacitance.

These chosen values of electrical resistance and capacitance must be carefully selected according to the following relationship:

$$(9) \qquad \frac{R_{th}\, C_{th}}{R_e\, C_e} = \frac{t_{th}}{t_e} = T$$

If T is large, the electrical response will be too fast and will be inaccurately recorded.

Table B-1 contains the values used in this analysis. The thermal resistance was computed using equations (7) and (8) instead of the following equation

$$(10) \qquad R_{th} = \frac{\ell n\ (r_{n+1}/r_n)}{2\ \pi\ k\ L}$$

because for small Δr_n, (r_{n+1}/r_n) approaches unity and R_{th} approaches zero. The given relationships (equations (7) and (8)) are accurate when Δr_n is small.

The convection resistance R_{th_h} is found from the following equation

$$(11) \qquad R_{th_h} = \frac{1}{hA} = \frac{1}{h\ 2\pi\ r_i\ L}$$

R_{th_h} must also be normalized with the same value used previously.

TABLE B-1

NOZZLE HEAT TRANSFER DESIGN PARAMETER VALUES

Radius (inches)	Δr (inches)	Mean Radius (inches)
0.5030		
	0.1365	0.5753
0.6395		
	0.1121	0.6978
0.7516		
	0.0974	0.8018
0.8490		
	0.0873	0.8938
0.9364		

etc. until r_0 = 1.61 inches

R_{th}	R_{th} (normalized)	R_e (used in circuit) KΩ
0.00256	8.78	
0.00202	6.91	126
0.00166	5.71	
0.00141	4.86	90.9
0.00123	4.23	
0.00109	3.74	71.0
0.00098	3.36	
0.00089	3.04	58.3

etc. for the remaining divisions

smallest R_{th} = 0.000291

Total R_{th} = 0.0222

Total Capacitance = 0.108 μ farads

C_e = 1.0 μ farads per volume element

T = 0.761

The electrical circuit is set up using decade resistors, decade capacitors, and a step input voltage source. The set up is shown schematically in Figure B-2. Both the input step voltage and output response are simultaneously recorded, thereby permitting the initial t = 0 point to be indicated on the graphical record along with the temperature versus time curve.

The procedure for recording the profiles is as follows:

1. Calibrate the output channel by connecting it to the step input. This output level corresponds to the step temperature of the chamber (T_o = 4500°R) or T_{aw} of the gas stream.

2. Short the capacitors to insure no initial voltage.

3. Connect the input channel to the desired node. These nodes correspond to certain known depths in the wall. Again, observe the recorder to insure that the zero level is maintained. This level is the ambient temperature value prior to ignition.

4. Apply the step input and record the response. Assure that the paper recording speed is fast enough to give reasonable accuracy and yet slow enough to yield an accurate response. If the paper speed must be increased to the point where the response is questionable, then the electrical resistance and capacitance values must also be increased such that the time constant of the circuit is raised.

The output trace from the recorder is in the form of a graph whose coordinates are temperature versus time. Knowing the failure temperature limit of copper($\sim$ 2000°R) it is a simple matter of proceeding along the output curve until this failure temperature line is intersected. At this point, the run duration time is noted. Based

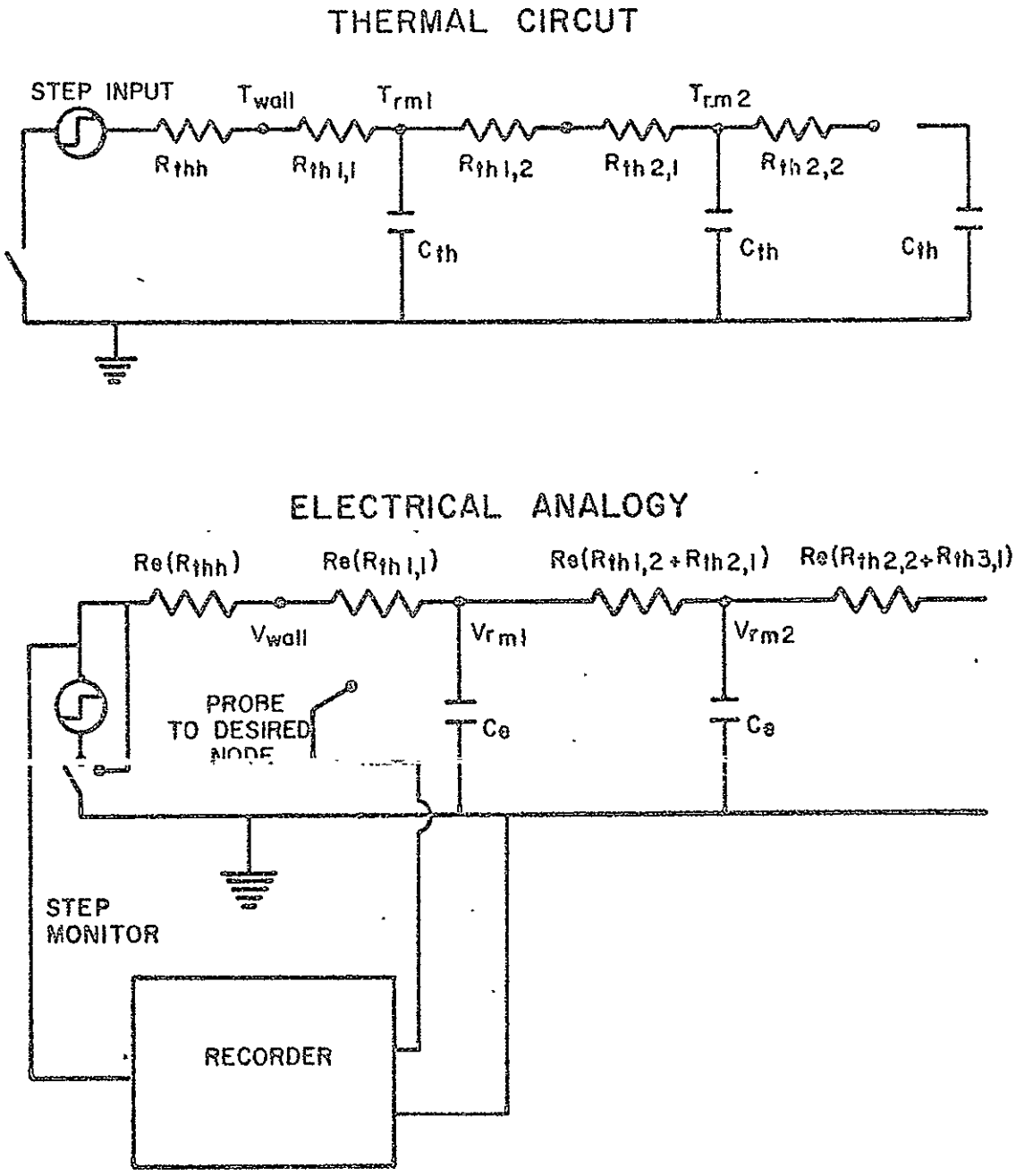

FIGURE B-2 SCHEMATIC OF ANALOG UNIT

on the previously specified initial and boundary conditions, it was analytically shown that the nozzle throat area would withstand a run duration up to approximately 14 sec. before failure. The design and employment of the all copper system was predicted on the outcome from this analysis. As mentioned earlier in this report, the total copper system performed successfully during all runs without any visible signs of deterioration.

APPENDIX C

HYDRAZINE FUEL TRANSFER CHECKLIST

Supersonic Combustion Program

Procedure for Transfer of Hydrazine into Fuel Storage Tank

1. Vent fuel (storage/run) tank by depressing D-27 on control console. _____
2. Remove Hydrazine drum from storage and deliver to loading area and set on weighing scales. _____
3. Install capped-off bung in Hydrazine fuel drum. _____
4. Install regulator, gauge, check valve and flex line on 150 psig N_2 line (see schematic drawing Figure C-1). _____
5. Locate water hose and turn on water. _____
6. Purge line and with small bleed flow connect N_2 line to small bung on Hydrazine fuel drum. _____
7. Install flex line to N_2H_4 inlet at wall from outlet of Hydrazine fuel drum. _____
8. Weigh fuel drum (Total Weight _____ lb_f). _____
9. USE CAUTION Bleed flex line full of N_2H_4 by cracking nut at wall inlet. _____
10. Set gauge pressure at 10 psig with regulator (continue to set to this pressure). _____
11. Crack fitting on 150 psig N_2 line located on top of Hydrazine storage/run tank. _____
12. Open N_2H_4 fuel inlet valve at wall and Hydrazine fuel drum outlet valve for 5 seconds. _____
13. Feel transfer line for hot spots. Secure transfer operations and leave area immediately if any hot areas are observed. _____

14. Proceed to transfer Hydrazine if no indication of hot spots. _____

15. On completion of the transfer of the desired amount of Hydrazine turn off Hydrazine valve at drum outlet. _____

16. Record weight of fuel drum (Total Weight _____ lb_f). _____

17. Retighten fitting on 150 psig N_2 line located on top of Hydrazine storage/run tank. _____

18. Turn off N_2H_4 fuel inlet valve at wall and disconnect fuel flex line at wall under blanket of water. USE CAUTION _____

19. Vent N_2 pressure from the N_2 pressure line to the Hydrazine fuel drum. _____

20. Remove depressurized N_2 pressure line from Hydrazine fuel drum and cap off bung. _____

21. Shut off N_2 valve at wall and disconnect line. _____

22. Disconnect and clean fuel flex lines with de-ionized water flush and wrap with polyethylene sheet. _____

23. Remove Hydrazine fuel drum and lines to storage area.

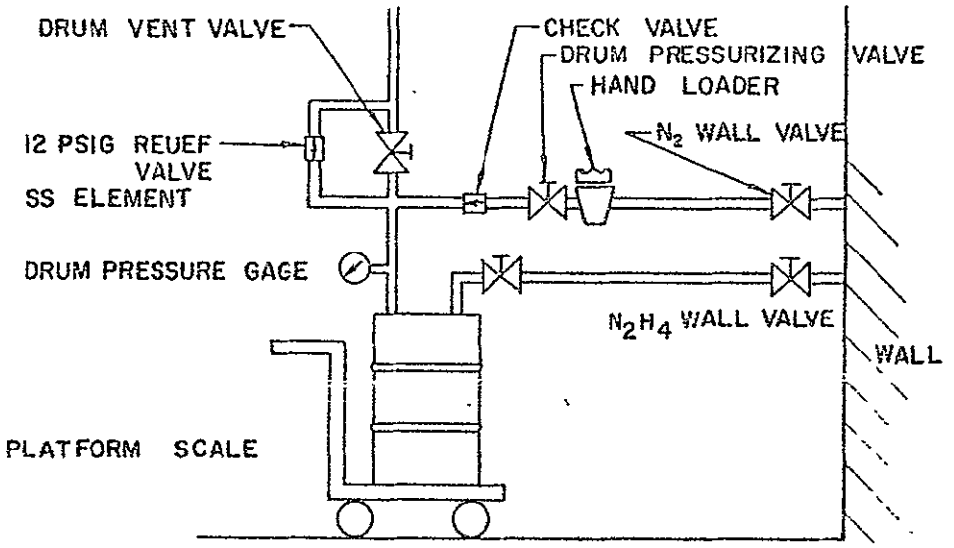

FIGURE C-1 SCHEMATIC DRAWING OF HYDRAZINE TRANSFER APPARATUS

APPENDIX D

CHECKLIST FOR TYPICAL SUPERSONIC COMBUSTION

IGNITION DELAY EXPERIMENTAL RUN

Supersonic Combustion Program

Operational Procedures

I. Prefire Operation

A. Hand Valve Adjustments
1. Open N-23 _____
2. Open water valves to sumps in run tank room _____

B. Test Preparation
1. Secure both cells _____
2. Close J-Boxes and turn on N_2 bleed _____
3. Close gates _____
4. Turn on warning lights _____

C. Pressurize N_2 supply
1. Adjust N-85 to 1500 PSI _____
2. Adjust PT-80 and PT-81 to 150 PSI _____
3. Set purge pressure using N-87 to ____ PSI _____

D. Start Up H_2 Heater
1. Open hand valve at propane tank _____
2. Turn power on for panel by throwing #12 in LP 2 box _____
3. Shut main fuel valve off _____
4. Push green reset button on flame safety relays _____
5. Check to see red lights are off on tube wall and exhaust temperature limit controls _____
6. Put control on manual and drive closed _____
7. Push start button and hold till all three blue lights come on _____
8. Turn on main fuel valve switch but do not open manual control _____

E. Load Oxidizer Run Tank and Fill Lines
   1. Follow standard facility procedure to load oxidizer tank
   2. Turn on Floor wash both sides
   3. Open O-11 (hand valve)
   4. Open O-10 and O-13
   5. Open B-10 and pressurize tank to 150 PSI
   6. Open catch tank isolation valve
   7. Open hand valve D-31 for 15 seconds
   8. Close D-31
   9. Close catch tank isolation valve

F. Fill Fuel Lines
   1. Set system deluge
   2. Open D-24 and F-13
   3. Open C-17 and pressurize fuel tank to 150 PSI, then close
   4. Open hand valve D-28 for 5 seconds
   5. Close D-28
   6. Check potters with magnet

G. Fill H_2 Lines
   1. Open hand valves to each bottle
   2. Open H-27 (hand valve)

H. Final System Pressurization
   1. Turn on high rate ventilators
   2. Close N-40
   3. Open N-10
   4. Open N-15
   5. Regulate N-81 to ____ PSI (Strip Chart)
   6. Open N-26
   7. Set oxidizer tank pressure using N-84 to ____ PSI (Strip Chart)
   8. Open N-42b
   9. Open P-35
   10. Set fuel tank pressure using N-80 at ____ PSI (Strip Chart)

I. Final Heater Preparation
   1. Open C-23 and allow process gas temperature to reach ____°F
   2. Regulate hydrogen pressure to ____ PSI using N-83

J. Sequencer
   1. Set malf. #1 timer at ___ seconds
   2. Set malf. #2 timer at ___ seconds
   3. Set malf. #3 timer at ___ seconds
   4. Set prefire purge at ___ seconds
   5. Set postfire purge at ___ seconds
   6. Set overall malf. timer at ___ seconds

7. Set test duration timer at ___ seconds _____
8. Set oscillograph to read oxidizer flow, fuel flow, and 60 Hz time line _____
9. Start countdown after initial purge _____
10. Operate manual valve to heater at the count of ___ _____
11. Operate fuel purge at count of ___ _____
12. Start camera at count of ___ _____
13. Hold oxidizer and fuel purge manually just before fire switch is thrown and release just after motor starts _____
14. Purge manually (before post-fire purge terminates) until gas generator stream is clean) _____
15. Shut down heater on post-fire purge, push stop button, close main fuel valve (manual) _____

II. Post Fire Operations

A. Depressurize Fuel and Oxidizer Tanks
1. Close N-10 _____
2. Close N-42b, N-15 and N-26 _____
3. Decrease N-80 to fully closed position _____
4. Decrease N-84 to fully closed position _____
5. Vent fuel tank to 0 PSI using D-27 and vent oxidizer tank to 150 PSI using N-38 _____

B. Depressurize N_2 System
1. Open N-40 _____
2. Open N-26 _____
3. Open N-42b _____
4. Open 0-15 - N_2 vents thru chamber _____
5. Open N-15 _____

C. Drain Oxidizer Lines
1. Open B-10 _____
2. Open D-10 and drain run tank _____
3. Close 0-10 and B-10 _____
4. Purge line using P-21 _____
5. Close 0-13 _____
6. Close D-10 _____

D. Drain Fuel Lines
1. Close D-24 _____
2. Open hand valve D-23 (1/4 turn) _____
3. Purge with P-15 (watch fuel flow recorder) _____
4. Close D-23 _____
5. Close F-13 _____
6. Drain fuel line at test stand _____

E. Shutdown H_2 System

1. Close C-23 after heater cools down _____
2. Decrease N-83 to fully closed position _____
3. Close hand valves on H_2 bottles _____
4. Open CC-21 _____
5. Increase N-83 to partially open position _____
6. Open hand purge H-28 and vent H_2 line _____
7. Close H-28 _____
8. Decrease N-83 to fully closed position _____
9. Close H-27 _____
10. Turn off propane valve at tank _____
11. Close CC-21 _____

F. Final Shutdown

1. Return all valves to normal position _____
2. Shutdown 150 PSI supply _____
3. Shutdown 1500 PSI supply _____
4. Turn off warning lights _____
5. Turn off floor washes and water to sumps _____
6. Turn off N_2 to J-boxes _____
7. Close O-11 and N-23 (hand valves) _____
8. Secure test cell _____

APPENDIX E

GAS SAMPLE APPARATUS DESCRIPTION AND OPERATIONAL PROCEDURE

The fundamental objective of gas sampling is to obtain a sample which is representative of the composition of the fluid at the sampling point. Probes employed in this program to capture a representative vitiated air sample were previously described in the section on instrumentation. This appendix is primarily concerned with the description of the associated gas sample apparatus and its overall operations.

Obtaining a vitiated air sample from the existing experimental apparatus presents a unique problem. During startup of the gas generator, there is a probability of obtaining erroneous specie concentration data due to contamination. Because an oxidizer lead is employed, nitrogen tetroxide could collect on the inside of the gas sample lines and invalidate any sample subsequently collected. To overcome this obstacle, a system was designed and tested (Run 36) which provides a high pressure nitrogen gas sample line purge (150 psig) until steady state gas generator operation is obtained. A photograph and schematic drawing of the gas sampling apparatus are respectively presented as Figures E-1 and E-2.

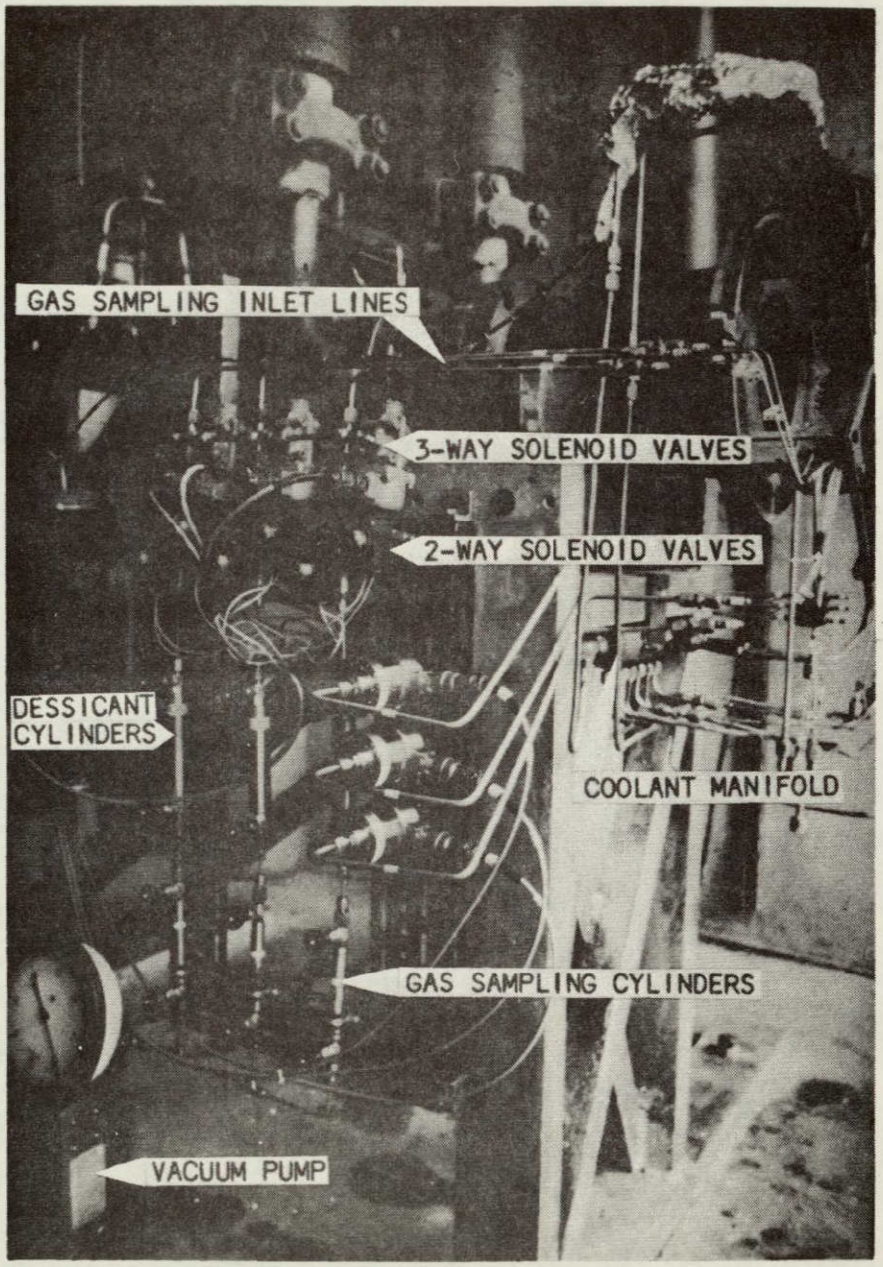

FIGURE E-1 PHOTOGRAPH GAS SAMPLING SYSTEM

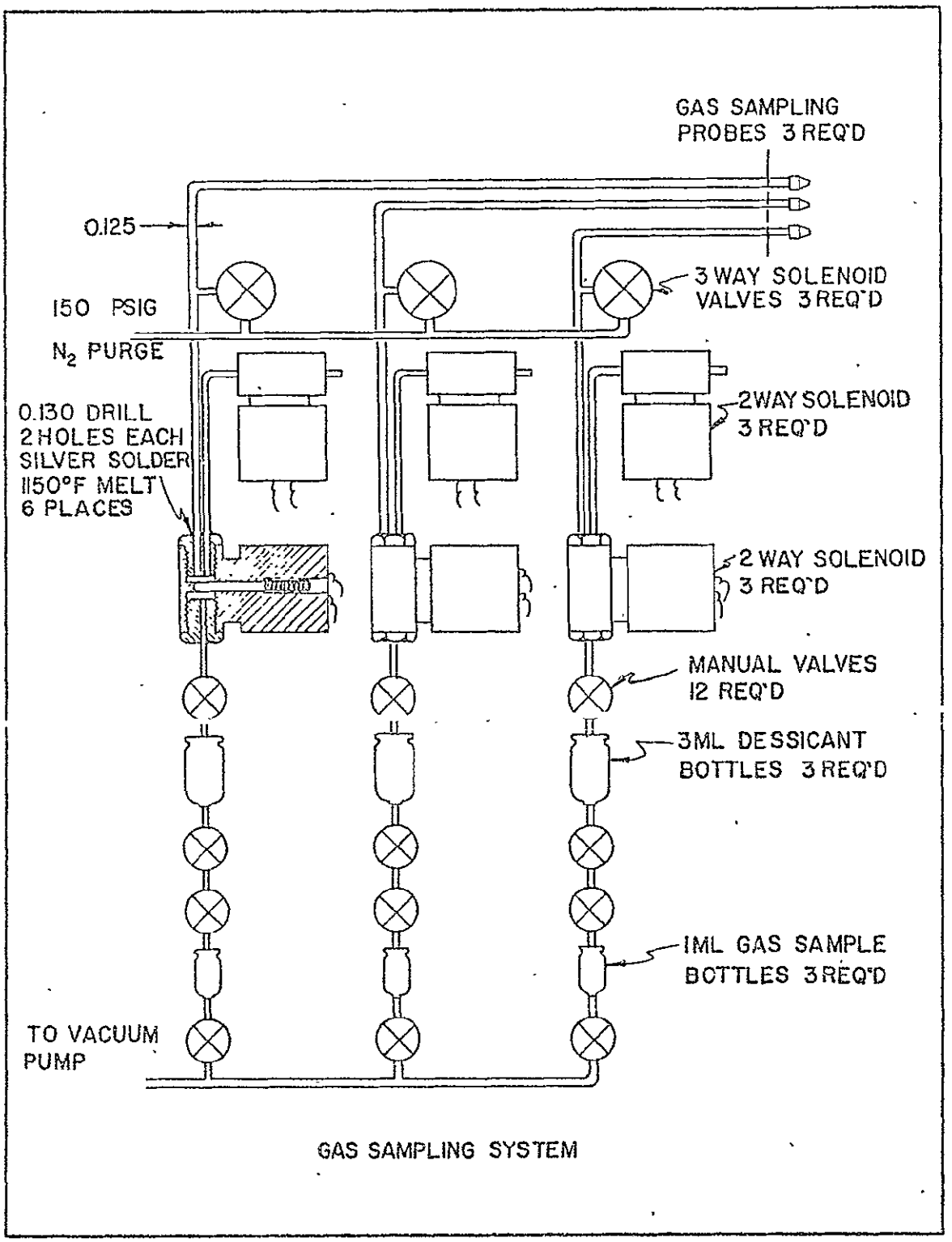

FIGURE E-2 SCHEMATIC GAS SAMPLING SYSTEM

In a typical vitiated air gas sampling experimental run the sequence of operations is as follows:

1. Prior to gas generator ignition, all manual valves are opened and the lines downstream of the two way solenoid valves, the dessicant and gas sample bottles are evacuated down to 0.15 psia.

2. The manual valves immediately upstream of the vacuum pump are closed and all others remain open.

3. The three way solenoid valves are opened and all other solenoid valves remain closed.

4. The 150 psig N_2 purge is activated and the gas sampling lines upstream are purged.

5. The gas generator is started and once steady operation is obtained the three way solenoid valves are closed and the upper two way solenoid valves opened; the lower two way solenoid valve remains closed. The N_2 purge is closed off and the combustion gases are allowed to blow through the lines down to the lower two way solenoid valves, up through the upper two way solenoid valves and overboard.

6. When the gas sample is to be taken, the upper valve closes and the lower valves opens allowing the evacuated bottles to capture the sample. Once the sample is taken, lower valves are closed and the three way valves opens which begins to purge the line during shutdown.

7. After shutdown all manual valves are closed and the bottles are taken for analysis.

APPENDIX F

COMBUSTION EFFICIENCY ANALYSIS FOR GAS GENERATOR - SAMPLE CALCULATION

The primary objective of any gas generator is to provide a given flow rate of a mixture of gases of known composition. Assuming that the chemical reactions of the injected propellants are known, together with other pertinent parameters, one can theoretically predict the flow rate and composition of an idealized system. Deviations from these idealized results, when the system is experimentally operated, are measures of the efficiency of the apparatus. For most "boiler-plate" rocket motors which are used as gas generators, the efficiency of combustion is measured by the deviation of the effective exhaust velocity (C^*) measured from the theoretically computed value. This parameter (C^*) is employed because of its relative ease of measurement in experimental systems. The values of chamber pressure, nozzle throat area and total propellant flow rate are the items required. The combustion efficiency based on C^* (η_{C^*}) is defined as the ratio of the actual C^* measured to that theoretically computed by thermochemical computer programs. A high η_{C^*} would indicate that the theoretically computed species composition would be reasonably accurate.

The following is a sample calculation of the gas generator η_{C^*} for the present system (Run 45):

1. Measured parameters

$$\dot{w}_f = 1.5 \text{ lb/sec}$$

$$\dot{w}_{ox} = 5.5 \text{ lb/sec}$$

$$\dot{w}_{N_2} = 2.0 \text{ lb/sec}$$

$$\dot{w}_{TOTAL} = 9.0 \text{ lb/sec}$$

$$P_c = 528 \text{ psia}$$

$$T_{N_2} = 510^\circ R$$

$$A_t = 1.97 \text{ in}^2$$

2. Calculate fuel fraction in order to determine from the thermochemistry computer output the $C^*_{Theor\ (f/ox)}$ for the anhydrous-hydrazine/nitrogen-tetroxide reaction.

$$\text{Fuel fraction} = \frac{\dot{w}_f}{\dot{w}_f + \dot{w}_{ox}} = 0.2129$$

Reading from the thermochemistry output

$$C^*_{Theor,(f/ox)} = 4798.75 \text{ ft/sec}$$

3. Gaseous diatomic nitrogen (N_2) is employed as a diluent. Therefore, its effect on the overall theoretical C^* must be determined. By definition,

$$C^* = \frac{g_c P_c A_t}{\dot{w}_{TOTAL}}$$

$$\dot{w}_{TOTAL} = \rho_t A_t V_t$$

(choked and constant flow rate assumed), for a perfect gas,

$$\rho_t = \frac{P_t}{RT_t}$$

substituting for ρ_t and $\dot{w}_{TOTAL}$ in the equation for C^*

$$C^* = g_c \frac{P_c \; R \; T_t}{P_t \; V_t}$$

The nozzle throat is choked, therefore, for N_2, ($\gamma \sim 1.3$) at $M = 1$.

$$T_t/T_{N_2} = 0.869$$

$$P_c/P_t = \frac{1}{0.545}$$

$$V_t = \sqrt{\gamma \; RT_t}$$

substituting for T_t/T_{N_2}, P_c/P_t and V_t in the equation for C^* and rearranging yields

$$C^*_{N_2} = \frac{1}{0.545} \sqrt{\frac{0.869 \; T_{N_2} \; R \; g_c}{\gamma}}$$

substitution measured values

$$C^*_{N_2} = 1420 \text{ ft/sec}$$

4. To get the overall $C^*_{Theor,Mean}$, the $C^*_{Theor,(f/ox)}$ and $C^*_{N_2}$ must be weighted.

$$C^*_{Theor,Mean} = \frac{(\dot{w}_f + \dot{w}_{ox}) \; C^*_{Theor,(f/ox)} + \dot{w}_{N_2} \; C^*_{N_2}}{\dot{w}_{TOTAL}}$$

Substituting values specified

$$C^*_{Theor,Mean} = 4051 \text{ ft/sec}$$

5. The actual C^* is calculated by the equation

$$C^*_{actual} = \frac{P_c \, A_t \, g_c}{\dot{w}_{TOTAL}}$$

Substituting measured values

$$C^*_{actual} = 3885 \text{ ft/sec}$$

6. The η_{C^*} is calculated as

$$\eta_{C^*} = \frac{C^*_{actual}}{C^*_{Theor,Mean}} = \frac{3886}{4052} = 0.96$$

APPENDIX G

PROPOSED METHOD FOR DETERMINING COMBUSTION EFFICIENCY OF THE SUPERSONIC TEST SECTION

The method for evaluation of overall combustion efficiency involves a comparison of the actual non-adiabatic, finite-rate thermochemistry combustion process in which certain quantities are measured experimentally to the adiabatic, equilibrium thermochemistry case determined analytically. The combustor analytical model consists of an open system with fuel (H_2) and oxidizer (vitiated air) being added with instantaneous mixing and without shocks. The assumption of no heat transfer through the walls of the combustor and equilibrium thermochemistry allows one to write the energy equation (first law of thermodynamics) for the system.

$$\dot{w}_f H_f + \dot{w}_{ox} H_{ox} = \dot{w}_{cp} H_{cp}$$

This equation may be manipulated through the use of the concept of total enthalpy and a definition of a quantity called the "sensible enthalpy" to give a constant, Q_{chm}, called the heat of reaction, as follows:

$$H = h + \frac{V^2}{2}$$

Also

$$h = \Delta H_f^\circ + \int_{T_1}^{T} c_p \, dT$$

Thus

$$H = \Delta H_f^\circ + \int_{T_1}^{T} c_p \, dT + \frac{V^2}{2}$$

Defining sinsible enthalpy as

$$h_s \equiv \int_{T_1}^{T} c_p dT + \frac{V^2}{2}$$

Hence

$$H = \Delta H_f^\circ + h_s$$

Substituting into the energy equation

$$\dot{w}_f \left(\Delta H_{f_f}^\circ + h_{s_f}\right) + \dot{w}_{ox} \left(\Delta H_{f_{ox}}^\circ + h_{s_{ox}}\right) = \dot{w}_{cp} \left(\Delta H_{f_{cp}}^\circ + h_{s_{cp}}\right)$$

Rearranging

$$\dot{w}_{cp} \, h_{s_{cp}} - \dot{w}_f \, h_{s_f} - \dot{w}_{ox} \, h_{s_{ox}} = - \dot{w}_{cp} \, \Delta H_{f_{cp}}^\circ + \dot{w}_f \, \Delta H_{f_f}^\circ + \dot{w}_{ox} \, \Delta H_{f_{ox}}^\circ$$

Defining the heat of reaction, Q_{chm}, as the right side of the above equation

$$Q_{chm} \equiv - \dot{w}_{cp} \, \Delta H_{f_{cp}}^\circ + \dot{w}_f \, \Delta H_{f_f}^\circ + \dot{w}_{ox} \, \Delta H_{f_{ox}}^\circ$$

By conservation of mass

$$\dot{w}_{cp} = \dot{w}_f + \dot{w}_{ox}$$

The heat of reaction may be determined analytically by knowing the weight flow rates and heats of formation of the fuel, oxidizer and combustion products. This task may be accomplished by using the 1D equilibrium SS Combustion program [18] in conjunction with the JANAF Tables. This computed heat of reaction, Q_{chm}, based on the idealized model, will be used later in the determination of overall combustion efficiency.

The actual supersonic combustion of hydrogen and vitiated air occurs non-adiabatically, with heat transfer through the walls of the combustor and with finite-rate thermochemistry that deviates from equilibrium. Thus, the energy equation cannot be written for the actual open system unless some modification is made. A modified energy equation may be written with the inclusion of a term Q_L, which comprises the heat transfer through the walls of the combustor and losses due to nonequilibrium thermochemistry, as follows:

$$\dot{w}_f H_f + \dot{w}_{ox} H_{ox} = \dot{w}_{cp} H_{cp} + Q_L$$

Manipulation of this modified energy equation gives $Q' = Q_{chm} - Q_L$, where Q' may be expressed in terms of weight flow rates and sensible enthalpies of fuel, oxidizer, and combustion products as follows:

$$\dot{w}_f \left(\Delta H^\circ_{f_f} + h_{s_f}\right) + \dot{w}_{ox} \left(\Delta H^\circ_{f_{ox}} + h_{s_{ox}}\right) = \dot{w}_{cp} \left(\Delta H^\circ_{f_{cp}} + h_{s_{cp}}\right) + Q_L$$

Rearranging

$$\dot{w}_{cp}\, h_{s_{cp}} - \dot{w}_f\, h_{s_f} - \dot{w}_{ox}\, h_{s_{ox}}$$

$$= - \dot{w}_{cp}\, \Delta H^{\circ}_{f_{cp}} + \dot{w}_f\, \Delta H^{\circ}_{f_f} + \dot{w}_{ox}\, \Delta H^{\circ}_{f_{ox}} - Q_L$$

$$= - Q_{chm} - Q_L$$

$$= Q'$$

Thus

$$Q' = \dot{w}_{cp}\, h_{s_{cp}} - \dot{w}_f\, h_{s_f} - \dot{w}_{ox}\, h_{s_{ox}}$$

where

$$h_{s_{cp}} = \int_{T_1}^{T_{s_{cp}}} c_{p_{cp}}\, dT + \frac{V_{cp}^2}{2}$$

$$h_{s_f} = \int_{T_1}^{T_{s_f}} c_{p_f}\, dT + \frac{V_{cp}^2}{2}$$

$$h_{s_{ox}} = \int_{T_1}^{T_{s_{ox}}} c_{p_{ox}}\, dT + \frac{V_{cp}^2}{2}$$

Determination of the fuel and oxidizer flow rates and sensible enthalpies presents no particular difficulty since inlet conditions to the supersonic combustor are known. Thus, the determination of Q' reduces to the problem of calculating the sensible enthalpy of the combustor products. The determination of $h_{s_{cp}}$, as described below, for determining combustion efficiency, may be carried out by measuring wall static pressure at the combustor exit and cone-static pressure, pitot pressure, species composition, and static temperature

at radial locations at the combustor exit.* Assuming the flow is axisymmetric, a knowledge of these quantities provides information needed to determine sensible enthalpies at radial locations of the combustor exit. An integrated sensible enthalpy at the exit plane then provides a knowledge of Q'. Finally, combustion efficiency is determined by forming the ratio

$$\eta_c = \frac{Q'}{Q_{chm}} = \frac{\left(Q_{chm} - Q_L\right)}{Q_{chm}}$$

The following described analysis will provide information needed to determine $h_{s_{cp}}$ at one radial location at the combustor exit. As seen above, this is all that is needed to arrive at a combustion efficiency. Due to the presence of supersonic flow, the measured values of static and total pressure are not the true values and therefore means must be devised to correct the measured values. In order to estimate the free-stream Mach number at the exit, M_e, the measured combustor exit wall static pressure, p_{s_w}, and the indicated local impact pressure, P_t', are used with the Rayleigh pitot formula

$$\frac{p_{s_w}}{P_t'} = \frac{\left\{\left[\left(\frac{2\gamma}{\gamma+1}\right) M_e^2 - \frac{(\gamma-1)}{(\gamma+1)}\right]^{1/(\gamma-1)}\right\}}{\left[\frac{(\gamma+1)}{2M_e^2}\right]^{\gamma/(\gamma-1)}}$$

The specific heat ratio, γ, may be determined from an analysis of species. The M_e obtained from the above relation is then used to

---

*Instrumentation needed for these measurements were described in the section entitled "Description of Instrumentation."

convert the indicated cone-static pressure to a more nearly correct local value by a useful approximation technique in Reference 30.

$$C_p = \frac{\left(p_s' - p_{s_{cp}}\right)}{q_{cp}} = \frac{\left(p_s'/p_{s_{cp}} - 1\right)}{1/2\ \gamma\ M_e^2}$$

$$C_p = \frac{1}{2}\left(f_2 + f_1 \sin^2\delta - \left\{\left(f_2 - f_1 \sin^2\delta\right)^2 - \left[\left(f_3 - f_1\right)\sin^2\delta\right]^2\right\}^{1/2}\right)$$

where

$$f_1 = \frac{(\gamma+7)}{4} - \left(\frac{(\gamma-1)}{4}\right)^2 + \frac{6}{M_e^6} + \frac{(M_e^2-1)}{M_e^4}\sin\delta$$

$$f_2 = \frac{1/2\ (\gamma+7)}{(\gamma+1)}\left(1 - \frac{1}{M_e^2}\right)\left(1 + \frac{1}{M_e^6}\right)$$

$$f_3 = \frac{\gamma/2\ (\gamma+7)}{(\gamma+1)}\left(1 + \frac{1}{M_e^2}\right)\left(1 + \frac{1}{M_e^6}\right)$$

The newly calculated value of $p_{s_{cp}}$ is used together with P_t' to repeat the above process and determine a new M_e. This process is continued until satisfactory convergence is obtained.

Total pressure is determined using the following formula

$$P_{t_{cp}} = p_{s_{cp}}\left\{1 + \left[\frac{(\gamma-1)}{2}\right] M_e^2\right\}^{\gamma/(\gamma-1)}$$

The total temperature is arrived at using the following weight flow function

$$\frac{G\left(T_{t_{cp}}\right)^{1/2}}{P_{t_{cp}}} = M_e\ (\gamma/R)^{1/2}\ \frac{\left\{1/\left[1+\left(\frac{(\gamma-1)}{2}\right)M_e^2\right]\right\}^{(\gamma+1)}}{2(\gamma-1)} = f(\gamma,M_e)$$

Manipulation of this equation gives

$$T_{t_{cp}} = \left[f(\gamma,M_e)\ P_{t_{cp}}\ G\right]^2$$

The static temperature is determined by the following equation

$$T_{s_{cp}} = \frac{T_{t_{cp}}}{\left\{1+\left[\frac{(\gamma-1)}{2}\right]M_e^2\right\}}$$

The velocity is determined by using the Mach number relation

$$M_e = \frac{V_{cp}}{A_{cp}}$$

$$M_e = \frac{V_{cp}}{\left(\gamma R T_{s_{cp}}\right)^{1/2}}$$

$$V_{cp} = M_e\ \left(\gamma R T_{s_{cp}}\right)^{1/2}$$

The sensible enthalpy at a specific radial location may be determined knowing, cp, $T_{s_{cp}}$, and V_{cp} as follows:

$$h_{s_{cp}} = \int_{T_1}^{T_s} c_{p_{cp}}\ dT + \frac{V_{cp}^2}{2}$$

Thus, the combustion efficiency may be determined using the equations previously described.

In addition to analytically determining the radial static temperature, the static temperature profile across the supersonic combustor exit may be measured optically utilizing the intensity comparison scheme as previously described in the section entitled "Description of Instrumentation."

Due to the presence of non-uniform concentration and velocity gradients across the exit plane of the combustor, some type of mixing analysis and local determination of the mass velocity is required. This information may be obtained by employment of the GASL "Supersonic Mixing and Combustion of Hydrogen in Air Streams" computer program as in Reference 28.